Modelling the transient strain behaviour of concrete exposed to elevated temperatures

Thesis submitted in fulfilment of degree of *Doctor of Philosophy*

Christopher James Robson

Supervisor: Dr Colin Thorpe Davie

School of Civil Engineering and Geosciences, Newcastle University

September, 2012

ABSTRACT

The available transient strain models for concrete are investigated and, where appropriate, modified through a multi-level analysis procedure in which the models are explored in general, in terms of qualitative behaviour in FE simulations of generic experimental conditions, and in terms of FE simulations of specific experimental conditions. The previously ignored issue of the nature of the transient strain response to states of tension is explored through simulation of the resultant axial strain behaviour of three mathematical models for tensile transient strain, defined a priori.

An original analytical tool and a novel calibration technique are developed to allow this work to be performed. The method of 'Gauss point mean variables' plotting allows the values of any model parameters to be explicitly examined throughout a simulation, while the 'iterative feedback technique' allows for rapid parametric calibration while maintaining the accuracy of the FE method.

Using these techniques, it is found that the Nielsen model and the Terro model allow the reproduction of experimental results, with the remaining models, including the commonly applied Anderberg model, shown to be a relatively poor approximation. Application of these models to three realistic examples of concrete technology shows that transient strain is extremely important in conditions of heating, consistently increasing structural resilience. In particular, simulation of concrete beams subjected to restrained expansion shows convincingly that the Anderberg model is fundamentally unable to reproduce experimental behaviour.

Results suggest that no transient strain develops due to conditions of tension. However, due to the relatively small specimen size of the experimental conditions, this conclusion may be considered to be tentative. A continuation of this research using experimental data obtained using larger specimens is recommended. The response of transient strain to states of tension is shown to have a profound effect on the development of damage in columns subjected to fire conditions.

Further, a brief investigation into the load-dependence of transient strain implied by the experimental data reveals that a small deviation from linearity may be suitable. A further exploration of this deviation, including into the effects on overall results in experimental conditions, may be useful for transient strain modelling.

Acknowledgements

First and foremost, I offer my sincerest gratitude to my supervisor, Dr Colin Davie, who has offered both guidance and a degree of creative freedom during the course of this work. This thesis would not have been possible without the knowledge, experience, and significant investment of time that he provided throughout the entire duration of the project. It is not possible to imagine a supervisor who would provide a more fertile environment in which to carry out research.

I also acknowledge the assistance of a contemporary research colleague of mine, Dr Ini Edem, who provided significant encouragement and good general advice when required throughout my work.

I must also thank Dr Diya Kuruvilla who provided support in numerous ways throughout some of the most difficult periods of this research and gave me the inspiration to carry on. She has acted as my rock, my light, and my constant companion. I hope that she realises how much she means to me.

Performing research is, at times, a very stressful endeavour. Therefore, I thank all of the friends and colleagues who helped to alleviate this stress throughout my research. I shall certainly miss our lunch time chats.

I would also like to thank my parents for supporting me throughout my education and for acting as role models that showed me the value of hard work. I could not be where I am today without them.

Finally, I acknowledge Halcrow for the financial support provided through a CASE award for this project. I sincerely hope that they will continue to support the wonderful research being performed at Newcastle University.

Table of contents

Chapter 1. Introduction..... 1

Chapter 2. Literature review..... 5

2.1 Key experimental observations..... 7

2.1.1 Temperature-dependence of transient strain..... 9

2.1.2 Rate of development of transient strain..... 13

2.1.3 Effects of cooling and re-heating on transient strain..... 15

2.1.4 Load-dependence of transient strain..... 18

2.2 Physical origins of transient strain..... 21

2.2.1 Basic creep as the origin of transient strain..... 22

2.2.2 Dehydration process as the origin of transient strain..... 24

2.2.3 Stress concentration due to pore evacuation..... 27

2.2.4 Local mesoscale stresses due to thermal mismatch..... 28

2.2.5 Final remarks..... 30

2.3 Mathematical models of transient strain..... 30

2.3.1 Anderberg and Thelandersson..... 31

2.3.2 Gawin et al..... 33

2.3.3 Terro 35

2.3.4 Nielsen et al..... 36

2.3.5 Schneider..... 38

2.3.6 Final Remarks..... 40

2.4 Final remarks..... 42

Chapter 3. Methodology..... 46

3.1 Governing equations..... 46

3.2 Constitutive laws for energy and fluid transport behaviour..... 47

3.3 Constitutive laws for mechanical behaviour..... 48

3.3.1 Elastic strain..... 49

3.3.2 Basic creep..... 53

3.3.3 Thermal strain..... 53

3.3.4 Transient strain..... 54

3.4 Numerical model..... 54

3.4.1 Finite element formulation..... 55

3.4.2 Boundary conditions..... 60

3.5 Mean variable analysis..... 60

Chapter 4. Analytical review of proposed transient strain models..... 63

4.1 Bažant model..... 63

4.2 Anderberg model..... 74

4.3 Gawin model..... 77

4.4 Sabeur model..... 81

4.5 Terro model..... 85

4.6 Nielsen model..... 92

4.7 Wu model..... 95

4.8 Schneider model..... 96

4.9 Thienel model..... 103

4.10 Brooks model..... 106

4.11 Final model list..... 108

4.12 Final remarks..... 110

Chapter 5. Qualitative investigation of model behaviour..... 113

5.1 Methodology..... 114

5.1.1 Experimental conditions of simulations..... 115

5.1.2 Material properties..... 117

5.1.3 FE model parameters..... 119

5.2 Transient strain in tension..... 130

5.3 Predictions of models in various high temperature conditions..... 130

5.4 Modifications of models..... 141

5.4.1 Modification of Bažant model..... 141

5.4.2 Modification of Anderberg model..... 143

5.4.3 Modification of Nielsen model..... 144

5.4.4 Modification of Terro model..... 144

5.4.5 Modification of Schneider model..... 145

5.5 Closing remarks..... 146

Chapter 6. Quantitative analysis of model performance..... 150

6.1 Methodology..... 151

6.1.1 The iterative feedback technique..... 153

6.1.2 The Parametric Permutation Iterator (PPI)..... 154

6.1.3 Conventional fitting technique..... 157

6.2 The Experimental Data Sets..... 158

6.3 Details of application of model..... 161

6.3.1 Accounting for the cylindrical cavity..... 163

6.3.2 Applying the basic creep model..... 165

6.3.3 Thermal damage..... 169

6.3.4 Test of FE model parameters..... 172

6.4 Results and Discussion..... 173

6.4.1 The Nielsen model/TTS analysis..... 174

6.4.2 The Anderberg model..... 186

6.4.3 The Terro model..... 192

6.4.4 The Schneider model..... 196

6.4.5 The Bažant model..... 201

6.4.6 Overall discussion..... 207

6.4.7 The load-dependence..... 213

Chapter 7. Structural case studies..... 219

7.1 Restrained beam..... 220

7.2 Column in fire conditions..... 227

7.3 Nuclear reactor pressure vessel in service conditions..... 231

7.4 Final remarks..... 235

Chapter 8. Conclusions and further work..... 237

8.1 Conclusions..... 237

8.1.1 Analytical review of proposed transient strain models..... 238

8.1.2 Qualitative investigation of model behaviour..... 239

8.1.3 Quantitative analysis of model performance..... 241

8.1.4 Structural case studies..... 243

8.1.5 Wider implications..... 244

8.2 Further work..... 246

Appendix A..... 248

Appendix B..... 250

Appendix C..... 252

Appendix D..... 255

References..... 280

List of figures

	Page
Figure 2-1: The difference in total shear strain in specimens identically loaded, one heated 18 hours before load was applied and the other heated immediately after loading [14].	7
Figure 2-2: Total LITS observed due to heating of a concrete specimen in a torsional loading state at a level of approximately 20% of the ultimate torsional load at room temperature. Strain decomposition is based on previous results [31].	8
Figure 2-3: (a) The LITS master curve found using five different concrete specimens heated at 1°C/min up to 600°C at three different load levels [31] and (b) the LITS curves for five different concrete types heated at 1°C/min up to 600°C under a compressive uniaxial load equal to 10% of the initial compressive strength [17].	8
Figure 2-4: The sum of elastic strain and creep observed when two identically loaded specimens undergo different heating regimes to the same temperature (approximately 60°C) [13].	12
Figure 2-5: The period of time required following temperature equilibration for the daily dimensional change of a cement paste specimen to become relatively stable when heated at 1°C/min to elevated target temperatures [43].	14
Figure 2-6: The total axial strain in excess of the strain recorded when heated under no load for two concrete cylindrical specimens loaded in uniaxial compression to different magnitudes [22].	16
Figure 2-7: The sum of elastic strain and creep strain reported by Fahmi et al. [15] for specimens under uniaxial compression (left) or torsion (right), and in conditions of 50% relative humidity (top) or 100% relative humidity (bottom). Each specimen is subjected to a cyclic temperature history between a minimum of 23°C and a maximum of 60°C as denoted in the upper portion of each graph.	17
Figure 2-8: Results for (a) total shear strain of saturated mortar specimens in conditions of thermal cycling loaded in torsion [14] and (b) LITS and shrinkage induced by thermal cycling of concrete specimens (according to temperature histories, denoted E1 and E2) while under compressive load [19].	18
Figure 2-9: Results showing, for a range of elevated temperatures, (a) the octahedral deviatoric LITS against the ratio of the octahedral deviatoric stress to the initial compressive strength, and (b) the octahedral volumetric LITS against the ratio of the octahedral volumetric stress to the initial compressive strength [36].	20
Figure 2-10: A comparison of the microprestress evolution due to the imposed temperature history shown at the top of the figure and that due to no change in temperature [56].	22
Figure 2-11: (a) The development of the equilibrium value of the mass of dehydrated material with temperature increase and (b) the dehydrated mass of material with time at four elevated temperatures [64].	24
Figure 2-12: Comparison of the creep observed on concrete specimens, where one specimen undergoes carbonation after three days of loading [68].	26
Figure 2-13: The stress distribution of a material under axial compressive load in the region surrounding (a) a rigid spherical inclusion and (b) a spherical cavity [77].	27
Figure 2-14: Comparison of the total strain output of the model of Grassl and Pearce [78] in comparison to experimental data sets obtained using concrete cylinders heated while unloaded and while under three different load levels (22.5%, 45%, and 67.5%) [33].	29
Figure 2-15: Comparison of model output with transient strain experimental data found for heated specimens (a) preloaded at three different load levels and (b) restrained and heated at two different rates [33].	31
Figure 2-16: Comparison of total strain results produced using the model of Gawin et al. [87] and experimental data.	33
Figure 2-17: Relationships between the calculated values of (a) thermo-chemical strain, and (b) normalised transient strain and the thermo-chemical damage parameter [87].	34
Figure 2-18: Comparison of the polynomial approximation and experimental data for (a) basalt, limestone, lightweight, and gravel (T<400°C) aggregate concretes, and (b) gravel aggregate concretes (T>400°C) [88].	35
Figure 2-19: Comparisons of LITS model predictions and that deduced from experimental data for concrete of (a) 68% quartzite aggregate content, (b) 70% siliceous aggregate	36

content, and (c) 71.5% quartzite aggregate content [88].
Figure 2-20: Comparison of the predictions of a fourth-order polynomial transient strain model [39] and those of this model with two different sets of parameter values [90]. 37
Figure 2-21: Comparison of the model predictions and experimental data (a) for preloaded heated concrete specimens [33] and (b) for stress development in axially restrained heated concrete specimens, where the nature of each of the curves is explained in the text. 38
Figure 2-22: Comparison of the experimentally determined transient strain functions for three different types of concrete [34]. 39
Figure 4-1: A Kelvin-Voigt-type rheological model. 64
Figure 4-2: Representations of the simulated evolution of (a) temperature and (b) microprestress of concrete specimens in three sets of heating conditions. 68
Figure 4-3: Representations of the simulated evolution of (a) pore relative humidity and (b) microprestress of concrete specimens in three sets of drying conditions. 69
Figure 4-4: The variation in the ultimate microprestress value (as defined by Equation 4-11) with (a) time since start of heating and (b) time since start of drying. Note that the initial value of microprestress is indicated in the graphs by a dashed line. 69
Figure 4-5: Simulations of evolution of (a) relative humidity and (b) microprestress of a specimen heated to 100°C and held at constant temperature thereafter for four different magnitudes of the effect of temperature on rate of drying. 70
Figure 4-6: Simulations of (a) evolution in time of both microprestress and hypothetical microprestress and (b) resultant transient strain for a specimen linearly heated to 50°C in one day (and subsequently held at constant temperature) while simultaneously dried to 50% relative humidity. 72
Figure 4-7: Simulated results showing the transient strain that develops for specimens heated to (a) 100°C, (b) 200°C, (c) 500°C, and (d) 800°C. Two sets of results are shown in the graphs, one set in which no drying is allowed and another in which the specimens are simultaneously dried to a relative humidity of 0.01. 73
Figure 4-8: Transient strain history at three different uniaxial load levels (as percentage of initial value of $\boldsymbol{f_c}$) calculated using both Equation 4-17 ('original') and Equation 4-19 ('modified') for concrete containing (a) siliceous aggregates and (b) carbonate aggregates. 76
Figure 4-9: Comparison of the evolutions of normalised transient strain and the thermo-chemical strain calculated from experimental data [87]. Also shown are bilinear functions calibrated to these data. 78
Figure 4-10: Comparison of the thermal strain data and the proposed strain decomposition of the authors [87]. 80
Figure 4-11: (a) The evolution of $\boldsymbol{m_{dehyd} - m_{eq}}$ and (b) the evolution of $\boldsymbol{m_{eq}}$ measured at high temperatures. Note that the value of $\boldsymbol{m_{dehyd}}$ after 600 minutes at high temperature is assumed to be approximately equal to $\boldsymbol{m_{eq}}$ [64]. 83
Figure 4-12: (a) The fitted temperature function, defined by Equation 4-34, for $\boldsymbol{m_{eq}}$ and (b) the decomposed functions of Equation 4-34. 84
Figure 4-13: The fitted LITS temperature functions of (a) Equations 4-37 and 4-38, and (b) Equations 4-39 and 4-40. 87
Figure 4-14: Comparison of the load function proposed by Terro [39, 88] and the modified version proposed here to prevent a prediction of non-zero LITS development in conditions of zero local stress. 88
Figure 4-15: Effect of aggregate content by volume on the (a) specific creep of concrete (after unspecified time under load) [118] and (b) LITS of concrete predicted by Equation 4-43. 89
Figure 4-16: Comparison of the model predictions (a) as originally presented by Terro [88], (b) using the model without the factor $\boldsymbol{\varepsilon_{LITS}^{V_a}}$, (c) with the factor $\boldsymbol{\varepsilon_{LITS}^{V_a}}$ proposed by Terro [39, 88], and (d) using the factor $\boldsymbol{\varepsilon_{LITS}^{V_a}}$ given by Equation 4-43. The concrete tested contains 71.5% (quartzite) aggregate content by volume. 90
Figure 4-17: Comparison of experimental data and the function $\boldsymbol{\varepsilon_{LITS}^{V_a}}$ proposed by Terro [39, 88] (Equation 4-42), along with a modified version (Equation 4-44), and the model proposed here (Equation 4-43). 91
Figure 4-18: Example of typical output of the Nielsen transient strain model for five different load levels. 94
Figure 4-19: Comparison of the strain outputs predicted by the Nielsen model and the Wu model. 96

Figure 4-20: The temperature-dependent functions of the Schneider model, (a) the degradation of elastic modulus and (b) the transient strain function. 98
Figure 4-21: The transient strain output of the Schneider model, (a) axial transient strain for five different levels of preload and (b) the mean of the preload-normalised transient strain output of the model (mean calculated over ten different evenly-spaced preload levels between 10% and 100%). 99
Figure 4-22: Comparison of the proposed functions $\boldsymbol{f_R}$. 101
Figure 4-24: The normalised transient strain model for the three types of concrete for which parameters are fitted [34]. 102
Figure 5-1: The heating regimes used in the simulations. 116
Figure 5-2: The FE mesh to be applied for simulations in this work. 119
Figure 5-3: Graphical representation of $\boldsymbol{g_{tr}}$ *for each TTS assumption. Note that it is assumed that the tensile strength is 10% of the compressive strength.* 122
Figure 5-4: The hypothetical axial strain of a concrete specimen heated under load (0%, 30%, and 60%) to 800°C. 123
Figure 5-5: (a) Net transient strain and (b) total strain that are found to develop in unloaded FHTHT conditions for different TTS assumptions, The dotted line shows the intended total strain development. 124
Figure 5-6: The axial component of total strain and of thermal strain for heated unloaded cylindrical specimens of materials TTS0, TTS1, and TTS2. 125
Figure 5-7: The axial component of total strain for cylindrical specimens modelled using three different TTS assumptions (TTS0, TTS1, and TTS2) heated at 5°C/min under uniaxial compression equal to 30% of the initial compressive strength. 126
Figure 5-8: The axial component of transient strain for cylindrical specimens modelled using three different TTS assumptions heated at 5°C/min under uniaxial compression equal to 30% of the initial compressive strength. Also included for comparison are the 'ideal' transient strain behaviour at this load level and the transient strain behaviour found to develop in unloaded conditions for each TTS assumption. 127
Figure 5-9: The total strain observed in conditions of heating under load for the three TTS assumptions (TTS0, TTS1, and TTS2), along with the total strain history calculated by superposition of total strain in unloaded conditions with elastic strain and transient strain in loaded conditions. 127
Figure 5-10: Active ranges of $\boldsymbol{g_{tr}}$ *during FHTHT test in (a) unloaded conditions and (b) conditions of constant external uniaxial compressive load equal to 30% of the initial compressive strength.* 128
Figure 5-11: The total axial strain of a loaded concrete cylinder subjected to FHTHT conditions. The TTS assumptions applied are (a) TTS0 (with $\boldsymbol{C}$*=13×10-3) and (b) TTS2 (with* $\boldsymbol{C}$*=9×10-3).* 129
Figure 5-12: Total strain results in unloaded FHTHT conditions using all five transient strain models. 132
Figure 5-13: Total strain results in unloaded SHTHT conditions using all five transient strain models. 132
Figure 5-14: Total strain results for unloaded specimen in FHTHT conditions and SHTHT conditions, modelled using the Nielsen transient strain model. 133
Figure 5-15: Average measures of transient strain that develops in unloaded specimens in FHTHT conditions, due to local thermal stresses calculated using all five transient strain models. 134
Figure 5-16: Total strain results for loaded specimens in conditions of FHTHT. Note that the Bažant model deforms at constant temperature beyond the minimum strain value shown in the graph. 135
Figure 5-17: Total strain results for the loaded specimen in SHTHT conditions modelled using the Bažant transient strain model. 135
Figure 5-18: Total strain results for loaded specimens in FHTLT conditions. Note that the Bažant model develops at constant temperature beyond the minimum strain value shown in the graph. 136
Figure 5-19: Deduced transient strain component that develops in the loaded specimens in FHTHT conditions, calculated using the Nielsen model. 137

Figure 5-20: Deduced transient strain component that develops in the loaded specimens in FHTHT conditions, calculated using the Bažant model. 137
Figure 5-21: Total strain results for loaded specimens in HC1 conditions using all of the transient strain models. 138
Figure 5-22: Total strain results for both loaded and unloaded specimens subjected to the HC2 conditions using the Nielsen model, the Anderberg model, the Terro model, and the Schneider model. 138
Figure 5-23: Deduced transient strain results for specimens loaded and subjected to the HC2 conditions using the Nielsen model, Anderberg model, Terro model, and Schneider model. 139
Figure 5-24: The total strain results of both loaded and unloaded specimens subjected to the HC2 conditions calculated using the Bažant model, shown in (a) the low temperature region only and (b) the entire temperature range of heating. 140
Figure 6-1: Flow diagram representing the IFT procedure. 153
Figure 6-2: The finite element mesh used to simulate the experimental conditions of §6.2. 162
Figure 6-3: Comparison of the simulation of the evolution of the radial temperature profile of the concrete specimens heated at 5°C/min for use of (a) the filled BCs, (b) the sealed BCs, and (c) the unsealed BCs. 165
Figure 6-4: Comparison of the mathematical model for the changing compressive strength parameter with increasing temperature and experimental data on which it is based. 168
Figure 6-5: The experimental results for the evolution of the elastic modulus in heated conditions. The line represents the average behaviour found experimentally for unloaded concrete and the data points that of preloaded concrete. 169
Figure 6-6: The output of Equation 6-11 calibrated to the unloaded and loaded specimens. 171
Figure 6-7: Comparison of the different evolutions of (a) thermal strain and (b) transient strain that develop during heating of specimens described by transient strain models of differing TTS assumptions. 178
Figure 6-8: Comparison of simulated total strain in unloaded heated conditions and experimental data. 179
Figure 6-9: Comparison of the transient strain (TTS0) curves found to be most appropriate for the total strain results using each of the individual loaded data sets. 179
Figure 6-10: Mean error calculated across all permutations of parameter values for each value of the transition temperature considered (TTS0 assumption applied). 180
Figure 6-11: Minimum error associated with each transition temperature for (a) AT225, (b) AT35, (c) AT45, and (d) AT675 data sets. 181
Figure 6-12: The total strain predicted for each load level in comparison with the experimental data sets using the Nielsen model and (a) the TTS0 assumption, (b) the TTS1 assumption, and (c) the TTS2 assumption. The parameters $\boldsymbol{A}$, $\boldsymbol{B}$, *and* $\boldsymbol{C}$ *for each graph are chosen according to the data of all four load levels with* $\boldsymbol{\theta}^*$ *chosen independently for each individual load level.* 183
Figure 6-13: The total strain predicted for each load level in comparison with the experimental data sets using the Nielsen model and (a) the TTS0 assumption, (b) the TTS1 assumption, and (c) the TTS2 assumption. The parameters for each graph are chosen according to the data of all four load levels. 184
Figure 6-14: The total strain predicted for each load level in comparison with the experimental data sets using the Nielsen model and (a) the TTS0 assumption, (b) the TTS1 assumption, and (c) the TTS2 assumption. The parameters for each curve are chosen according to each individual data set. 185
Figure 6-15: Comparison of the total strain results obtained through FE simulations using the transient strain model (Anderberg) calibrated to the experimental data (AT45) via the PPI program. The further modified model results are for a similar simulation in which a non-zero value of $\boldsymbol{B_A}$ *is applied.* 190
Figure 6-16: The total strain predicted by FE simulations for each load level in comparison with the experimental data sets using the Anderberg model. The parameters for each graph are chosen according to each individual data set. 191
Figure 6-17: The total strain predicted for each load level in comparison with the experimental data sets using the Anderberg model. The parameters for each graph are chosen according to the data of all four load levels. 191
Figure 6-18: The total strain predicted by FE simulations for each load level in comparison with the experimental data sets, using the Terro model. The parameters for each graph are 195

chosen according to each individual data set.
Figure 6-19: The total strain predicted by FE simulations for each load level in comparison with the experimental data sets, using the Terro model. The parameters for each graph are chosen according to the data of all four load levels. 195
Figure 6-20: The total strain predicted by FE simulations for each load level in comparison with the experimental data sets, using the Schneider model. The parameters for each graph are chosen according to each individual data set. 199
Figure 6-21: The total strain predicted for each load level in comparison with the experimental data sets using the Anderberg model. The parameters for each graph are chosen according to the data of all four load levels. 200
Figure 6-22: Development of (a) microprestress and (b) transient strain during heating to 800°C at 5°C/min heating for a range of minimum values of the model relative humidity parameter. 202
Figure 6-23: Comparison of the experimental data (AT35) and model output. 205
Figure 6-24: Comparison of the experimental data and simulated results using the Bažant transient strain model calibrated to results using trial and error. 206
Figure 6-25: Comparison of experimental data and the model predictions using the Bažant transient strain model calibrated with the initial default set of values of parameters. 206
Figure 6-26: Target transient strain data calculated for each of the four data sets. 209
Figure 6-27: Comparison of the load-dependent functions found to best describe the experimental data sets using the IFT applied to the data sets and Equations 6-22 (a)–(e). 216
Figure 7-1: FE mesh used to simulate the heated restrained concrete beams (plane stress). 220
Figure 7-2: Thermal strain data for various concrete types and the derived thermal strain model applied to the beam specimens (modified to indicate the model curve) [2]. 221
Figure 7-3: Axial stress evolution obtained by Pearce et al. [2], using (1) the Nielsen model with a lower bound set of parameter values (no preload), (2) the Nielsen model with an upper bound set of parameter values (no preload), (3) the Nielsen model with an upper bound set of parameter values (preloaded), (4) no transient strain model (no preload), and experimental data obtained for (5) specimens with no preload [3] and (6) preloaded specimens [4]. 222
Figure 7-4: Comparison of the experimental results for the heated concrete beam in both unloaded and preloaded conditions and model results for (a) the Nielsen model, (b) the Anderberg model, (c) the Terro model, and (d) no transient strain model. 223
Figure 7-5: Comparison of the experimental results for the heated concrete beam in both unloaded and preloaded conditions and model results, using a thermal damage model that accounts for preload, for (a) the Nielsen model, (b) the Anderberg model, (c) the Terro model, and (d) no transient strain model. 227
Figure 7-6: (a) The ISO fire curve, as applied to the concrete cylinder in the numerical simulation and (b) FE mesh used (plane strain). 228
Figure 7-7: Profiles of the (a) first, (b) second, and (c) third principal stress components in the column cross section five seconds prior to the initiation of mechanical damage in the region of the upper right hand corner (Nielsen model). 228
Figure 7-8: Profile of mechanical damage in the column cross section after (a) 230 seconds, (b) 295 seconds, and (c) 490 seconds of exposure to fire conditions (Nielsen model). 229
Figure 7-9: The mechanical damage profile for the column in fire conditions (a) after 300 seconds of heating (Nielsen model and TTS1) and (b) after 415 seconds of heating (Nielsen model and TTS2). 231
Figure 7-10: The FE mesh used for numerical modelling of NPV in service conditions. 232
Figure 7-11: The stationary temperature profile at the peak operating temperature of the service conditions. 233
Figure 7-12: The profile of mechanical damage that develops in the NPV in the absence of the transient strain development after the first period of cooling is complete. 234
Figure B-1: Comparison of the displacement values found at the surface of the mesh approximately (a) one day after start of heating for 30x20 mesh simulated using various values of the time step parameter, and (b) two days after start of heating for a mesh composed of various numbers of elements simulated using a time step of 2 s. 250

List of tables

	Page
Table 2-1: The lengths associated with the scales of observation of concrete [24].	6
Table 4-1: Table of suggested values for the free parameters of Equation 4-56 [34].	98
Table 5-1: Material parameters to be used in the simulations.	118
Table 6-1: Material properties given by Anderberg and Thelandersson [1] for relevant experimental tests.	160
Table 6-2: Experimental parameters of tests performed by Anderberg and Thelandersson [1].	161
Table 6-3: Values of default initial thermal strain parameters used in FE simulations.	176
Table 6-4: Values of default initial transient strain parameters used in the FE simulations.	177
Table 6-5: Range of values of parameters and incremental values used in the PPI procedure.	177
Table 6-6: Default initial values of the free parameters of the Anderberg transient strain model (Equation 6-14).	188
Table 6-7: Range of values of parameters and incremental values used throughout the PPI procedure.	188
Table 6-8: The maximum, minimum, and incremental values of the model parameters applied in the first application of the PPI program within the IFT analysis of the Terro model.	194
Table 6-9: Default set of transient strain parameters for the Schneider model.	198
Table 6-10: Range of values of parameters and incremental values used in the PPI analysis procedure (third iteration).	199
Table 6-11: Default initial parameter values for the Bažant model.	204
Table 6-12: The relative error measures calculated for each of the transient strain models calibrated to each individual data set.	211
Table 6-13: The relative error measures calculated for each of the transient strain models calibrated to all data sets.	212
Table 6-14: The values of the free parameters of the load-dependent functions applied to the data sets using the IFT.	215
Table 6-15: The parameters of the loading functions found to produce the lowest overall error using the IFT.	217
Table B-1: Parameter values associated with minimum error values for results of each data set and combinations of data sets, where the Nielsen model is implemented, with the TTS0 assumption.	252
Table B-2: Parameter values associated with minimum error values for results of each data set and combinations of data sets, where the Nielsen model is implemented, with the TTS1 assumption.	253
Table B-3: Parameter values associated with minimum error values for results of each data set and combinations of data sets, where the Nielsen model is implemented, with the TTS2 assumption.	253
Table B-4: Parameter values associated with minimum error values for results of each data set and combination of data sets, where the Anderberg model is implemented (with the TTS0 assumption).	254
Table B-5: Parameter values associated with minimum error values for results of each data set and combination of data sets, where the Terro model is implemented (with the TTS0 assumption).	254
Table B-6: Parameter values associated with minimum error values for results of each data set ad combinations of data sets, where the Schneider model is used (with the TTS0 assumption).	254

Chapter 1. Introduction

Concrete, the most used manmade material on the planet, could be said to be the ubiquitous foundation on which the urban world is built. Applications include tunnels, roads, high-rise buildings, car parks, nuclear reactor pressure vessels (NPVs), and many more features of the planet's engineered landscape.

This dominance of concrete as a building material, the use of which outstrips that of the second most used building material (timber) roughly by a factor of three[1] [1], is a result of many positive factors, including relatively low price, durability, and its ability to be cast. In addition, due to the common use of local resources and relatively low production energy requirements, concrete usage can be considered environmentally friendly. Moreover, although properly addressed on a structural level rather than a material level, concrete is widely considered to be highly fire resistant due to a low thermal conductivity, an increased specific heat in temperature ranges prior to structural failure, and a non-flammable nature [1, 2]. Although there are several properties of concrete that are not ideal from a construction point of view (such as low tensile strength, tendency to undergo volume changes in ambient conditions, and a fairly low strength to weight ratio), there are several techniques that can be applied to mitigate the effects of these weaknesses, including use of reinforcement, prestress, and chemical admixtures.

The high temperature resistance of concrete is particularly advantageous as several uses of concrete are required to operate in conditions of increased temperature, such as the heating of airfield pavement by hot exhaust gases. It is important that the performance of the concrete application after such exposure remains of a high standard in order to maintain appropriate levels of safety and reduce repair costs. Moreover, for safety reasons, all concrete structures must be designed to withstand all feasible sets of conditions without complete loss of structural integrity.

Rapid heating to high temperature is one of the most extreme sets of conditions that may act on a structure. For NPVs, such conditions may occur, for instance, due to loss of coolant in the reactor, while fire is the main potential cause for most other

[1] This guideline figure is accurate for the volume of respective materials used in the U.S.A. construction industry in the year 2000.

applications. Concrete is known to undergo severe material degradation in these conditions, with thermal spalling found to be common [3-6]. The resultant loss of outer material in severe cases tends to expose inner material directly to rapid temperature change, thus accelerating the progress of damage. This is particularly deleterious to structural integrity if steel is a component of the concrete as the mechanical properties of steel at elevated temperatures are very poor in comparison to those at moderate temperatures.

Thus, it is essential that the thermo-mechanical response of concrete to high temperatures is well understood. Design codes exist to which structural designs must adhere in order to be considered safe (e.g. [7, 8]). However, these codes are largely based on direct extrapolation of experimental tests that are far removed from the scales and shapes of practical concrete structures. Therefore, the safety factors involved must be high in order to ensure structural reliability. Conversely, the costs of direct experimental testing of specific structural designs are prohibitively high and the value of experimental tests on scale models limited. Thus, numerical modelling is the most practical option for designers who wish to make cost effective or non-standard designs of concrete structures able to withstand service conditions over many years and short term accidental conditions.

There are several disparate aspects of the thermo-mechanical behaviour of concrete in high temperature conditions that are of significant importance to such analysis. This work shall focus on the modelling of transient strain, a dominant component of strain found to develop in preloaded concrete specimens in conditions of virgin heating. A thorough analytical review of the relevant experimental observations and applied mathematical models is performed, with recommendations for potential improvements. Through qualitative and quantitative analysis, these modelling techniques are objectively compared and mutually evaluated. Finally, the consequent effects of the transient strain models on material performance in realistic applications are directly observed.

As this work focuses on transient strain modelling, the conditions which are here most relevant are the experimental conditions in which transient strain is found to develop, i.e. increasing temperature with an applied external load. However, the model must be

formulated such that the predictions in all conditions are consistent with experimental observations. Therefore, conditions of constant or reducing temperature and unloaded conditions are not explicitly beyond the scope of this work.

Although there is a great deal of existing research into transient strain, both experimental and theoretical, there are a number of research areas that can be identified in a review of the literature that may require further investigation. It is the aim of this body of work to supplement this research through identification each of these areas and application of techniques of numerical analysis to attempt to resolve these issues or to identify the methodology and scope of work required for future investigations to reach such a resolution.

Based on the review of the literature in chapter 2, these areas of particular research interest may be identified as:

- Of the large number of transient strain models available, there appears to be no clear indication of which models result in behaviour that is most consistent with experimental observations. Moreover, links between hypothesised physical origins for transient strain and successful mathematical models may be explored.
- The nature of the transient strain response of concrete to states of tension is an area of research in which little progress has been made. There appears to be no work that establishes the importance of this potential effect or examines experimental results for evidence for this nature.

The principal methodology of this work is the use of a thermo-mechanical model for concrete implemented in the finite element (FE) framework, as briefly detailed in chapter 3. The total strain model applied by the model is thermal strain, transient strain, elastic strain (dependent on the thermo-mechanical damage state of the specimen), and basic creep.

It is necessary to restrict the investigation to a subset of the large number of available models. This is achieved through critical analysis of the models using an explicit set of criteria, detailed in chapter 4.

Many of the models are developed using individual data sets and may require modifications in order to adequately reproduce experimental observations. Thus, in chapter 5, the transient strain models are applied to a number of sets of plausible experimental conditions in order to assess the qualitative performance of the models. This allows potential modifications to be identified for subsequent quantitative investigations of the models. Moreover, several assumptions for the tensile transient strain models are identified in chapter 5 as plausible and their qualitative effects on simulated total strain behaviour in the sets of experimental conditions are shown.

In order to critically assess the relative performances of the transient strain models in experimental conditions through comparison with related experimental data, it is necessary to perform a stage of parametric calibration to the experimental data in order to find the closest fit to the data sets as is possible. As it is critically important that the contribution of transient strain can be identified in the experimental results for this calibration, the data sets of a comprehensive experimental investigation [9], in which the non-transient strain models may also be calibrated, are used for this purpose. In chapter 6, the methodology to complete these objectives is developed and applied and the results compared.

Finally, in chapter 7, each of a short list of the calibrated models of strongest performance is applied to three different sets of realistic experimental conditions for the purpose of examination of the importance of the modelling techniques to these conditions. These conditions are a column in fire conditions, an axially restrained beam in conditions of rapid heating, and a nuclear reactor pressure vessel in service conditions.

Chapter 2. Literature review

Since 1962, researchers have been aware that concrete that is heated while under load undergoes a greater degree of deformation in the loading direction than would be predicted using a 'conventional' strain decomposition [10]. Many experimental investigations into this behaviour have since been performed [9, 11-23] and this increased deformation magnitude is now known to be due to the development of transient strain.

Several different terms are commonly used in the literature to refer to transient strain. To avoid confusion, the terminology used in this work shall be explicitly defined. *Load-induced thermal strain* (*LITS*) is the name of the strain component most often reported in experimental work. It is defined as follows.

$$\varepsilon_{LITS}(T,\sigma) = \varepsilon_{tot}(T,\sigma) - \varepsilon_{th}(T) - \varepsilon_{el}(T_0,\sigma) \qquad \text{Equation 2-1}$$

where ε_{LITS} and ε_{tot} are the LITS and total strain respectively that develop during heating to temperature T while under a constant applied load σ, ε_{th} is the thermal strain that develops due to this temperature increase, and ε_{el} is the elastic strain caused by this applied load at the original temperature T_0.

LITS can be considered, thus, to be composed mainly of changes in elastic strain due to heating, basic creep, and transient strain. As the first two strain components tend to be of a fairly low magnitude, LITS and transient strain are often used interchangeably. However, this practice is both inaccurate and can lead to confusion.

Moreover, transient strain can be decomposed into two strain components, known as *transitional thermal creep*[2] (*TTC*) and *drying creep* (*DC*). In terms of relative magnitude, TTC is the principal strain component of LITS. DC is a strain component that develops in concrete specimens that are allowed to dry while under load. As concrete specimens undergo drying when heated, DC develops in identical conditions to TTC. It is found that it is very difficult to distinguish the strain contributions of TTC and DC, both in

[2] The term '*transient creep*' is sometimes used in place of '*transient strain*' in the literature. This practice is avoided in this work in order to avoid potential confusion with '*transitional thermal creep*' (which is occasionally known as '*transient thermal creep*').

practice and in theory. Thus, the combined contribution is usually discussed, though TTC is understood to be the dominant strain component.

In the following review, the key experimental observations relating to LITS are first discussed (§2.1). In turn, the various hypotheses that have been proposed for the physical origins of transient strain are then reviewed (§2.2). Then, the mathematical models commonly used to simulate transient strain are briefly examined (§2.3). Finally, the research areas that this work is intended to address shall be defined, based on the contents of this review (§2.4).

Concrete is a complex multiscale material, the structure of which is highly dependent on the scale of observation. Thus, it is common to define scales of observation on which discussed phenomena are considered to occur. Four such scales may be commonly defined: the *nanoscale*, the *microscale*, the *mesoscale*, and the *macroscale*. Processes active on lower scales of observation are extremely important to macroscale behaviour of concrete.

Table 2-1: The lengths associated with the scales of observation of concrete [24].

Name of length scale	Lengths associated with this length scale (m)
Nanoscale	$10^{-8} - 10^{-6}$
Microscale	$10^{-6} - 10^{-4}$
Mesoscale	$10^{-3} - 10^{-2}$
Macroscale	$10^{-2} - 10^{-1}$

While there is no universally agreed convention on the precise lengths associated with each length scale, the scales can be chosen such that the nature of concrete is compositionally distinct on each. Therefore, following the convention applied by some researchers [24, 25], the group of scales applied here are defined in table 2-1. On the macroscale, concrete is simply a single-phase material. On the mesoscale, concrete is composed of aggregates (both coarse and fine) and a cement matrix[3]. On the microscale, the hardened cement paste is observed to be composed of unreacted cement particles and hydration products (*cement gel*). Finally, on the nanoscale, the substructure of the main component of hydration, *calcium silicate hydrate* (C-S-H[4]), can be observed. A review of the nature of concrete on each of the scales of

[3] The cement matrix can also be found to be composed of two phases on this scale, bulk cement paste and interfacial transition zone.

[4] Conventional cement notation is applied here, in which *CaO*, *SiO*, and H_2O are represented by *C*, *S*, and *H* respectively

observation is considered to be beyond the scope of this work, though reference to processes on different length scales is inevitable for concrete research.

2.1 Key experimental observations

That concrete can not only reach a temperature of $100℃$ without complete material failure but also increase in strength for temperatures up to about $300℃$ was once considered to run counter to theoretical arguments [26]. The internal thermal stresses induced by thermal incompatibility of the components of concrete were expected to be of too great a magnitude for the material to endure. The authors suggested that the intrinsic porosity of cement paste somehow prevents the stresses in the region of the aggregate inclusions from increasing to sufficient magnitude to cause material failure. This unsatisfactory explanation had no compelling alternative until TTC was discovered in the 1960s and allowed the thermal stability of concrete to be explained.

The existence of TTC gained interest in 1966, when the first experimental investigation into this behaviour was performed [12]. Subsequently, several investigations [13-16, 27] helped to confirm TTC as an established experimental phenomenon in concrete specimens exposed to moderate elevated temperatures ($T < 100℃$), with the existence of TTC in temperature ranges above $100℃$ later demonstrated by Thelandersson and Anderberg [9, 28]. An example of these early results is shown in figure 2-1.

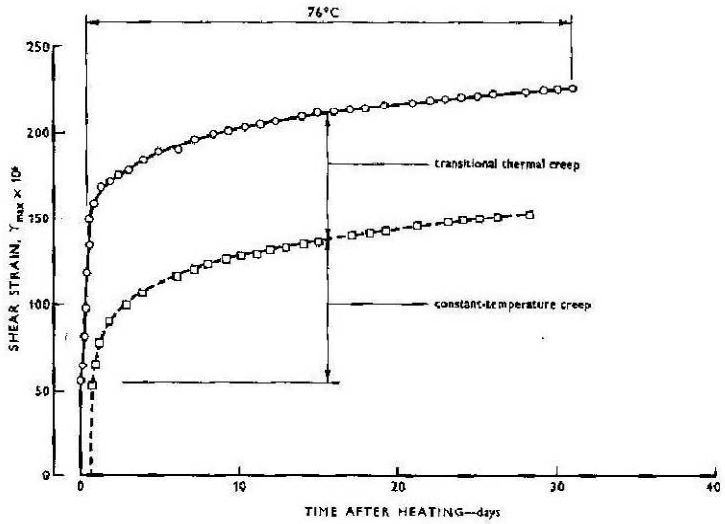

Figure 2-1: The difference in total shear strain in specimens identically loaded, one heated 18 hours before load was applied and the other heated immediately after loading [14].

The results of figure 2-1 show the shear strain found to develop in preloaded mortar specimens heated to $76℃$ in comparison to that in preheated mortar specimens loaded while at a constant temperature of $76℃$. Clearly marked in the figure by the authors [14] is the contribution of TTC (no drying creep is expected to have developed).

All investigations show that LITS makes a substantial contribution to the total deformation of concrete specimens when simultaneously heated and loaded. Based on experimental results [29], a characteristic value of "specific" LITS (i.e. per unit of applied load and temperature increase) is $0.45 \times 10^{-6}℃^{-1}MPa^{-1}$ [30]. This can be compared with corresponding values for ε_{el} and ε_{th} of the order of $33 \times 10^{-6}MPa^{-1}$ and $10 \times 10^{-6}℃^{-1}$ respectively. These values are consistent with observations [9] that suggest that an axial load equivalent to between 30% and 45% of f_c completely suppresses the net expansion of heated concrete caused by ε_{th}. Evidently, fairly modest values of applied load and temperature increase are required for LITS to become the dominant strain component.

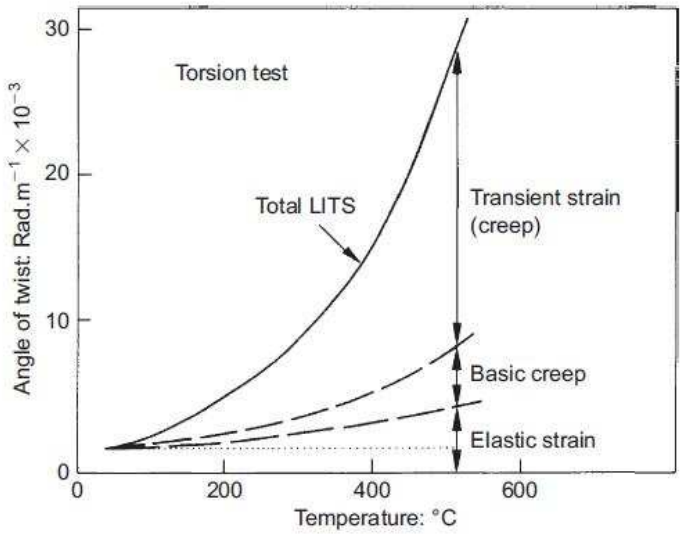

Figure 2-2: Total LITS observed due to heating of a concrete specimen in a torsional loading state at a level of approximately 20% of the ultimate torsional load at room temperature. Strain decomposition is based on previous results [31].

Results show that, for mature cementitious specimens, transient strain is the largest component of LITS, several times larger than both increases with temperature of basic creep and elastic strain [28, 32, 33]. The relative magnitudes of the LITS components for temperatures below $500℃$, estimated by Khoury [31] from previous results, are shown in figure 2-2. Given the large magnitude of LITS, the results of figure 2-2

underlines the importance of accurate modelling of transient strain for simulations of the hygro-thermo-mechanical behaviour of concrete in general conditions of heating and loading.

In this section, the main experimental observations regarding LITS are described. Firstly, in §2.1.1, the temperature-dependence of LITS is described. Then, observations relating to the rate of development and effects of cooling and reheating on LITS are discussed in §2.1.2 and §2.1.3 respectively. Finally, in §2.1.4, key observations related to the load-dependence of LITS are outlined.

2.1.1 *Temperature-dependence of transient strain*

Analysis of experimental results shows that LITS develops according to a '*master curve*' for temperatures below about $450℃$ [17]. The existence of the master curve, which implies that the nature of the aggregate is relatively unimportant, greatly simplifies the analysis of heated concrete specimens and remains the most important experimental finding relating to transient strain.

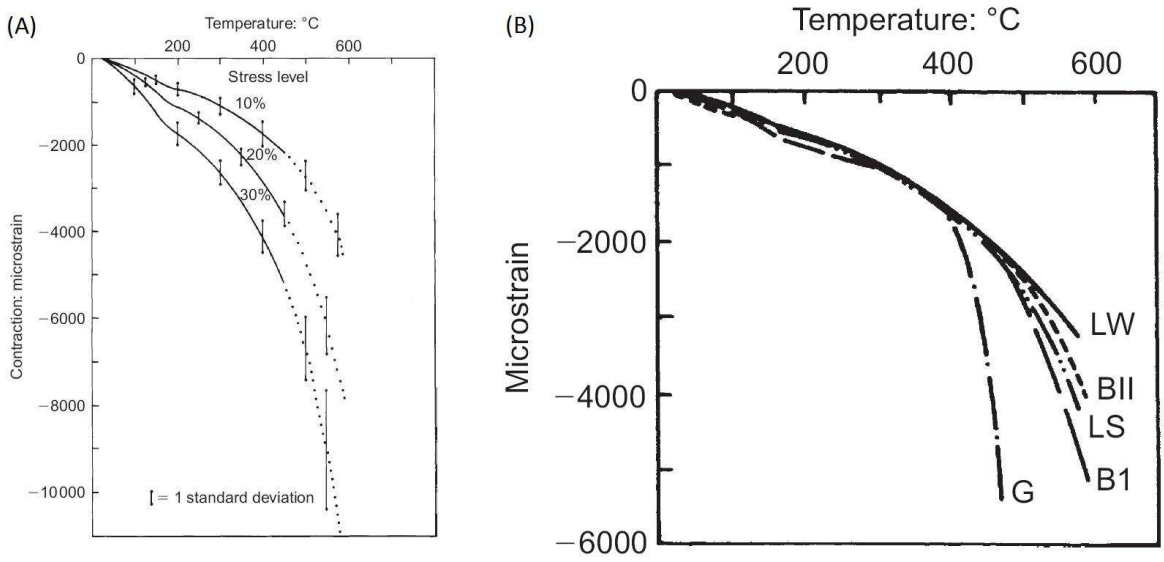

Figure 2-3: (a) The LITS master curve found using five different concrete specimens heated at 1°C/min up to 600°C at three different load levels [31] and (b) the LITS curves for five different concrete types heated at 1°C/min up to 600°C under a compressive uniaxial load equal to 10% of the initial compressive strength [17].

An example of the master curve is shown in figure 2-3 (a) from analysis of experimental results of five different specimens heated at $1℃/min$ with coarse aggregate types of limestone (LS), two types of basalt (B1 and BII), lightweight (LW), and gravel (G) under three different axial compressive load magnitudes. It is found that the master curve is valid only for temperatures below about $450℃$. Above this

temperature, results suggest that a degree of LITS divergence develops for different concrete specimens and, thus, that the master curve concept is no longer valid. This is demonstrated in figure 2-AAA (b), which shows the LITS curves for the five different concrete types heated under 10% load level.

It is found that several different criteria must be met to ensure that application of the master curve is valid for two different heated concrete specimens. The specimens should

- have similar aggregate content by volume,
- not undergo significant damage during heating,
- have similar preheating regimes,
- be heated at a similar rate, and
- be composed of a cement of a C-S-H nature.

If any of the above criteria are not met, the LITS behaviour of two heated concrete specimens would not be expected to be identical. For instance, it has been consistently shown that the magnitude of LITS is reduced in materials of higher aggregate content [12, 17, 18, 34]. Results show that the ratio of LITS of a concrete (of aggregate content of about 67% by volume) to that of neat cement paste is approximately constant at $0.35-0.40$ for the temperature range $75-400℃$ (the cement paste was not tested beyond $400℃$) [17]. Thus, the aggregate content is an important parameter for accurate prediction of LITS behaviour but can be considered to act primarily as a scaling parameter.

The development of damage in heated and loaded CM specimens is found to lead to significant differences in macroscopic LITS behaviour [17, 18]. This is illustrated, for instance, in figure 2-3 (b) in which the LITS of the concrete containing a gravel aggregate undergoes a major deviation from the LITS of the other concretes due to the development of significant damage during heating caused by thermo-chemical instability of the gravel.

Specimens that undergo different preheating regimes may exhibit profoundly different LITS behaviour during subsequent experimental tests. These results, which are an

important consideration for the accuracy of prediction models, are discussed in more detail in §2.1.3.

Results are not consistent on the importance of heating rate on the magnitude of LITS. For heating rates between about $4℃/min$ and $3℃/day$, some researchers find that there is little difference between the results of rapidly heated specimens and slowly heated specimens [10, 17], while others suggest that there may be a potentially large effect on results [18].

Based on experimental evidence [19, 28, 32], it is generally accepted that heating rate is fairly unimportant to the development of LITS, particularly in the range in which most experimental tests are performed, $2–5℃/min$. In fact, the range of heating rates in which this general observation may be considered to be valid is likely to be wider than this, e.g. $0.2–5.0℃/min$ [17, 34].

These observations are mainly found using experimental results acquired using concrete specimens under fairly low load levels. Some results appear to suggest that the LITS that develops for concrete specimens under high compressive load may be dependent on the heating rate, unlike that which develops when under a low applied load level [30]. However, the origin of this phenomenon is thought to be nonlinearity caused by the combination of macroscopic stress redistribution during heating and the strong spatial variation of material mechanical properties induced by temperature gradients. At an applied load level of 60% for instance, this nonlinearity is far more significant than at a load level of 30%. Thus, it appears that results support the assumption that direct effects of heating rate on LITS are fairly minimal and that apparent effects at high load levels should be largely reproducible using realistic thermo-mechanical and material models.

Only C-S-H cement types were used in the experimental work from which the master curve behaviour was first observed [17]. Potentially different observations were anticipated for concretes made using different types of cement. Based on previous work [35], some researchers [36] have suggested that the cement type is important for the magnitude of LITS observed at temperatures higher than about $200℃$, with aluminate content, for instance, found to be important for temperature ranges above

400°C [36, 37]. Therefore, cement type is likely to be a relevant consideration for predictions of LITS behaviour.

For temperature ranges above about 450°C, as stated above, the master curve is no longer found to apply to the results. An intensification of the rate of increase of the LITS magnitude is generally found to develop in this temperature range, with some authors considering a transition in behaviour to occur at approximately 450°C. It appears that, whereas the aggregate type is unimportant in the low temperature range, this is not the case in the high temperature range.

Despite this limit to range of applicability, the master curve is a powerful tool for modelling LITS behaviour of concrete. It allows a simple method to predict the LITS behaviour of different concrete specimens, despite differences in aggregate type [17, 38], water/cement ratio [19, 34], and age [16, 30, 34] (provided that the age is above three months [18, 39]).

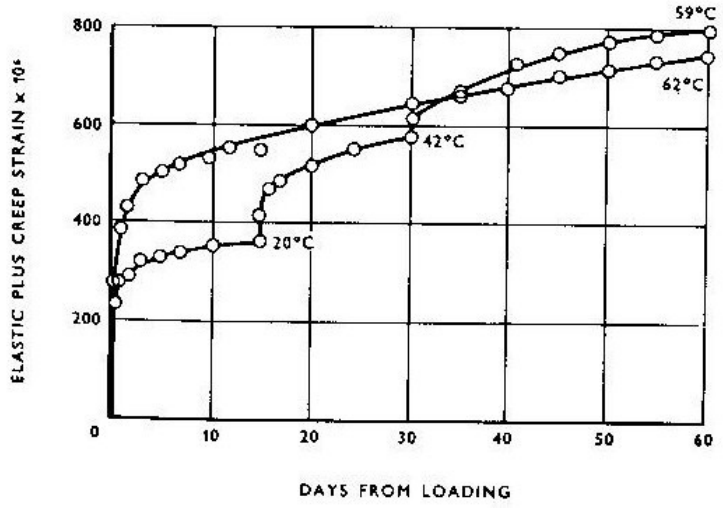

Figure 2-4: The sum of elastic strain and creep observed when two identically loaded specimens undergo different heating regimes to the same temperature (approximately 60°C) [13].

It has been observed several times that the number of heating periods in which the temperature is increased from an initial value to a final value is found to have little effect on the magnitude of LITS [13, 14, 16, 19] as is demonstrated in the results of figure 2-4 for instance. This relative insensitivity to the number of heating periods suggests that LITS can be expressed as a unique function of temperature, without path-dependence, which further simplifies application of LITS models.

2.1.2 *Rate of development of transient strain*

As the basic creep component of strain always appears concurrently with transient strain, it is very difficult to accurately identify the contribution of transient strain in the experimental measurements, particularly as the effects of high temperature on basic creep are fairly poorly understood at present. As a result, it is plausible that a proportion of transient strain develops in the period of time after a target temperature is reached but is not reported as such. In fact, the rate of development of transient strain is an area of interest that receives very little attention currently.

Most experimental investigations of LITS are performed with strain measurements made at set points in time during continuous heating. Depending on the size of the heated specimens, it may be of significant importance at which location within the specimens the temperature sensors are located. For even moderately sized specimens, the temperature values in the core and at the surface may be significantly different [40]. To counter this, researchers tend to apply either a low heating rate or to use a specimen of fairly small dimensions. Based on experimental work, it is found that the most appropriate position for a temperature sensor, in cylindrical specimens heated by a furnace, is at a position that is approximately 58% from the central axis of the specimen [41].

For similar reasons, Anderberg and Thelandersson [9] defined specimen temperature as the value recorded at a sensor located at a radial distance of 60% of the length of the radius from the central axis of the specimen. Typically, the LITS component derived from the experimental results by the authors is calculated assuming that LITS develops quasi-instantaneously. Thus, any time-dependence of the strain of the specimens are considered to be due to basic creep only.

Thus, the time-dependence of LITS is difficult to determine from these types of experimental tests. However, there are some experimental investigations that suggest that LITS has a non-zero rate of development. For example, some researchers [31, 42] believe that investigations of basic creep at high temperatures, which should in theory exhibit no LITS (due to the lack of an applied load during the phase of temperature increase), invariably produce a total strain behaviour that contains a component of '*delayed LITS*'.

A demonstration of this is provided by the investigation of Dias et al. [43] in which the quantity of time after cessation of heating required for dimensional stability to be reached was measured for a range of temperatures using samples of cement paste. These results, shown in figure 2-5, suggest that a period of time of around two weeks is required for the samples to reach a stable deformation state.

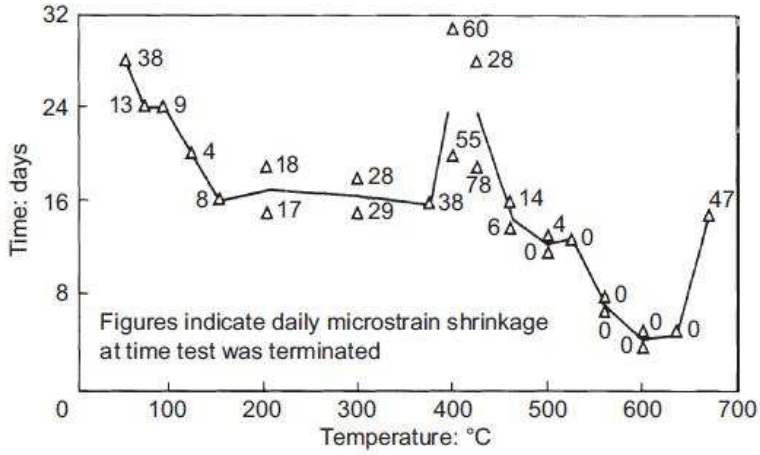

Figure 2-5: The period of time required following temperature equilibration for the daily dimensional change of a cement paste specimen to become relatively stable when heated at 1°C/min to elevated target temperatures [43].

The results of the authors, shown in figure 2-5, demonstrate that the time required for relative dimensional stability of the specimen is a non-linear function of temperature that appears to reflect the underlying processes at work within the cement paste, such as loss of evaporable water in the low temperature range and dehydration of C-S-H for temperatures close to $450℃$. Consistent with figure 2-5, it was found in an experimental investigation [20] that the period of time required for full development of LITS at $400℃$ is longer than the period of time required at temperatures below this point (and above $150℃$).

Similarly, in tests designed to investigate the high temperature behaviour of concrete [38], it is found that the deformation following heating to high temperatures is in advance of that expected on the basis of 'true' basic creep tests [44]. In particular, basic creep is found to peak in value at about $400-500℃$ [38]; this is considered to be delayed LITS on the basis that no such peak is observed in 'true' basic creep tests.

Based on an analysis of available experimental data, Khoury et al. [30] conclude that the rate of development of LITS decreases with specimen age. Experimental results suggest that specimens of age under 40 days fully develop LITS components within

roughly ten days of loading [10, 12, 14, 22], while the corresponding period of time for specimens of ages above six months at the time of loading is approximately one month [18, 45]. However, this finding may be of lesser importance in the temperature range above $100℃$, for which suitable experimental results are uncommon.

It is difficult to identify the parameters that affect LITS development rate as there are an insufficient number of investigations which allow this experimental observable to be reliably determined. Of these investigations [10, 13, 15, 18, 22, 46], it is consistently suggested that LITS fully develops in the temperature range below $100℃$ after a loading period of between a few days and a month. For higher temperatures, the period of time required for full LITS development appears to be typically less than one day [17, 20, 21, 46].

Hence, regarding the development time required for LITS, it appears that results suggest that the assumption of a quasi-instantaneous development of LITS may be of questionable accuracy. It appears that a period of time of up to 24 hours may be characteristic of LITS development time in concrete specimens heated to high temperatures, with a larger period of time required in the temperature range around $400℃$. However, a greater quantity of experimental evidence is required in order to draw firm conclusions. Currently, the assumption of quasi-instantaneous LITS development appears to be the most appropriate approach.

2.1.3 *Effects of cooling and re-heating on transient strain*

Results show that LITS is irreversible upon cooling and unloading, both for moderate temperatures [10, 13-16, 22, 30] and for high temperatures [17, 20, 21, 28, 32, 47-52]. It is likely that all of the components of LITS share the characteristic that cooling does not result in a recovery of the strain component but that only the transient strain component is fully irreversible upon unloading.

As can be seen in figure 2-6, an increase in temperature leads to a rapid development of mechanical strain, whereas a much slower increase in mechanical strain occurs at constant temperature. During cooling, there is a very small increase in mechanical strain, which is of a far lesser degree than that which develops during heating.

It is almost always found either that no increase in LITS is observed in cooling conditions or that any increase in LITS during cooling is of a very low magnitude [12, 14-16, 18, 20-22, 34, 38, 42, 47, 53]. There are no examples known to the present author which demonstrate that LITS-like behaviour is active during cooling of a magnitude equal to that observed during virgin heating.

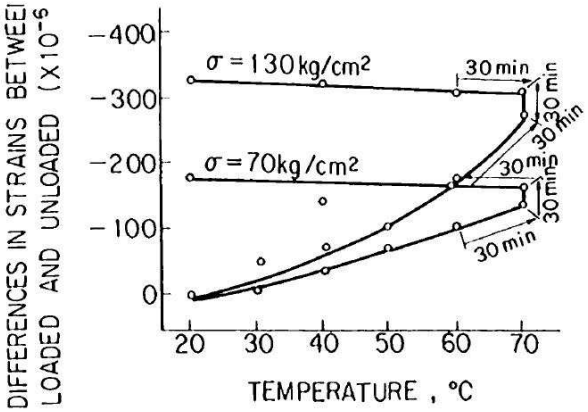

Figure 2-6: The total axial strain in excess of the strain recorded when heated under no load for two concrete cylindrical specimens loaded in uniaxial compression to different magnitudes [22].

While it is clear from figure 2-6 that decreasing temperatures do not lead to an increase in creep rate, the results of figure 2-7 are inconsistent with respect to this characteristic. In conditions of 100% relative humidity, temperature cycling leads to generally increasing creep behaviour, with a small increase in creep observed to coincide with some of the cooling periods. In contrast, no increase in creep due to cooling or re-heating is found in the specimens in conditions of 50% relative humidity. As the results of figure 2-7 are obtained in relatively moist conditions, it cannot be considered that moisture-dependence of LITS explains this behaviour.

The effects of unloading on mechanical strain are evident in figure 2-7. For each set of conditions, when load is removed, there is a relatively large immediate strain recovery, followed by a gradual slow continuing recovery, properly described as elastic strain and basic creep respectively. For each example, a residual strain component remains after unloading that demonstrates the irreversibility of transient strain due to unloading.

On the subject of LITS behaviour in conditions of second heating, there is some disagreement between experimental observations. Some studies suggest that the

magnitude of LITS does not increase during reheating [14, 16, 21, 22, 47], while others indicate that a development of LITS of a reduced magnitude may occur [12, 18].

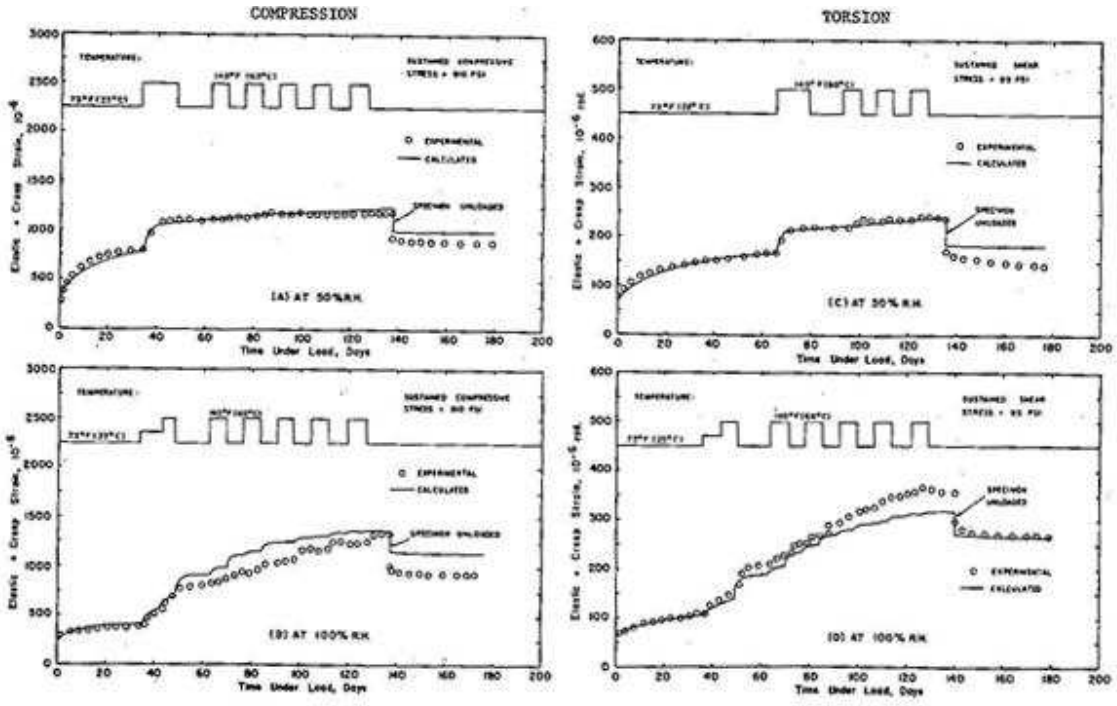

Figure 2-7: The sum of elastic strain and creep strain reported by Fahmi et al. [15] for specimens under uniaxial compression (left) or torsion (right), and in conditions of 50% relative humidity (top) or 100% relative humidity (bottom). Each specimen is subjected to a cyclic temperature history between a minimum of 23°C and a maximum of 60°C as denoted in the upper portion of each graph.

The results of Hansen and Eriksson [12] are quite revealing with regard to this issue. It is found that a small degree of LITS is observed if the second heating period immediately follows the initial heating cycle, whereas a more substantial degree of LITS is recorded if there is a significant period of time between first and second heating cycles. A similar investigation [18] has found similar behaviour to occur, despite differences in the specifics of the experiments (particularly with regard to the loading condition during the earliest heating cycle).

On the basis of observations such as these, it has been postulated that a regeneration of '*LITS potential*' may occur within a CM specimen if a sufficiently long period of time at ambient temperature is allowed before reheating takes place [18, 38]. Similarly, some researchers believe that the LITS potential may not be exhausted during a period at a particular peak temperature (due to a finite rate of LITS development) such that reheating to the same temperature results in further LITS associated with the remaining potential [30].

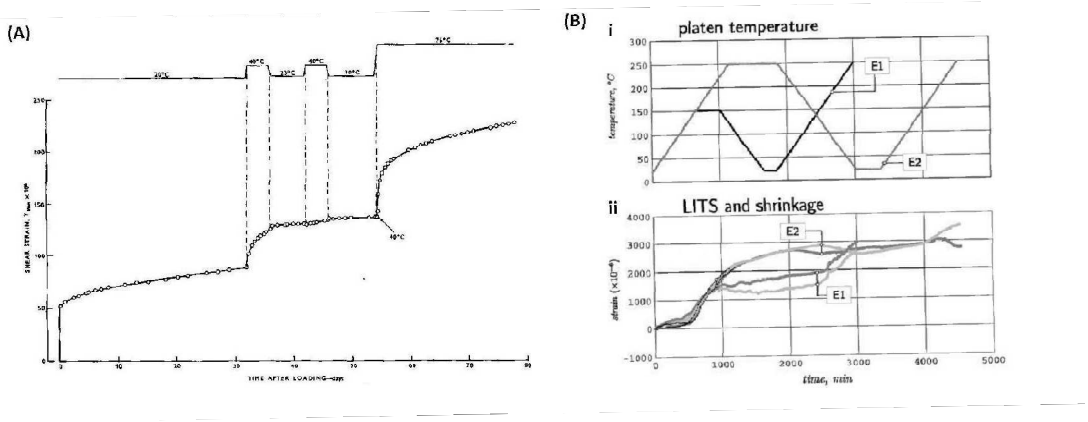

Figure 2-8: Results for (a) total shear strain of saturated mortar specimens in conditions of thermal cycling loaded in torsion [14] and (b) LITS and shrinkage induced by thermal cycling of concrete specimens (according to temperature histories, denoted E1 and E2) while under compressive load [19].

While LITS sometimes develops in conditions of reheating, if the temperature exceeds the peak temperature of the previous temperature cycle, LITS is consistently observed to develop [14, 19-22]. This behaviour is shown, for instance, in the results of figures 2-8 (a) and (b). In each sets of results, it can be seen that a large increase in strain occurs during any period in which virgin heating takes place. This observation is consistent with the observation that transient strain can be considered to be a function of temperature with no path dependence.

2.1.4 *Load-dependence of transient strain*

It is found that, for a wide range of values of compressive strength and applied loads, LITS is linearly related to the ratio of applied load to compressive strength [9, 16, 17, 21, 22, 28, 30, 31, 34]. Although slight deviations from linearity may develop at high load levels (e.g. 70% of the compressive strength [39]) and low load levels (e.g. 10% of the compressive strength [17]), the assumption of linearity in the whole loading range is considered to be unlikely to lead to significant errors. Moreover, if there is a lower bound for the level of applied load necessary to initiate LITS, it must be very low [20].

Most experimental investigations into LITS are performed in conditions of uniaxial compression. Although these investigations have allowed significant progress in the understanding of LITS, little insight is provided into the nature of LITS in states of tensile or multiaxial loading states. In fact, no LITS tests, known to the present author, have been performed in which concrete specimens are heated in a state of direct applied tension.

Experimental results on heated concrete specimens in conditions of biaxial compression [23, 36, 54] suggest that the temperature-dependence of LITS measured in a loading direction is very similar to that of an identically heated specimen in conditions of uniaxial compression. However, the expansive strain in the unloaded direction is found to be relatively large in comparison to the equivalent elastic expansion at room temperature (governed by a Poisson's ratio of about 0.2). An average value for a '*transient strain Poisson's ratio*' measured in the temperature range $20-250℃$ is found in different investigations to be in the range $0.34-0.46$ [19, 54]. Moreover, some work suggests that transient strain should properly be considered to be anisotropic [19]. Thus, although LITS tests performed using torsional loading, for instance, exist, it is not currently feasible to use these data sets to indirectly study the LITS response of concrete to states of tension.

As a result, the LITS response of concrete to states of tension is an area of interest about which very little is known and which receives very little attention. Typically, this has not been considered an issue as states of tension in practical applications of concrete are avoided in the design phase wherever possible due to the relatively low tensile strength of the material. However, it means that assumptions must be made for LITS modelling in multiaxial analyses that may be of critical importance in some sets of conditions. Also, the LITS behaviour of concrete in conditions of tensile loading may allow the underlying physical mechanisms to be better understood.

Qualitatively, the axial LITS observed to occur in conditions of uniaxial compression is found to be similar to that observed in torsion when in roughly equivalent loading conditions at temperatures less than about $60℃$ [15]. However, quantitatively, it is observed that the ratio of the total mechanical strain to the initial elastic strain in conditions of applied torsion and heating is higher than that observed in roughly equivalent conditions of uniaxial compression [15]. These results are consistent with other observations [17, 29], for torsional and flexural loading states. These observations may reflect the weakness of concrete in states of tension, imposed by the external loading states. Increased temperature may lead to states of significant tension on the mesoscale due to thermal mismatch, which results in significant microcracking. Consequently, mechanical strain may be enhanced in these loading conditions, when

compared to states of pure compression, due to the more rapid drying, increased material softness, and enhanced local mesoscale stresses.

Although the present author has reservations regarding the experimental procedure applied by Thienel and Rostásy [36] due to the use of the octahedral axial system and consequent dependence on the value of Poisson's ratio for interpretation of results, the results are revealing with respect to the multiaxial nature of LITS. As shown in figures 2-9 (a) and (b) respectively, results show that the deviatoric LITS component is linearly related to the deviatoric stress component, whereas a nonlinear relationship exists between the volumetric LITS component and the volumetric stress measure, which reaches an approximate maximum value at about 30% of the initial compressive strength. The authors suggest that volumetric LITS remains fairly constant thereafter, though results are not provided to confirm this observation.

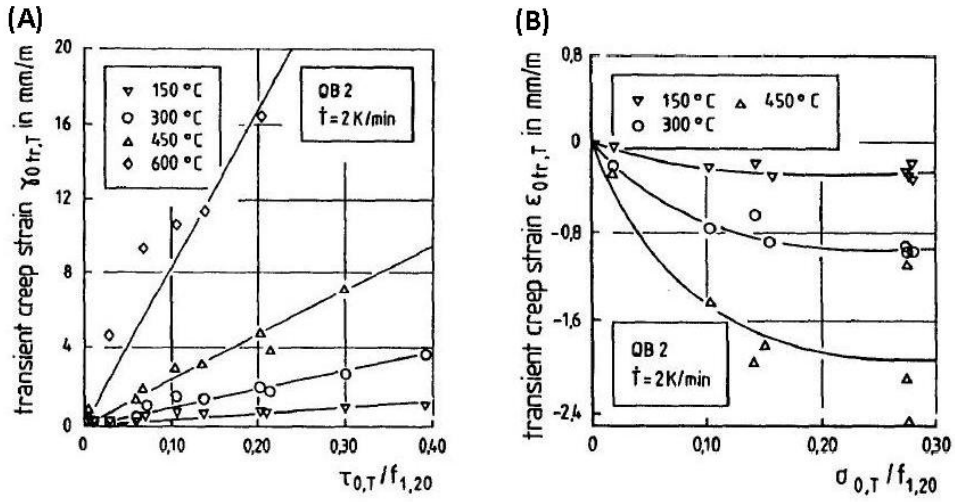

Figure 2-9: Results showing, for a range of elevated temperatures, (a) the octahedral deviatoric LITS against the ratio of the octahedral deviatoric stress to the initial compressive strength, and (b) the octahedral volumetric LITS against the ratio of the octahedral volumetric stress to the initial compressive strength [36].

The results of figures 2-9 (a) and (b) may be interpreted as showing that the role of volumetric stresses is largely to prevent or reduce the formation of microcracks. The degree of microcracking is expected to increase with temperature. Therefore, the threshold volumetric stress, required to prevent the microcracking process, also must increase with temperature. Applied volumetric stress in excess of this threshold, results in a very small quantity of additional LITS. The original authors consider the explanation to be supported by results obtained by means of acoustic emission analysis [55]. However, due to the use of the octahedral axial system and consequent high dependence on the value of transient strain Poisson's ratio for interpretation of

results, the conclusions of this work should be considered tentative until confirmed by more reliable analyses.

2.2 Physical origins of transient strain

Despite significant research efforts in the last $40 - 50$ years, due to the complex underlying physicochemical nature of cement gel, there is currently no universally accepted theory for the sub-macroscopic mechanism that leads to the development of transient strain. Any such theory must explain the observed characteristics of transient strain behaviour on the macroscale, which are broadly,

- that the magnitude of LITS observed is reduced by the presence of aggregate inclusions,
- that, for temperatures below $450℃$, LITS is observed to obey a master curve,
- that all observations show that LITS is irrecoverable both on unloading and on cooling,
- that many investigations suggest that LITS develops only during virgin heating,
- that some investigations indicate that some LITS can develop in conditions of non-virgin heating,
- that almost all observations demonstrate that LITS does not develop in conditions of decreasing temperature,
- that the load-dependence of LITS is roughly linear and normalised by the initial compressive strength, and
- that LITS develops in specimens that do not undergo drying during the heating period.

It is important that the physical origin of transient strain can be identified such that the experimental observations can be explained more readily and that more robust predictions can be made. There are several different proposed physical origins for TTC in the literature that shall be discussed in the following, including the basic creep mechanism (§2.2.1), the dehydration process (§2.2.2), stress concentration due to pore evacuation (§2.2.3), and nonlinear strains due to local stresses on the mesoscale (§2.2.4).

2.2.1 *Basic creep as the origin of transient strain*

The physical mechanism that causes basic creep, the time-dependent deformation that develops when concrete is placed under a sustained load for a period of time, has been theorised to be the same as that which causes transient strain [56]. In this model, basic creep is composed of two distinct components, viscoelastic creep and viscous flow. A parameter representing particular microscale hygro-thermo-mechanical effects (such as hindered adsorption), named the '*microprestress*', is key in defining the material viscosity and, thus, the viscous flow rate due to an applied load. The effects of temperature (and relative humidity) change on the microscale processes that define this parameter are theorised to lead to transient strain on the macroscale.

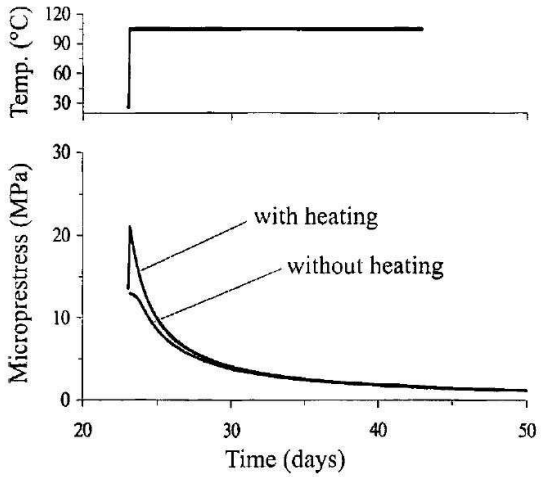

Figure 2-10: A comparison of the microprestress evolution due to the imposed temperature history shown at the top of the figure and that due to no change in temperature [56].

When a concrete specimen is heated, the microprestress term is considered to increase in magnitude, whereas the magnitude of the parameter decays continuously when temperature remains at a constant value. An illustration of this type of behaviour is shown in figure 2-10. It can be seen that the microprestress term associated with the heated specimen is of a magnitude greater than that of the unheated specimen for a period of approximately seven days. During this period of time, if an identical preload is applied to both specimens, a greater magnitude of irreversible viscous flow creep would be expected for the heated specimen. According to this theory, the resultant strain difference would be identified as LITS.

The basic creep mechanism as an origin of transient strain in the manner described here is consistent with several of the experimental observations. A model formulated in this way must be consistent with the observation that the role of aggregate in

transient strain in concrete is one of restraint. Aggregates are also known simply to restrain the magnitude of basic creep that develops in loaded concrete specimens [19, 30, 36, 43, 57-61] (it has been shown that, even accounting for the stress transfer mechanism that occurs due to creep of the cement paste [62], the stresses that are placed on the aggregates during sustained periods of loading are insufficient to cause inelastic stresses in most materials used as aggregate [57]).

Moreover, as transient strain is described as a component of viscous flow creep, the requirement that the proposed physical origin results in irrecoverable strain on unloading is automatically satisfied. It also seems reasonable to assume that cooling will not cause any recovery of the additional viscous flow (transient strain) that develops during the heating phase. In fact, inspection of the mathematical model associated with this theory confirms that this is the case.

Consistently, transient strain is found to develop in virgin heating conditions. Several sets of experiments have been performed that suggest that transient strain does not develop during second heating until the peak temperature of the previous heat cycle is exceeded (at which point, transient strain is found to spontaneously develop once again). This theory for the origin of transient strain appears to be unable to explain these observations.

Similarly, the observation that LITS obeys a master curve suggests that a similar master curve should exist for the flow creep formulation of concrete if this theory is valid. To the best of the current author's knowledge, no research has been conducted into this possibility.

It is unclear if this model for transient strain is valid in temperature ranges above $100℃$ due to potential conceptual difficulties caused by loss of evaporable water, which is considered to be the main agent by which microprestress is imposed on the concrete solid microstructure. In fact, the original authors do not apply the mathematical model for temperatures higher than $100℃$. Clearly, such a restriction on this model weakens considerably the credibility of the hypothesis that basic creep is the origin of transient strain.

2.2.2 *Dehydration process as the origin of transient strain*

The molecular and microstructural phase changes that take place within heated cement paste are theorised to be the cause of TTC by several authors [20, 30, 63-65], with the dehydration of C-S-H specifically identified by some as the principal cause of TTC in the temperature range between about $105℃$ and $400℃$ [20, 64]. Also identified as phase changes likely to contribute to the development of this strain component are CH dehydration [30] and silicate polymerisation [65].

While no specific physical mechanism appears to have been proposed, Sabeur and Meftah [64] formulate a mathematical model based on the hypothesis that physical transformations that occur under sustained stress fields result in the evolution of a rearranged cement microstructure when compared to equivalent physical transformations in conditions of zero applied stress. The difference in the two microstructures is observed to be a difference in total strain on the macroscale. Thus, based on this hypothesis, the dehydration process induced by heating should lead to an additional strain component. The authors [46, 64] postulate that this strain component may entirely account for TTC.

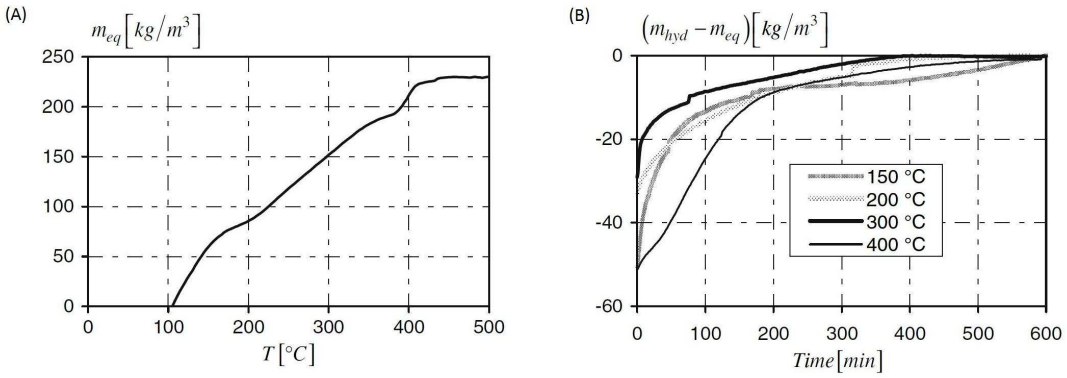

Figure 2-11: (a) The development of the equilibrium value of the mass of dehydrated material with temperature increase and (b) the dehydrated mass of material with time at four elevated temperatures [64].

In this model, it is necessary that transient strain is decomposed into drying creep and '*dehydration creep*'. Dehydration is widely known to occur in temperature ranges exceeding $100℃$. Thus, in order to account for the existence of transient strain in the temperature range below this temperature, a drying creep model must be applied. The model chosen by the authors [46, 64] is that of Bažant et al. [66], known as the '*stress-induced shrinkage*' model in which the drying creep is considered to be given as drying shrinkage modified by a linearly stress-dependent multiplicative factor.

The dehydration process, measured using the change in mass of ground samples of heated cement paste, tends to develop asymptotically towards a temperature-dependent limiting value. Thus, it is necessary to experimentally determine the relationship between the limiting value of dehydration and temperature, $m_{eq}(T)$, as well as to establish a reliable model for the development of dehydration with time, $m_{hyd}(t)$. Figures 2-11 (a) and (b) show the results of the experimental investigation carried out to determine $m_{eq}(T)$ and $m_{hyd}(t)$ respectively [46, 64].

It can be seen from figure 2-11 (a) that m_{eq} is a monotonically increasing function of temperature, consistent with experimental observations. However, in the temperature range of $400 - 500℃$, m_{eq} appears to reach a plateau in contrast to experimental observations that suggest that transient strain tends to increase in magnitude rapidly in this temperature range. The authors do not address this potential issue with the model as experimental results are simulated only in temperature ranges less than $400℃$. However, it may be noted that many tests of heated concrete specimens are performed with a constant heating rate (i.e. without measurements made during temperature plateaus). Therefore, an advanced development of transient strain at temperatures close to $450℃$ may, in some instances, be explained by the rapid development of m_{hyd} despite no similar increase in the value of m_{eq}.

The results of figure 2-11 (b) indicate that m_{hyd} develops in a highly similar manner for each of the temperature plateaus. 10 hours is found to be a sufficient quantity of time for dehydration to be approximately complete at each temperature range. An exponential model is applied by the authors [46, 64] to describe the evolution of m_{hyd}. As a result, this model shall produce predictions for transient strains that fully develop only approximately 10 hours following the start of heating. Thus, heating rate shall be important to model output.

There are several experimental justifications for use of a model such as this. The dehydration process is widely considered to be irreversible on cooling, which is consistent with experimental observations that transient strain does not develop or recover in cooling conditions [67]. Also, this hypothesis therefore provides a physical justification for the consistently observed condition that virgin heating always causes transient strain to develop.

Moreover, as the dehydration process has a finite rate of development, this hypothesis allows observations that transient strain may, in some instances, develop in conditions of non-virgin heating if the period of time spent at the peak temperature is insufficient to allow the development of the equilibrium transient strain magnitude associated with that temperature. Also, it may be speculated that, if a significant quantity of time is spent at temperatures below $100℃$ after a heat cycle (particularly in moist conditions), a degree of rehydration may occur. Subsequent heating may lead to a degree of second dehydration for temperatures below the peak temperature of the first temperature cycle. Thus, transient strain may be possible in this temperature range.

Moreover, as dehydration is clearly a physical process that occurs in the cement paste phase of concrete and not the aggregates, the role of the aggregates in a model based on this hypothesis must be principally one of restraint. As with the basic creep origin hypothesis, this is consistent with experimental observations.

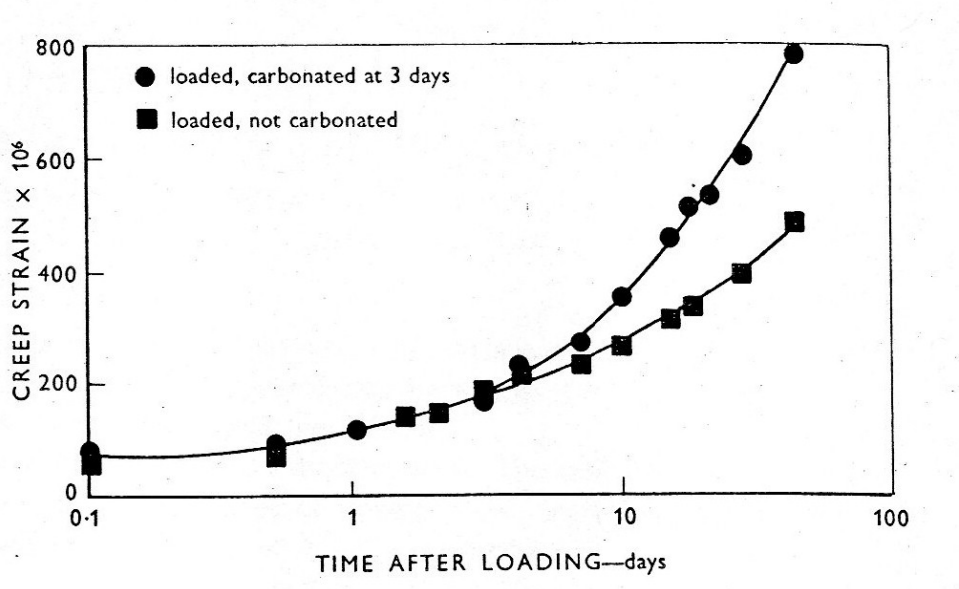

Figure 2-12: Comparison of the creep observed on concrete specimens, where one specimen undergoes carbonation after three days of loading [68].

Although no consensus presently exists regarding which physical origin for transient strain is best supported by experimental results, there is a strong indication that disruption of the microstructure of cement paste results in increased inelastic strain compliance. It has been shown that the creep rate of a cement paste slab specimen increases by a considerable degree (more than 50%) when conditions that promote carbonation are applied to concrete specimens while under load, despite the

decreased creep rate of carbonated specimens [68]. This behaviour, which is shown in figure 2-12, is similar to that of transient strain. Thus, these results may be considered to support a general hypothesis that any physical or chemical transformation that occurs in concrete while under a sustained load leads to an increase in local creep compliance (and therefore, when averaged over a whole specimen, an increase in global creep compliance), apparently due to molecular rearrangements [65].

Thus, it is possible to speculate further that other physical transformations occur during heating may lead to transient strain. For example, concrete is known to undergo a process known as silicate polymerisation over long periods of time [69-73]. High temperatures increase the rate at which this process occurs [69, 72, 74-76]. Thus, these physical transformations that occur during heating may also result in transient strain-like effects.

2.2.3 *Stress concentration due to pore evacuation*

A novel physical origin of transient strain was suggested by Brooks [77]. Stress distribution within solid materials is significantly affected due to the presence of rigid inclusions and cavities, as shown in figures 2-13 (a) and (b) respectively. In fact, it can be shown that the average stress within the solid matrix (surrounding the inclusions and/or cavities) is lowered by the presence of rigid inclusions and elevated by the presence of cavities.

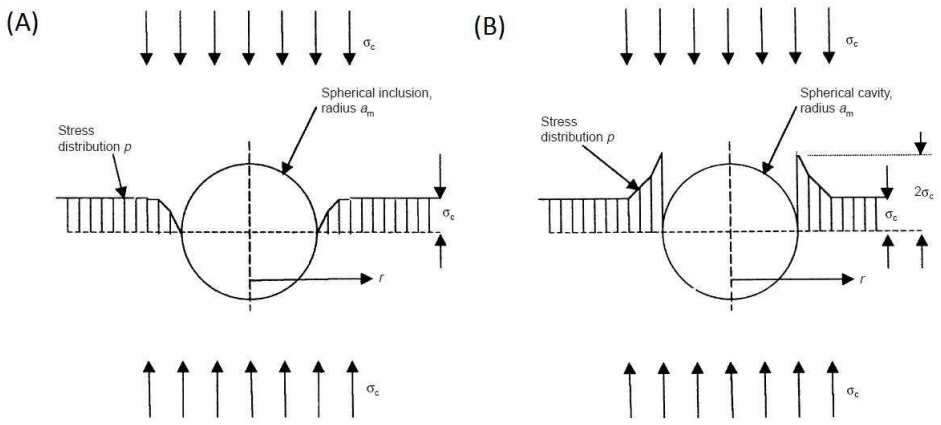

Figure 2-13: The stress distribution of a material under axial compressive load in the region surrounding (a) a rigid spherical inclusion and (b) a spherical cavity [77].

According to this theory, in the cement paste, a filled pore can be considered to play a similar role to a rigid inclusion in defining the stress distribution in concrete, with

empty pores playing a similar role to cavities. Thus, if a pore that is initially filled with water loses the water while under a constant externally applied load, according to this theory, the average stress within the cement matrix increases by a fairly significant degree. As a result of this, an increased degree of creep would be observed to develop.

Though this physical mechanism was principally intended to provide an explanation of drying creep, the author considers it to provide a satisfactory model for TTC also. It is argued that heating leads to a reduction in the degree of water saturation within the cement paste and, thus, leads to similar effects. However, this argument conflicts with experimental observations that suggest that TTC develops in non-drying conditions. It is unclear if this physical model may be made consistent with these observations.

Moreover, the model faces problems in explaining the reason that, if considered to be of a basic creep nature, TTC and drying creep are only considered to be temporary increases in creep compliance. According to this model, the stress enlargement caused by evacuation of pores is apparently a permanent change. However, the author [77] counters this objection with the suggestion that the creep potential of the material decays in time such that subsequent loading (a significant period of time after the end of heating and drying) would not result in increased creep. However, there appears to be apparent cause of this mechanism, which is vital for this physical model to correctly describe experimental observations and, therefore, must be considered a significant weakness of this model.

2.2.4 *Local mesoscale stresses due to thermal mismatch*

It has been suggested that the transient strain of concrete can be explained using an explicit mesomechanical model [78]. The combination of the externally applied loads and the mesoscale stresses that develop within concrete during heating due to thermal mismatch of the components is postulated as leading to significant nonlinear strains that are observed on the macroscale as TTC.

Consistent with other researchers, concrete is assumed to be a three phase model on the mesoscale, with aggregate inclusions surrounded by a layer of ITZ and embedded in a matrix of cement paste [79-83]. Using a sophisticated two-dimensional three phase model for concrete applied on the mesoscale, the authors [78] demonstrate that the effects of simultaneous loading and heating can lead to total strain behaviour that

appears to be very similar to those of experimental observations, as shown in figure 2-14. It is a significant strength of this approach that no phenomenological models are assumed for concrete behaviour (though phenomenological models are necessary to describe the behaviour of the three components of concrete).

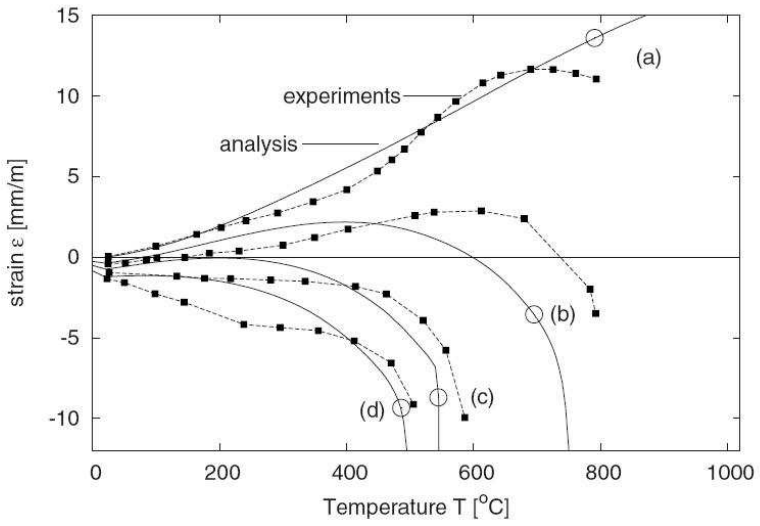

Figure 2-14: Comparison of the total strain output of the model of Grassl and Pearce [78] in comparison to experimental data sets obtained using concrete cylinders heated while unloaded and while under three different load levels (22.5%, 45%, and 67.5%) [33].

Although this model has been shown to be capable of performing fairly well in comparison to experimental data, this type of model disagrees with experimental observations that suggest that the role of the aggregate phase of concrete in transient strain is one of restraint only (at least in the range of temperatures in which aggregates are chemically stable). An increased aggregate content is found to cause a decreased transient strain (all else being equal). In the framework of the approach used for this model, there must be a mid-range aggregate content at which the transient strain development is at a maximum. According to experimental observations, this value is zero [17, 39]. Therefore, this model cannot be consistent with experimental observations of transient strain behaviour.

An explicit mechanistic approach to transient strain modelling may be valid on the microscale, with thermal mismatch of cement gel phases responsible for the development of transient strain. However, while a microscale mechanistic transient strain model of this type would be of questionable validity due to the considerable number of assumptions necessary in terms of the morphology, distribution, mutual interactions, relative quantities, thermal properties and stress-strain behaviour of each

of the phases, as well as the necessary multiscale translation, no example of such a model exists of which the present author is aware.

2.2.5 *Final remarks*

Four potential physical origins for transient strain have been discussed here. Although not previously mentioned, some researchers have considered internal moisture migration between gel pores and capillary pores to be the principal cause of TTC [12, 84]. This possibility has been rejected, primarily due to the difference between the rate of development of TTC and the moisture migration rates at different temperatures [30]. However, this mechanism is thought to play an important role in the development of isothermal drying creep [19, 66]. Thus, internal moisture migration may play a significant role in the development of LITS due to the drying creep component of transient strain.

Each of the physical origins discussed in this chapter are plausible as causing potentially transient strain-like effects. Thus, it is possible that more than one of these physical mechanisms are active in heated concrete and, therefore, that any mathematical model based on just one of these physical origins is necessarily incomplete. This represents a serious complication for this research area as it is extremely difficult to calibrate transient strain models by any other means than retrofitting to experimental data. Thus, if two mathematical models must be simultaneously calibrated, the task is far more complex.

2.3 Mathematical models of transient strain

Although there are several theories regarding the physical origin of transient strain and corresponding proposed mathematical models, most models for transient strain (or LITS) are of a phenomenological nature. This is reasonable due to the existence of a LITS master curve, though a model based on a hypothesis for the physical processes in cement paste responsible for transient strain is very desirable, particularly for predictions of ‘non-standard’ behaviour, such as the development of transient strain in non-virgin heating conditions.

The mathematical models are typically very similar in form, generally consisting of a function of temperature and a function of applied load, the product of which is the

axial component of transient strain at any given temperature. As transient strain increases in magnitude only when temperature increases, it is usual for the models to be written in incremental form, though this is not reproduced here.

Five of the most widely used and plausible models are briefly discussed in turn in this section. The main mathematical formulae for each model are presented and discussed, followed by a review of the results of simulations using the models as presented by researchers in the literature.

2.3.1 *Anderberg and Thelandersson*

The model proposed by Anderberg and Thelandersson [9, 33] is given, for the case of applied uniaxial compression, by the following.

$$\dot{\varepsilon}_{tr} = \beta_A \frac{\partial \varepsilon_{th}}{\partial T} \frac{\sigma}{f_c(T_0)} \dot{T} \qquad \text{Equation 2-2}$$

where β_A is the coupling coefficient for this model and ε_{th} is thermal strain.

The transient strain component, originally referred to by the authors as the *thermomechanical interaction*, is assumed to develop in direct proportion to ε_{th} in heated conditions, with an applied scaling factor given by the product of β_A and the ratio of σ to f_c. A value of β_A found to be accurate for an experimental data set is 2.35 [9, 33], which suggests that a constant value of σ equal to approximately $0.43 f_c$ throughout heating should lead to the evolution of transient strain that is identical to that of thermal strain in magnitude in the axial direction. This is approximately consistent with experimental results.

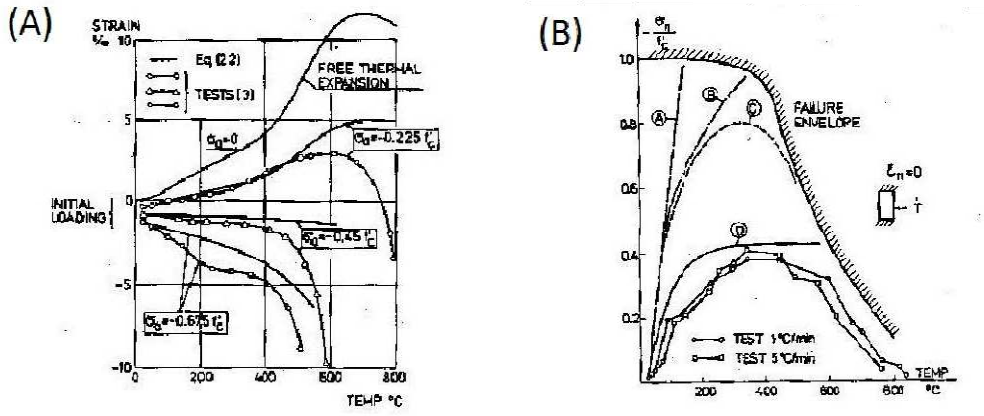

Figure 2-15: Comparison of model output with transient strain experimental data found for heated specimens (a) preloaded at three different load levels and (b) restrained and heated at two different rates [33].

Application of the model to realistic heating conditions is found to produce results of varying quality, such as those of figures 2-15 (a) and (b). The results of figure 2-15 (a) suggest that model output quantitatively matches the experimental data most closely for the specimen placed under the applied load level of lowest magnitude, with a lesser quantitative match for the specimen under the highest magnitude of applied load. Significant deviations are consistently found in the results for high temperature ranges ($T > 400$℃). These results suggest that an increasing degree of compressive strain develops in this temperature range that the model does not reproduce.

Similarly, the results of figure 2-15 (b) suggest that the model output (denoted '*D*' in the figure) underestimates the degree of stress relaxation in the high temperature range. While significant improvement is obtained by use of a transient strain model (cf. curve D with curves A–C, each of which is produced using no transient strain model), qualitative agreement with the experimental results is present only in the temperature range below approximately 400℃.

Moreover, the thermal strain behaviour of concretes that contain significant quantities of quartz exhibits a characteristic change in behaviour at temperatures of around 573℃ due to α-β phase inversion. In contrast, a corresponding change in behaviour of transient strain is not observed in the experimental results [17], which suggests that the evolutions of transient strain and thermal strain in high temperature conditions may be distinct.

Due to poor model performance in the low temperature range, this model may be applied with a modification to the governing equation whereby, for temperatures higher than 550℃, the following relationship is valid [63, 85].

$$\dot{\varepsilon}_{tr} = \mathrm{B}_A \frac{\sigma}{f_c(T_0)} \dot{T}\,, \qquad T > 550℃ \qquad \text{Equation 2-3}$$

where B_A is the coupling coefficient for the model in the high temperature range.

No experimental results are known to the present author that suggest that concretes that exhibit a stronger thermal strain behaviour also undergo a greater magnitude of transient strain. In fact, some experimental results have suggested that an inverse relationship is valid [21], though recent analysis suggests that it may not be

appropriate to draw strong conclusions from these results. However, similar criticisms of this model have been expressed by other researchers [86].

2.3.2 *Gawin et al.*

The model proposed by Gawin et al. [87] is given, for the case of uniaxial compression, by the following.

$$\dot{\varepsilon}_{tr} = \beta_G \frac{d\chi}{dT} \frac{\sigma}{f_c(T_0)} \dot{T} \qquad \text{Equation 2-4}$$

where β_G is the coupling coefficient for this model and χ is the thermo-chemical damage parameter, defined as the relative difference in material stiffness between heated and unheated specimens (unloaded during heating). It should be noted that, although not suggested in Equation 2-4, the model is formulated in a manner that the stress term applied by the authors is the *Bishop's effective stress parameter*, which accounts for the apparent magnifying effects of damage and hygro-mechanical phenomena on the local stress term applied to the solid material of concrete.

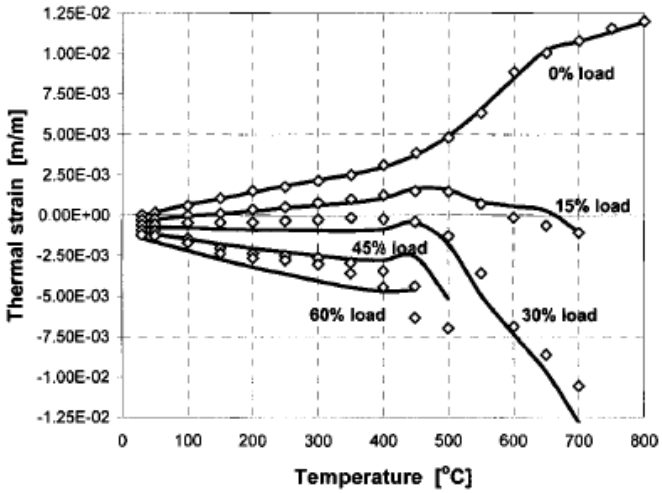

Figure 2-16: Comparison of total strain results produced using the model of Gawin et al. [87] and experimental data.

As can be deduced from Equation 2-4, this model assumes that the temperature-dependence of the degradation in elastic stiffness due to heating and that of ε_{tr} are identical (ignoring the effects of heating on the effective stress). No physical mechanism is proposed for this link. However, if the model is found to be highly accurate, it may be speculated that the physical mechanisms that lead to the reduction in elastic modulus are also those that lead to transient strain. These mechanisms are

largely related to the dehydration process. Thus, this model may have a link to the hypothesis for the physical origins of transient strain discussed in §2.2.2.

As shown in figure 2-16, the transient strain model proposed by Gawin et al. [87] can be used to reproduce total strain behaviour of concrete specimens in conditions of heating and loading fairly accurately. The accuracy of the model appears to be highest for simulations of tests performed at lower load levels, with larger deviations appearing to develop for load levels of 45% and 60% than for 15% and 30%.

The results of figure 2-16 were obtained using a piecewise form of Equation 2-4 in which the value of β_G changes discontinuously at a *critical value* of V (approximately 0.55, which corresponds with a temperature of $450-500℃$). The justification for use of this bilinear model is illustrated in figure 2-17 (b) in which the normalised transient strain measure is plotted against derived values of χ.

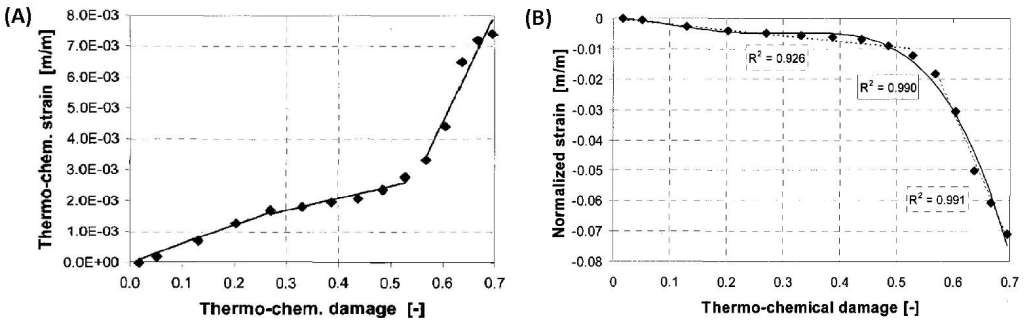

Figure 2-17: Relationships between the calculated values of (a) thermo-chemical strain, and (b) normalised transient strain and the thermo-chemical damage parameter [87].

The authors consider this behaviour to be consistent with results for the thermo-chemical strain component [87] (i.e. strain that develops due to thermally-induced chemical transformations) in which a discontinuous change in behaviour occurs at an identical value of χ, as shown in figure 2-17 (a). This behaviour is suggested to be caused by an advanced thermo-chemical decomposition of the cement matrix, specifically C-S-H and CH, and the beginning of decomposition of the calcareous aggregate, which is an important process in the accelerated development of microcracks. This observation indicates that transient strain and thermo-chemical strain may share a common origin, i.e. dehydration and material microcracking.

It is generally advantageous to use of this model that the conditions in which transient strain is found to develop and those in which χ is found to increase in value (i.e.

conditions of virgin heating) may be considered to be identical. Moreover, processes such as '*healing*' in which a degree of material stiffness may be recovered in the period of time following a heat cycle [2] may potentially allow an explanation for observations of the development of transient strain in non-virgin heating conditions to be made in the future. Significant research is required in this area.

2.3.3 *Terro*

The model proposed by Terro [39, 88] is given by the following.

$$\varepsilon_{LITS} = 3.05V_a\left(0.032 + 3.3226\frac{\sigma}{f_c(T_0)}\right)\sum_{n=0}^{N} a_n T^n \qquad \text{Equation 2-5}$$

where V_a is the aggregate content, a_n are the polynomial coefficients, and N is the maximum order of the equation (taken to be four, unless the aggregate material is Thames river gravel, in which case it is taken to be five).

The model, intended for LITS rather than transient strain, is explicitly intended to reproduce the temperature-dependence of the LITS master curve [17]. In order to account for the effects of aggregate content on this curve, a scaling factor dependent on the aggregate content parameter is included in the model, as shown in Equation 2-5.

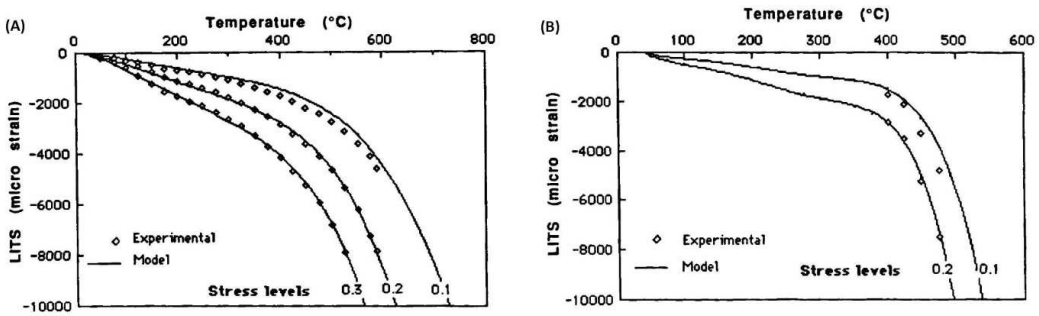

Figure 2-18: Comparison of the polynomial approximation and experimental data for (a) basalt, limestone, lightweight, and gravel (T<400°C) aggregate concretes, and (b) gravel aggregate concretes (T>400°C) [88].

This model has been criticised [86] because, according to Equation 2-5, the magnitude of LITS calculated to develop in heated conditions under no applied load is non-zero, a prediction that cannot be accurate when compared to experimentally determined LITS data. However, it should be noted that the experimental results on which this model is based [17] suggest that the relationship between LITS and applied load level appears statistically to be a decreasing function (rather than linear) for the loading range below

approximately 10% of the compressive strength. Therefore, it is unsurprising that a model calibrated to result sets obtained in load ranges above this value (like this model) predicts a non-zero value of LITS in unloaded conditions. When adopting this model however, this poor model behaviour should be addressed.

The performance of the model is shown in figures 2-18 (a) and (b), calibrated to "normal" aggregate types (i.e. limestone, basalt, and lightweight) and gravel aggregates (from the Thames River) respectively for three levels of applied load. It can be seen that the model is capable of reproducing target data sets accurately.

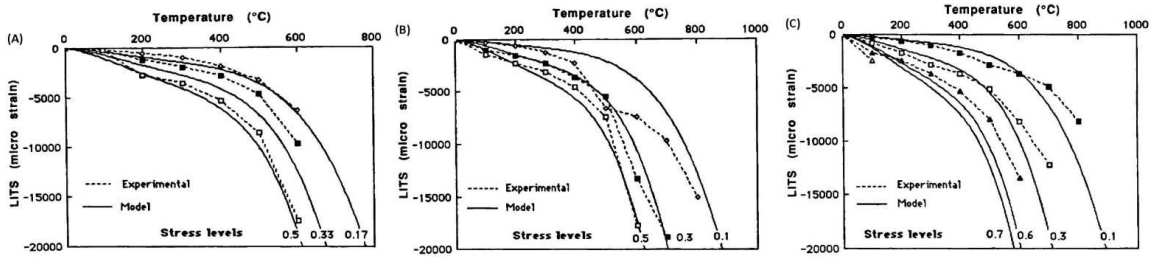

Figure 2-19: Comparisons of LITS model predictions and that deduced from experimental data for concrete of (a) 68% quartzite aggregate content, (b) 70% siliceous aggregate content, and (c) 71.5% quartzite aggregate content [88].

When applied to different experimental data sets, as shown in figures 2-19 (a)–(c), results suggest that the model predicts LITS curves that match experimental results to a varying degree of accuracy. The most accurate overall model predictions are obtained for the concrete with an aggregate content of 68% (figure 2-19 (a)) which is also the concrete most similar to that used in model calibration in terms of aggregate content, though the variation in this parameter is small between all concretes tested. The model results shown in figure 2-19 (b) are also close to the experimental results, for those obtained using the two highest load levels. The remaining result, obtained on a specimen under a load of 10% of the compressive strength, is fairly poor. This contrasts sharply with the results obtained for the results of application of the previously discussed models.

2.3.4 *Nielsen et al.*

The model proposed by Nielsen et al. [89], which is bi-parabolic in temperature-dependence, is defined the following governing equation.

$$\varepsilon_{tr} = \begin{cases} \frac{\sigma}{f_c}\left(A\theta^2 + B\theta\right), & T \leq 470℃ \\ \frac{\sigma}{f_c}\left[C(\theta - \theta_{tr})^2 + A\theta_{tr}(2\theta - \theta_{tr}) + B(\theta - \theta_{tr})\right], & T > 470℃ \end{cases}$$ Equation 2-6

where A, B, and C are free parameters of the model, θ_{tr} is the transition temperature ($470℃$), defined using a reduced temperature scale, given by the following.

$$\theta = \frac{T - T_0}{100°C}$$ Equation 2-7

Use of the reduced temperature scale allows the values of the model parameters to be of a similar magnitude, which is generally good practice for computational modelling.

It can be seen from Equation 2-6 that the model is developed such that continuity of the first derivative of ε_{tr} with respect to temperature is guaranteed for any values of the free parameters. The inclusion of this constraint must be considered an explicit model assumption as no experimental investigations of which the present author is aware have shown that this continuity is necessary over the entire temperature range, though equally no experimental observations have suggested that this continuity is broken. Nonetheless, the assumption of continuity allows the model to contain one fewer free parameter than is otherwise necessary, which is advantageous for simplicity of the model.

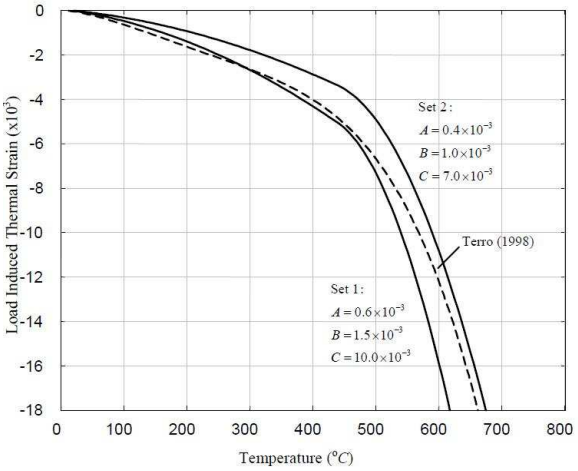

Figure 2-20: Comparison of the predictions of a fourth-order polynomial transient strain model [39] and those of this model with two different sets of parameter values [90].

With appropriate choice of the values of free parameters, the transient strain output of this model has been shown to be qualitatively good in comparison to the LITS master curve, as represented by the strain produced by the model of Terro [39], shown

in figure 2-20. Two different curves produced by this model can be defined that represent approximate 'upper' and 'lower' bounds for the master curve.

When the model performance is compared with experimental data sets, as shown in figures 2-21 (a) and (b), it can be seen that a fairly good match with experimental observations can be obtained. In contrast with results obtained using the models of Anderberg and of Gawin et al., model results appear to more closely match experimental data for larger levels of applied load. The results for the lowest applied load level suggest that the transient strain development is significantly underestimated in the high temperature range.

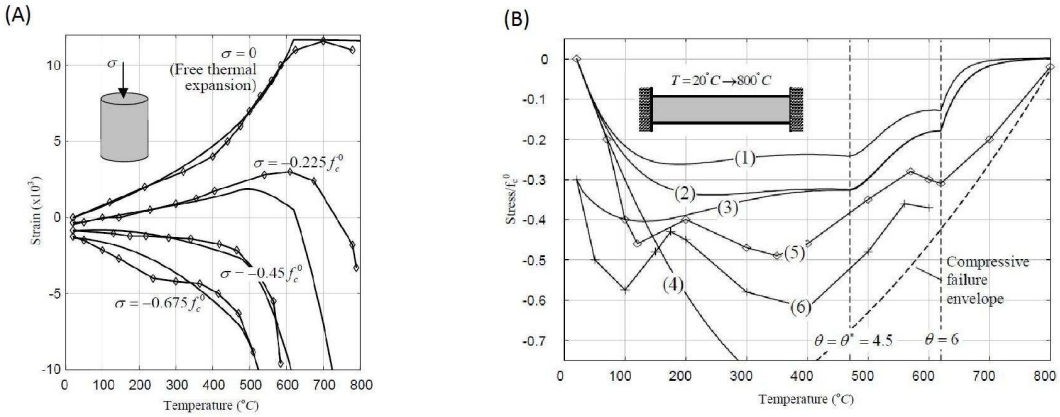

Figure 2-21: Comparison of the model predictions and experimental data (a) for preloaded heated concrete specimens [33] and (b) for stress development in axially restrained heated concrete specimens, where the nature of each of the curves is explained in the text.

The results of simulation of axially restrained heated concrete specimens demonstrate that the model broadly reproduces qualitatively the experimental data, as shown in figure 2-21 (b). Quantitatively, the results deviate significantly from the experimental data sets and suggest that the model overestimates the magnitude of stress relaxation provided by transient strain in these conditions.

2.3.5 Schneider

The principal temperature-dependence of the model proposed by Schneider [34] is given by the '*transient strain function*', ϕ, which is defined as follows.

$$\phi(T, w) = C_1 \tanh[\gamma_w (T - T_0)] + C_2 \tanh\left[\gamma_0 \left(T - T_g\right)\right] + C_3 \qquad \text{Equation 2-8}$$

where C_1, C_2, γ_0, and T_g are free parameters of the model, γ_w is a moisture-dependent parameter, and C_3 is a constant that ensures that ϕ is zero when T is equal to T_0.

In this model, transient strain is calculated using the following equation.

$$\varepsilon_{tr} = \left(g\phi + \frac{\sigma}{f_c}\theta \right) \frac{\sigma}{E(T,\sigma)} \qquad \text{Equation 2-9}$$

where E is the temperature- and preload-dependent elastic modulus and g is defined as follows.

$$g = \begin{cases} 1 + \frac{\sigma}{f_c}\theta, & \sigma \leq 0.3 f_c \\ 1 + 0.3\theta, & \sigma > 0.3 f_c \end{cases} \qquad \text{Equation 2-10}$$

As can be seen from Equations 2-8–10, unlike most phenomenological transient strain models, the load-dependence of this model is nonlinear. It is expected that deviation from linearity must be fairly small to maintain a good agreement with experimental data. However, it is difficult to determine that this is the case from examination of Equations 2-8–10 and no demonstrations are provided by the author [34].

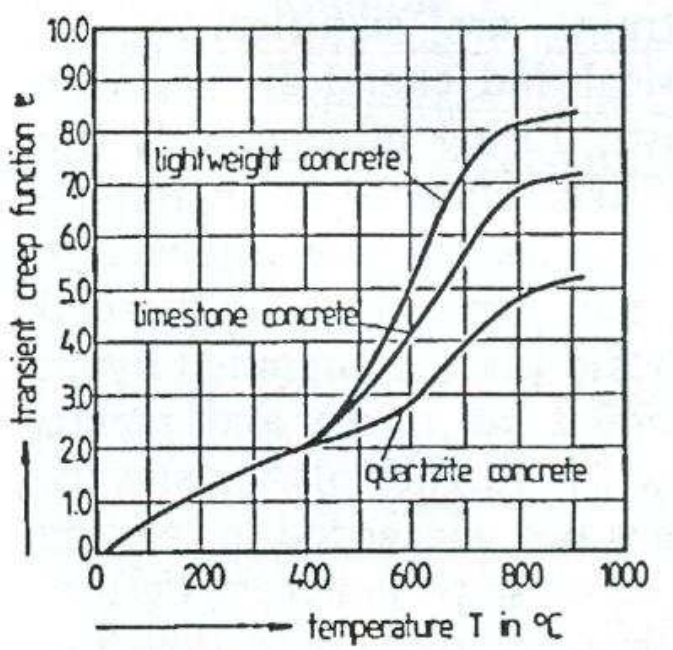

Figure 2-22: Comparison of the experimentally determined transient strain functions for three different types of concrete [34].

Although no physical model is explicitly associated with this transient strain model, the author [34] suggests that transient strain is the result of an increase in creep associated with redistribution of moisture in the cement microstructure, principally due to loss of both physically bound water and chemically bound water. However, no

indication of this physical mechanism appears to be reflected in the mathematical form of the model chosen.

Direct comparison of model predictions with experimental data sets has not been presented for this model; experimental data have been used for model calibration only. It is found that generally unique sets of values are required for the free parameters of Equation 2-8, dependent on aggregate type, as illustrated in figure 2-22, which shows the evolution of ϕ for three different concretes heated to about $900℃$. It can be seen in the figure that significant deviations of ϕ occur only in the temperature range above about $400℃$, which is broadly consistent with the LITS master curve concept.

It would be very useful to compare directly the transient strain predictions made using this model with experimental data sets. The unique mathematical form of the model, in terms of both temperature- and load-dependence, is worthy of further investigation.

2.3.6 *Final Remarks*

In this section, the existing mathematical models used to describe transient strain in the research field have been briefly examined. In addition to these, each of the hypotheses for the physical origin of transient strain has been used to develop mathematical models for transient strain. As each of the presented mathematical formulations are derived from uniaxial experimental data (experimental data on lateral transient strain evolution are sparse), it is necessary to make an assumption on the lateral behaviour of transient strain. It is most common that transient strain is assumed to be described as an isotropic phenomenon that is well described using a '*transient strain Poisson's ratio*' parameter that is generally distinct from the conventional (elastic) Poisson's ratio parameter [39, 56, 64, 87, 90].

There is also a model that was proposed by Thienel and Rostásy [36], which is a modification of a simple analytical method used to model the incremental multiaxial elastic response of concrete to a monotonically increasing multiaxial load [91-93]. This multiaxial elastic model, which requires the octahedral stress system, is directly adapted using linearly varying temperature-dependent parameters in order to describe transient strain.

Although it is an advantage of the model, in comparison to most others, that the model explicitly accounts for multiaxial stresses and strains, the validity of the model may be questionable as, for instance, previous work [91-93] suggests that the adapted methodology is not generally applicable to concrete, except in the case of axisymmetric analysis. Moreover, due to the presentation provided [36], mathematical details of the model are ambiguous and, in practice, the multiple axial transformation calculations necessary to implement the model are likely to be computationally demanding. Thus, further details of this model are not provided here.

The assumptions applied to define the transient strain response of concrete to states of tension are generally under-reported in the literature. Very few researchers indicate the nature of these assumptions used in their work; Pearce et al. [90, 94] assumed that transient strain does not develop in tension but accepted that there is insufficient experimental evidence to justify this decision. Presumably, this information is generally omitted due to the assumption that tensile stresses are largely irrelevant for the thermo-mechanical modelling of heated concrete loaded in compression. However, it can be envisioned that states of tension may develop during heating in practical structures due to complex shapes or rapid heating. Thus, it is a valid area of research to investigate that appears to have been paid little attention.

It is worthy of note that, in the research field, the calculated transient strain output of individual models tends to be presented alongside sets of experimental data without comparison with those of other models in similar conditions. Each set of researchers who have adopted one of the transient strain models and presented results has done so using a unique set of models to describe the thermo-mechanical behaviour of concrete, such as those describing thermal transport, hygral transport, and the evolution of non-transient strain components during heating. As a result, it is very difficult to make an objective comparison of the relative performances of all of the models here discussed using presently existing results in the literature.

Some researchers have performed limited comparisons of model output for some of the models presented here [63, 85]. However, the comparisons lack objectivity because the simulations are performed using values of the model parameters defined by the original authors. As the models are not calibrated to the same experimental

data sets, the comparison is likely to be inherently biased towards those models calibrated to experimental data most similar to those used in the comparisons. Moreover, for these comparisons, the models were not implemented into a realistic numerical simulation framework, such as finite element modelling. This may be expected to limit the reliability of any conclusions reached from such a process. Thus, reliable guidance about which transient strain model of the many available is not available in the literature, which is concerning due to the high importance of the transient strain model to the total strain behaviour of heated concrete.

2.4 Final remarks

It is clear that a naming convention would be useful in transient strain research. The use of terminology is frequently inconsistent between different research groups, which may lead to confusion and misinterpretation of results. However, a theoretical agreement on the physical causes of transient strain and the strain decomposition of heated and loaded concrete may first be required for standard nomenclature to be accepted. Thus, such a convention should not be expected for some time.

As shown in the review of the key experimental observations of LITS (§2.1), LITS is a dominant strain component for concrete specimens heated while under applied load, with a magnitude of the order of thermal strain. Transient strain is the dominant strain component of LITS. Thus, understanding transient strain and developing accurate models to predict the evolution of transient strain is extremely important.

Much experimental evidence suggests that LITS is governed by a ‘master curve’. Thus, in particular, the aggregate type has only a negligible influence on the evolution of LITS, provided that the temperature range is below about $450℃$ and that the aggregate is chemically stable in this temperature range. Note that this contrasts sharply with mechanical properties of concrete, such as compressive strength, and other strain components, such as thermal strain, which are typically strongly affected by aggregate type.

Moreover, experimental evidence shows that the presence of aggregate in concrete strongly affects the magnitude of LITS that develops. Generally, a decreased aggregate content leads to a greater development of LITS, roughly by a constant factor. Due to

these experimental observations, transient strain is here considered to be seated in the cement paste.

Experimental evidence is found to suggest that LITS has a finite rate of development. Clearly, a component of this time-dependent deformation should be considered to be basic creep. In fact, due to the poorly understood rate of development of transient strain, experimental data are extremely difficult to interpret and, as a result, little reliable evidence for the temperature-dependence of basic creep exists. Thus, a physical model for transient strain that can establish the rate of development of transient strain may be extremely useful.

Similarly, some experimental evidence suggests that LITS may sometimes develop in non-virgin heating conditions. It may be hypothesised that this is due to the existence of a 'LITS potential' that is depleted during virgin heating but that may regenerate when significant time is spent at ambient temperatures. This theoretical framework allows the explanation of the development of LITS in non-virgin heating conditions as, thus, being due either to this regeneration of the potential or to a degree of residual LITS potential remaining after cooling has ceased. However, no systematic experimental study of this phenomenon has been performed that would allow the behaviour of the LITS potential during heating to be determined. Thus, the LITS potential is presently a hypothetical theoretical construct only. The development of a reliably physical model would certainly allow this research area to progress.

It is clear from a review of the available experimental evidence that there has been very little research into the development of LITS in concrete specimens placed under states of direct tension. Although states of direct tension are never deliberately applied to concrete structures in practice (in fact, structures are always designed to avoid any application of tension to concrete), an understanding of the transient strain response of concrete to states of tension may be important in some extreme situations, such as when concrete structures are subjected to fire. Due to fires, spalling may occur at the heated surface of concrete, which can expose the steel reinforcement to fire and, thus, lead to loss of effective reinforcement. In such conditions, the transient strain response of the unreinforced regions of concrete to

states of tension may be quite important, particularly if any flexural or torsional loading is present for example.

Moreover, no evidence exists of which the present author is aware that demonstrates that the total strain response of unloaded concrete specimens that are rapidly heated are unaffected by the applied mathematical formulation for transient strain in states of tension. It may be envisioned that, in these conditions, different formulations may profoundly affect the relaxation of thermal stresses throughout the body of the specimens. Thus, the absence of research into the effects of different assumed formulations for the tensile response of the transient strain model is an issue that should be addressed.

As was discussed in the review of the hypotheses for the physical origin of transient strain (§2.2), several different potential physical origins for transient strain have been proposed in the literature, including basic creep, cement dehydration, silicate polymerisation, microdiffusion of pore water, nonlinear strains due to mesoscale stresses caused by thermal mismatch. None of these models have been shown convincingly to explain transient strain, though some appear to be promising avenues for future research efforts.

It is very important that the physical origin of transient strain can be identified as this will significantly aid the development of reliable mathematical models and allow predictions of 'non-standard' behaviour, such as the development of transient strain in conditions of non-virgin heating. It should be noted however that it is entirely plausible that more than one of the proposed physical origins of transient strain contribute to result in the development of the strain component experimentally determined as LITS. Thus, if any of the hypotheses are found to be unable to fully explain transient strain, this possibility should be considered.

Numerous mathematical models have been developed to predict the transient strain that will develop in conditions of elevated temperature. These models, discussed in this review (§2.3), tend to reproduce chosen sets of experimental data, with extrapolation to other concrete types justified by the existence of the master curve. Although most of the models share a common general form, there is much variation in

the temperature functions chosen to represent the temperature-dependence of transient strain.

No reliable objective comparisons have been performed to demonstrate the relative performances of these models. Thus, there is no guidance available for researchers who require a transient strain model, despite the evident importance of the transient strain to the total strain development of concrete in heated conditions. This is an issue that should be addressed.

As a result of this review of the literature, this work will attempt to address the following issues.

- The lack of understanding of the transient strain response of concrete to states of tension, including testing the hypothesis that this response may directly affect results in some cases and the determination of the most appropriate form of this aspect of transient strain modelling using numerical techniques.
- The absence of objective direct comparisons of the relative performances of existing transient strain models. This process may also allow some insight into the underlying physical processes that lead to the development of transient strain, which may help to guide future research efforts.

Chapter 3. Methodology

In this chapter, the methodology of this work is outlined. The governing hygro-thermo-mechanical equations are first defined, before the key constitutive laws for the energy and fluid transport behaviour and the strain model for concrete are given. Details of the overall numerical model are then provided, from which the FE model is given. Note that this work builds on the work of Davie et al. [95, 96], who base much of their work on that of Tenchev et al. [97]. Therefore, many of the details of the hygro-thermomechanical framework applied here is available in the published work of these researchers. Finally, a method of analysing the output of FE simulations proposed in this work is outlined.

Concrete is considered in this work to be an isotropic homogeneous porous medium on the macroscale that is multiphase in nature, containing a solid phase, an air phase, and typically liquid water and water vapour phases. The solid skeleton is a stiff material that undergoes isotropic damage when sufficient temperatures and strain states are imposed. In conditions of loading and temperature change, several distinct strain components are found to develop and material parameters are generally inconstant. The pores of concrete contain the fluid phases. It is energetically favourable for water to be in a physically adsorbed state up to a critical liquid saturation level (known as the *solid saturation point*). Thus, no liquid water is considered to exist until the liquid saturation exceeds this level. The gas phases are a mixture of air and water vapour, each of which assumed to behave as ideal gases.

3.1 Governing equations

The governing equations of the hygro-thermo-mechanical model used herein are defined as follows.

$$\frac{\partial}{\partial t}\left(\epsilon_G \tilde{\rho}_A\right) = -\nabla \cdot \boldsymbol{J}_A \qquad \text{Equation 3-1}$$

$$\frac{\partial}{\partial t}\left(\epsilon_G \tilde{\rho}_V\right) + \frac{\partial}{\partial t}\left(\epsilon_L \rho_L\right) - \frac{\partial}{\partial t}\left(\epsilon_D \rho_L\right) = -\nabla \cdot \left(\boldsymbol{J}_V + \boldsymbol{J}_L\right) \qquad \text{Equation 3-2}$$

$$\left(\underline{\rho C}\right)\frac{\partial T}{\partial t} - \lambda_E \frac{\partial}{\partial t}\left(\epsilon_L \rho_L\right) + \left(\lambda_D + \lambda_E\right)\frac{\partial}{\partial t}\left(\epsilon_D \rho_L\right) = \nabla \cdot (k \nabla T) + \lambda_E \nabla \cdot \boldsymbol{J}_L \qquad \text{Equation 3-3}$$

$$\nabla \cdot \left(\boldsymbol{\sigma}' - \alpha P_{pore}\boldsymbol{I}\right) + \boldsymbol{b} = 0 \qquad \text{Equation 3-4}$$

where ϵ_θ is the volume fraction of phase θ ($\theta = L, V, A, G, D$, which refer to liquid water, water vapour, dry air, gas, and dehydrated water phases respectively), $\tilde{\rho}_\theta$ is the mass of phase θ per unit volume of gaseous material, $\boldsymbol{J}_\theta$ is the mass flux of phase θ, ρ_θ is the mass density of phase θ, $\underline{\rho C}$ is the heat capacity of concrete, T is the absolute temperature, t is time, λ_D is the specific heat of dehydration, λ_E is the specific heat of dehydration, k is the thermal conductivity of concrete, $\boldsymbol{\sigma}'$ is the effective stress (defined below), α is the Biot coefficient, P_{pore} is the pore pressure, $\boldsymbol{I}$ is the identity tensor, and $\boldsymbol{b}$ is the body force.

3.2 Constitutive laws for energy and fluid transport behaviour

It is assumed that Darcy's law of pressure-driven flow is applicable to transport of both the liquid and gas phases, while Fick's law of concentration-driven diffusion is also applicable to transport of the gaseous phases. Thus, the flux terms of Equations 3-1–3 may be written as follows.

$$\boldsymbol{J}_A = -\epsilon_G \tilde{\rho}_A \frac{KK_G}{\mu_G}\nabla P_G - \epsilon_G \tilde{\rho}_G D_{AV} \nabla\left(\frac{\tilde{\rho}_A}{\tilde{\rho}_G}\right) \qquad \text{Equation 3-5}$$

$$\boldsymbol{J}_V = -\epsilon_G \tilde{\rho}_V \frac{KK_G}{\mu_G}\nabla P_G - \epsilon_G \tilde{\rho}_G D_{AV} \nabla\left(\frac{\tilde{\rho}_V}{\tilde{\rho}_G}\right) \qquad \text{Equation 3-6}$$

$$J_L = -\epsilon_L \rho_L \frac{KK_L}{\mu_L}\nabla P_L \qquad \text{Equation 3-7}$$

where K is the intrinsic permeability of concrete, K_θ, P_θ, and μ_L are the relative permeability, the pressure, and the dynamic viscosity of phase θ respectively, and D_{AV} is the diffusion coefficient for the mixture of air and water vapour within concrete.

The gas phases are assumed to behave as ideal gases. Thus, the pressure terms are calculated as follows.

$$P_A = R_A \tilde{\rho}_A T \qquad \text{Equation 3-8}$$

$$P_V = R_V \tilde{\rho}_V T \qquad \text{Equation 3-9}$$

where R_A and R_V are the gas constants for the air and vapour phases respectively. The sum of Equations 3-8 and 3-9 give the gas pressure, P_G.

Liquid pressure is calculated based on the known equation relating liquid pressure, gas pressure, and capillary pressure P_C.

$$P_L = P_G - P_C \qquad \text{Equation 3-10}$$

where P_C is defined as follows.

$$P_C = \begin{cases} 0 & , \quad S \leq S_{SSP} \\ -R_V T \rho_L \ln\left(\frac{P_V}{P_{sat}}\right), & S > S_{SSP} \end{cases} \qquad \text{Equation 3-11}$$

where P_{sat} is the saturation vapour pressure, S is the liquid saturation, and S_{SSP} is the solid saturation point (i.e. the saturation degree at which all liquid water is physically adsorbed to the internal surface of the concrete [98]).

Saturation is calculated based on the ratio of ϵ_L (which is modelled using a sorption isotherm [97]) to the accessible pore space, ϕ. Similarly, the difference between ϕ and ϵ_L gives ϵ_G.

The pore pressure term of Equation 3-4 is calculated as follows.

$$P_{pore} = \begin{cases} P_G - P_{G,\infty} & , \quad S \leq S_{SSP} \\ \left(\frac{S - S_{SSP}}{1 - S_{SSP}}\right) P_L + \left(\frac{1 - S}{1 - S_{SSP}}\right) P_G - P_{G,\infty}, & S > S_{SSP} \end{cases} \qquad \text{Equation 3-12}$$

where $P_{G,\infty}$ is the gas pressure of the atmosphere surrounding the concrete. This formulation for pore pressure assumes that adsorbed water applies no pressure and that 2the combined effect of gas and liquid pressures is given by a weighted sum of each individual contribution.

3.3 Constitutive laws for mechanical behaviour

In general conditions of temperature change and loading, total strain of concrete is here considered to be decomposed as follows.

$$\dot{\boldsymbol{\varepsilon}}_{tot} = \dot{\boldsymbol{\varepsilon}}_{el}(\boldsymbol{\sigma}', T) + \dot{\boldsymbol{\varepsilon}}_{cr}(\boldsymbol{\sigma}', T, t, t') + \dot{\boldsymbol{\varepsilon}}_{th}(T) + \dot{\boldsymbol{\varepsilon}}_{tr}(\boldsymbol{\sigma}', T) \qquad \text{Equation 3-13}$$

where ε_{tot}, ε_{el}, ε_{cr}, ε_{th}, and ε_{tr} are total strain, elastic strain, basic creep, thermal strain, and transient strain respectively, t and t' are the present time and the time at which effective stress $\boldsymbol{\sigma}'$ was applied respectively.

3.3.1 *Elastic strain*

Conditions that cause damage are considered here to result in a distribution of microcracking throughout the material. As a result, externally applied stress is apparently concentrated on the 'undamaged' material due to the reduced resisting area. This magnified stress is the effective stress, $\boldsymbol{\sigma}'$.

$$\boldsymbol{\sigma}' = (1 - \omega)(1 - \chi)\boldsymbol{E}_0 : \boldsymbol{\varepsilon}_{el} \qquad \text{Equation 3-14}$$

where ω and χ are scalar measures of the mechanical damage and thermal damage respectively. The secant modulus is defined by the following.

$$\boldsymbol{E}_{sec} = (1 - \omega)(1 - \chi)\boldsymbol{E}_0 \qquad \text{Equation 3-15}$$

Damage functions can be defined that govern the development of mechanical and thermal damage. Mechanical damage is governed by the following.

$$f^{md} = \tilde{\varepsilon} - \kappa^{md} \qquad \text{Equation 3-16}$$

where f^{md} is the mechanical damage function, $\tilde{\varepsilon}$ is the equivalent strain measure, and κ^{md} is the mechanical damage history parameter.

The equivalent strain measure is calculated as follows.

$$\tilde{\varepsilon} = AI_1 + \sqrt{A^2 I_1^2 + BJ_2} \qquad \text{Equation 3-17}$$

where I_1 is the first invariant of the strain tensor, J_2 is the second invariant of the strain deviator tensor, and A and B are defined as follows.

$$A = \frac{g - 1}{2g(1 - 2v)} \qquad \text{Equation 3-18}$$

$$B = \frac{1}{2g(1+\nu)^2}$$ Equation 3-19

where g is the ratio of compressive strength to tensile strength and ν is Poisson's ratio.

$$g = \frac{f_c}{f_t}$$ Equation 3-20

The mechanical damage history parameter is calculated as follows.

$$\kappa^{md} = \begin{cases} \kappa_0^{md} , & \tilde{\varepsilon} \leq \kappa_0^{md} \\ \tilde{\varepsilon} , & \tilde{\varepsilon} > \kappa_0^{md} \end{cases}$$ Equation 3-21

where κ_0^{md} is the temperature-dependent threshold for the initiation of mechanical damage, given as the ratio of tensile strength to elastic modulus.

$$\kappa_0^{md} = \frac{f_t(T)}{E(T)}$$ Equation 3-22

where the temperature-dependence of the elastic modulus is defined by the thermal damage model (see below) and temperature-dependence of tensile strength is defined as follows.

$$f_t(T) = f_t^0\left(1 - 0.016\hat{\theta}^2\right)$$ Equation 3-23

where $\hat{\theta}$ is a history variable that represents a measure of the maximum temperature reached by the material (defined below).

If $f^{md} = 0$ and $\frac{\partial \tilde{\varepsilon}}{\partial t} > 0$, the existing conditions are sufficient to cause mechanical damage. Thus, the scalar mechanical damage variable ω, which may never decrease, increases in value.

$$\omega = 1 - \frac{\kappa_0^{md}(T)}{\kappa^{md}} e^{-\gamma(T)[\kappa^{md} - \kappa_0^{md}(T)]}$$ Equation 3-24

where γ is the temperature-dependent strain-softening parameter that is controlled by the fracture energy release rate [94].

In a similar manner, thermal damage is governed by the following.

$$f^{td} = T - \kappa^{td} \qquad \text{Equation 3-25}$$

where f^{td} is the thermal damage function and κ^{td} is the thermal damage history parameter, which is calculated as follows.

$$\kappa^{td} = \begin{cases} T_o, & T \leq T_0 \\ T, & T > T_0 \end{cases} \qquad \text{Equation 3-26}$$

If $f^{td} = 0$ and $\frac{\partial T}{\partial t} > 0$ (i.e. virgin heating), the existing conditions are sufficient to cause thermal damage. Thus, the scalar thermal damage variable χ, which may never decrease, increases in value.

$$\chi = 0.2\hat{\theta} - 0.01\hat{\theta}^2 \qquad \text{Equation 3-27}$$

where $\hat{\theta}$ is defined by the following.

$$\hat{\theta} = \frac{\kappa^{td} - T_0}{100°C} \qquad \text{Equation 3-28}$$

The generalised form of Equation 3-27 can be written as follows.

$$1 - \chi = \left(1 - \zeta\hat{\theta}\right)^2 \qquad \text{Equation 3-29}$$

where ζ is the free parameter of the thermal damage model, set by default to 0.1 as in Equation 3-27.

In chapter 6, a modified form of Equation 3-29 is applied in order to account for the effects of preload on thermal damage development. Compressive preload is frequently found to suppress the magnitude of damage that develops during heating. As no mechanical damage develops in the unloaded heated specimen, the difference in thermal damage development cannot be considered to be a reduction in mechanical damage (negative mechanical damage is not allowed). Thus, preload must suppress the development of thermal damage.

Based on the experimental results considered in chapter 6, the following form of Equation 3-29 is applied to account for the effects of preload on thermal damage.

$$1-\chi_\sigma = \begin{cases} 1, & \theta < \theta_\chi^* \\ \left[1-\zeta_\sigma\left(\theta-\theta_\chi^*\right)\right]^2, & \theta \geq \theta_\chi^* \end{cases} \qquad \text{Equation 3-30}$$

where χ_σ is the thermal damage parameter for preloaded concrete specimens and replaces χ in Equations 3-14 and 3-15, is the free parameter of the model, and θ_χ^* is the (reduced) transition temperature of the model.

It is here proposed that thermal damage may be broadly considered to be composed of two components, herein referred to as *intrinsic thermal damage* and *thermal mismatch damage*. Broadly, intrinsic thermal damage is an unavoidable component of damage that develops due to thermo-chemical transformations and thermal mismatch develops due to material microcracking that is driven by inter-phase stresses within concrete (which builds at the boundaries between phases due to incompatible thermal expansion behaviour for instance). As it is the build up of tensile stresses that lead to thermal mismatch thermal damage, the pre-application of a compressive stress may reduce or remove the influence of these tensile stresses and the consequent development of microcracking. Thus, in the presence of preload, a reduced magnitude of thermal damage is observed to develop in heated conditions.

Equations 3-14 and 3-15 are mathematically consistent with this model for thermal damage. χ_σ is a measure of intrinsic thermal damage. It is initiated at a transition temperature corresponding to the initiation of chemo-thermal processes within the cement paste. The combination of thermal mismatch damage and intrinsic thermal damage is given by χ.

It is here assumed that Poisson's ratio is unaffected by damage, which appears to be a reasonable assumption for thermal damage and a good approximation for mechanical damage due to typical load ranges. Thus, as isotropy is assumed, Equation 3-14 can be rewritten as follows.

$$\boldsymbol{\sigma}' = (1-\omega)(1-\chi)E_0\boldsymbol{D} : \boldsymbol{\varepsilon}_{el} \qquad \text{Equation 3-31}$$

where E_0 is the elastic constant and $\boldsymbol{D}$ is defined as the (isotropic) elastic tensor with the common factor E_0 taken out.

3.3.2 *Basic creep*

Although it is recognised that basic creep may be a significant component of strain in concrete specimens loaded for a significant period of time, no specific basic creep model is adopted in this work. This is because basic creep is a very difficult strain component to predict and the adoption of a generic model may introduce as large a degree of error as it is intended to remove, particularly as the magnitude of basic creep that develops in the conditions of interest to this work is typically of relatively minor importance. However, any model that can be shown to reproduce the basic creep behaviour of a particular concrete in conditions similar to those of interest shall be adopted when modelling that particular material.

3.3.3 *Thermal strain*

Thermal strain, considered to be the combined effect of FTS and drying shrinkage, is modelled here using the following model.

$$\dot{\boldsymbol{\varepsilon}}_{th} = \alpha_{th}\dot{\theta}\boldsymbol{I} \qquad \text{Equation 3-32}$$

where $\boldsymbol{I}$ is the identity tensor and α_{th} is given as follows.

$$\alpha_{th} = \begin{cases} \dfrac{6 \times 10^{-5}}{7 - \theta}, & 0 \leq \theta \leq 6 \\ 0, & \theta > 6 \end{cases} \qquad \text{Equation 3-33}$$

This model, developed to describe the thermal strain behaviour of quartzite concretes matches experimental behaviour fairly well [86]. The discontinuous transition in model behaviour at a temperature of 620°C reflects the transition in observed thermal strain behaviour at this temperature due to chemo-thermal degradation of the quartzite aggregates at temperatures close to this value.

To ensure that the model can be calibrated to experimental data for further work, Equation 3-32 may be rewritten as follows.

$$\alpha_{th} = \begin{cases} \dfrac{\beta}{\theta' - \theta} & , \quad 0 \leq \theta \leq \theta_1 \\ \gamma & , \quad \theta_1 > 6 \end{cases}$$ Equation 3-34

where β, θ', γ, and θ_1 are free parameters of the model, set equal to 6×10^{-5}, 7, 0, and 6 respectively by default if no calibration occurs. It should be noted that θ' must be greater in value than θ_1 for sensible model behaviour.

3.3.4 *Transient strain*

Several transient strain models shall be adopted in the course of this work. For the purposes of forming the numerical model, the following general form of the transient strain model shall be assumed, though some transient strain models do not follow this general form.

$$\dot{\boldsymbol{\varepsilon}}_{tr} = \boldsymbol{M}\boldsymbol{\sigma}'\dot{T}$$ Equation 3-35

where $\boldsymbol{M}$ is the tensor that defines the multiaxial nature of transient strain, as well as the temperature-dependence and magnitude. As it is assumed that transient strain is isotropic, $\boldsymbol{M}$ shall be similar in form to $\boldsymbol{B}$, with additional factors and an equivalent transient strain Poisson's ratio in place of the elastic Poisson's ratio.

3.4 Numerical model

The stress increment can be obtained from Equation 3-14.

$$d\boldsymbol{\sigma}' = \boldsymbol{E}_{sec} : d\boldsymbol{\varepsilon}_{el} - (1-\omega)\widehat{\boldsymbol{\sigma}}' d\chi - (1-\chi)\widehat{\boldsymbol{\sigma}}' d\omega$$ Equation 3-36

where $\widehat{\boldsymbol{\sigma}}'$ is the stress required to produce equivalent elastic strain $\boldsymbol{\varepsilon}_{el}$ in an otherwise identical undamaged material.

$$\widehat{\boldsymbol{\sigma}}' = \boldsymbol{E}_0 : \boldsymbol{\varepsilon}_{el}$$ Equation 3-37

Equation 3-31 can be rewritten as follows.

$$\dot{\boldsymbol{\varepsilon}}_{th} = \boldsymbol{m}\dot{T}$$ Equation 3-38

Thus, assuming no basic creep, Equation 3-35 can be rewritten as follows.

$$d\boldsymbol{\sigma}' = \boldsymbol{E}_{sec}: d\boldsymbol{\varepsilon}_{tot} - \boldsymbol{E}_{sec}: (\boldsymbol{m} + \boldsymbol{M}: \boldsymbol{\sigma}')dT - (1-\omega)\widehat{\boldsymbol{\sigma}}' d\chi - (1-\chi)\widehat{\boldsymbol{\sigma}}' d\omega \quad \text{Equation 3-39}$$

This equation is essential for the formation of the finite element formulation that follows. Definition of $\boldsymbol{M}$, which is very important to the evolving stress and strain state of concrete in heated conditions, is the area that this work is principally intended to investigate.

3.4.1 *Finite element formulation*

The weak form of the governing equations is obtained using the standard Galerkin weighted residual method and application of the divergence theorem. Furthermore, using the standard Finite Element approximation, the chosen primary variables of displacements, u, temperature, T, gas pressure, P_G, and vapour content, $\tilde{\rho}_V$, may be expressed in terms of their nodal quantities.

$$\boldsymbol{u} = \boldsymbol{N}_u \boldsymbol{a} \quad \text{Equation 3-40}$$

$$T = \boldsymbol{N}_T \boldsymbol{T} \quad \text{Equation 3-41}$$

$$P_G = \boldsymbol{N}_P \boldsymbol{P}_G \quad \text{Equation 3-42}$$

$$\tilde{\rho}_V = \boldsymbol{N}_\rho \widetilde{\boldsymbol{\rho}}_V \quad \text{Equation 3-43}$$

where $\boldsymbol{N}_u$, $\boldsymbol{N}_T$, $\boldsymbol{N}_P$, and $\boldsymbol{N}_\rho$ are the shape functions for displacement, temperature, gas pressure, and vapour content respectively and $\boldsymbol{a}$, $\boldsymbol{T}$, $\boldsymbol{P}_G$, and $\widetilde{\boldsymbol{\rho}}_V$ are the respective nodal values.

The governing equations for this hygro-thermo-mechanical model may be expressed as follows.

$$\boldsymbol{C}\dot{\boldsymbol{x}} + \boldsymbol{K}\boldsymbol{x} = \boldsymbol{f}_{ext} \quad \text{Equation 3-44}$$

where the coefficient matrices $\boldsymbol{C}$ and $\boldsymbol{K}$, as well as the vector of nodal values are given as follows

$$\boldsymbol{C} = \begin{bmatrix} 0 & 0 & 0 & 0 \\ 0 & \boldsymbol{C}_{TT} & \boldsymbol{C}_{TP} & \boldsymbol{C}_{TV} \\ 0 & \boldsymbol{C}_{AT} & \boldsymbol{C}_{AP} & \boldsymbol{C}_{AV} \\ 0 & \boldsymbol{C}_{MT} & \boldsymbol{C}_{MP} & \boldsymbol{C}_{MV} \end{bmatrix} \quad \text{Equation 3-45}$$

$$\boldsymbol{K} = \begin{bmatrix} \boldsymbol{K}_{uu} & \boldsymbol{K}_{uT} & \boldsymbol{K}_{uP} & \boldsymbol{K}_{uV} \\ 0 & \boldsymbol{K}_{TT} & \boldsymbol{K}_{TP} & \boldsymbol{K}_{TV} \\ 0 & \boldsymbol{K}_{AT} & \boldsymbol{K}_{AP} & \boldsymbol{K}_{AV} \\ 0 & \boldsymbol{K}_{MT} & \boldsymbol{K}_{MP} & \boldsymbol{K}_{MV} \end{bmatrix} \quad \text{Equation 3-46}$$

$$\boldsymbol{x} = \begin{Bmatrix} \boldsymbol{a} \\ \boldsymbol{T} \\ \boldsymbol{P}_G \\ \widetilde{\boldsymbol{\rho}}_V \end{Bmatrix} \quad \text{Equation 3-47}$$

$$\boldsymbol{f}_{ext} = \begin{Bmatrix} f_{ext}^{u} \\ f_{ext}^{T} \\ f_{ext}^{P} \\ f_{ext}^{V} \end{Bmatrix} \quad \text{Equation 3-48}$$

The sub-matrices of the above are the standard FE volume integrals. For instance, $\boldsymbol{C}_{TT}$, $\boldsymbol{K}_{TT}$, and f_T^{ext} are given by the following.

$$\boldsymbol{C}_{TT} = \int_V C_{TT} \boldsymbol{N}_T^T \boldsymbol{N}_T \, dV \quad \text{Equation 3-49}$$

$$\boldsymbol{K}_{TT} = \int_V K_{TT} \nabla \boldsymbol{N}_T^T \nabla \boldsymbol{N}_T \, dV \quad \text{Equation 3-50}$$

$$f_T^{ext} = \oint_S \left(K_{TT} \frac{\partial T}{\partial n} + K_{TP} \frac{\partial P_G}{\partial n} + K_{TV} \frac{\partial \tilde{\rho}_V}{\partial n} \right) dS \quad \text{Equation 3-51}$$

where the terms describing heat and mass transport $K_{\theta\phi}$ and $C_{\theta\phi}$ ($\theta = T$, A, and M and $\phi = T$, P, and V) are provided in Appendix A. The terms $\boldsymbol{K}_{uu}$, $\boldsymbol{K}_{uT}$, $\boldsymbol{K}_{uP}$, and $\boldsymbol{K}_{uV}$ are of significant importance to this work. Thus, they are described in more detail here.

$$d\boldsymbol{\sigma} = d\boldsymbol{\sigma}' - d\boldsymbol{P}_{pore} \quad \text{Equation 3-52}$$

As expressed in Equation 3-12, pore pressure is given by a weighted sum of the pressures of the fluids within the pores. In incremental form, pore pressure can be expressed as follows.

$$d\boldsymbol{P}_{pore} = \left(\frac{\partial \boldsymbol{P}_{pore}}{\partial T} \right)_{P_G, \tilde{\rho}_V} dT + \left(\frac{\partial \boldsymbol{P}_{pore}}{\partial P_G} \right)_{T, \tilde{\rho}_V} dP_G + \left(\frac{\partial \boldsymbol{P}_{pore}}{\partial \tilde{\rho}_V} \right)_{T, P_G} d\tilde{\rho}_V \quad \text{Equation 3-53}$$

where the partial differential terms can be determined from Equations 3-8–12 to be given by the following.

$$\left.\begin{aligned}
&\left(\frac{\partial \boldsymbol{P}_{pore}}{\partial T}\right)_{P_G,\,\tilde{\rho}_V} = \boldsymbol{0} && \text{Equation 3-54 (a)}\\
&\left(\frac{\partial \boldsymbol{P}_{pore}}{\partial P_G}\right)_{T,\,\tilde{\rho}_V} = \boldsymbol{I} && \text{Equation 3-55 (a)}\\
&\left(\frac{\partial \boldsymbol{P}_{pore}}{\partial \tilde{\rho}_V}\right)_{T,\,P_G} = \boldsymbol{0} && \text{Equation 3-56 (a)}
\end{aligned}\right\} S \le S_{SSP}$$

$$\left.\begin{aligned}
&\left(\frac{\partial \boldsymbol{P}_{pore}}{\partial T}\right)_{P_G,\,\tilde{\rho}_V} = -\left(\frac{S - S_{SSP}}{1 - S_{SSP}}\right)\frac{\partial P_C}{\partial T}\boldsymbol{I} && \text{Equation 3-54 (b)}\\
&\left(\frac{\partial \boldsymbol{P}_{pore}}{\partial P_G}\right)_{T,\,\tilde{\rho}_V} = \boldsymbol{I} && \text{Equation 3-55 (b)}\\
&\left(\frac{\partial \boldsymbol{P}_{pore}}{\partial \tilde{\rho}_V}\right)_{T,\,P_G} = -\left(\frac{S - S_{SSP}}{1 - S_{SSP}}\right)\frac{\partial P_C}{\partial \tilde{\rho}_V}\boldsymbol{I} && \text{Equation 3-56 (b)}
\end{aligned}\right\} S > S_{SSP}$$

To be concise in notation, we shall replace the partial differential terms with the following terms.

$$\boldsymbol{p}_T \equiv \left(\frac{\partial \boldsymbol{P}_{pore}}{\partial T}\right)_{P_G,\,\tilde{\rho}_V} \qquad \text{Equation 3-57}$$

$$\boldsymbol{p}_G \equiv \left(\frac{\partial \boldsymbol{P}_{pore}}{\partial P_G}\right)_{T,\,\tilde{\rho}_V} \qquad \text{Equation 3-58}$$

$$\boldsymbol{p}_V \equiv \left(\frac{\partial \boldsymbol{P}_{pore}}{\partial \tilde{\rho}_V}\right)_{T,\,P_G} \qquad \text{Equation 3-59}$$

Therefore, Equation 3-52 can be rewritten as follows.

$$\begin{aligned} d\boldsymbol{\sigma} = \boldsymbol{E}_{sec}{:}\, d\boldsymbol{\varepsilon} - \boldsymbol{E}_{sec}{:}\,(\boldsymbol{m} + \boldsymbol{M}\boldsymbol{\sigma}')dT - (1-\omega)\widehat{\boldsymbol{\sigma}}'d\chi - (1-\chi)\widehat{\boldsymbol{\sigma}}'d\omega \\ - \boldsymbol{p}_T dT - \boldsymbol{p}_G dP_G - \boldsymbol{p}_V d\tilde{\rho}_V \end{aligned} \qquad \text{Equation 3-60}$$

Thus, the stiffness sub-matrices of Equation 3-44 can be written as follows.

$$\boldsymbol{K}_{uu} = \int_V \boldsymbol{B}^T\left[\boldsymbol{E}_{sec} - H_1^{md}(1-\chi)\widehat{\boldsymbol{\sigma}}'\boldsymbol{s}^T\right]\boldsymbol{B}\,dV \qquad \text{Equation 3-61}$$

$$\begin{aligned} \boldsymbol{K}_{uT} = -\int_V \boldsymbol{B}^T\big[&\boldsymbol{E}_{sec}{:}\,(\boldsymbol{m} + \boldsymbol{M}\boldsymbol{\sigma}') + (1-\omega)H^{td}\widehat{\boldsymbol{\sigma}}' \\ &+ (1-\chi)H_2^{md}\widehat{\boldsymbol{\sigma}}' \\ &- (1-\chi)H_1^{md}\widehat{\boldsymbol{\sigma}}'\boldsymbol{s}^T(\boldsymbol{m} + \boldsymbol{M}\boldsymbol{\sigma}') + \boldsymbol{p}_T\big]\boldsymbol{N}_T^T\,dV \end{aligned} \qquad \text{Equation 3-62}$$

$$\boldsymbol{K}_{uP} = -\int_V \boldsymbol{B}^T \boldsymbol{p}_G \boldsymbol{N}_P^T \, dV \quad \text{Equation 3-63}$$

$$\boldsymbol{K}_{uV} = -\int_V \boldsymbol{B}^T \boldsymbol{p}_V \boldsymbol{N}_\rho^T dV \quad \text{Equation 3-64}$$

where H_1^{md} and H_2^{md} define the effects of mechanical damage, H^{td} defines the effects of thermal damage, and $\boldsymbol{s}$ translates between a given strain state and the equivalent strain measure of the mechanical damage model.

$$H_1^{md} = \frac{\partial \omega}{\partial \kappa^{md}} \quad \text{Equation 3-65}$$

$$H_2^{md} = \frac{\partial \omega}{\partial \kappa_0^{md}} \frac{\partial \kappa_0^{md}}{\partial T} + \frac{\partial \omega}{\partial \gamma} \frac{\partial \gamma}{\partial T} \quad \text{Equation 3-66}$$

$$H^{td} = \frac{\partial \chi}{\partial \kappa^{td}} \quad \text{Equation 3-67}$$

$$\boldsymbol{s} = \frac{d\tilde{\varepsilon}}{d\boldsymbol{\varepsilon}} \quad \text{Equation 3-68}$$

Equations 3-42 are further discretised in time using a finite difference scheme defined as follows.

$$\boldsymbol{x}^{t+\xi\Delta t} = (1-\xi)\boldsymbol{x}^t + \xi \boldsymbol{x}^{t+\Delta t} \quad \text{Equation 3-69}$$

$$\dot{\boldsymbol{x}}^{t+\xi\Delta t} = \frac{\boldsymbol{x}^{t+\xi\Delta t} - \boldsymbol{x}^t}{\Delta t} \quad \text{Equation 3-70}$$

where Δt is the time increment, $\boldsymbol{x}^t$ and $\boldsymbol{x}^{t+\Delta t}$ are the values of the state variables at times t and $t + \Delta t$ respectively, and ξ is a constant in the range 0–1.

As is appropriate for a nonlinear set of equations, the Newton-Raphson method is used. Thus, the discrete system of equations is linearised and the state variables are decomposed as follows.

$$\boldsymbol{x}_j = \boldsymbol{x}_{j-1} + d\boldsymbol{x} \quad \text{Equation 3-71}$$

where the subscripts j and $j-1$ represent iteration numbers. Similarly, the stress tensor is decomposed.

$$\boldsymbol{\sigma}_j = \boldsymbol{\sigma}_{j-1} + d\boldsymbol{\sigma} \qquad \text{Equation 3-72}$$

Thus, Equations 3-42 can be rewritten as follows.

$$\bar{\boldsymbol{K}} d\boldsymbol{x} = \boldsymbol{f}_{ext} - \boldsymbol{f}_{int} \qquad \text{Equation 3-73}$$

where $\bar{\boldsymbol{K}}$ is the '*effective stiffness matrix*' and is defined as follows.

$$\bar{\boldsymbol{K}} = \begin{bmatrix} \boldsymbol{K}_{uu} & \boldsymbol{K}_{uT} & \boldsymbol{K}_{uP} & \boldsymbol{K}_{uV} \\ \boldsymbol{0} & \frac{1}{\Delta t}\boldsymbol{C}_{TT} + \xi \boldsymbol{K}_{TT} & \frac{1}{\Delta t}\boldsymbol{C}_{TP} + \xi \boldsymbol{K}_{TP} & \frac{1}{\Delta t}\boldsymbol{C}_{TV} + \xi \boldsymbol{K}_{TV} \\ \boldsymbol{0} & \frac{1}{\Delta t}\boldsymbol{C}_{AT} + \xi \boldsymbol{K}_{AT} & \frac{1}{\Delta t}\boldsymbol{C}_{AP} + \xi \boldsymbol{K}_{AP} & \frac{1}{\Delta t}\boldsymbol{C}_{AV} + \xi \boldsymbol{K}_{AV} \\ \boldsymbol{0} & \frac{1}{\Delta t}\boldsymbol{C}_{MT} + \xi \boldsymbol{K}_{MT} & \frac{1}{\Delta t}\boldsymbol{C}_{MP} + \xi \boldsymbol{K}_{MP} & \frac{1}{\Delta t}\boldsymbol{C}_{MV} + \xi \boldsymbol{K}_{MV} \end{bmatrix} \qquad \text{Equation 3-74}$$

The internal force vector, denoted by $\boldsymbol{f}_{int}$, is a result of rearrangements of the equations when deriving Equation 3-71. Thus, for instance, the term $\boldsymbol{f}_{int}^{T}$ is defined as follows.

$$\begin{aligned} \boldsymbol{f}_{int}^{T} = \frac{1}{\Delta t}[\boldsymbol{0} \quad \boldsymbol{C}_{TT} \quad \boldsymbol{C}_{TP} \quad \boldsymbol{C}_{TV}]\left(\boldsymbol{x}_{j-1}^{t+\Delta t} - \boldsymbol{x}^{t}\right) \\ + [\boldsymbol{0} \quad \boldsymbol{K}_{TT} \quad \boldsymbol{K}_{TP} \quad \boldsymbol{K}_{TV}]\left(\xi \boldsymbol{x}_{j-1}^{t+\Delta t} - (1-\xi)\boldsymbol{x}^{t}\right) \end{aligned} \qquad \text{Equation 3-75}$$

Most commonly, a value of 0.5 is assigned to ξ.

This work, as stated previously, is principally concerned with the tensor $\boldsymbol{M}$ of Equation 3-35. This tensor is important in the definition of the sub-matrix $\boldsymbol{K}_{uT}$, as shown by examination of Equation 3-62. This is the point of entry for any changes introduced in this work into the behaviour of the FE simulations. Thus, it is clear from Equation 3-62 that several other aspects of the model are critically important to such an investigation. It is essential that the thermomechanical damage model is well-defined, due to the central role of $\boldsymbol{\sigma}'$ in Equation 3-62. Also, the thermal strain model, which plays a large role in the definition of $\boldsymbol{K}_{uT}$, must be based on reliable experimental observations. Moreover, the hygral aspects are critically important to reliable determination of $\boldsymbol{K}_{uT}$, both directly through the effects of accurate profiles of gas pressure and vapour content on model results and indirectly through the coupling effects, such as that represented by Equation 3-54 (b). Therefore, in this work, the

transient strain model cannot be considered in isolation. Particular effort must be made to ensure that the hygral aspects of the model, the thermal strain constitutive model, and the damage model are well suited to experimental evidence.

3.4.2 *Boundary conditions*

In terms of the mechanical aspects of the model, the boundary conditions are chosen to match the experimental conditions. Most often lines of symmetry are sought in the body of the specimen to be modelled at which conditions of restraint can be applied. If a load is also to be applied, constant nodal forces may be applied at the boundaries (weighted to give an even distribution of stress across the body). Similarly, if a specimen is restrained in a certain direction, spatial restraint can be imposed at this boundary of the body.

In terms of temperature and vapour content, Neumann type boundary conditions are applied. Thus, for temperature, the equation that defines the boundary conditions is as follows.

$$\frac{\partial T}{\partial n} = \frac{h_{qr}}{k}(T_\infty - T) \qquad \text{Equation 3-76}$$

where h_{qr} is the coefficient of the combined effects of convection and radiation at the boundary and T_∞ is the temperature of the surrounding atmosphere.

Similarly, for vapour content, the equation that defines the boundary condition is as follows.

$$\frac{\partial \tilde{\rho}_V}{\partial n} = -\frac{K_{VT}}{K_{VV}}\frac{h_{qr}}{k}(T_\infty - T) + \frac{\beta}{K_{VV}}\left(\tilde{\rho}_{V,\infty} - \tilde{\rho}_V\right) \qquad \text{Equation 3-77}$$

where β is the coefficient of water vapour mass transfer at the boundary, $\tilde{\rho}_{V,\infty}$ is the vapour content of the surrounding atmosphere, and K_{VT} and K_{VV} are matrix terms defined in Appendix A.

3.5 Mean variable analysis

During a simulation in a FE environment, calculations of key parameters and state variables are made at a typically large number of points distributed throughout the

mesh used to simulate the body of the modelled structure, known as *Gauss points*. After a number of iterations, a stable and mutually consistent solution is reached throughout the mesh and the time variable is advanced (at which point, further calculation iterations are made). Typically, a FE package can be set to provide as output for analysis any desired parameter or state variable throughout the simulation; a user of the package must only specify the location (or locations) within the mesh at which the data are required.

Although this method is highly useful for analysis of results in general, it is found to be inadequate for this work, which requires the transient strain component and its influence on results to be isolated as much as possible. For example, data for the local axial transient strain component at any single point within the mesh are unlikely to be globally representative if inhomogeneous load and temperature fields exist. Thus, a novel technique is here applied in which a measure of any desired parameter or state variable calculated within the model may be output throughout the simulation; this measure is defined as the mean value of the variable over all unique[5] Gauss points within the body of the mesh. Hence, this measure is global in nature and may avoid issues related to determining post hoc the contributions made by each strain component to the total strain measure.

The calculation of the *Gauss point mean* (GPM) value is intended to approximate a simple volume-averaging procedure. Thus, for this approximation to be accurate, the Gauss points should be approximately evenly spaced throughout the volume occupied by the FE mesh. This is easily achievable for most simple problems. However, for more complex shapes, it may be necessary to calculate a weighted mean value to account for differences in volume associated with each Gauss point.

Specifically, it may be noted that a Gauss point mean value of a variable shall not be representative of the volume-averaged value of the variable if a mesh of uniform 2D elements is used with axisymmetric geometrical constraints to represent a 3D cylindrical body. This is due to the shape of the 3D body approximated by the mesh; Gauss points at a large distance from the central axis of the cylinder 'represent' a

[5] The term *unique* is used here as boundary elements may sometimes occupy the same space as body elements. Thus, uniqueness is required to avoid double counting.

greater volume than those at a shorter distance. Thus, a weighted mean would certainly be desirable for this example.

However, in tests, when the GPM values of total strain are compared to those calculated from nodal displacement values (i.e. the most accurate technique that would otherwise be applied), results obtained for axisymmetric simulations of cylindrical concrete specimens in typical conditions of heating and loading show that the accuracy of the (unweighted) GPM measure is very good. Moreover, GPM measures of each of the hygro-thermal state variables are found to be near identical to those calculated directly using nodal values and the GPM measures of each of the strain components are consistent with the GPM measure of total strain, i.e. the following equation is found to be satisfied to a high degree of accuracy.

$$\varepsilon_{tot}^{GPM} = \varepsilon_{el}^{GPM} + \varepsilon_{th}^{GPM} + \varepsilon_{cr}^{GPM} + \varepsilon_{tr}^{GPM} \qquad \text{Equation 3-78}$$

where ε_{tot}^{GPM}, ε_{el}^{GPM}, ε_{th}^{GPM}, ε_{cr}^{GPM}, and ε_{tr}^{GPM} are the GPM measures of total strain, elastic strain, thermal strain, basic creep, and transient strain respectively.

Chapter 4. Analytical review of proposed transient strain models

It was determined in chapter 2 that the lack of objective comparisons of the performances of the existing transient strain models is an issue that should be addressed in this work. In this chapter, each of the existing models for transient strain is examined in turn. In particular, the capacity of the model to reproduce experimental data (either in the form presented in the literature or following any potential modifications identified as necessary by the present author) is the most important consideration in this analysis. Based on a set of explicit criteria, a shortlist of transient strain models for further work is then determined.

Note that a system of nomenclature is here employed in which each model is labelled using the surname of the researcher principally associated with the model. Most often, this is the researcher listed as first author on the publication in which the model is proposed.

4.1 Bažant model

As was discussed in §2.2.1, the transient strain model of Bažant et al. [56] is based on the principle that a change in temperature (or relative humidity) leads to a temporary increase in creep compliance of the cement gel. The presence of an external load during heating, thus, leads to the development of transient strain. In order to examine this transient strain model, a brief description of the basic creep model (named '*microprestress-solidification theory*') developed by Bažant and colleagues over many years [56, 66, 99-108] is necessary.

Within microprestress-solidification theory, the macroscale creep behaviour of CMs is considered to be due to two physical causes on the microscale, intrinsic viscoelasticity of the cement gel and shear slip between layers of cement gel. The resultant contributions of the two different processes to creep are separately modelled and are known as *viscoelastic creep* and *viscous flow creep* respectively. Only the latter creep component contributes to transient strain.

The viscous flow component, caused by shear slip of layers of cement gel, is governed by a rheological-type relation.

$$\dot{\varepsilon}_f(t) = \frac{\psi(t)}{\eta(S_\mu)}\sigma(t) \qquad \text{Equation 4-1}$$

where ψ is a factor that is used to account for the effects of temperature and relative humidity on the *reduced time* parameter[6] and η is a viscosity parameter which is largely dependent on a parameter named *microprestress*, S_μ.

In the framework of this model, transient strain must be caused by a temporary increase in creep rate triggered by a period of increasing temperature. The term in Equation 4-1 that exhibits this behaviour is η, which is modelled as follows.

$$\frac{1}{\eta(S_\mu)} = cbS_\mu^{b-1} \qquad \text{Equation 4-2}$$

where c and b are free parameters of the model. The value of b consistently found to most adequately reproduce the basic creep experimental data is 2.0. The value of c is found to vary between data sets simulated in the range 1.0×10^{-8}– $3.0 \times 10^{-8} MPa^{-1} day^{-1}$ [56].

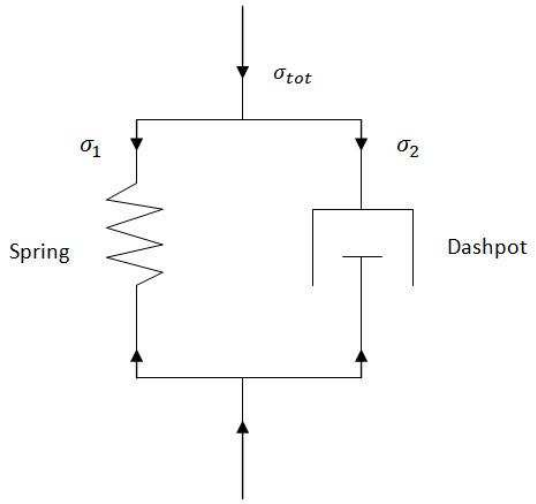

Figure 4-1: A Kelvin-Voigt-type rheological model.

Microprestress is a volume-averaged scalar measure of internal stresses proposed by the authors [56] to represent the net effect of stresses on the internal solid-fluid interfacial area due to various hygro-thermo-mechanical phenomena (i.e. capillary

[6] This parameter is used by the authors to account for the effects of experimental conditions on the rate of bond breakages and restorations on the microstructural level which can have a considerable effect on the creep rate.

tension, surface energy, disjoining pressure, and crystal growth pressure). According to the model, microprestress alters the energy required for shear slip to take place such that an increased value of S_μ leads to more compliant viscous flow creep behaviour. Therefore, as shown in Equation 4-2, η decreases with increasing S_μ.

Mathematically, the evolution of S_μ is assumed to be governed by a Kelvin-Voigt-type rheological model, an example of which is shown in figure 4-1. The well-known governing equation of a model such as this is given by the following.

$$\dot{\sigma}_2 + \frac{K_{K-V}}{\eta_{K-V}}\sigma_2 = \dot{\sigma}_{tot} \qquad \text{Equation 4-3}$$

where σ_{tot} and σ_2 are the overall stress applied to the rheological model and the stress transmitted through the dashpot respectively, and K_{K-V} and η_{K-V} are the spring constant and the dashpot viscosity respectively. According to the Bažant model, η_{K-V} is dependent on σ_2 in an identical manner to the dependence of η on S_μ. Also, the presence of the rate term, $\dot{\sigma}_{tot}$ and $\dot{\sigma}_2$, lead to the inclusion of a factor to account for the reduced time, as in Equation 4-1. Hence, Equation 4-3 can be rewritten as follows.

$$\dot{\sigma}_2 + \psi_S(t) c_0 \sigma_2^b = \dot{\sigma}_{tot} \qquad \text{Equation 4-4}$$

where $\psi_S(t)$ is the reduced time factor and c_0 is a dummy parameter included for mathematical brevity. The reduced time factor is defined as follows.

$$\psi_S(t) \equiv exp\left[\frac{Q_S}{R}\left(\frac{1}{T_0} - \frac{1}{T}\right)\right] \qquad \text{Equation 4-5}$$

where Q_S and R are the activation energy associated with the microprestress evolution process and the gas constant respectively; the value of the ratio term involving these terms suggested by Bažant et al. is $3000K$ [56]. The factor c_0 of Equation 4-4 is defined by the following.

$$c_0 = cbk \qquad \text{Equation 4-6}$$

Though the application of Equations 4-4—4-6 to reproduce the governing equation of S_μ is not explicitly explained by Bažant et al. [56], the model presented by the authors may be reproduced if it is assumed that σ_{tot} represents a measure of the total stress

imposed on the solid cement gel material by the various hygro-thermo-mechanical processes and σ_2 is equivalent to S_μ. Thus, an equation for the evolution of S_μ requires the mathematical description of the term $\dot{\sigma}_{tot}$.

The authors assume that σ_{tot}, which is a measure of the stress imposed on the cement gel due to the hygro-thermo-mechanical phenomena, is dependent on T and h in a manner identical to the Kelvin equation [56]. Therefore, $\dot{\sigma}_{tot}$ can be described as follows.

$$\dot{\sigma}_{tot} = -k_1\left(\dot{T}\ln h + T\frac{\dot{h}}{h}\right) \qquad \text{Equation 4-7}$$

where k_1 is a free parameter that accounts for the parameters of the Kelvin equation and any scaling parameters that may be present. Initially, the authors considered direct substitution of Equation 4-7 into Equation 4-4 to fully define the evolution of S_μ. The resultant model would predict an increasing value of S_μ in conditions of heating or drying (and increased $\dot{\varepsilon}_f$). However, cooling or wetting conditions would lead to a rapidly decreasing value of S_μ (and decreased $\dot{\varepsilon}_f$, as well as possible transient strain recovery). The authors [56] considered this to be inconsistent with their interpretation of transient strain in which cooling or wetting leads to a short-term decrease in $\dot{\varepsilon}_f$ (due to 'deactivation of creep sites'), and a long-term increase in $\dot{\varepsilon}_f$ (due to the formation of new creep sites in different locations, at which S_μ is large in magnitude and opposite in sign to that prior to cooling). Therefore, the authors proposed an amendment to Equation 4-7.

$$\dot{\sigma}_{tot} = k_1\left|\dot{T}\ln h + T\frac{\dot{h}}{h}\right| \qquad \text{Equation 4-8}$$

As can be seen from Equation 4-8, $\dot{\sigma}_{tot}$ is assumed to depend on the absolute value of the hygro-thermal terms derived from the Kelvin equation. Thus, cooling leads to broadly the same effects on $\dot{\varepsilon}_f$as heating. The original authors accept that this model does not fully behave as intended (as the initial period of $\dot{\varepsilon}_f$ decrease due to cooling cannot occur), though consider Equation 4-8 to be more realistic than Equation 4-7. It is clear however that the motivation for the definition of Equation 4-7 is not consistent with the subsequent modification of Equation 4-8. Thus, application of Equation 4-8

cannot be considered to be justified by the assumption of Kelvin model behaviour. Instead, use of Equation 4-8 should be considered heuristic.

Substitution of Equation 4-8 into Equation 4-4 gives an equation for the evolution of S_μ.

$$\dot{S}_\mu + \psi_S c_0 S_\mu^2 = k_1 \left| \dot{T} \ln h + T \frac{\dot{h}}{h} \right| \qquad \text{Equation 4-9}$$

where b is set equal to 2 as is consistently suggested to be the most appropriate value in comparisons with experimental data by the authors [56].

In ambient conditions, the closed form solution of Equation 4-9 is given as follows.

$$S_\mu = \left[\frac{1}{S_{\mu,0}} + \psi_s c_0 (t - t_0) \right]^{-1} \qquad \text{Equation 4-10}$$

where $S_{\mu,0}$ is the value of the microprestress variable at the initial time t_0. Thus, in conditions of ambient temperature, S_μ (and, thus, also $\dot{\varepsilon}_f$) decays in time monotonically, with a characteristic rate of decrease of microprestress dependent on material parameters and temperature.

For general temperature and relative humidity histories, numerical integration is necessary to calculate the evolution of S_μ. However, if it is assumed that $S_\mu = S_{\mu,\infty}$, the limiting value of S_μ, when $\dot{S}_\mu = 0$, the general evolution of S_μ can be determined. Substitution of these values into Equation 4-9 yields the following.

$$S_{\mu,\infty} = \sqrt{\frac{k_1 \left| \dot{T} \ln h + T \frac{\dot{h}}{h} \right|}{\psi_s c_0}} \qquad \text{Equation 4-11}$$

It can easily be seen by substitution into Equation 4-9 that if $S_\mu < S_{\mu,\infty}$, $\dot{S}_\mu > 0$, while if $S_\mu > S_{\mu,\infty}$, $\dot{S}_\mu < 0$. Thus, it is clear that $S_\mu \to S_{\mu,\infty}$ for all times, such that $S_{\mu,\infty}$ may be referred to as the '*ultimate microprestress*'. Therefore, for instance, if idealised constant rates of heating and of drying, say, are maintained for a sufficiently long period, microprestress tends towards a positive finite constant. This behaviour is confirmed by numerical integration of Equation 4-9. An example calculation, using

typical values for the material parameters as given by Bažant et al. [56], for three different temperature histories is illustrated in figures 4-2 (a) and (b).

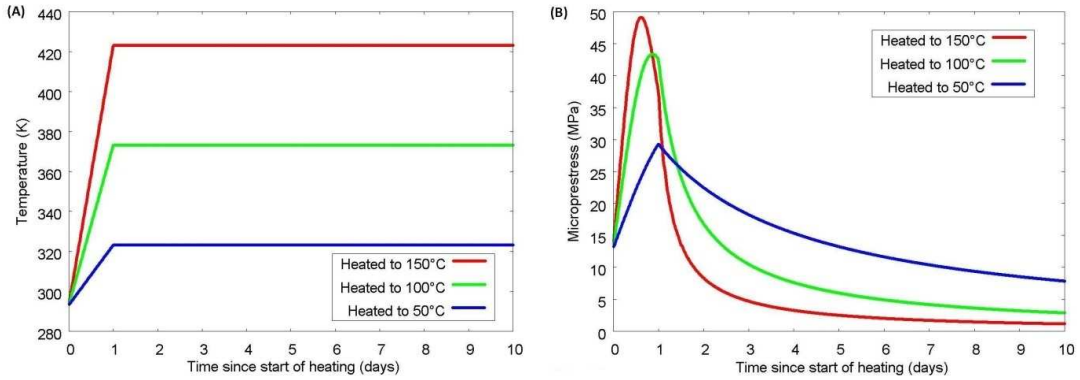

Figure 4-2: Representations of the simulated evolution of (a) temperature and (b) microprestress of concrete specimens in three sets of heating conditions.

Figure 4-2 (b) gives a general idea of the nature of the evolution of S_μ in conditions of changing temperature, albeit in idealised conditions. The results show that, unsurprisingly, the greater the temperature increase, the higher is the increase in S_μ (and the rate of subsequent decrease in S_μ). The time at which S_μ begins to decrease is not shown clearly in figure 4-2 (b) but decreases slightly with increased rate of heating.

Similar results can be shown for a drying specimen. For the purpose of observing the effects of a decreasing relative humidity on the microprestress, it is assumed that relative humidity can be represented using an exponential decay function.

$$(\Delta h)_n = \alpha_{RH}\left(h_{n+1/2} - h_{lim}\right)(\Delta t)_n \qquad \text{Equation 4-12}$$

where α_{RH} is a scaling parameter, h_{lim} is the final relative humidity of the dried specimen, Δt is the quantity of time over which the relative humidity changes by Δh, and the subscripts refer to the timestep value.

The evolution of h described by Equation 4-12 is shown in figure 4-3 (a) (where the initial value of h is 0.8 and the value of α_{RH} is $-1.07 \times 10^{-6} s^{-1}$). The subsequent evolution of S_μ in these conditions is shown in figure 4-3 (b).

The results of figure 4-3 (b) contrast with those of figure 4-2 (b) in that the conditions that result in the largest increase in S_μ do not also lead to a more rapid subsequent decrease in S_μ. Aside from this, the results are broadly similar.

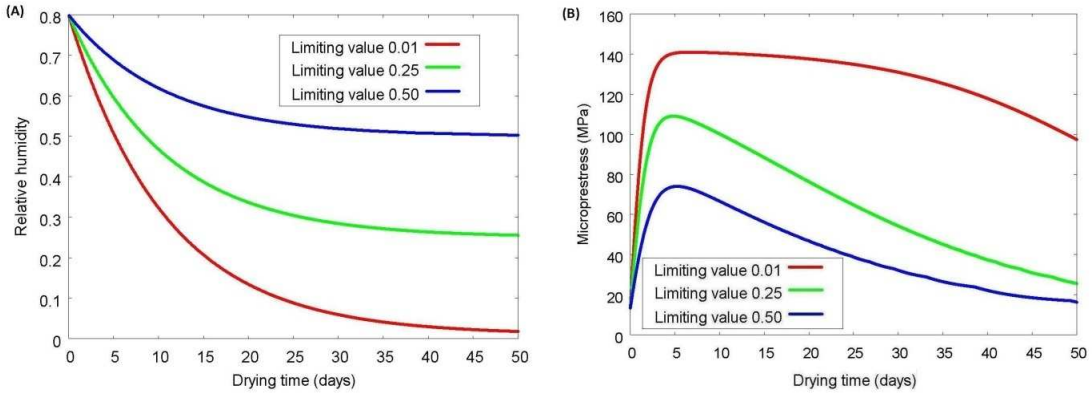

Figure 4-3: Representations of the simulated evolution of (a) pore relative humidity and (b) microprestress of concrete specimens in three sets of drying conditions.

Equation 4-11 largely explains the results of figures 4-2 (b) and 4-3 (b). If the value of $S_{\mu,\infty}$ (defined by Equation 4-11) is plotted, as in figures 4-4 (a) and (b), it can easily be confirmed, from comparison with the results of figures 4-2 (b) and 4-3 (b) respectively, that the variation in $S_{\mu,\infty}$ strongly defines the evolution of the S_{μ}.

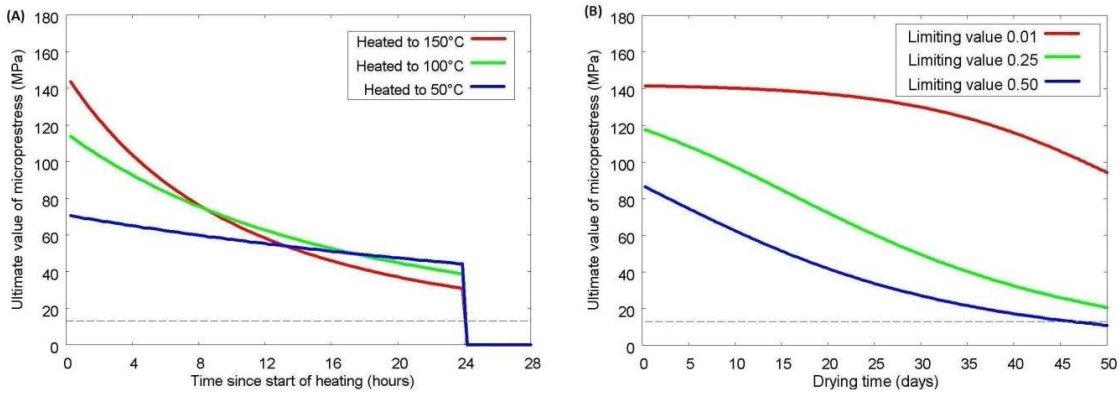

Figure 4-4: The variation in the ultimate microprestress value (as defined by Equation 4-11) with (a) time since start of heating and (b) time since start of drying. Note that the initial value of microprestress is indicated in the graphs by a dashed line.

As shown in figures 4-4 (a) and (b), $S_{\mu,\infty}$ begins at a much higher value than the initial value of S_{μ} (shown as a dashed line in the figures). This leads in all cases to a rapid initial increase in the value of S_{μ}. Subsequently, $S_{\mu,\infty}$ diminishes rapidly for the heated specimens within the first 24 hours (and collapses to zero at 24 hours due to the cessation of heating). This closely matches the evolution of the value of S_{μ} of the heated specimens. Similarly, the initial values of $S_{\mu,\infty}$ for the drying specimens are very similar to those of the heated specimens. However, the value of $S_{\mu,\infty}$ undergoes a much slower subsequent decline in value. This is due to the relatively low value of ψ_s (1.0) throughout and the gradual decay in $\dot{h}$, rather than the corresponding discontinuous transition of $\dot{T}$ to zero for the heating case.

It can be noted from figure 4-4 (a) that even a specimen that is continuously heated shall undergo a phase of decreasing S_μ. Results of simulations generally show that the initial value of $S_{\mu,\infty}$ is strongly influenced by $\dot{T}$, such that a larger value of $\dot{T}$ leads to a larger initial value of $S_{\mu,\infty}$. However, the larger values of T leads to an increase in the value of ψ_S, which causes a more rapid decay of $S_{\mu,\infty}$ (as can be determined from Equation 4-11). As ψ_S is not dependent on h in a similar manner, a comparable increased rate of decay is not observed for rapidly dried specimens.

To account for the simultaneous effects of heating and drying, Equation 4-12 must be modified to account for the effects of T on $\dot{h}$. Temperature is broadly expected to increase the rate of drying and reduce the value of h_{lim}. While this latter effect is ignored here, the former effect is assumed to be governed by an Arrhenius-type factor. Thus, the following relationship between drying rate and temperature is assumed.

$$(\Delta h)_n = \left\{1 + \lambda_{RH} - \lambda_{RH} exp\left[-\frac{Q_{RH}}{R}\left(\frac{1}{T_0} - \frac{1}{T_{n+1/2}}\right)\right]\right\} \alpha_{RH} h_{n+1/2} (\Delta t)_n \qquad \text{Equation 4-13}$$

where Q_{RH} and λ_{RH} are parameters that define the increase in rate of drying caused by a change in temperature.

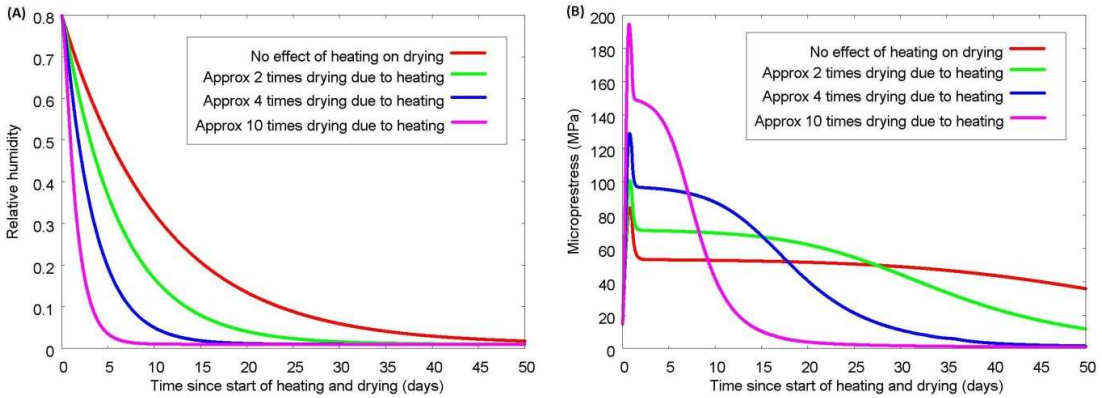

Figure 4-5: Simulations of evolution of (a) relative humidity and (b) microprestress of a specimen heated to 100°C and held at constant temperature thereafter for four different magnitudes of the effect of temperature on rate of drying.

It is highly important, for a more complete analysis of this model, that the temperature and relative humidity histories are each accurately modelled. The results show that the effects of the relative humidity variation on the microprestress evolution are significant. As an example, the dependence of the evolution of microprestress in time for a specimen heated to $100℃$ in one day and subsequently held at constant

temperature is shown in figure 4-5 (b) for several different drying histories represented by the evolution of h in figure 4-5 (a).

As shown in figure 4-5 (b), the effect of the specific drying rate on the evolution of relative humidity in heated conditions is large. Though the curves are qualitatively identical, more rapid drying is found to cause a larger peak and faster subsequent decrease in the evolution of S_μ. Thus, significant differences in transient strain magnitude and rate of development may be observed.

The general shape of the evolution of S_μ suggested in figure 4-5 (b) is clearly strongly influenced by that due to the heating alone and that due to the drying alone (viz. figures 4-2 (b) and 4-3(b) respectively). The effects of temperature on drying serve to increase the rate of decrease of S_μ in the period of time after heating has ceased. This general shape is to be expected for all cases of heating and drying, though the magnitude of the initial 'spike' in S_μ is dependent on the initial value of $\dot{T}$. The effects of heating alone should in most cases dominate the period in which heating occurs with dominance of the effects of drying in the subsequent period of time. As microprestress leads to transient strain effects in conditions of changing temperature and relative humidity, the Bažant model appears to suggest that an increased period of development of transient strain is necessary in the low temperature range.

Despite the nature of this model, which is not written to produce separate components of transient strain and (the remainder of) basic creep, it is possible to calculate these separate components. To do this, parallel calculations of the history of S_μ must be made for two concrete specimens in identical conditions, one of which accounts for transient strain effects and the other does not ($k_1 = 0$). The parallel evolutions of the *actual* microprestress and the *hypothetical* microprestress, S_μ^{hyp}, can be separately applied to Equation 4-1 to yield two distinct flow creep histories, ε_f and ε_f^{hyp} respectively. Thus, transient strain is given as follows.

$$\varepsilon_{tr} = \varepsilon_f - \varepsilon_f^{hyp} \qquad \text{Equation 4-14}$$

An example of the evolution of S_μ and S_μ^{hyp} are shown, for instance, in figure 4-6 (a) for the case of a specimen heated to 50°C in one day (and subsequently held at constant temperature) while drying to a relative humidity of 0.50 (λ_{RH} is equal to 3.0).

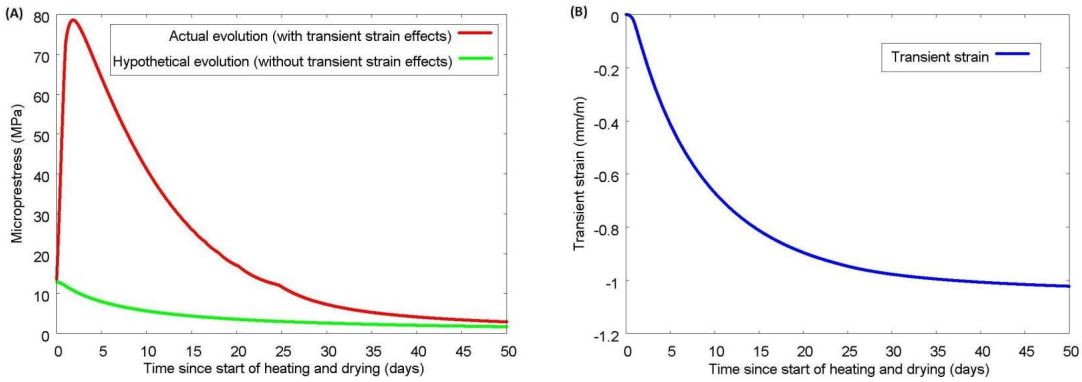

Figure 4-6: Simulations of (a) evolution in time of both microprestress and hypothetical microprestress and (b) resultant transient strain for a specimen linearly heated to 50°C in one day (and subsequently held at constant temperature) while simultaneously dried to 50% relative humidity.

As is clearly shown in figure 4-6 (a), the development of S_μ^{hyp} is very distinct from S_μ in heated conditions. The difference between the microprestress values $S_\mu - S_\mu^{hyp}$ increases to a maximum up to approximately the point at which heating ceases. Subsequently, $S_\mu - S_\mu^{hyp}$ steadily decreases with time until the value is very small after a period of 50 days. At this point, $\dot{\varepsilon}_{tr}$ should be of a negligible value. This is observed in the evolution of ε_{tr}, as seen in figure 4-6 (b) (where parameters suggested by Bažant et al. [56] are used). Some results suggest that full development of ε_{tr} generally occurs within 30 days from the start of heating [13, 14, 16, 18, 30], whereas some researchers assume that a rapid (near instantaneous) development of ε_{tr} is a good approximation of experimental results [9, 34, 39, 89]. It is clear from the application of the Bažant model that this model has the potential to qualitatively match the former sets of observations, while predictions of rapid development of ε_{tr} may require modifications of model parameters.

According to the Bažant model, a majority of the component of ε_{tr} that develops due to an increase in temperature occurs after the temperature has been reached by the specimen. Therefore, to examine the Bažant model output, it is necessary to allow ε_{tr} to reach the limiting value by holding temperature constant until $\dot{\varepsilon}_{tr} = 0$.

As already stated, results indicate that a more intense early peak in S_μ and a subsequent rapid decline are generally found to occur for more rapidly heated

specimens when compared with more slowly heated specimens. It is unclear how this affects the development of ε_{tr} however. Figures 4-7 (a)–(d) show the evolution of ε_{tr} for specimens heated to the same temperature at different rates.

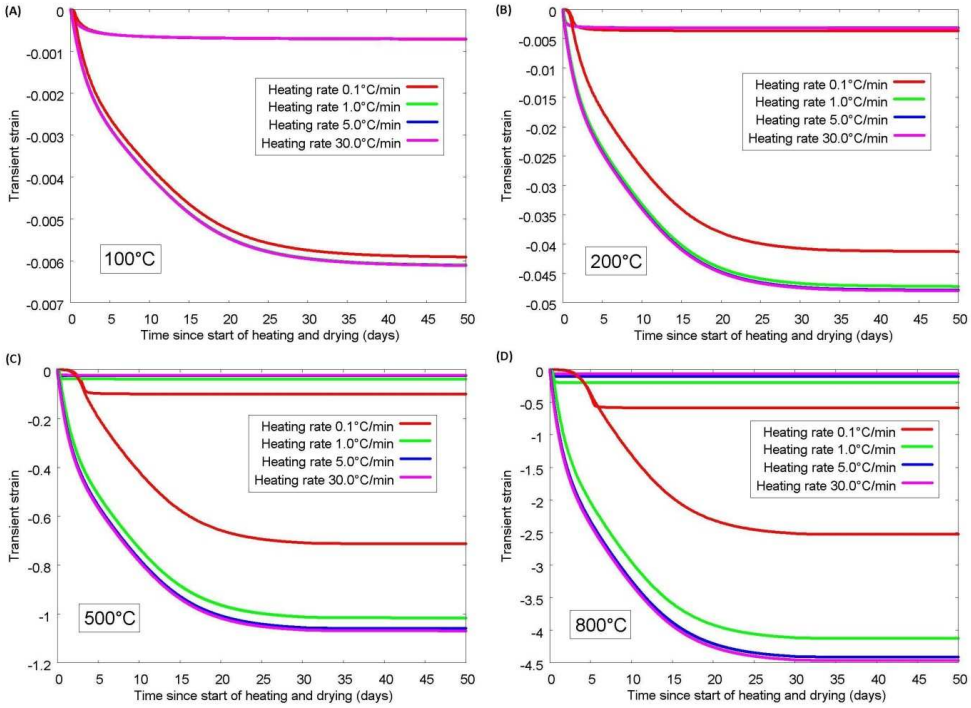

Figure 4-7: Simulated results showing the transient strain that develops for specimens heated to (a) 100°C, (b) 200°C, (c) 500°C, and (d) 800°C. Two sets of results are shown in the graphs, one set in which no drying is allowed and another in which the specimens are simultaneously dried to a relative humidity of 0.01.

Several observations can be made based on these results.

- The final value of ε_{tr} is reached within about 30 days of the start of heating. The non-drying specimens reach the final value very much faster than the drying specimens.
- Different heating rates generally cause only slight variation in the final value of ε_{tr}. In comparison to the large changes in heating rate, these differences are relatively small.
- The difference in final ε_{tr} value induced by different heating rates appears to depend strongly on whether drying is allowed. If no drying is allowed, a larger heating rate leads to lower final ε_{tr}. The reverse is observed in drying conditions.
- The final value of ε_{tr} in drying conditions is found to be approximately an order of magnitude larger than that which develops in non-drying conditions.

- The model predicts ε_{tr} of approximately correct magnitudes for lower temperatures but appears to vastly overestimate ε_{tr} for higher temperatures, even exceeding unity in some cases.

4.2 Anderberg model

The Anderberg model posits that the temperature-dependences of transient strain and thermal strain are identical [9]. As the load-dependence of the model is linear, no original mathematical functions are necessary to describe transient strain in the framework of this model. This may be a significant reason that the Anderberg model is relatively popular [109-112].

The Anderberg model is defined by the following.

$$\dot{\boldsymbol{\varepsilon}}_{tr} = \Gamma \boldsymbol{Q} : \boldsymbol{\sigma} \dot{T} \qquad \text{Equation 4-15}$$

where Γ is a temperature-dependent function and $\boldsymbol{Q}$ is the tensor that defines the multiaxial nature of transient strain behaviour (isotropy is assumed by the authors, with a value of 0.28 found to be approximately consistent with experimental data [9, 33]).

In the formulation of the Anderberg model, it is assumed that the temperature-dependence of transient strain is identical to that of thermal strain. Thus, Γ is defined as follows.

$$\Gamma = \frac{\beta_A}{f_c(T_0)} \frac{\partial \varepsilon_{th}}{\partial T} \qquad \text{Equation 4-16}$$

where β_A is a free parameter of the model, assumed to be independent of temperature. The factor of f_c is included to normalise the load level, as is typical in transient strain modelling. Substitution of Equation 4-16 into Equation 4-15 gives the final form of the Anderberg model.

$$\dot{\boldsymbol{\varepsilon}}_{tr} = \frac{\beta_A}{f_c(T_0)} \frac{\partial \varepsilon_{th}}{\partial T} \boldsymbol{Q} : \boldsymbol{\sigma} \dot{T} \qquad \text{Equation 4-17}$$

Anderberg and Thelandersson [9, 33] found that a value of 2.35 for β_A produces results that correspond reasonably well to available experimental data on siliceous

concrete specimens loaded in uniaxial and biaxial compression, while a value of 2.36 was found more suitable in another study [109]. Anderberg and Thelandersson [9] also reported that a value of 2.00 is appropriate for the experimental data of another investigation [113].

As discussed in §2.3.1, the model, as defined by Equation 4-17, appears to be best suited to modelling concrete transient strain behaviour in the low temperature range. An increase in the magnitude of $\frac{\partial \varepsilon_{tr}}{\partial T}$ is observed for temperatures larger than about 450℃ that is not reproduced by application of Equation 4-17. Evidently, this is because a comparable increase in $\frac{\partial \varepsilon_{th}}{\partial T}$ is not observed to take place in this temperature range.

Therefore, in order to address this issue, Equation 4-15 may be modified such that a discontinuous change in the value of Γ occurs at a transition temperature, given as 550℃ [32].

$$\Gamma = \begin{cases} \dfrac{\beta_A}{f_c(T_0)} \dfrac{\partial \varepsilon_{th}}{\partial T} , & T \leq 550℃ \\ \dfrac{\mathrm{B}_A}{f_c(T_0)} , & T > 550℃ \end{cases} \qquad \text{Equation 4-18}$$

where B_A is a free parameter found to have a value of 1.0×10^{-4} [32]. Thus, Equation 4-17 must be rewritten as follows.

$$\dot{\boldsymbol{\varepsilon}}_{tr} = \begin{cases} \dfrac{\beta_A}{f_c(T_0)} \dfrac{\partial \varepsilon_{th}}{\partial T} \boldsymbol{Q} : \boldsymbol{\sigma} \dot{T} , & T \leq 550℃ \\ \dfrac{\mathrm{B}_A}{f_c(T_0)} \boldsymbol{Q} : \boldsymbol{\sigma} \dot{T} , & T > 550℃ \end{cases} \qquad \text{Equation 4-19}$$

Thus, at the transition temperature, the relationship between ε_{tr} and T becomes linear. It is unclear from Equation 4-19 whether this will lead to a discontinuous change in $\frac{\partial \varepsilon_{tr}}{\partial T}$ sufficient to improve model behaviour in the high temperature range. By comparison of the predictions of Equations 4-17 and 4-19 in the range $T > 550$℃ for a range of different empirical models for ε_{th} (and the values of β_A and B_A provided in the literature), it is found that, in all cases examined, Equation 4-19 results in a marked increase in ε_{tr} in the range $T > 550$℃, compared to that found through use of Equation 4-17. As an example of this is illustrated in figures 4-8 (a) and (b), which

shows the evolution of ε_{tr} calculated using Equation 4-17 ('*original*') and using Equation 4-19 ('*modified*') using as input two different empirical models for ε_{th} that were proposed in the literature to represent concrete types containing siliceous aggregates and carbonate aggregates respectively [114].

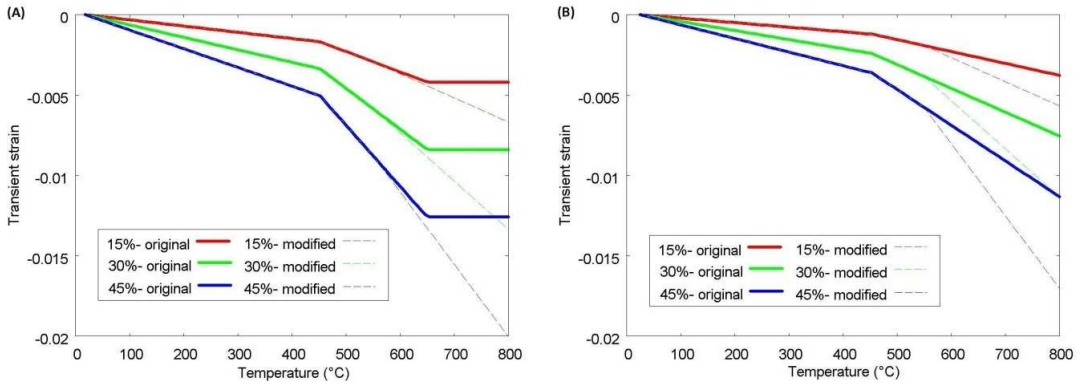

Figure 4-8: Transient strain history at three different uniaxial load levels (as percentage of initial value of f_c) calculated using both Equation 4-17 ('original') and Equation 4-19 ('modified') for concrete containing (a) siliceous aggregates and (b) carbonate aggregates.

The results of figures 4-8 (a) and (b) show that Equation 4-19 results in a more rapid development of ε_{tr} in the high temperature range than that produced by Equation 4-17. As this is qualitatively more consistent with experimental observations, the form of the Anderberg model defined by Equation 4-19 should be retained for the remainder of this work.

As it is well known that ε_{th} is strongly dependent on the nature of the aggregates present in concrete, use of the Anderberg model suggests that the magnitude of ε_{tr} must be similarly related to the nature of the aggregates. However, this is counter to observations which suggest that transient strain is seated in the cement paste and that the role of the aggregates is one of restraint only (§2.1.1). Thus, the Anderberg model must be considered to be in disagreement with experimental observations.

In addition, LITS can be shown to obey a master curve for temperatures below about 450°C (§2.1.1), whereas no similar observation has ever been made for ε_{th}. Thus, the value of β_A must vary between different concrete types. It is a fairly severe weakness of the Anderberg model that the model parameters must be calibrated for application to different concrete types, though model output should remain broadly consistent.

4.3 Gawin model

The *Gawin model* is a model in which the development of transient strain is linked to thermo-chemical damage [87]. This relationship is based on similarities of the conditions in which the two phenomena are found to develop and a perceived similarity of the development of ε_{tr} and the strain component that is proposed to develop directly as a result of this damage, the thermo-chemical strain, ε_{tc}.

The increment of transient strain may be expressed in terms of the increment of thermo-chemical damage parameter, $\Delta\chi$, as follows.

$$\Delta\boldsymbol{\varepsilon}_{tr} = \beta_G \frac{\Delta\chi}{f_c(T_0)} \boldsymbol{Q} : \tilde{\boldsymbol{\sigma}} \qquad \text{Equation 4-20}$$

where β_G is a function of χ defined as follows.

$$\beta_G = \frac{\partial \bar{\varepsilon}_{tr}(\chi)}{\partial \chi} \qquad \text{Equation 4-21}$$

where $\bar{\varepsilon}_{tr}$ is (axial) transient strain normalised by load. $\tilde{\boldsymbol{\sigma}}$ is the effective stress measure defined as follows.

$$\tilde{\boldsymbol{\sigma}} = \frac{1}{(1-\omega)(1-\chi)} (\boldsymbol{\sigma} + \alpha_B \mathrm{X}_s^{ws} p_s \boldsymbol{I}) \qquad \text{Equation 4-22}$$

where α_B is Biot's coefficient, X_s^{ws} is the fraction of the internal concrete surface in contact with the pore water phase, $\boldsymbol{I}$ is the identity tensor, and p_s is the solid phase pressure (the pressure applied to the internal surface of the concrete by the pore fluids).

The original authors explicitly define all softening that occurs in unloaded heating conditions as due to the development of χ. Thus, χ is given by the following.

$$\chi(T) = 1 - \frac{E_0(T)}{E_0(T_0)} \qquad \text{Equation 4-23}$$

where $E_0(T)$ is the elastic modulus of a concrete specimen heated to temperature T in unloaded conditions.

As already stated, one of the motivations for the Gawin model is that the conditions in which both χ and ε_{tr} increase in value are identical. Thus, application of Equation 4-20 requires no further explicit assumptions regarding conditions in which ε_{tr} development occurs, which is advantageous. Moreover, if subsequent research into phenomena, such as stiffness recovery, demonstrates conditions in which this model can be tested, this model has the potential to predict the development of ε_{tr} in non-virgin heating conditions, which would be a significant achievement.

One potential implication of this formulation here identified is that experimental evidence suggests that χ is dependent on the magnitude of preload present during heating [3, 34, 39, 52, 115]. Thus, this suggests that Equation 4-23 should be modified to account for this load-dependence. However, this may have significant consequences for the Gawin model output, potentially introducing a significantly nonlinear load-dependence.

The original authors present results that indicate that β_G is piecewise in value, such that ε_{tr} is a bilinear function of χ, with the transition occurring at a value of χ of 0.55 [87]. Moreover, a similar bilinear relationship is found to exist between ε_{tc} and χ, where the bilinear transition also occurs at a value of χ of 0.55. These results, reproduced in figure 4-9, are considered by the original authors to demonstrate that there is a direct link between the underlying mechanisms that lead to both ε_{tc} and ε_{tr}.

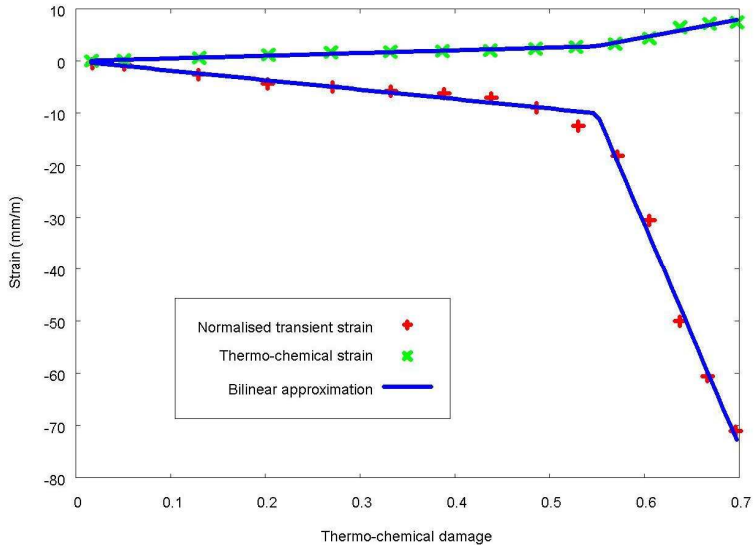

Figure 4-9: Comparison of the evolutions of normalised transient strain and the thermo-chemical strain calculated from experimental data [87]. Also shown are bilinear functions calibrated to these data.

To properly evaluate the results shown in figure 4-9, the derivation of ε_{tc} should be analysed. When a concrete specimen is heated in unloaded conditions, the total strain is considered by the original authors to be made up of the following strain components.

$$\boldsymbol{\varepsilon}_{tot} = \boldsymbol{\varepsilon}_{FTS} + \boldsymbol{\varepsilon}_{sh} + \boldsymbol{\varepsilon}_{tc} \qquad \text{Equation 4-24}$$

where $\boldsymbol{\varepsilon}_{FTS}$ and $\boldsymbol{\varepsilon}_{sh}$ are free thermal strain and drying shrinkage respectively.

$\boldsymbol{\varepsilon}_{FTS}$ is determined using experimental results obtained on a cooling concrete specimen. It is assumed that this is the only strain component that is reversible. The contribution of $\boldsymbol{\varepsilon}_{sh}$ is calculated using a poromechanical model, defined as follows.

$$\mathrm{d}\boldsymbol{\varepsilon}_{sh} = \frac{\alpha_B(\mathrm{X}_s^{ws}\mathrm{d}p_s + \mathrm{d}\mathrm{X}_s^{ws}p_s)}{(1-\omega)(1-\chi)K(T_0)}\boldsymbol{I} \qquad \text{Equation 4-25}$$

where $K(T_0)$ is the bulk modulus of the concrete evaluated at temperature T_0.

Due principally to considerable uncertainty in the evaluation of X_s^{ws}, particularly in temperature-dependence, it is extremely difficult to calibrate Equation 4-25 to experimental data. Therefore, significant uncertainty must exist in the determination of $\boldsymbol{\varepsilon}_{sh}$. Consequently, $\boldsymbol{\varepsilon}_{tc}$ must also be uncertain as it is calculated by the rearranged form of Equation 4-24.

$$\boldsymbol{\varepsilon}_{tc} = \boldsymbol{\varepsilon}_{tot} - \boldsymbol{\varepsilon}_{FTS} - \boldsymbol{\varepsilon}_{sh} \qquad \text{Equation 4-26}$$

Therefore, it cannot be strongly asserted that the relationships shown in figure 4-10 are evidence for the validity of the assumptions of this model as the data reported for $\boldsymbol{\varepsilon}_{tc}$ may be unreliable.

It is questionable whether the concept of a normalised transient strain parameter is valid for this model due to the explicit use of the effective stress, $\widetilde{\boldsymbol{\sigma}}$, in the calculations. As the value of $\widetilde{\boldsymbol{\sigma}}$ in any normal direction may fluctuate significantly during a heating test, the assumption of a linear relationship between ε_{tr} and σ that is assumed in evaluating $\bar{\varepsilon}_{tr}$ may be unreliable.

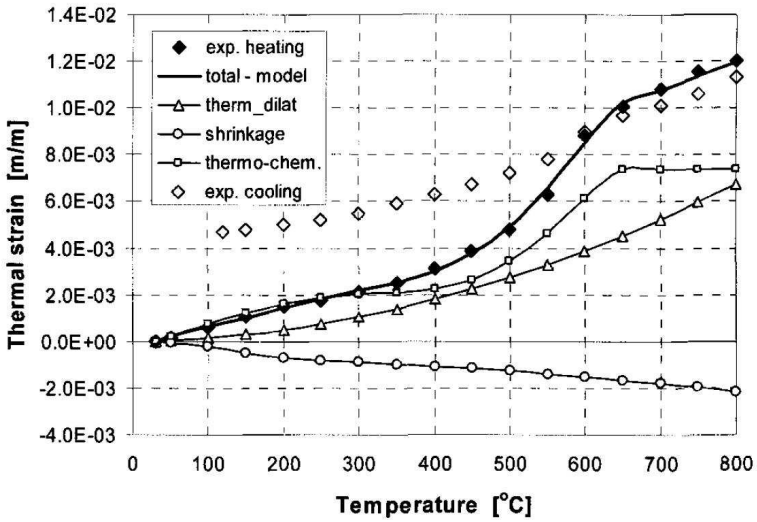

Figure 4-10: Comparison of the thermal strain data and the proposed strain decomposition of the authors [87].

No explicit indication of the deviation between $\tilde{\sigma}$ and σ is explicitly provided by the original authors. However, according to the model proposed, $d\tilde{\sigma} - d\sigma$ is the direct cause of ε_{sh}. Thus, since the original authors suggest that complete drying leads to a final value of ε_{sh} of between 400 and 500×10^{-6} [87], it can be calculated that this corresponds to a final value of $d\tilde{\sigma} - d\sigma$ of around 20% of the initial value of f_c. When accounting for the magnification caused by the increase in χ due to heating, this final value of ε_{sh} can easily be shown to be approximately consistent with that shown in figure 4-10. Therefore, a comparable increase in $d\tilde{\sigma} - d\sigma$ can be deduced to have taken place during heating. Due to the magnitude of this value, it is clear that the evaluation of $\bar{\varepsilon}_{tr}$ is likely to be very unreliable.

Furthermore, it may also be noted that this considerable increase in $\tilde{\sigma}$ during heating should also result in the development of ε_{tr}, even though no load is externally applied. That no such component is represented in the results of figure 4-10 suggests that Equation 4-20 is not applied to produce the results of figure 4-10. Instead, it is likely that the strain components are calculated directly using the equations (without use of, say, a FE model). Thus, it may be suggested that this practice may have caused inaccuracy in model derivation. Also, the evaluation of ε_{tc} from experimental data must be considered to be unreliable and, therefore, observations of similarities between ε_{tc} and ε_{tr} should be re-examined.

4.4 Sabeur model

According to the Sabeur model, transient strain is made up of two distinct strain components, drying creep [116] and '*dehydration creep*' [46, 64].

$$\dot{\boldsymbol{\varepsilon}}_{tr} = \dot{\boldsymbol{\varepsilon}}_{dc} + \dot{\boldsymbol{\varepsilon}}_{hc} \qquad \text{Equation 4-27}$$

where $\boldsymbol{\varepsilon}_{dc}$ and $\boldsymbol{\varepsilon}_{hc}$ are drying creep and dehydration creep respectively.

Since it is widely believed that $\boldsymbol{\varepsilon}_{tr}$ is composed of $\boldsymbol{\varepsilon}_{dc}$ and $\boldsymbol{\varepsilon}_{TTC}$, it can be concluded that ε_{hc} is equivalent to ε_{TTC}. Moreover, while it is commonly acknowledged that $\boldsymbol{\varepsilon}_{tr}$ may be decomposed in such a manner, it is rare that this decomposition is reflected explicitly in applied models.

According to the Sabeur model, $\boldsymbol{\varepsilon}_{dc}$ and $\boldsymbol{\varepsilon}_{hc}$ are active in neighbouring but distinct temperature regimes, such that the mathematical description of ε_{tr} is effectively piecewise, increasing as $\boldsymbol{\varepsilon}_{dc}$ for $T \leq 105℃$ and as $\boldsymbol{\varepsilon}_{hc}$ for $T > 105℃$. This model assumption is very convenient as experimental data can easily be examined to identify the contributions of $\boldsymbol{\varepsilon}_{dc}$ and $\boldsymbol{\varepsilon}_{hc}$ to $\boldsymbol{\varepsilon}_{tr}$ for model calibration.

$\boldsymbol{\varepsilon}_{dc}$ is modelled by the original authors using a modified form of the *stress-induced shrinkage* model [66], in which an applied load is assumed to linearly magnify the magnitude of drying shrinkage, $\boldsymbol{\varepsilon}_{sh}$, that develops in drying conditions. This model is expressed as follows.

$$\dot{\boldsymbol{\varepsilon}}_{dc} = \frac{\beta_S^{dc}}{f_c(T_0)} |\dot{h}| \boldsymbol{Q} : \boldsymbol{\sigma} \qquad \text{Equation 4-28}$$

where β_S^{dc} is the free parameter of this model. By calibrating Equation 4-28 to experimental data obtained in the low temperature region ($T \leq 105℃$), a value of approximately $2.7 \times 10^{-3} MPa^{-1}$ is found to be appropriate for β_S^{dc} [64]. The absolute value of $\dot{h}$ is used by the original authors in Equation 4-28 to ensure that $\boldsymbol{\varepsilon}_{dc}$ is irreversible and may also develop during periods of moisture increase (which is at variance with the original stress-induced shrinkage model).

According to the Sabeur model, $\boldsymbol{\varepsilon}_{hc}$ is governed by a similar model to Equation 4-28.

$$\dot{\boldsymbol{\varepsilon}}_{hc} = \mathcal{H}(T - T_{hc0}) \frac{\beta_S^{hc}}{f_c(T_0)} \dot{m}_{dehyd} \boldsymbol{Q} : \boldsymbol{\sigma} \qquad \text{Equation 4-29}$$

where β_S^{hc} is the free parameter of this model, $\mathcal{H}$ is the Heaviside step function, T_{hc0} is the temperature at which the dehydration process begins (105℃), and m_{dehyd} is the mass of dehydrated water, the rate of which is assumed to be given by the following.

$$\dot{m}_{dehyd} = \frac{\langle m_{eq}(T) - m_{dehyd} \rangle}{\tau_{hyd}} \qquad \text{Equation 4-30}$$

where τ_{hyd} is the *dehydration relaxation time*, m_{eq} is the temperature-dependent equilibrium mass of dehydrated water, and Macaulay brackets are applied as defined by the following.

$$\langle x \rangle = \begin{cases} 0, & x < 0 \\ x, & x \geq 0 \end{cases} \qquad \text{Equation 4-31}$$

for any x. The use of Macaulay brackets in Equation 4-30 ensures that $\boldsymbol{\varepsilon}_{hc}$ is irreversible and only increases in magnitude in conditions of virgin heating, consistent with experimental observations.

The original authors explicitly restrict application of the Sabeur model to conditions in which $\sigma_c < 0.4 f_c$[7] and $T \leq 400$℃. These model restrictions are intended to minimise the development of mechanical damage and to avoid issues of uncertainty regarding the effects on the model of the changing nature of the dehydration process for temperatures in the range $T > 400$℃, respectively. While the former concern may be mitigated by use of a sophisticated model to account for mechanical damage (such as that described in §3.3.1), the latter issue may only be addressed by extension of the model into the temperature range $T > 400$℃, which would require further experimental data than provided by the authors and, potentially, development of a novel mathematical model complementary to Equation 4-29.

The governing transient strain model is given by the substitution of Equations 4-28 and 4-29 into Equation 4-27, which gives the following.

[7] Note that σ_c is written to emphasise that compressive loading is intended by the original authors.

$$\dot{\boldsymbol{\varepsilon}}_{tr} = \left(\frac{\beta_S^{dc}}{f_c(T_0)} |\dot{h}| + \frac{\beta_S^{hc}}{f_c(T_0)} \mathcal{H}(T - T_{hc0}) \dot{m}_{dehyd} \right) \boldsymbol{Q} : \boldsymbol{\sigma} \qquad \text{Equation 4-32}$$

Data-fitting shows that, for the concrete specimens used to produce the experimental results presented by the authors [64], β_S^{hc} is may be expressed as a linear function of m_{dehyd}, as follows.

$$\beta_S^{hc} = 7 \times 10^{-3} m_{dehyd} \qquad \text{Equation 4-33}$$

Thus, in order to apply the Sabeur model, it is necessary to determine appropriate empirical temperature functions to describe m_{eq} and τ_{hyd}. Experimental data presented by the original authors [46, 64], shown in figure 4-11 (a), suggest that τ_{hyd} may be considered to be independent of temperature, with a value of 120 minutes found to reproduce experimental results fairly well.

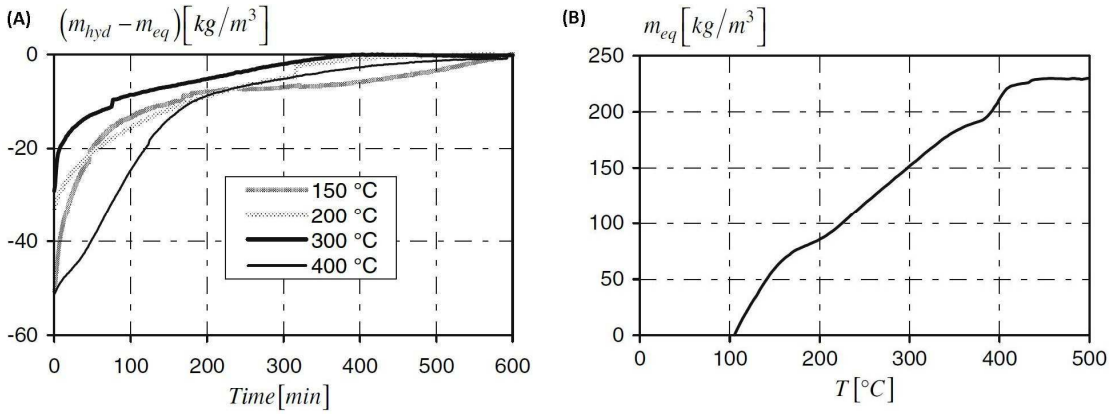

Figure 4-11: (a) The evolution of $m_{dehyd} - m_{eq}$ and (b) the evolution of m_{eq} measured at high temperatures. Note that the value of m_{dehyd} after 600 minutes at high temperature is assumed to be approximately equal to m_{eq} [64].

The temperature function, shown in figure 4-11 (b), is derived from thermogravimetric analysis (TGA) results obtained using cement paste samples heated at $0.2°C/min$. This low heating rate allows sufficient time for the dehydration process to reach equilibrium for high temperatures ($T < 400°C$). The results show that m_{eq} increases relatively steadily in the temperature range $100 - 400°C$ and reaches a plateau for higher temperatures. This is consistent with the suggestion by Parry-Jones et al. [117] that almost all of the water available to the dehydration process is released by the point that a temperature of $450°C$ is reached.

It is unclear if the authors use a temperature function to represent $m_{eq}(T)$ or if direct interpolation of the results of figure 4-11 (b). However, based on inspection of the data, it is here proposed that superimposition of three distinct temperature functions represent the data very well. The model used to fit the experimental data is defined as follows.

$$m_{eq} = \sum_{i=0}^{2} M_i \tanh[p_i(T - T_i)] \qquad \text{Equation 4-34}$$

where M_i, p_i, and T_i are free parameters of the model. Calibration of Equation 4-34 to the experimental data produces the results shown in figure 4-12 (a), with the decomposed functions demonstrated in figure 4-12 (b).

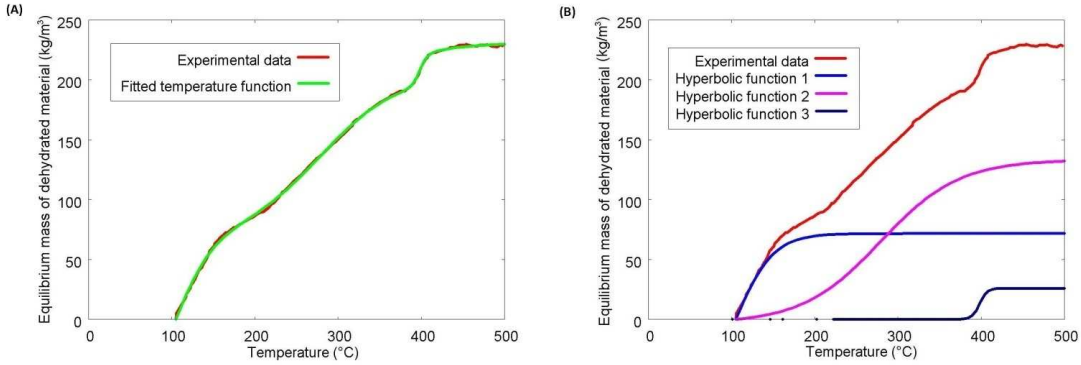

Figure 4-12: (a) The fitted temperature function, defined by Equation 4-34, for m_{eq} and (b) the decomposed functions of Equation 4-34.

It is possible to speculate that the good fit provided by calibration of Equation 4-34 to the experimental data reflects the underlying chemical processes. Dehydration is an extremely complex process, broadly consisting of the removal of chemically bound water from the many chemical species of cement paste. The dehydration of C-S-H is thought to be the dominant process in the temperature range of figure 4-12 (a). However, there are thought to be several metastable states in which C-S-H can exist during dehydration. The results of figures 4-12 (a) and (b) may be speculated to indicate that there are three such dominant states. However, a study of the chemistry of the dehydration process is beyond the scope of this work.

According to the Sabeur model, no decrease in m_{dehyd} may occur. This constraint is included due to the absence of a reliable model for rehydration and, thus, to prevent the development of ε_{tr} in conditions of cooling (and during the subsequent post-

cooling period). Thus, research into the rehydration of cement paste would be extremely useful as the subsequent predictions of the Sabeur model in conditions of (non-virgin) re-heating would be potentially of great interest to the research field.

The Sabeur model may be applied to conditions in which a concrete specimen that is submerged in water is heated in the temperature range $T < 100$℃. According to the model defined by Equation 4-32, absolutely no transient strain should develop in these conditions. However, this result disagrees with experimental observations, which suggest that some transient strain does develop in these conditions [13, 16, 18]. Therefore, it must be noted that this model is not fully consistent with experimental observations at present, though future model developments may address this issue.

4.5 Terro model

The *Terro model* is a mathematical model in which LITS is modelled using a fitted polynomial temperature function [39, 88]. As it is explicitly based on experimental data for LITS, it is a LITS model, rather than a transient strain model [17].

The Terro model is defined as the product of three separate functions as follows.

$$\varepsilon_{LITS}(T, \sigma, V_a) = \varepsilon_{LITS}^{V_a} \varepsilon_{LITS}^{\sigma} \varepsilon_{LITS}^{T} \qquad \text{Equation 4-35}$$

where $\varepsilon_{LITS}^{V_a}$, $\varepsilon_{LITS}^{\sigma}$, and ε_{LITS}^{T} are the functions that define the aggregate content-dependence, load-dependence, and temperature-dependence of the Terro model respectively.

LITS temperature-dependence is found to be well described if ε_{LITS}^{T} is expressed as a polynomial of fourth-order in temperature (in ℃). The following equation for ε_{LITS}^{T} is fitted to LITS experimental data for concrete specimens of $V_a = 0.65$ (where V_a is aggregate content by volume) and $\sigma = -0.3 f_c$, in the temperature range $20 – 590$℃ [17].

$$\varepsilon_{LITS}^{T} = (A_0 + A_1 T + A_2 T^2 + A_3 T^3 + A_4 T^4) \times -10^{-6} \qquad \text{Equation 4-36}$$

where A_0, A_1, A_2, A_3, and A_4 are model coefficients, given as -43.87, 2.73℃$^{-1}$, 6.35×10^{-2}℃$^{-2}$, -2.19×10^{-4}℃$^{-3}$, and 2.77×10^{-7}℃$^{-4}$ respectively. Equation 4-

36 must be modified if Thames river gravel is used due to divergent LITS behaviour (the aggregate undergoes chemo-thermal transition that significantly affects results).

$$\varepsilon_{LITS}^{T} = 1.48 \times (B_0 + B_1 T + B_2 T^2 + B_3 T^3 + B_4 T^4 + B_5 T^5) \times -10^{-6} \qquad \text{Equation 4-37}$$

where B_0, B_1, B_2, B_3, B_4, and B_5 are model parameters, found to be -1098.50, $39.21℃^{-1}$, $-0.43℃^{-2}$, $2.44 \times 10^{-3}℃^{-3}$, $-6.27 \times 10^{-6}℃^{-4}$, and $5.95 \times 10^{-9}℃^{-5}$. The factor of 1.48 in Equation 4-37 is a relic of the derivation process and may be absorbed into the values of the coefficients.

Equations 4-36 and 4-37 should be defined such that $\varepsilon_{LITS}^{T} = 0$ when $T = T_0$. Although unimportant when ε_{LITS}^{T} is calculated iteratively, according to direct calculation of ε_{LITS}^{T} using both Equations 4-36 and 4-37, this constraint is not satisfied with the values of the free parameters provided by the original author. It is found that $\varepsilon_{LITS}^{T} = 0$ when $T = 12.5℃$ for Equation 4-36 and when $T = 45.6℃$ for Equation 4-37.

In order to guarantee the condition that $\varepsilon_{LITS}^{T} = 0$ when $T = T_0$, it is here proposed that Equations 4-36 and 4-37 are replaced with equivalent functions to describe temperature-dependence of ε_{LITS} in terms of θ, rather than T. This also reduces the number of free parameters of each equation because A_0 and B_0 must be zero. Thus, Equation 4-36 may be rewritten as follows.

$$\varepsilon_{LITS}^{\theta} = (A_1'\theta + A_2'\theta^2 + A_3'\theta^3 + A_4'\theta^4) \times -10^{-6} \qquad \text{Equation 4-38}$$

where A_1', A_2', A_3', and A_4' are the new free parameters of the model, which are here determined to be 573.996, 465.772, -186.551, and 26.8912 respectively. Similarly, Equation 4-37 may be rewritten as follows.

$$\varepsilon_{LITS}^{\theta} = (B_1'\theta + B_2'\theta^2 + B_3'\theta^3 + B_4'\theta^4 + B_5'\theta^5) \times -10^{-6} \qquad \text{Equation 4-39}$$

where B_1', B_2', B_3', B_4', and B_5' are the updated parameters of the model, which are similarly determined to be 1538.550, -2427.010, 2122.530, -702.804, and 79.255 respectively.

Figure 4-13 (a) shows the output of the models defined by Equations 4-36 and 4-37, while figure 4-13 (b) shows the respective outputs of the models defined by Equations

4-38 and 4-39. It can be seen that the updated form of the model reproduces the previous model predictions well.

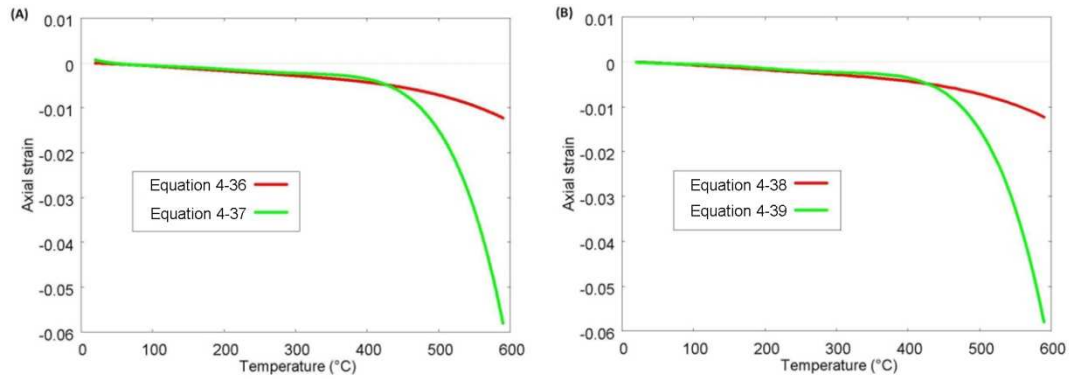

Figure 4-13: The fitted LITS temperature functions of (a) Equations 4-37 and 4-38, and (b) Equations 4-39 and 4-40.

The load-dependent factor of Equation 4-36, $\varepsilon_{LITS}^{\sigma}$, is given by the following.

$$\varepsilon_{LITS}^{\sigma} = 0.032 + 3.226\frac{\sigma_c}{f_c(T_0)} \qquad \text{Equation 4-40}$$

where σ_c is written to underline that it is compressive load that is explicitly considered here (and that the ratio of σ_c to f_c is numerically positive).

According to Equation 4-40, $\varepsilon_{LITS}^{\sigma} = 1$ when $\sigma_c = 0.3f_c$, which is consistent with the data to which Equation 4-35 is calibrated. However, also according to Equation 4-40, if $\sigma_c = 0$, $\varepsilon_{LITS}^{\sigma} = 0.032$. Thus, the Terro model predicts non-zero ε_{LITS} when a concrete specimen is heated in unloaded conditions. This cannot be assumed to represent the net effect of effective stresses or thermal stresses that develop during heating as there is no dependence on experimental conditions (e.g. heating rate). The model is calibrated to experimental data obtained using a range of values of σ_c. Therefore, this poor model behaviour suggests that extrapolation of the model to applied load levels outside of this range may be unreliable.

In order to constrain the model such that $\varepsilon_{LITS} = 0$ when $\sigma_c = 0$, it is proposed here that $\varepsilon_{LITS}^{\sigma}$ should be replaced with a new multiplicative factor, $\varepsilon_{LITS}^{\sigma,0}$, which may be defined as follows.

$$\varepsilon_{LITS}^{\sigma,0} = \left[1.0 - e^{-\alpha_\sigma\left(\frac{\sigma_c}{f_c(T_0)}\right)^2}\right]\left(0.032 + 3.226\frac{\sigma_c}{f_c(T_0)}\right) \qquad \text{Equation 4-41}$$

where α_σ is a free parameter that may be defined such that the predictions of $\varepsilon_{LITS}^{\sigma,0} \approx \varepsilon_{LITS}^{\sigma}$ for a range of values of σ_c of practical interest. It may be shown that if $\alpha_\sigma = 460$, $\left|\varepsilon_{LITS}^{\sigma,0} - \varepsilon_{LITS}^{\sigma}\right| \leq 0.01$ for $\sigma_c \geq 0.1 f_c$. Thus, this value of α_σ may be applied for this modified form of the Terro model to improve model behaviour in the range of low load levels. Figure 4-14 demonstrates the output of Equations 4-40 and 4-41 in this loading range.

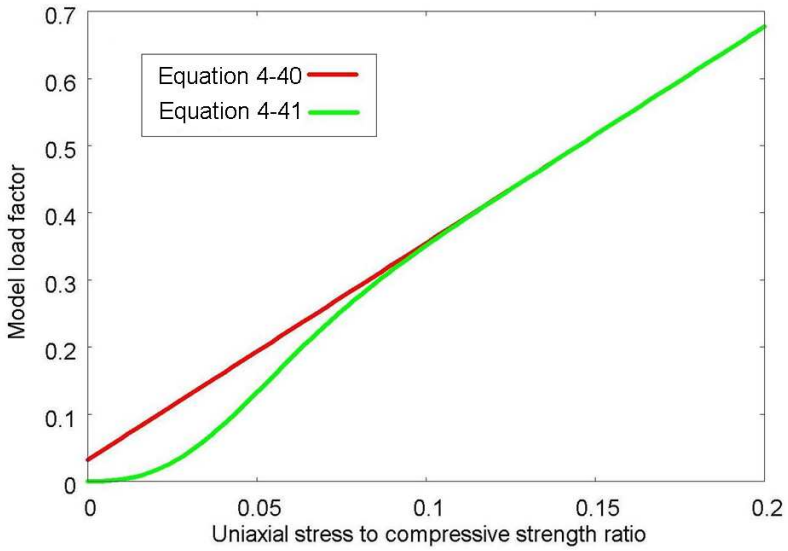

Figure 4-14: Comparison of the load function proposed by Terro [39, 88] and the modified version proposed here to prevent a prediction of non-zero LITS development in conditions of zero local stress.

Finally, there is one further multiplicative function in Equation 4-35 that must be defined in order to calculate ε_{LITS}. According to the Terro model, this function is defined as follows.

$$\varepsilon_{LITS}^{V_a} = 3.05 V_a \qquad \text{Equation 4-42}$$

Under the assumption that the V_a-dependences of basic creep and LITS are approximately identical, Equation 4-42 is empirically determined using experimental data for the specific basic creep of a range of different concretes. This appears to be a reasonable assumption as both LITS and basic creep may be considered to be seated in the cement paste phase (§2.2.1), with the primary role of aggregate in each case one of restraint.

However, the V_a-dependence of ε_{LITS} implied by Equation 4-42 is inconsistent with the experimental results on which the calibration of $\varepsilon_{LITS}^{V_a}$ is based, which are shown in figure 4-15 (a). According to the experimental results, the effect of increasing V_a is a

reduction in the magnitude of basic creep (and therefore LITS). On the contrary, Equation 4-42 indicates that the reverse relationship between V_a and ε_{LITS} exists. Furthermore, the value of $\varepsilon_{LITS}^{V_a}$ should be unity when $V_a = 0.65$ (as this is the value used to produce the original LITS experimental data). According to Equation 4-42, at this value of V_a, $\varepsilon_{LITS}^{V_a} \approx 2$.

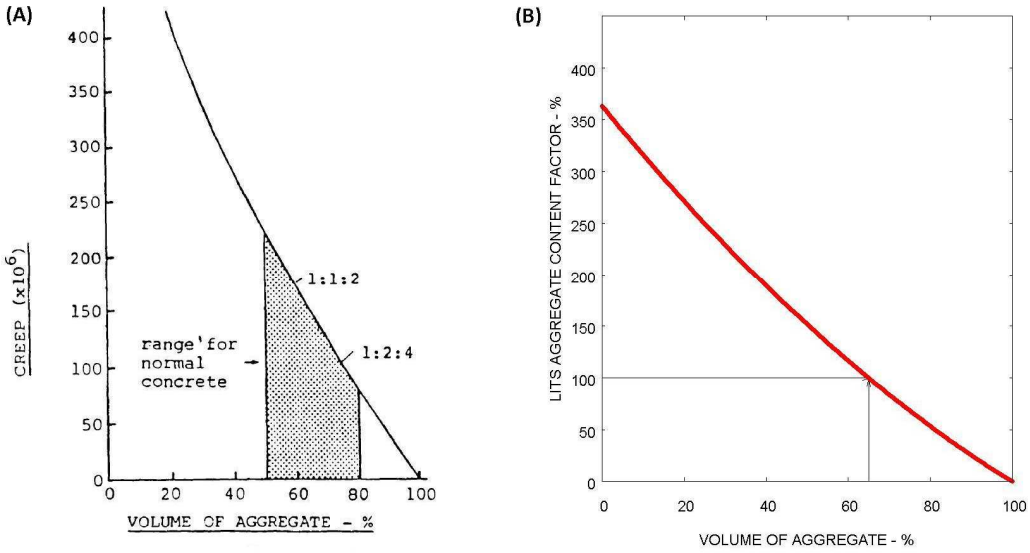

Figure 4-15: Effect of aggregate content by volume on the (a) specific creep of concrete (after unspecified time under load) [118] and (b) LITS of concrete predicted by Equation 4-43.

Therefore, it is clear that Equation 4-42 cannot reproduce experimental results. In order to address this issue, it is here proposed that the formulation of $\varepsilon_{LITS}^{V_a}$ should be recalibrated to the results of figure 4-15 (a), such that $\varepsilon_{LITS}^{V_a} = 1$ when $V_a = 0.65$ as follows.

$$\varepsilon_{LITS}^{V_a} = 1.188(1 - V_a)^2 + 2.441(1 - V_a) \qquad \text{Equation 4-43}$$

This model, as shown in figure 4-15 (b), reproduces the shape of the experimental data very well and satisfies the condition that $\varepsilon_{LITS}^{V_a} = 1$ when $V_a = 0.65$. As shown, extrapolation suggests that neat cement should undergo a LITS magnitude of between 350% and 400% of that of a concrete of $V_a = 0.65$, which is roughly consistent with experimental evidence [30].

The original author produced a comparison of the model output and experimental data, as shown in figure 4-15 (a) [88]. It can be seen that, despite the model issues highlighted in this work (i.e. poor model behaviour at $T = T_0$, $\sigma_c = 0$, and all values of V_a), the model reproduces the experimental results fairly well.

This is surprising in particular because the formulation of $\varepsilon_{LITS}^{V_a}$ given by Equation 4-42 should lead to poor model behaviour as demonstrated by a direct calculation of model output as defined by the original author [88], shown in figure 4-16 (c). Thus, due to dissimilarity between these results, it may be concluded that the models used to produce figures 4-16 (a) and (c) are not the same. This indicates that the exact form of the published Terro model contains typographical errors that are not applied in practice.

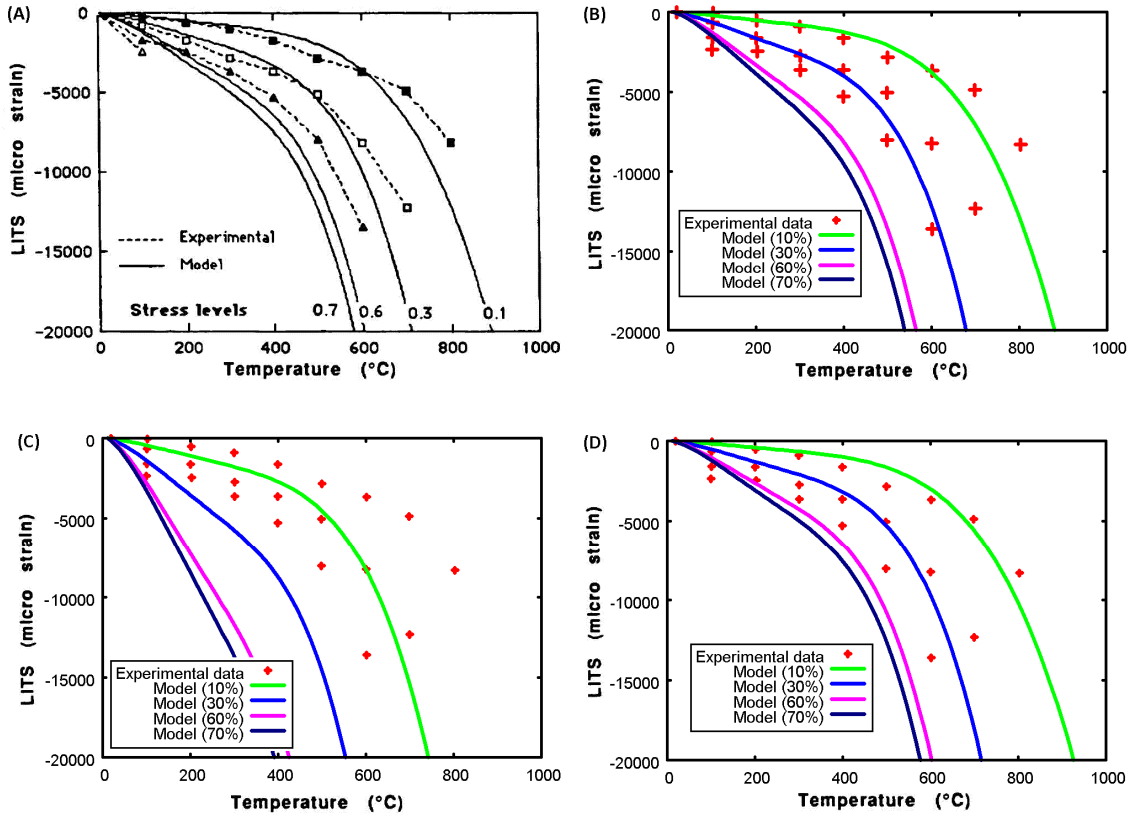

Figure 4-16: Comparison of the model predictions (a) as originally presented by Terro [88], (b) using the model without the factor $\varepsilon_{LITS}^{V_a}$, (c) with the factor $\varepsilon_{LITS}^{V_a}$ proposed by Terro [39, 88], and (d) using the factor $\varepsilon_{LITS}^{V_a}$ given by Equation 4-43. The concrete tested contains 71.5% (quartzite) aggregate content by volume.

Figures 4-16 (a) and (d) show the results of application of two modified forms of the Terro model. In figure 4-16 (a), the factor $\varepsilon_{LITS}^{V_a}$ is removed from the formulation of ε_{LITS}, such that no V_a-dependence is assumed. It is found that a relatively close match is obtained with experimental data and that the model output is similar to that shown in figure 4-16 (a). Similarly, in figure 4-16 (d), the factor $\varepsilon_{LITS}^{V_a}$ is applied to the model as defined in the modification proposed here, Equation 4-43. This is found to produce a very good match to experimental data and appears to be very similar to the model results of figure 4-16 (a). Therefore, it may be deduced that the intended form of the V_a-dependence of the Terro model is similar to that defined by Equation 4-43.

The most likely typographical error in Equation 4-42 is that $(1 - V_a)$ should replace V_a, i.e. the argument of the equation is intended to be cement content, not aggregate content. Therefore, Equation 4-42 should be rewritten as follows.

$$\varepsilon_{LITS}^{V_a} = 3.05(1 - V_a) \qquad \text{Equation 4-44}$$

Although Equation 4-44 does not exactly satisfy the condition that $\varepsilon_{LITS}^{V_a} = 1$ when $V_a = 0.65$, the difference is very small. A comparison of the predictions of Equations 4-42, 4-43, and 4-44 for $\varepsilon_{LITS}^{V_a}$ are shown in figure 4-17, along with the experimental data of figure 4-15 (a). It is found that the predictions of Equations 4-43 and 4-44 are very similar for typical ranges of V_a. Thus, it is very likely that Equation 4-44 defines the intended V_a-dependence of the Terro model.

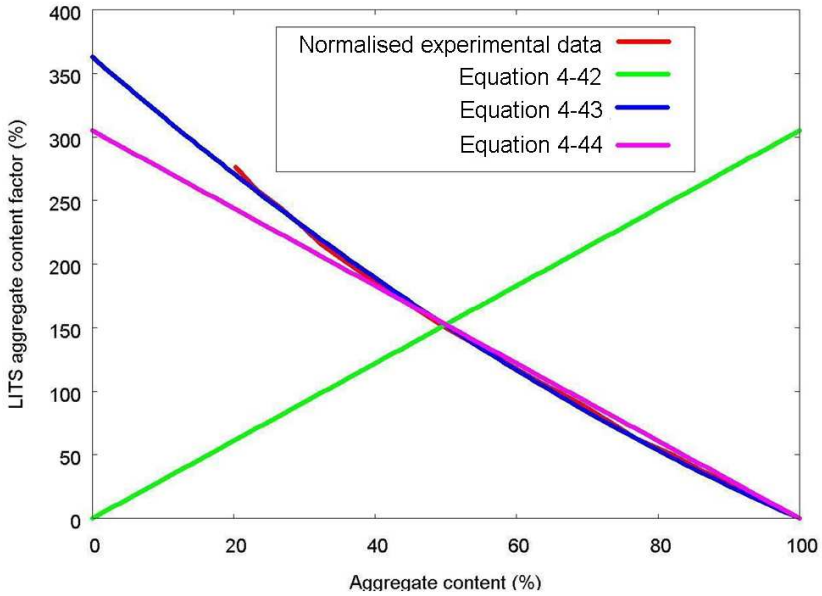

Figure 4-17: Comparison of experimental data and the function $\varepsilon_{LITS}^{V_a}$ proposed by Terro [39, 88] (Equation 4-42), along with a modified version (Equation 4-44), and the model proposed here (Equation 4-43).

It is important that the intended mathematical formulation of $\varepsilon_{LITS}^{V_a}$ is clarified as the demonstrably incorrect form of the model of Equation 4-42 has been presented twice [39, 88] and has been reproduced unmodified in at least two comparative studies of LITS models, in 2005 [63] and in 2007 [85]. This propagation of errors may lead to a misrepresentation of the performance of the Terro model.

Overall, the polynomial temperature function is well suited to use for LITS modelling because it is relatively simple to calibrate to experimental data and can be fitted to data to an arbitrary accuracy depending on the order of the polynomial. However, the

local behaviour of polynomials can be difficult to control and can result in undesirable behaviour. A relevant issue in LITS modelling is that transient strain should be a monotonically increasing function of temperature. Therefore, the temperature-dependent polynomial of the model should contain no local minima or maxima within the temperature range of the model. This condition is difficult to enforce for polynomials in general. For example, to ensure that this condition is met for Equation 4-36, it is necessary that the specific coefficient values used in the model result in no roots in the temperature range $20 - 590$℃, found by solution of

$$0 = A_1 + 2A_2T + 3A_3T^2 + 4A_4T^3 \qquad \text{Equation 4-45}$$

There is no general analytical method to solve cubic equations (or polynomials of higher order) however, so the solution can be difficult to find for a specific set of coefficients. Using numerical methods, it can be shown that only one root exists to the above equation for the values of the coefficients given by Terro [39]. This occurs at a value of T of approximately -19.5℃. A similar procedure shows that there is no value of T for which Equation 4-37 results in a local maximum or minimum.

4.6 Nielsen model

The *Nielsen model* reproduces the transient strain behaviour of concrete using a piecewise temperature function [89]. Load-dependence is considered to be linear and proportional to the ratio of the applied axial load to initial strength.

Temperature-dependence of the model is bi-parabolic in nature; two quadratic functions of temperature are active in different ranges of temperature, defined as follows.

$$y(\theta) = \begin{cases} A\theta^2 + B\theta, & \theta \leq \theta^* \\ C(\theta - \theta^*)^2 + A\theta^*(2\theta - \theta^*) + B\theta, & \theta > \theta^* \end{cases} \qquad \text{Equation 4-46}$$

where A, B, and C are free parameters of this model and θ^* is the reduced temperature at which the transition between quadratic functions occurs. This is determined by the authors to be 4.5 (470℃).

As with the Terro model, the use of a normalised measure of temperature is good practice because it ensures that the parameters of the model are of a similar order of magnitude. In this instance, typical values for A, B, and C suggested by the authors are 0.6×10^{-3}, 1.5×10^{-3}, and 10.0×10^{-3} respectively.

From the chosen form of Equation 4-46, it is clear that the function is continuous-valued for all temperatures. The gradient of the function is also continuous, including at the transition point of the function. It is unclear whether this behaviour is considered to be necessary for consistency with experimental predictions or if this technique is chosen in order to reduce the number of parameters of the model.

The transient strain model is expressed as the product of y and the axial load normalised by compressive strength.

$$\boldsymbol{\varepsilon}_{tr} = \frac{y(\theta)}{f_c(T_0)}\, \boldsymbol{Q}\!:\boldsymbol{\sigma} \qquad \text{Equation 4-47}$$

Whereas most transient strain models are intended to be applied to conditions of compressive loading with the case of tension not considered, the Nielsen model is explicitly formulated to distinguish between tensile and compressive loads [90, 94].

$$\boldsymbol{\varepsilon}_{tr} = \frac{y^{+}(\theta)}{f_t(T_0)}\boldsymbol{Q}\!:\boldsymbol{\sigma}^{+} + \frac{y^{-}(\theta)}{f_c(T_0)}\boldsymbol{Q}\!:\boldsymbol{\sigma}^{-} \qquad \text{Equation 4-48}$$

where the superscript '+' refers to the tensile component of the variable and '−' to the compressive component. This model, in which tensile transient strain can develop with a different temperature-dependence and relative magnitude in comparison to applied load, is more general than that of Equation 4-47.

Equation 4-48 can be considered to be equivalent to Equation 4-47 in conditions of compressive loading only; hence, y^{-} is identical to the function y of Equation 4-47. As the authors state, insufficient data are available to create a reliable transient strain model for concrete in tension and almost all applications of heated concrete do not place concrete under significant tensile stress [90, 94]. Thus, y^{+} is set to zero for all

temperatures such that it is assumed that no transient strain may develop in states of tension.

The typical axial transient strain output of the Nielsen model is shown in figure 4-18 for a range of applied uniaxial compressive load levels. The model produces transient strain behaviour that develops somewhat gradually up to a temperature $470°C$ (marked in the figure), above which the rate of development is much more rapid.

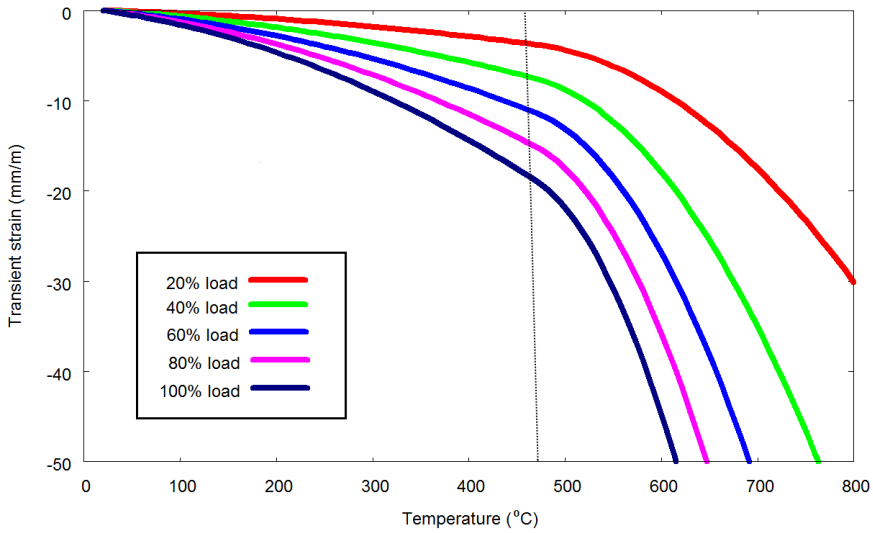

Figure 4-18: Example of typical output of the Nielsen transient strain model for five different load levels.

The value of the transition temperature of this model is given as $470°C$ [89]. This discontinuous change in material behaviour, shown in figure 4-18, suggests a rapid change in material composition, such as the α-β conversion of quartz which also occurs rapidly at a well-defined temperature (about $573°C$). However, no similar process is known to occur at $470°C$ in cement paste. It is far more likely that any changing process responsible for the change in behaviour, observed broadly for temperatures greater than and less than $470°C$, is gradual in development. Therefore, the model presented is simply a mathematical approximation and, as a result, the value of the transition temperature may be considered to be another free parameter of the model.

Including the transition temperature, the Nielsen model has four free parameters that can be calibrated to experimental data. Since it is fairly clear how adjustments to the values of the parameters affect the transient strain output of the model, there is a high degree of control associated with this model. This compares favourably with several other models, such as the Terro model, for which it is difficult to determine in advance the effects on model output made by changes to the values of model parameters.

4.7 Wu model

The *Wu model*, similarly to the Nielsen model, is modelled using a piecewise temperature function of quadratic nature. Load-dependence is also assumed to be linear and normalised using the initial material compressive strength.

However, the Wu model is intended to be applied to a particular type of material, concrete that contains PP-fibres. Materials that contain PP-fibres are found to undergo a sudden change in behaviour in a temperature range close to that at which the fibres melt (approximately $170℃$). When this occurs, moisture transfer properties of the material are significantly affected (due to the associated increase in pore space). Therefore, this model is unlikely to be appropriate for use in modelling of general concrete materials. However, it may be useful to examine the form of the model.

The temperature-dependence of the model can be written in a manner similar to that of the Nielsen model (Equation 4-46).

$$y_W(\theta) = \begin{cases} A_W\theta^2 + B_W\theta, & \theta \leq \theta_W^* \\ A_W(\theta_W^*)^2 + B_W\theta_W^* + C_W(\theta - \theta_W^*)^2 + D_W(\theta - \theta_W^*), & \theta > \theta_W^* \end{cases} \quad \text{Equation 4-49}$$

where θ_W^* is the normalised transition temperature of this model (set equal to 2.0) and A_W, B_W, C_W, and D_W are free parameters of the model, given as 1.2256×10^{-3}, 7.4884×10^{-4}, 1.3366×10^{-3}, and 1.3679×10^{-3} respectively. The load-dependence of the Wu model is identical to that of the Nielsen model. Therefore, the Wu model is defined as follows.

$$\varepsilon_{tr} = \frac{\sigma}{f_c(T_0)} y_W \quad \text{Equation 4-50}$$

When typical output of the Wu model is plotted, as in figure 4-19, the dissimilar behaviour of the Wu model in comparison with the Nielsen model is immediately obvious; $\frac{\partial \varepsilon_{tr}}{\partial T}$ is not continuous at the transition temperature. This behaviour likely reflects the rapid change in behaviour associated with the relatively fast process of melting of PP fibres.

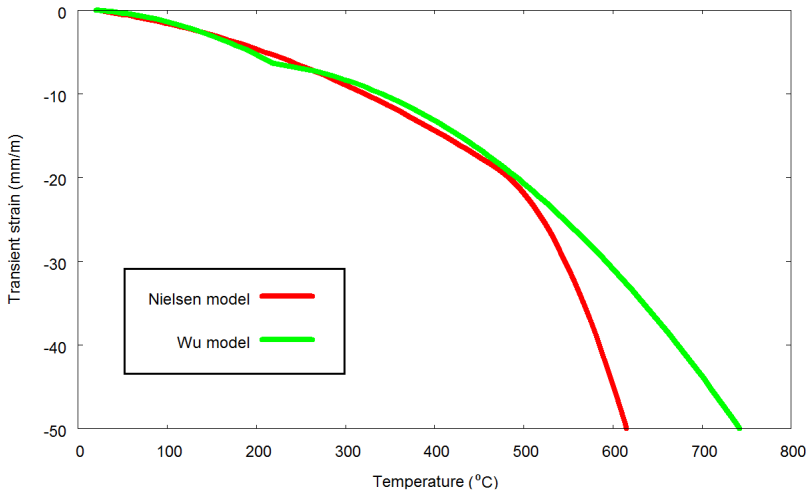

Figure 4-19: Comparison of the strain outputs predicted by the Nielsen model and the Wu model.

Also demonstrated by figure 4-19 is the similarity of the model predictions for temperatures below about $500℃$, despite the distinction in the natures of the materials intended for simulation by the models. It is only for temperatures above the transition temperature of the Nielsen model that the predicted results diverge significantly. As the temperature range of figure 4-19 is within the range used when developing both models, this divergent behaviour must be considered to be intentional.

4.8 Schneider model

The Schneider model is a method of simulating ε_{tr} using a nonlinear load-dependence and a complex temperature-dependence, dominated by temperature functions of hyperbolic nature [34, 119]. Further temperature-dependence is provided by the explicit dependence of the model output on the reducing material stiffness.

The original author suggests that the loss of moisture, from capillary pores, gel pores, and the chemical structure of the cement, leads to transient strain, though no associated physical mechanism is postulated [34]. No derivation or attempt at further physical justification for the mathematical model is provided.

The mathematical form of the Schneider model is presented within a full strain model for (rapidly) heated concrete [34]. Total strain is first decomposed into mechanical strain, ε_m, and thermal strain, ε_{th}.

$$\varepsilon_{tot}(T,\sigma) = \varepsilon_{th}(T) + \varepsilon_m(T,\sigma) \qquad \text{Equation 4-51}$$

ε_{th} is described by a temperature function fitted to experimental data, while ε_m is decomposed into elastic strain, plastic strain, and transient strain. Transient strain is defined in uniaxial form as follows.

$$\varepsilon_{tr}(T,\sigma) = \frac{\Phi(T,\sigma)}{E(T,\sigma)}\sigma \qquad \text{Equation 4-52}$$

where E is the preload- and temperature-dependent elastic modulus and Φ is the transient strain function, which is defined as follows.

$$\Phi(T,\sigma) = g(T,\sigma)\phi(T,w) + \frac{(T-T_0)}{100°C}\Sigma_{0.3}(\sigma) \qquad \text{Equation 4-53}$$

where w is moisture content per unit volume of the specimen and $\Sigma_{0.3}$ is a value-limited normalised axial load factor defined as follows.

$$\Sigma_{0.3}(\sigma) = \begin{cases} \dfrac{\sigma_c}{f_c(T_0)}, & \dfrac{\sigma_c}{f_c(T_0)} \leq 0.3 \\ 0.3 \quad , & \dfrac{\sigma_c}{f_c(T_0)} > 0.3 \end{cases} \qquad \text{Equation 4-54}$$

The function g of Equation 4-53 is given by the following.

$$g(T,\sigma) = 1.0 + \frac{(T-T_0)}{100}\Sigma_{0.3}(\sigma) \qquad \text{Equation 4-55}$$

The function ϕ of Equation 4-53, which is the dominant temperature-dependence of the Schneider model, is defined as follows.

$$\phi(T,w) = C_1 \tanh[\gamma_w(T-T_0)] + C_2 \tanh\left[\gamma_0\left(T-T_g\right)\right] + C_3 \qquad \text{Equation 4-56}$$

where C_1, C_2, γ_0, and T_g are free parameters, and C_3 is a parameter chosen to ensure that $\phi = 0$ when $T = T_0$.

$$C_3 = -C_2 \tanh\left[\gamma_0\left(T_0 - T_g\right)\right] \qquad \text{Equation 4-57}$$

Parametric values found by calibration of the model to the experimental data for three different types of concrete are shown in table 4-1. Consistent with experimental results, there is little variation between values for different concretes.

Moisture-dependence is introduced into the transient strain model via the parameter γ_w.

$$\gamma_w = (0.3w + 2.2) \times 10^{-3} \qquad \text{Equation 4-58}$$

where w should be expressed as a percentage.

Table 4-1: Table of suggested values for the free parameters of Equation 4-56 [34].

Parameter	Quartzite concrete	Limestone concrete	Lightweight concrete
C_1	2.60	2.60	2.60
C_2	1.40	2.40	3.00
T_g	700°C	650°C	600°C
γ_0	7.5×10^{-3}	7.5×10^{-3}	7.5×10^{-3}

Equations 4-52–58 do not fully describe the transient strain output of this model. It is also necessary to define the preload- and temperature-dependence of E. Based on experimental observations, the original author proposed a load-dependent formulation for stiffness degradation due to temperature increase [34].

$$E(T, \sigma) = E_0 f_0(T) g(T, \sigma) \qquad \text{Equation 4-59}$$

where f_0 is a temperature function that may be identified directly from experimental results using unloaded heated concrete specimens. In this work, f_0 can be identified as equivalent to $1 - \chi$.

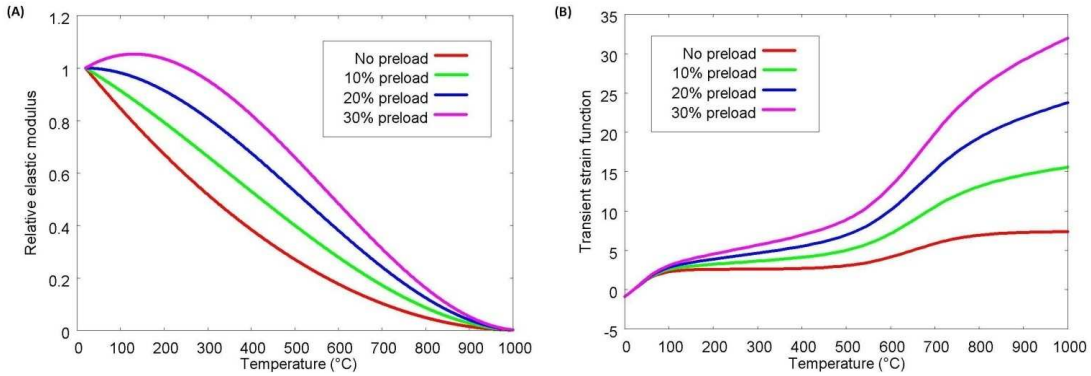

Figure 4-20: The temperature-dependent functions of the Schneider model, (a) the degradation of elastic modulus and (b) the transient strain function.

It should be noted that Equation 4-59 is explicitly a thermal damage formulation of the elastic stiffness of concrete; the load-dependence of the equation does not account for mechanical damage effects. The presence of load is found to reduce the stiffness

degradation caused by thermal damage (and can even lead to increased stiffness), as can be seen in figure 4-20 (a).

The two principal temperature-dependencies of the model are shown in figures 4-20 (a) and (b) at a range of preload levels. When $\sigma_c > 0.3f_c$, the equivalent temperature functions are identical to those for $\sigma_c = 0.3f_c$.

The Schneider model output is defined by the product of the function shown in figure 4-20 (b) and the inverse of the function shown in figure 4-20 (a). An example of the resultant ε_{tr} is shown in figure 4-21 (a) for several different load levels.

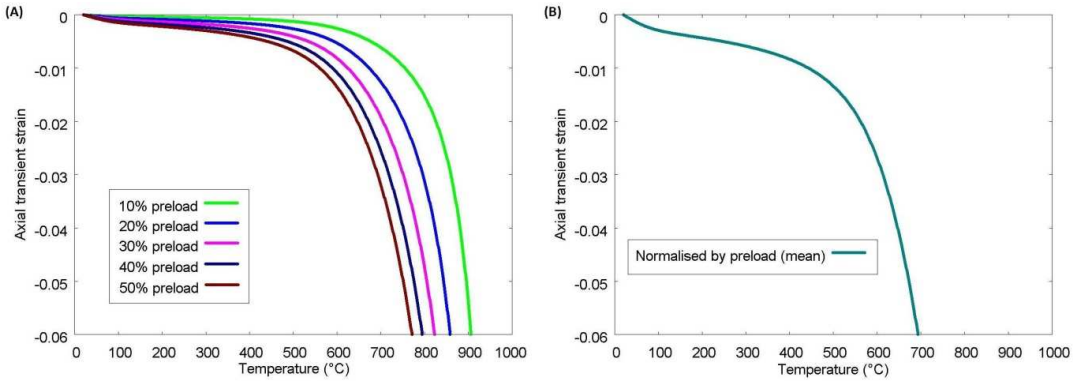

Figure 4-21: The transient strain output of the Schneider model, (a) axial transient strain for five different levels of preload and (b) the mean of the preload-normalised transient strain output of the model (mean calculated over ten different evenly-spaced preload levels between 10% and 100%).

Despite the nonlinear model formulation, an examination of the model output demonstrates that the dependence of transient strain on applied load is very close to linear. The deviation from linearity is very small for $\sigma_c < 0.3f_c$ and zero for $\sigma_c > 0.3f_c$. Therefore, ε_{tr} may be normalised by preload as in figure 4-21 (b).

No guidance is provided by Schneider for the correct method with which to generalise Equation 4-52 to multiaxial states [34]. The replacement of the uniaxial terms, ε_{tr} and σ, with isotropic multiaxial counterparts, $\boldsymbol{\varepsilon}_{tr}$ and $\boldsymbol{Q}:\boldsymbol{\sigma}$ respectively, is insufficient as the model also applies the axial load-dependent factor $\Sigma_{0.3}$. Thus, the axial load must be replaced with a scalar variable that represents the load level. In this work, the first invariant of the stress tensor (i.e. the *trace* of the stress tensor, $tr(\boldsymbol{\sigma})$) shall be applied in place of the axial load factor, such that $\Sigma_{0.3}$ may be rewritten as follows.

$$\Sigma'_{0.3} = \begin{cases} 0\,, & tr(\boldsymbol{\sigma}) > 0.0 \\ -\dfrac{tr(\boldsymbol{\sigma})}{f_c(T_0)}\,, & -0.3 < tr(\boldsymbol{\sigma}) \leq 0.0 \\ 0.3\,, & -0.3 \geq tr(\boldsymbol{\sigma}) \end{cases}$$ Equation 4-60

Equation 4-60 can also be seen to set a lower bound on the allowed values of $\Sigma'_{0.3}$. This prevents the presence of a tensile preload from influencing the model in a manner unintended by the original author.

Though the original author makes no attempt at physical justification for the mathematical form of the Schneider model, it is here proposed that ϕ is consistent as the mathematical description of the progress of an underlying temperature-dependent asymptotic process that develops only during heating, such as a chemo-thermal process. A strong candidate for such a process is cement paste dehydration.

It is assumed that the evolution of a parameter representing the degree of such a chemo-thermal process may be principally defined by two competing effects, i.e. the rate-increasing temperature-dependence of the process and the reducing quantity of remaining 'reactant' material.

$$\dot{N} = N(t)R_0 f_R(T)$$ Equation 4-61

where N is the parameter that represents the quantity of remaining reactant material (such as the number of available reactant molecules), R_0 is a characteristic rate of reaction, and f_R defines the temperature-dependence of the reaction rate.

In order to demonstrate that the solution of Equation 4-61 may be of a similar mathematical form to ϕ, three different monotonic functions of temperature are assumed for f_R. To allow some variability in outcome, the functions are a convex function, a concave function, and a linear function of temperature. The constraints that $f_R = 0$ when $T \leq 105$℃ and $f_R = 0.8$ when $T = 805$℃ are imposed as dehydration does not occur for $T \leq 105$℃ and to ensure that the functions are similar in magnitude throughout the temperature range of interest, respectively. These functions are presented in figure 4-22.

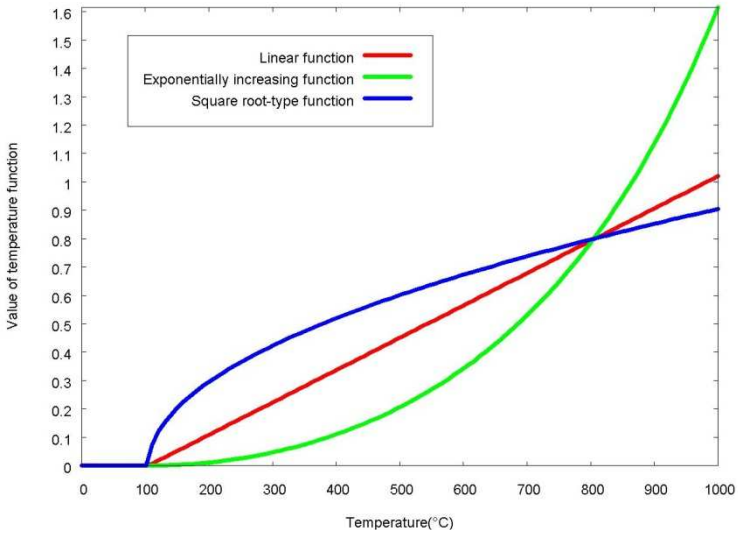

Figure 4-22: Comparison of the proposed functions f_R.

Using numerical integration, Equation 4-61 can be solved for each of these functions f_R in conditions of linearly increasing temperature. The corresponding evolution of $1.0 - N(t)$, shown in figure 4-23(a) for each of the three forms of f_R, can be seen to be qualitatively similar for any formulation of f_R, though the quantitative behaviour is strongly dependent on f_R.

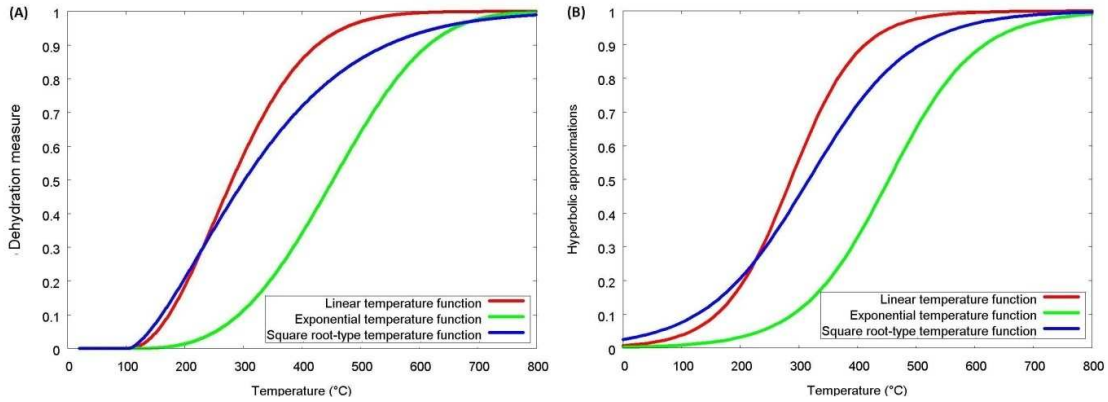

Figure 4-23: Comparison of (a) the calculated evolution of hypothetical dehydration measure evolution for each different form of the temperature-dependence of the reaction rate and (b) the hyperbolic approximation of these behaviour types.

In order to demonstrate that the results of figure 4-23 (a) can be well reproduced by a hyperbolic tangent function, the following function is fitted to each of the curves.

$$(1 - N)_{hyp} = 0.5\{tanh[\alpha_R(T - T_R)] + 1.0\} \qquad \text{Equation 4-62}$$

where α_R and T_R are free parameters. The resultant functions $(1 - N)_{hyp}$ are shown in figure 4-23 (b).

The form of Equation 4-62 is not ideal as a description of the dehydration process as it implies that dehydration occurs, albeit at a low rate, for $T < 105℃$, which is not supported by experimental observations. However, further development of the model would easily address this issue.

This example demonstrates in principle that the progress of a chemo-thermal process, such as dehydration, may be well described using a hyperbolic tangent temperature function. Thus, it may be suggested that the use of hyperbolic temperature functions to describe transient strain may be evidence that the underlying processes that lead to transient strain may be strongly related to the dehydration process. Similarly, it was demonstrated in §4.4 that the sum of three hyperbolic tangent temperature functions could very accurately describe experimental data for the temperature-dependence of the mass of water dehydrated from cement paste in the temperature range $20 – 500℃$.

Inspection of Equation 4-56 reveals that one of the hyperbolic tangent functions of ϕ develops in the temperature range in which no dehydration occurs ($T \leq 105℃$). Although it may seem that this term is representative of drying creep, in a manner analogous to the Sabeur model (§4.4), this interpretation is not consistent with the model predictions. It can easily be shown that a decrease in w during heating causes a decrease in the magnitude of $\frac{d\phi}{dT}$ and therefore also $\frac{d\varepsilon_{tr}}{dT}$. Moreover, if w is held constant during heating, a greater magnitude of ϕ is found to occur.

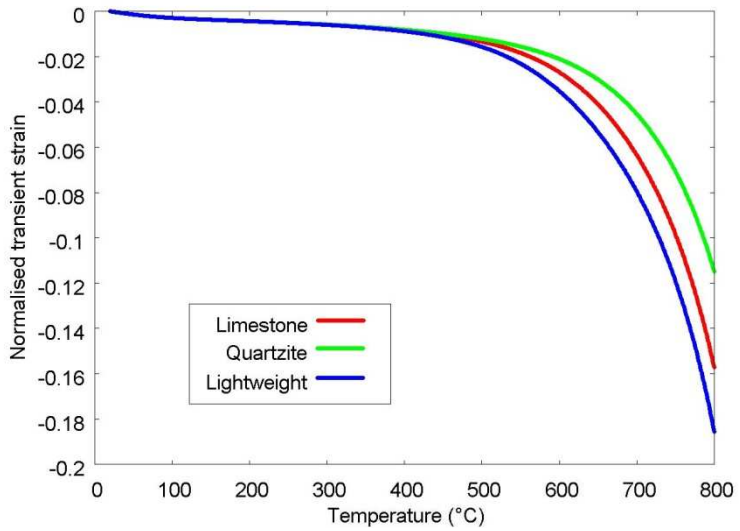

Figure 4-24: The normalised transient strain model for the three types of concrete for which parameters are fitted [34].

Finally, it should be noted that adherence to master curve-type behaviour can be seen to be observed, despite the dissimilar values of free parameters quoted for different concrete types (table 4-1). If it is assumed that $\frac{E_0}{f_c}$ is approximately the same for each type of concrete, normalised transient strain is found to be near identical for each of the concretes for the temperature range below about $450℃$, as shown in figure 4-24.

4.9 Thienel model

The *Thienel model* describes transient strain using the octahedral stress-strain coordinate system. The model is necessarily multiaxial, unlike most models which focus only on the axial transient strain response of a material.

Transient strain is modelled in the octahedral coordinate system using a formulation that is adapted from that of elasticity, with the associated material stiffness parameters modelled as both linearly temperature-dependent and load-dependent. The formulation is given as follows.

$$\begin{Bmatrix}\Delta\varepsilon_{0tr}\\ \Delta\gamma_{0tr}\end{Bmatrix} = \begin{bmatrix}\frac{1}{3K_{tr}} & \frac{1}{H_{tr}}\\ \frac{1}{Y_{tr}} & \frac{1}{2G_{tr}}\end{bmatrix}\begin{Bmatrix}\frac{\Delta T}{T_0}\sigma_0\\ \frac{\Delta T}{T_0}\tau_0\end{Bmatrix} \qquad \text{Equation 4-63}$$

where $\Delta\varepsilon_{0tr}$ and $\Delta\gamma_{0tr}$ are the octahedral hydrostatic and shear transient strain components respectively, induced by temperature increase ΔT and applied octahedral hydrostatic and shear stress components σ_0 and τ_0, and K_{tr}, G_{tr}, H_{tr} and Y_{tr} are given as the transient strain bulk modulus, shear modulus and (two) coupling moduli respectively.

The transient strain bulk modulus is defined as follows.

$$K_{tr} = K_{0tr}\left(1 - C_{kt}\frac{T_0}{T}\right) \qquad \text{Equation 4-64}$$

where C_{kt} is a parameter given as 0.02 and K_{0tr} is defined as follows.

$$K_{0tr} = K_{0,20}\left(1 + C_{k,tr}\sigma_0\right)\left(\frac{\tau_0}{C_{k,t}}\right)^{3/2} \qquad \text{Equation 4-65}$$

where $C_{k,tr}$ and $C_{k,t}$ are parameters given as $0.25\ MPa^{-1}$ and $45\ MPa$ respectively, and $K_{0,20}$ is the initial bulk modulus.

The transient strain shear modulus is defined by the following.

$$G_{tr} = G'_{0tr}\left(1 - \frac{\tau_0}{\tau_{0u,T}}\right) \geq C_{g,tr}G \qquad \text{Equation 4-66}$$

where $C_{g,tr}$ is given as 0.2, G is not defined[8], $\tau_{0u,T}$ is the temperature-dependent shear strength, and G'_{0tr} is defined as follows.

$$G'_{0tr} = G_{0tr}\left(1 - \frac{T}{T_{cr}}\right) \qquad \text{Equation 4-67}$$

where T_{cr} is a critical temperature of the model and G_{0tr} is defined by the following.

$$G_{0tr} = G_{0,20}\left(1 - C_g\sigma_0\right) \geq C'_g G_{0,20} \qquad \text{Equation 4-68}$$

where C_g is given as $0.021\ MPa^{-1}$, C'_g is given as 0.47, and $G_{0,20}$ is the initial shear modulus.

The coupling modulus H_{tr} is given as follows.

$$H_{tr} = 50 + \frac{250}{\left(\frac{T}{T_0} - 20\right)\sigma_0}, \qquad \frac{T}{T_0} > 20 \qquad \text{Equation 4-69}$$

No indication is provided for the formulation of the model for $T < 20T_0$, though it may be assumed that the value is essentially infinite (and, hence, that the inverse value, which is important to the model, is zero). Note that the units of the coupling modulus are GPa.

The coupling modulus Y_{tr} is given by the following.

[8] Although G is not defined, it seems logical to assume that the intention of the original authors, Thienel and Rostásy, is to use the parameter G'_{0tr}. However, this cannot be stated with certainty; hence, the equation given in the publication is reproduced.

$$Y_{tr} = \left(\frac{20}{\tau_0}\frac{T_0}{T}\right)^2$$ Equation 4-70

The units of Equation 4-70 are also GPa.

Note that the values of σ_0 and τ_0 should always be applied to the model in units of MPa and it appears that the temperature terms should be expressed in °C, though this is not clearly stated. This model is very unclear and poorly formulated in terms of units used. This is very undesirable as it increases the chance of poor application of the model and incidence of errors. Furthermore, it is generally bad practice to express temperature ratios in a measurement scale such as the Celsius scale.

This model is unique in that it is explicitly multiaxial. The model requires the principal stress state of the specimen to be converted to the octahedral stress state for application. Calculations according to Equations 4-64–70 then produce the resultant octahedral transient strain increment. From these two variables, it is necessary to subsequently calculate the three principal strain increments. Use of an assumption of the incidence of stress and strain deviator components (i.e. that the ratio of the first principal stress deviator to the first principal strain deviator is always identical to the equivalent ratio associated with the second component of the principal axis) allows three principal strain increments to be recovered from two octahedral strain increments. A general model also requires the eigenvalues of the initial stress state to apply the model (and the eigenvectors for conversion of the principal strain increments calculated to the original axial system). Evidently, this model is relatively computationally demanding.

Much of the model presented above is modified from an original version of this model intended for elastic analysis without explanation. It appears that the formulation of the Thienel model is based entirely on fitting an existing model for isothermal elastic strain to experimental observations for transient strain at elevated temperatures.

Preliminary attempts to apply the Thienel model suggest that the model is incorrectly written; for instance, the coupling modulus Y_{tr} of Equation 4-70 results in a very large contribution to octahedral transient strain from a modest value of octahedral hydrostatic stress for moderate temperatures and above. The source of the error is not clear from the formulation, possibly due to lack of clarity of the units to be used.

4.10 Brooks model

The transient strain model that is here referred to as the Brooks model was developed principally for drying creep. However, the author [77] also considers it to be valid for TTC and, thus, transient strain. Although the associated mathematical model is not sufficiently developed to be applied, the model is considered here because the physical model is highly original.

The model is based on the well-known local stress concentration effect found to occur at the boundary of holes in metals that is placed under external load. As the holes cannot transmit stress, the stresses tend to 'flow' around the holes in greater concentration than in regions far from the holes. This concentration leads to an increase in the average stress on the material, modelled using a stress enlargement factor (SEF) greater than unity. If rigid inclusions are embedded in the metal, the reverse effect is found to occur in the material, i.e. the stresses tend to flow through the inclusions and a lesser concentration is found in the matrix near the surface of the inclusions than far from the inclusions. This is modelled as a SEF of value less than unity.

The Brooks model posits that cement paste behaves in a similar manner to metals in this regard [77]; empty pores act as holes and saturated pores play a similar role to rigid inclusions. Partially filled pores act as rigid inclusions with a hole in the centre and result in a SEF of a value intermediate to those of holes and rigid inclusions. Therefore, as pore water is removed from the material by drying, the SEF increases and, according to the model, drying creep is observed on the macroscale. Heating is considered to lead to a similar reduction in pore water content and thus to TTC.

The mathematical model presented by Brooks is based on several idealisations (such as a pore system that is uniform in size, shape and spacing) [77]. These idealisations, which are necessary to enable a formulation to be presented and applied, are somewhat unrealistic and speculative. Therefore, the mathematical model is not reproduced here.

The form of the model described here clearly cannot explain drying creep (or TTC). The drying process should not induce a temporary change in SEF but a permanent one.

Therefore, pre-dried specimens that are subsequently loaded should undergo a greater degree of creep due to the SEF induced by drying; this is not consistent with drying creep observations. However, the author has considered this objection and speculated that, during pre-drying, the SEF is active with capillary stresses as the source; this causes a degree of creep that is observed as drying shrinkage. This action leads to decrease in 'creep potential' of the material and therefore the increased creep is not observed upon application of external load. This reasoning appears to be post hoc and is unconvincing. However, it is consistent with observations that dried specimens generally undergo a lesser magnitude of basic creep than specimens that have not been dried.

Furthermore, the model appears to be unable to explain results that show TTC in specimens that are heated to temperatures below $100°C$ while submerged in water (and therefore saturated throughout heating tests) [13, 16, 18]. The lack of increase in density of holes in the material cannot lead to an increase in SEF and, thus, no TTC should be observed.

One final objection to the model is that pore water is modelled using an equation that is derived for an infinitely stiff inclusion material. This is clearly not a good approximation as water has a stiffness that is far lower than cement gel (even if prevented from outward flow from the pore). In fact, if a more realistic value of the water stiffness is considered, a fully saturated pore should result in a SEF that is larger than unity, though less than when the material is fully dried. This significantly diminishes the capacity of the model to produce an increase in creep due to drying (or heating) as the effect due to drying must be necessarily small.

Although the model is very unlikely to be adequate as a mechanism for transient strain, the effects described in the model may play a role, albeit a small role, in the complicated hygro-thermomechanical behaviour of concrete. However, to apply this model accurately, a far more sophisticated model is required that can calculate an overall SEF for a concrete specimen using the detailed information regarding porosity, distributions of pore size and shape, and the moisture flow.

4.11 Final model list

The transient strain models presented in §4.1–10 represent the most up-to-date mathematical and physical models for transient strain that are presently available. The models that shall be applied in further work are detailed in this section.

There are a core set of criteria that are here applied in order to determine the shortlist of models to apply in further work. These criteria may be defined as follows. The final shortlist of models must contain only models that

- are unique, i.e. if there are two mathematical models that can clearly be calibrated to produce identical transient strain predictions, only one of these models should be included in the shortlist.
- have the potential to reproduce experimentally observed behaviour.
- may be well understood from the form presented in the literature without guesswork or numerous assumptions.

Thus, on the basis of these criteria, the shortlist of models selected to be the subject of further work is given by:

- the Nielsen model,
- the Anderberg model,
- the Terro model,
- the Schneider model, and
- the Bažant model.

The Wu model is not included in the shortlist because of the uniqueness criterion; the Nielsen model can be calibrated to produce identical transient strain output. As the Wu model is explicitly intended to describe the transient strain of concretes containing PP-fibres, it is likely that the Nielsen model is more widely applicable than the Wu model. Thus, the Nielsen model is here chosen for further investigation in preference to the Wu model.

The Brooks model is excluded from the shortlist because the mathematical model cannot be well understood from the literature. Moreover, the predictions of the model appear to be fundamentally inconsistent with experimental observations. Transient strain cannot be considered to be identical to drying creep.

The Thienel model is omitted from the shortlist because the presentation of the model in the literature is confusing and unclear. Preliminary attempts failed to reproduce the model results presented in the literature. Thus, as no clear inspiration for the model formulation can be derived, it appears unfeasible that the model can be investigated in further depth.

The Sabeur model cannot be considered further as the model is restricted to a temperature range under $400℃$. This is too restrictive for this investigation because the models are intended to be applied in a wide range, as is conventional in transient strain research. While the Bažant model is also intended for a restricted temperature range ($T < 100℃$), this restriction is of a far lower importance as the Bažant model may in principle be applied over a larger temperature range without the requirement of further development of the model. In contrast, the Sabeur model requires further experimental data in order to define the temperature-dependence of the model. Thus, there appears to be no rational way to apply this model in the intended temperature range.

The Gawin model is also not considered further as there are fundamental issues with the determination of the governing parameter of the model from experimental data sets. Thus, the model cannot reliably be used to produce results and the third criterion is not satisfied.

Thus, the remaining models that satisfy the criteria together form the shortlist that the remainder of this work shall investigate. This shall form a major part of the work to be carried out here. Work for which the particular transient strain model applied is not significant shall be here carried out using the Nielsen model (such as the investigation into the nature of the transient strain that develops due to states of tension). The reason for this is that the Nielsen model is relatively simple, with easily defined parameters, requires no further data to apply, and makes no assumptions about the nature of transient strain.

4.12 Final remarks

In this section, existing transient strain models have been examined in turn. The mathematical form of each has been scrutinised and, where appropriate, critically analysed. Some of the key findings are as follows.

The evolution of the microprestress parameter, S_μ, critical in defining the output of the Bažant model (§4.1), is found to be complex and difficult to predict in various hypothetical conditions of heating and drying, e.g. linear heating does not appear to lead to a monotonic increase in microprestress in all cases. Relative humidity plays a large role in the definition of the evolution of S_μ. Thus, it is important for application of the Bažant model that the drying behaviour of the concrete is modelled realistically.

It is here demonstrated that the transient strain output of the Bažant model can be decomposed from the total creep model output if a second set of creep calculations are made in parallel. Using this methodology, according to the Bažant model, transient strain is strongly time-dependent, with the majority of the strain developing in the period of time after the target temperature has been reached (within 30 days from the start of heating). In some cases, the final value of transient strain is extremely large, particularly for temperatures greater than $100℃$.

Furthermore, for application of the Bažant model, it was found that it is necessary to constrain the model such that values of relative humidity very close to zero are not included in calculations. Without this constraint, extremely large values of ε_{tr} may be produced. Though the exact value is relatively unimportant, use of an absolute value of $h_{min} = 0.05$ is found to markedly improve results. Thus, this modification of the Bažant model shall be applied in the remainder of this work.

Also, the modified form of the Anderberg model produces predictions that deviate fairly significantly from those of the unmodified model in all cases here examined (§4.2). It is also established that the model is fundamentally inconsistent with experimental observations regarding the effects of aggregate content on the magnitude of transient strain.

The Gawin model describes the temperature-dependence of transient strain using that of thermo-chemical damage (§4.3). However, in using experimental data for the

degradation of Young's modulus in unloaded heated conditions to determine the evolution of this parameter, the authors equate thermo-chemical damage with several processes that lead to stiffness degradation. It is here proposed that damaging effects, such as microcracking due to thermal mismatch, should be distinguished mathematically from those due to thermo-chemical processes in order to calibrate this model.

It is also shown here that the results presented by the original authors (of the Gawin model) do not include the contribution of ε_{tr} to the total strain of concrete heated in unloaded conditions [87]. Although this appears to be reasonable at first, this approach is inconsistent as the effective stress is used as input to the models for both ε_{sh} and ε_{tr}. Therefore, the development of ε_{sh} in heated conditions implies that there should be a simultaneous of ε_{tr}. This omission means that the evolution of the thermo-chemical strain component, ε_{tc}, which is considered by the original authors to support the physical basis of the model, is incorrectly defined from experimental data.

The Sabeur model must be extended to a wider range of temperatures to properly test model performance (§4.4). Also, it would be interesting to explore the possibility that hydration (or rehydration) may cause transient strain-like effects, though this possibility is explicitly forbidden in the mathematical formulation of the model presented by the original authors [46, 64]. However, it appears that the Sabeur model cannot fully describe transient strain as experimental data that suggest TTC develops in the temperature range below $100℃$ cannot be reproduced by this model [13, 16, 18].

The Terro model is described mathematically by three distinct functions, modifications (of the forms given in the literature) of each of which are here proposed (§4.5). The temperature function should be written in terms of the reduced temperature variable in order to decrease the number of free parameters and to allow the value of each to be of similar magnitude. The load function should include a factor that ensures that non-zero transient strain develops only when non-zero net stress exists. Finally, the mathematical definition of the aggregate-dependent factor is here shown to be contradictory to the intentions of the original author [39, 88]. It appears that the error is typographical; this issue should be addressed to prevent the propagation of this error.

Through the analysis of the kinetics of a hypothetical temperature-dependent chemical reaction, the principal temperature-dependence of the Schneider model is here shown to be consistent with the mathematical description of the progress of such a process (§4.8). Further evidence for this proposal is provided by the examination of the Sabeur model (§4.4) in which it was here shown that experimental data for the equilibrium mass of dehydrated water at high temperatures may be accurately reproduced using the sum of three hyperbolic tangent functions.

Moreover, in order to apply the Schneider model in conditions of multiaxial stress, it is necessary to make modifications to the model. A scalar preload term is applied in calculations of ε_{tr}. This term is replaced with the first invariant of the stress tensor in this work. Also, a maximum value restriction is placed on the magnitude of the preload term by the original author, equal to $0.3f_c$ [34]. It is assumed in this work that extrapolation to the tensile loading range is not intended. Therefore, a minimum preload value of 0 is also applied in this work.

Finally, following detailed examination of each of the models, on the basis of explicit criteria, a shortlist of transient strain models to be the subject of further work is here defined (§4.11) These models are the Bažant model, the Anderberg model, the Nielsen model, the Terro model, and the Schneider model.

Chapter 5. Qualitative investigation of model behaviour

In chapter 4, the available transient strain mathematical models were examined and a shortlist was created for the purposes of further work. In this chapter, the predictions of these models are explored in a number of realistic experimental conditions within the context of a hygro-thermo-mechanical model set in a FE environment (as detailed in chapter 3). The purpose of this is to further explore the plausibility of the current predictions of these models and, thus, to guide the application of these models for the next stage of the work (chapter 6).

The response of the transient strain model to states of tension is an area about which little is known. Some authors assume no significant difference from the response to states of compression [56], while others assume that transient strain is absent in states of tension due to lack of experimental evidence to the contrary [90]. However, most researchers [34, 39, 46, 64, 87, 120] ignore the issue on the basis that states of tension are rarely externally applied to concrete structures and that various techniques to support the structure in regions of tensile loading (such as precompression) can be implemented to effectively eliminate local states of tension in structural concrete in typical service conditions. However, such local states of tension may develop when temperature is increased, on the macroscale due to temperature differentials and on the mesoscale and microscale due to thermal mismatch. The potential significance of these states to the stress-strain state of concrete structures on the global scale, which is likely to depend heavily on the tensile aspect of the transient strain model formulation, has never been examined.

Thus, one of the key areas considered in this work is the correct response of transient strain models to states of tension, as identified based on comparisons of experimental evidence and model predictions obtained using distinct assumptions of the nature of tensile transient strain. The first step, carried out in this chapter, is a qualitative investigation into this phenomenon for the purposes of demonstrating that tensile transient strain can play a significant role in the development of total strain (measured globally) and to investigate whether distinct tensile transient strain formulations may be implemented in a manner that retains consistency between model predictions and experimental behaviour.

This is achieved through modelling standard concrete cylinders heated in realistic conditions to a high temperature in unloaded conditions and unloaded conditions in turn for three distinct assumed tensile transient strain (TTS) formulations. Comparison of the results allows the significance of the TTS formulation to be directly observed and for preliminary conclusions to be made regarding the plausibility of each of the model assumptions.

There are a large number of distinct mathematical formulations, with corresponding potential implications for the physical origin of transient strain, applied at present in the research field, as indicated by the number of models discussed in §2.2, §2.3, and chapter 4. An objective and unbiased investigation that evaluates the available transient strain models is necessary to provide guidance for researchers who require a reliable transient strain model and performing such an investigation is beyond the scope of their work. Such guidance is not currently available as transient strain models tend to be compared to separate experimental data sets with generally different non-transient strain models, without an independent selection of parametric values for a fair comparison.

It is the aim of this work to provide such an unbiased analysis. Following the formation of the shortlist of models, a key first step is to apply the models in realistic conditions for qualitative analysis of results. This is done for a number of reasons. Practically, this analysis ensures that the models are compatible with the hygro-thermo-mechanical model and that the process of adoption has been completed successfully, such that model output similar to that reported in the literature is possible. Moreover, for the purposes of increasing the effectiveness of quantitative analysis, potential changes to the models can be suggested at this stage that may potentially improve model performance in the intended experimental conditions or that may be suitable for further research.

5.1 Methodology

In order to investigate the qualitative behaviour of the transient strain models in various conditions of high temperature, the models are applied to six sets of realistic experimental conditions. These conditions are chosen in order to demonstrate the

effects of heating rate, temperature level, and cyclic heating on output of each of the models (§5.1.1).

In order to ensure that the material modelled in the simulations is realistic, the parameters of the material model are chosen based on those reported by other researchers (§5.1.2). Although the combination of the specific parametric values chosen is not necessarily identical to any reported, typical values are chosen, so that no extraordinary combination of properties shall be allocated to the material.

Finally, a suitable set of FE model parameters must be chosen for the simulations in order to ensure that the results are reliable. Such a set is here found through direct inspection of the solution using trial and error methodology (§5.1.3).

5.1.1 *Experimental conditions of simulations*

Six sets of heating conditions are here defined to carry out the qualitative investigation.

- *Slow heating to low temperature* (SHTLT)
- *Fast heating to low temperature* (FHTLT)
- *Slow heating to high temperature* (SHTHT)
- *Fast heating to high temperature* (FHTHT)
- *Heat cycle 1* (HC1)
- *Heat cycle 2* (HC2)

The heating (and cooling) rates of the conditions are always linear and either 'fast' ($5℃/min$) or slow ($0.1℃/min$). These heating rates are chosen because $5℃/min$ is a typical experimental heating rate that is considered to be relatively fast, while $0.1℃/min$ is chosen because it is intended to demonstrate effects of heating in conditions such as those encountered by concrete used in nuclear reactor pressure vessels (NPVs). Though the actual heating rates applied for NPVs are far lower than $0.1℃/min$, a higher heating rate is chosen here for practicality. More generally, a rapid heating rate and a slow heating rate are applied in order to examine the effects of temperature field inhomogeneity on the transient strain models.

The temperature history of each heating regime is shown in figure 5-1. As can be seen, all of the tests take place over the course of 30 days. This period is chosen in order to ensure that all state variables reach equilibrium values before the end of the tests. Moreover, some observations suggest that this period of time is sufficient in all cases to allow transient strain to fully develop. Thus, it is worthwhile to observe model output for this period, though only the Bažant model is formulated in such a way that this behaviour may be observed.

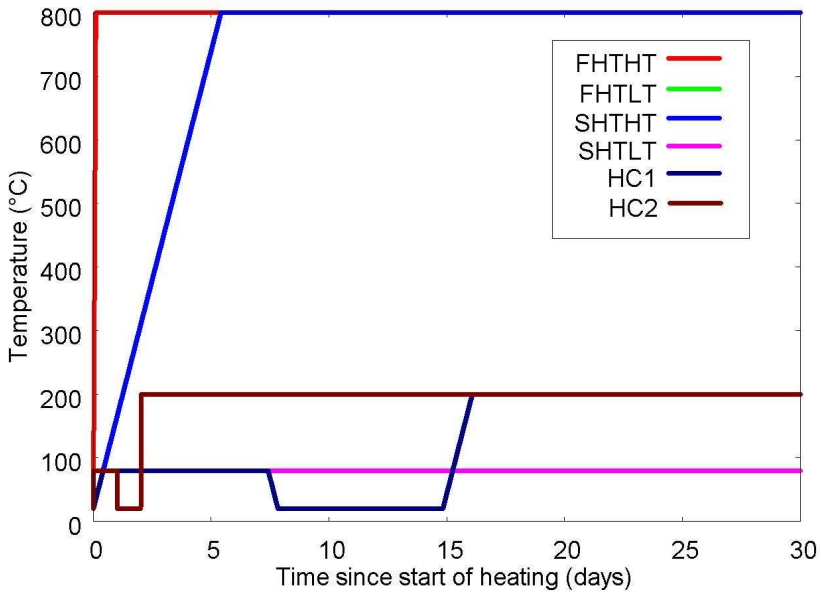

Figure 5-1: The heating regimes used in the simulations.

As shown in figure 5-1, two heat cycles are applied in the tests, HC1 and HC2. The two heat cycles are very similar, each begin with an initial period of temperature increase up to an intermediate value ($80℃$), which is held for a period of time before a subsequent period of cooling to the initial temperature (which is also held for a period of time) and subsequent second period of heating to a higher temperature ($200℃$). The distinguishing features of the two heat cycles are the rates of temperature change and the periods of time spent at constant temperature. HC1 is characterised by a heating (and cooling) rate of $0.1℃/min$ and a period of constant temperature of seven days, while HC2 is characterised by equivalent parameters of $5℃/min$ and one day respectively. These features are chosen to demonstrate any effects of the length of the period of time between heat cycles and at high temperature on the subsequent development of transient strain in non-virgin heating conditions (each of these factors were theorised as potentially critical in such development in §2.1.3).

The concrete specimens to be used for the simulations are of standard cylindrical dimensions similar to those commonly used in tests of heated and/or loaded concrete specimens, i.e. a diameter of $150\ mm$ and height $300\ mm$ [2]. These dimensions are expected to result in inhomogeneous temperature fields for the tests involving rapid heating, particularly to high temperatures.

Heating conditions applied to the specimens are those of a furnace. Thus, heat and moisture transfer occurs at the surface of the specimens. This is a very common experimental method.

Each of the tests is performed in two distinct loading cases, i.e. unloaded conditions and uniaxial constant compressive load equal to 30% of f_c. Only two load levels are considered as this aspect of the model is unlikely to yield useful results at this stage of qualitative analysis.

For the investigation into the nature of tensile transient strain, the FHTHT experimental conditions alone are applied. These conditions are chosen as they are expected to lead to thermal stresses of the largest magnitude and, thus, to local tensile stresses during heating.

The investigation of the transient strain response to conditions of tension may be investigated using these experimental conditions. As the set of conditions that causes thermal stresses of the largest magnitude is of particular interest to this analysis, it is only the FHTHT conditions that are applied for this analysis. Moreover, as the influence of the model on the specimen stress state is critical to this analysis, an additional loading case is considered, defined as a constant uniaxial compressive load equal to 60% of the initial compressive strength.

5.1.2 *Material properties*

Material properties are chosen here with reference to those that have been previously used in the research field in order that realistic material behaviour is assured. Table 5-1 shows the most important of these material parameters to be used in the relevant hygro-thermo-mechanical model defined in chapter 3.

In general, parameters not named in table 5-1 are found to vary little between analyses, are of a lesser importance to results of this analysis or are defined by specific experimental conditions (e.g. initial moisture content).

Table 5-1: Material parameters to be used in the simulations.

Name of parameter	Value of parameter used	Example references
Elastic modulus	$30\ GPa$	[121, 122]
Initial compressive strength	$40\ MPa$	[76, 123, 124]
Initial tensile strength	$4\ MPa$	[124-126]
Intrinsic permeability	$1.2 \times 10^{-17} m^2$	[125, 127, 128]
Initial porosity	8%	[122, 129, 130]
Initial thermal conductivity	$1.64\ WK^{-1}m^{-1}$	[121, 131]
Apparent density	$2400\ kgm^{-3}$	[131-133]

Total strain decomposition is given by the following.

$$\varepsilon_{tot} = \varepsilon_{th} + \varepsilon_{el} + \varepsilon_{tr} \qquad \text{Equation 5-1}$$

ε_{th} is modelled using Equations 3-32 and 3-34 (§3.3.3), which may be written as follows.

$$\varepsilon_{th}(\theta) = \begin{cases} \beta ln\left(\dfrac{\theta_1}{\theta' - \theta}\right) & \theta \leq \theta_1 \\ \beta ln\left(\dfrac{\theta'}{\theta' - \theta_1}\right) + \gamma(\theta - \theta_1) & \theta > \theta_1 \end{cases} \qquad \text{Equation 5-2}$$

where β, γ and θ' are free parameters of the thermal strain model, given by default as 6×10^{-3}, 0 and 7 respectively, and θ_1 is the transition (reduced) temperature, given as 6. In principle, these parameters may be calibrated to reproduce experimental data, though this is not performed here.

ε_{el} is largely defined by the concrete stiffness, which is found to decrease with temperature increase. Material stiffness degradation due to temperature increase is accounted for using the thermal damage formulation, defined principally by Equation 3-29. This model may be written as follows.

$$E(\theta) = \left(1.0 - 0.1\hat{\theta}\right)^2 E_0 \qquad \text{Equation 5-3}$$

where E_0 is the initial value of Young's modulus and $\hat{\theta}$ is a history variable that is equal to the highest (reduced) temperature reached by the material.

The final strain model considered in this qualitative analysis is ε_{tr}. As the mathematical formulation of the transient strain formulation is not expected to be significant for the tensile transient strain investigation, as indicated in §4.11, only the Nielsen model shall be applied (§4.6). For the qualitative investigation of the transient strain models, each of the Bažant model (§4.1), the Anderberg model (§4.2), the Terro model (§4.5), the Nielsen model (§4.6), and the Schneider model (§4.8) shall be applied.

5.1.3 *FE model parameters*

As previously mentioned, the concrete specimens to be used in simulations are cylinders of diameter $150\ mm$ and height $300\ mm$. Consistent with the methodology chosen for this work, the specimen is approximated by a mesh of finite elements. As the problem is axisymmetric, a two dimensional mesh can be used without loss of accuracy.

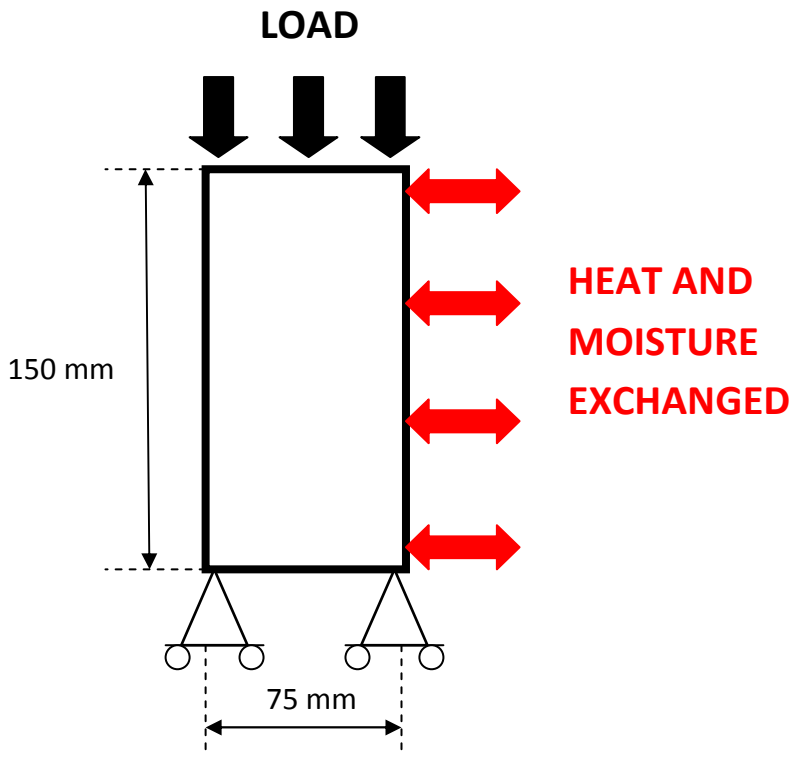

Figure 5-2: The FE mesh to be applied for simulations in this work.

The body of the mesh is composed of eight-noded (serendipity) quadrilateral elements and three-noded line elements along the rightmost edge to represent the curved surface of the cylinder. These line elements allow the exchange heat and moisture between the cylinder and the external atmosphere. External loading is applied to the uppermost edge of the mesh, which represents the cross-sectional surface of the

cylinder, as shown in figure 5-2. This loading is imposed by weighted position-dependent nodal forces that are constant in time. The loading is ideal in that no friction is assumed between the loading agent and the concrete specimen and because the loading is assumed to be distributed evenly over the cross section of the specimen throughout the test. No heat transfer is allowed across the loading surface.

As the loading and heating conditions are symmetrical, it is not necessary to simulate an entire 2D slice of the body. In fact, only one quarter of the area of a slice must be modelled, with displacement constrained on the lower edges in the axial direction, as shown in figure 5-2.

On the basis of direct tests of FE model output using a wide range of values of time step and mesh discretisation schemes (see Appendix B), a time step of two seconds and a mesh of 600 body elements (30×20) is applied for analysis. Results obtained using a mesh thus defined are found to be near-identical to results obtained using finer meshes and smaller time step values.

It should be noted that, unless otherwise stated, strain results presented in this work are the GPM measures (§3.5). Tests demonstrated that the GPM measures of all state variables are, to a high degree of accuracy, the same as the volume-averaged measures.

5.2 Transient strain in tension

The issue of the transient strain response to states of tension has received very little attention. Experimental data that allow for a thorough investigation into the existence and nature of tensile transient strain are sparse. Although there have been several examples of experimental transient strain investigation in which the nature of applied load is torsion [14, 16] or flexure [11], experiments are most often performed using applied uniaxial compression [9, 10, 13, 17, 18]. Moreover, experimental tests performed in direct tension appear to be extremely rare, due to the significant practical difficulties of loading a CM specimen in tension, particularly in heated conditions. Therefore, the lack of attention to modelling of transient strain of concrete in conditions of applied tension can be attributed to a relative scarcity of experimental tests to reproduce and a paucity of practical examples in which concrete structures undergo direct tension.

To investigate the nature of the transient strain response to states of tension, three distinct mathematical formulations for this aspect of the model are separately assumed. Application of each of these models (with all other aspects of the hygro-thermo-mechanical model identical) allows the effects of each of these distinct models on total strain results to be examined by comparison. This is intended to establish the potential importance of the tensile transient strain response of concrete in typical laboratory conditions and provide evidence for the most appropriate mathematical formulation for this phenomenon.

Partially following the suggestion of Pearce et al. [94], three forms for the materials' transient strain response to tensile states are adopted here; these are defined as follows. A component of tensile stress, in conditions of simultaneous virgin heating, causes

- no transient strain component (*TTS0*),
- a tensile component of transient strain identical in magnitude to that produced by an identical compressive stress (TTS1), and
- a tensile component of transient strain identical in magnitude to that produced by an identical compressive stress-strength ratio (TTS2).

Transient strain can be assumed to be governed by the following equation.

$$\varepsilon_{tr} = f_{tr}(T) g_{tr}(\sigma) \qquad \text{Equation 5-4}$$

where f_{tr} and g_{tr} are the temperature-dependent and load-dependent factors that govern transient strain respectively. Thus, g_{tr} is distinct for each of these assumptions and can be defined as follows.

$$g_{tr}^{TTS0} = \begin{cases} \dfrac{\sigma}{f_c}, & \sigma \leq 0 \\ 0, & \sigma > 0 \end{cases} \qquad \text{Equation 5-5 (a)}$$

$$g_{tr}^{TTS1} = \begin{cases} \dfrac{\sigma}{f_c}, & \sigma \leq 0 \\ \dfrac{\sigma}{f_c}, & \sigma > 0 \end{cases} \qquad \text{Equation 5-5 (b)}$$

$$g_{tr}^{TTS2} = \begin{cases} \dfrac{\sigma}{f_c}, & \sigma \leq 0 \\ \dfrac{\sigma}{f_t}, & \sigma > 0 \end{cases}$$ Equation 5-5 (c)

Each of the factors g_{tr} for the TTS assumptions, defined by Equations 5-5 (a)–(c), is illustrated in figure 5-3.

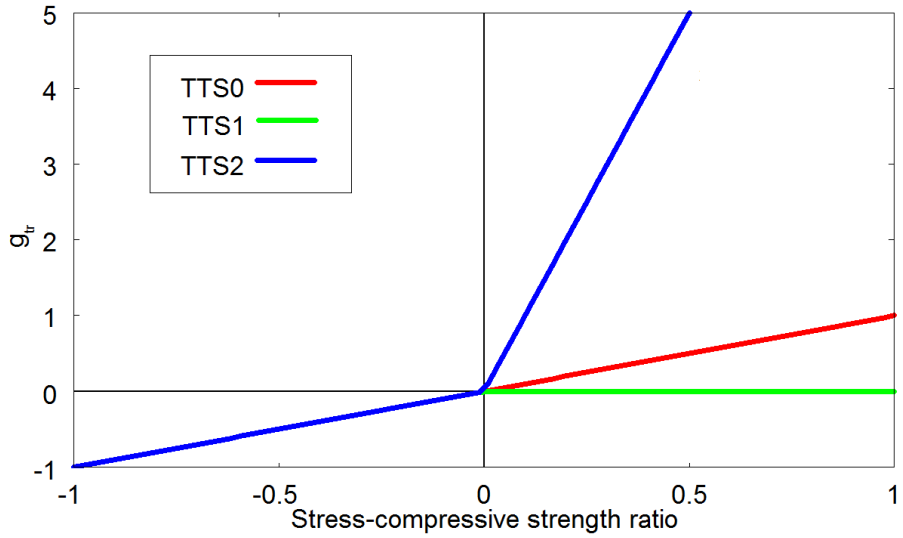

Figure 5-3: Graphical representation of g_{tr} for each TTS assumption. Note that it is assumed that the tensile strength is 10% of the compressive strength.

As shown in figure 5-3, g_{tr} is identical for each of the TTS assumptions in the compressive loading range (i.e. $\sigma < 0$). In the tensile loading range however, g_{tr} is very different for each. For TTS0, g_{tr} is given as zero regardless of the loading magnitude. Thus, no transient strain may develop for any tensile load. For TTS1, g_{tr} develops as for compressive loads. Thus, effectively no distinction is made between tensile transient strain and compressive transient strain. For TTS2, it can be seen that g_{tr} develops far more rapidly in the tensile loading range than in the compressive loading range. This is a direct result of the far lower tensile strength of concrete. As a result, a large magnitude of transient strain shall develop for relatively low magnitudes of tensile loading.

As can be intimated from Equation 5-4, it is assumed a priori that the temperature-dependence of transient strain due to tension is identical to that due to compression. The possibility that this is not the case is not explored as there appears to be no rational method with which to approach an investigation in this way at the present time.

In order to compare the effects of the assumptions TTS0, TTS1, and TTS2 on the total strain behaviour of concrete in heated conditions, simulations of concrete cylinders in FHTHT conditions are performed (§5.1.1). These conditions are expected to result in significant thermal stresses within the specimens during heating. When a material is heated rapidly, the tensile thermal stresses that develop are balanced by the compressive thermal stresses that also develop in heated conditions. Thus, the action of transient strain, which is far more rapid than the action of conventional creep, may significantly affect this balance during heating. As a result, the TTS assumption applied may play a significant role in defining the total strain behaviour observed in these conditions.

For comparison with model output, hypothetical 'experimental data sets' are here produced, using each of the strain models defined in §5.1.2, by direct application of the experimental parameters to the models. These data sets are illustrated in figure 5-4 It is expected that each of these models have been calibrated to experimental data sets using experimental methodology similar to that applied in these simulations. Thus, the total strain behaviour produced by each of these models should be similar.

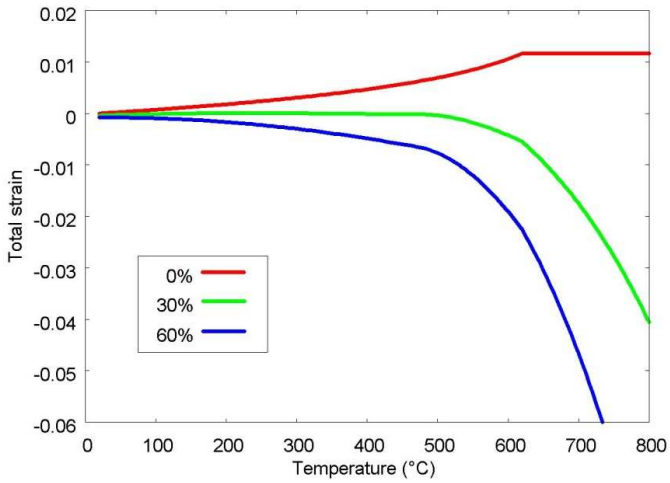

Figure 5-4: The hypothetical axial strain of a concrete specimen heated under load (0%, 30%, and 60%) to 800°C.

As previously mentioned, interaction between the thermal stresses produced during heating and the transient strain model should in principle have an effect on the total strain behaviour of the concrete specimens. As a result, a component of net transient strain may in theory develop during heating in unloaded conditions. Such a strain component in these conditions is not commonly reported in the literature to the best of the present author's knowledge. This may be due to the lack of an analytical tool

such as that applied here to directly record GPM measures of all strain components automatically during FE simulations.

If this strain component develops with a significant magnitude, experimental results should be interpreted in such a manner that this is taken into account. Thus, the total strain in unloaded heated experimental conditions should not be considered to be thermal strain. Instead, both models should be chosen to be mutually consistent in producing the total strain behaviour.

For the present work, the net transient strain found to develop in unloaded FHTHT conditions are shown in figure 5-5 (a) for each of the TTS assumptions defined by Equations 5-5 (a)–(c), alongside the hypothetical total axial strain for these conditions. It can be seen that this net transient strain measure is strongly affected by the TTS assumption applied.

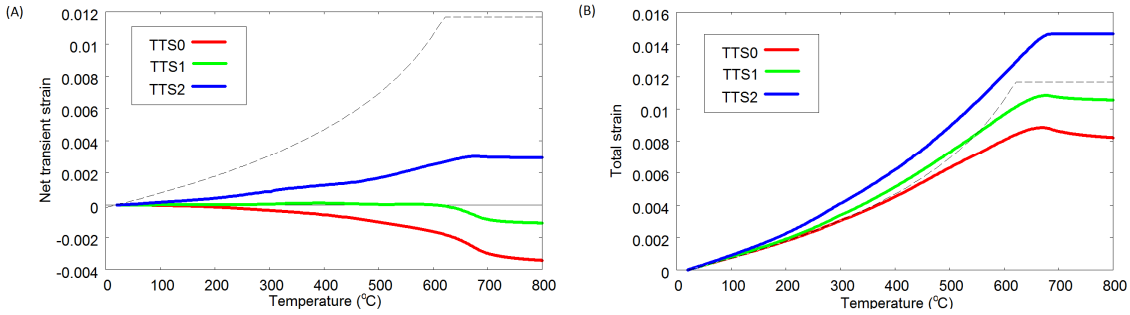

Figure 5-5: (a) Net transient strain and (b) total strain that are found to develop in unloaded FHTHT conditions for different TTS assumptions, The dotted line shows the intended total strain development.

The results of figure 5-5 (a), produced using the thermal strain model represented by the dotted line, show that the TTS0 assumption results in net transient strain that is consistently compressive in nature. This is unsurprising as there can be no direct tensile transient strain in this material (though net positive transient strain may develop due to lateral compression). In contrast, results obtained using the TTS1 assumption show very little net transient strain development. The strain does not appear to be consistently tensile or compressive in nature. The net transient strain that develops due to application of the TTS2 assumption is of a comparable magnitude to that of TTS0 throughout the test but of opposite sign.

The magnitude of the net axial transient strain that develops in the simulations where the TTS0 or TTS2 assumptions were implemented is approximately equal to one third of that of the thermal strain that develops. Thus, net transient strain that develops in

unloaded conditions must be considered to be significant in these conditions, dependent on the TTS assumption applied. Moreover, the thermal strain models must be recalibrated to account for this net transient strain in order to ensure that total strain results are consistent with the hypothetical experimental data set (the dotted curve in figure 5-5 (a)). The consequences of not calibrating thermal strain in this manner can be directly seen in the results of figure 5-5 (b), whereby the total strain found depends strongly on the TTS assumption applied.

Using *trial and error'* methodology, the thermal strain models of each of the materials can be calibrated such that the simulated total strain of each of the materials are approximately consistent with one another and very closely match the hypothetical total strain behaviour of heated concrete under no external loading. The results of this procedure are shown in figure 5-6.

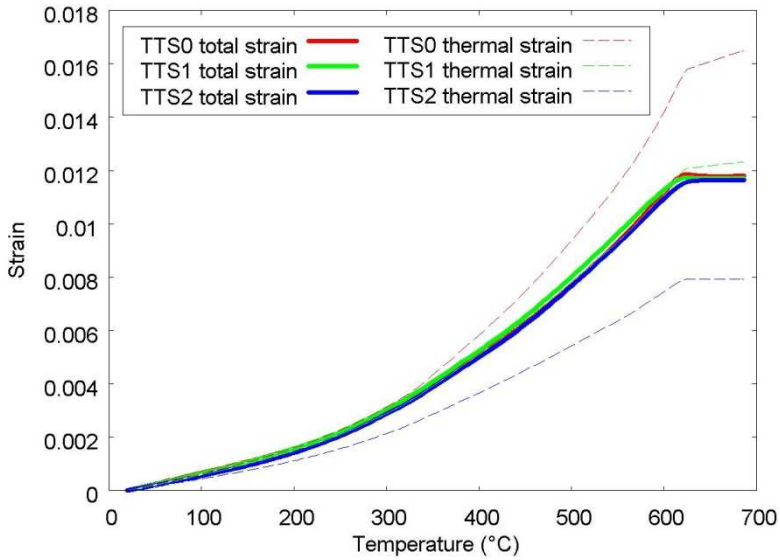

Figure 5-6: The axial component of total strain and of thermal strain for heated unloaded cylindrical specimens of materials TTS0, TTS1, and TTS2.

As shown in figure 5-6, the thermal strain component of materials TTS0 and TTS2 deviate significantly from the total strain of each material in the applied conditions. TTS0 requires a more thermally expansive behaviour and TTS2 a less thermally expansive behaviour in order to produce consistent total strain behaviour. Material TTS1 undergoes very little net transient strain; hence, the thermal strain is nearly identical to total strain.

Application of external uniaxial compressive loading (equal to 30% of initial compressive strength) to the three materials produces intriguing results. The axial

component of total strain observed for each of the TTS assumptions, shown in figure 5-7, depends strongly on TTS assumption. Where the TTS0 or TTS1 assumption has been applied, the specimens are found to undergo a small quantity of net expansion up to the point in time at which a temperature of between about $500℃$ and $600℃$ is reached, after which the materials contract. No similar expansion is found to occur for the specimen modelled using the TTS2 assumption. At the point when a temperature of $800℃$ has been reached by the specimens, each of the specimens has undergone a net contraction with an approximately evenly spaced range of axial contractive strains, between about $-25\ mm/m$ and $-40\ mm/m$ (the TTS2 assumption results in contraction of the largest magnitude and TTS0 the least).

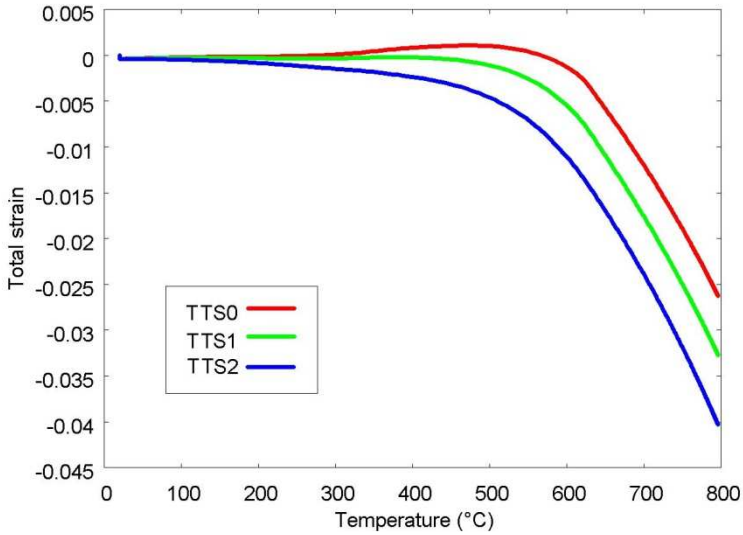

Figure 5-7: The axial component of total strain for cylindrical specimens modelled using three different TTS assumptions (TTS0, TTS1, and TTS2) heated at 5°C/min under uniaxial compression equal to 30% of the initial compressive strength.

This dissimilarity of total strain behaviour, as exhibited in figure 5-7, suggests that an assumption made in producing these results must be reconsidered. Examination of the axial transient strain behaviour of each of the materials, shown in figure 5-8, gives a strong indication of the nature of this incorrect assumption.

As can be seen in figure 5-8, the development of the transient strain component of the specimens in loaded conditions is very nearly independent of the TTS assumption applied. In turn, the FE model output is nearly identical to the ideal transient strain (given by direct application of the Nielsen model to the experimental conditions). Thus, the measure of transient strain that develops in unloaded conditions (also shown in figure 5-8) has a negligible influence on that which develops in loaded conditions.

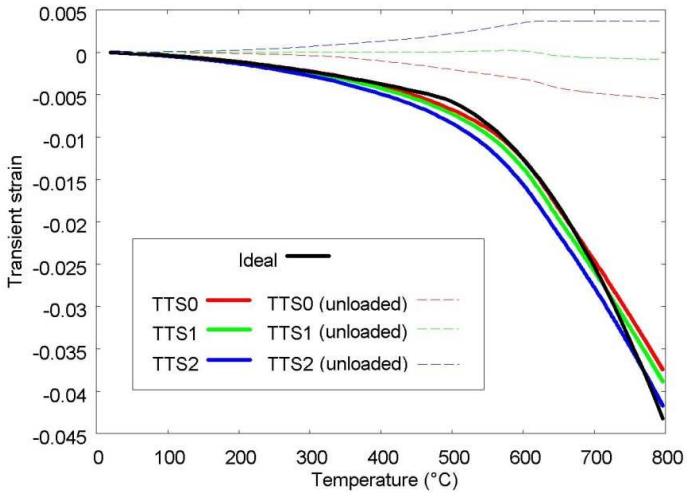

Figure 5-8: The axial component of transient strain for cylindrical specimens modelled using three different TTS assumptions heated at 5°C/min under uniaxial compression equal to 30% of the initial compressive strength. Also included for comparison are the 'ideal' transient strain behaviour at this load level and the transient strain behaviour found to develop in unloaded conditions for each TTS assumption.

Therefore, it is clear that the cause of the difference in the total strain curves of figure 5-7 is that it was assumed that it is valid to apply the superposition principle to the total strain that develops in unloaded conditions and the mechanical strain components that develop when load is applied. In fact, due to the development of significant transient strain in unloaded conditions, this is not valid, as can be shown easily.

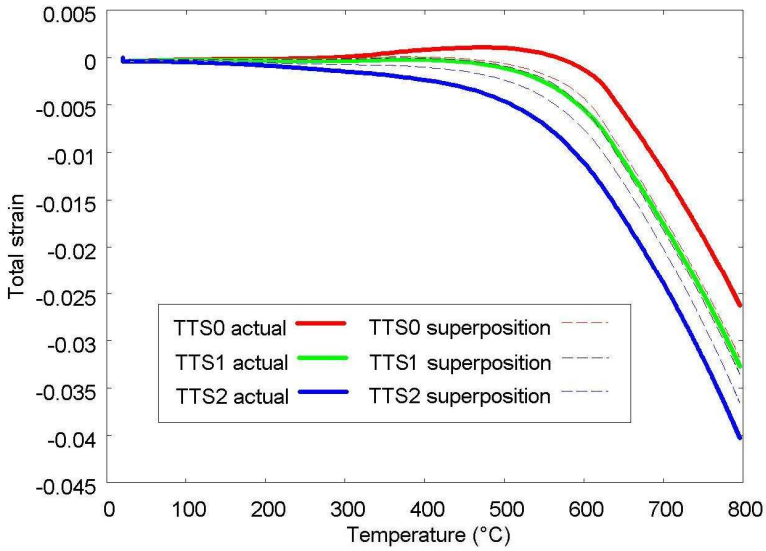

Figure 5-9: The total strain observed in conditions of heating under load for the three TTS assumptions (TTS0, TTS1, and TTS2), along with the total strain history calculated by superposition of total strain in unloaded conditions with elastic strain and transient strain in loaded conditions.

This is illustrated in the results of figure 5-9, which shows the total strain curves for each TTS assumption found through direct FE simulation and by superposition of the total strain in unloaded conditions and the additional mechanical strain components that develop in loaded conditions.

The apparent failure of the superposition principle for materials TTS0 and TTS2, illustrated in figure 5-9, can be considered to be due to the reduction in influence of transient strains caused by thermal stresses when external loading is applied. This can be explained with a very simple model. Assume that the position-dependent axial stress state of concrete can be approximately described by the following.

$$\sigma(\boldsymbol{r}) = \pm\delta(\boldsymbol{r})|\bar{\sigma}_{th}^{max}| \qquad \text{Equation 5-6}$$

where σ is the instantaneous axial stress at any location $\boldsymbol{r}$ within the concrete specimen, δ is a position-dependent proportionality factor normalised to unity, and $|\bar{\sigma}_{th}^{max}|$ is the maximum thermal stress magnitude within the specimen. Based on the results of figure 5-9, $|\bar{\sigma}_{th}^{max}|$ can be assumed to be less than 10% of the compressive strength. Thus, in unloaded conditions, the active range of the g_{tr} function for each TTS assumption is illustrated by figure 5-10 (a). It can be seen that the TTS assumption is significant to the transient strain output of the model as the loading range in which the TTS assumptions are divergent in model predictions is active.

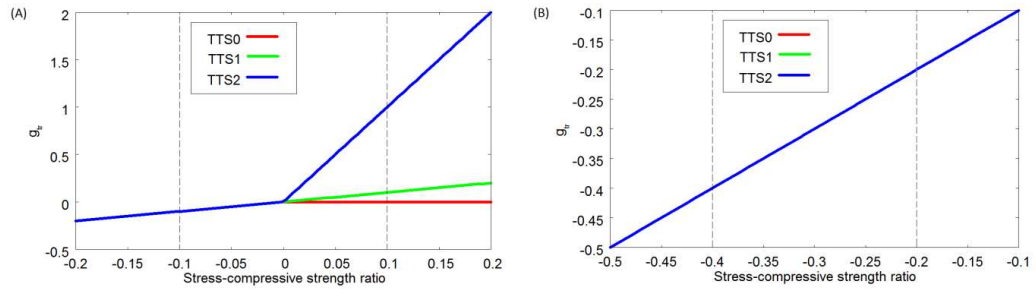

Figure 5-10: Active ranges of g_{tr} during FHTHT test in (a) unloaded conditions and (b) conditions of constant external uniaxial compressive load equal to 30% of the initial compressive strength.

When a load of 30% of the initial compressive strength is applied, it is clear from the results of figure 5-10 (b) that the TTS assumptions no longer produce different transient strain predictions as the loading range does not include the tensile region. Thus, in these conditions, the transient strain model outputs for all three TTS assumptions are identical.

In order to make the total strain predictions consistent for each TTS assumption in both loaded and unloaded conditions, it is necessary to allow the transient strain parameters to vary by TTS assumption. It is very difficult to simultaneously determine appropriate values for the parametric set of both the transient strain and thermal

strain models in this manner. Therefore, in order to simplify the analysis, only the parameter of the transient strain model that is active for temperatures higher than $470℃$ for the Nielsen model, C, is considered to deviate from the initial value applied here. As much of the difference in total strain results, shown in figure 5-9, is in this temperature range, this may be an effective technique to improve model results.

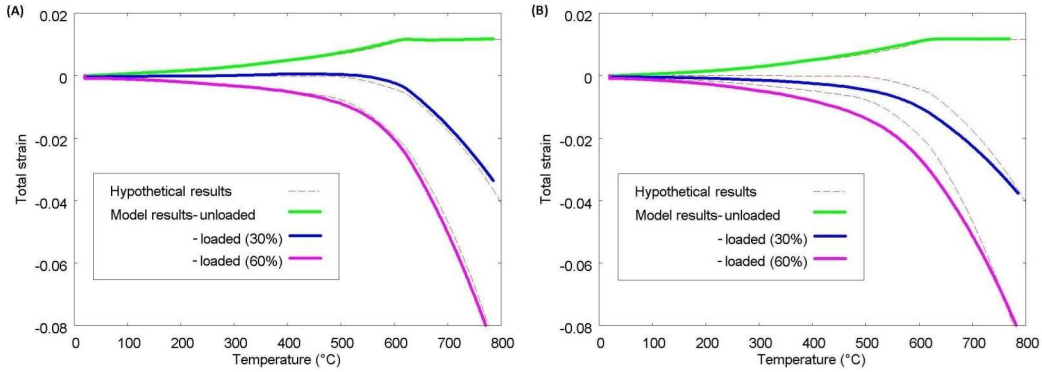

Figure 5-11: The total axial strain of a loaded concrete cylinder subjected to FHTHT conditions. The TTS assumptions applied are (a) TTS0 (with C=13×10^{-3}) and (b) TTS2 (with C=9×10^{-3}).

As shown in 5-11 (a) and (b), after trials of several different values of C for the cases where the assumptions TTS0 and TTS2 are applied, an obvious improvement can be achieved when using the TTS0 assumption if $C = 13 \times 10^{-3}$. However, no significant improvement in model results can be found for the case where assumption TTS2 is applied by changing the value of this parameter. The results indicate that total strain results deviate from the hypothetical total strain results by a significant degree in the low temperature range. Thus, in order to further improve model performance, it is likely to be necessary to recalibrate further parameters of the transient strain model.

Therefore, it can be concluded that use of the TTS0 and TTS1 assumptions may produce results that are consistent with experimental observations. There is no basis at this stage to state that evidence supports either of these models. Moreover, even though use of the TTS2 assumption could not be here shown to be also capable of producing results consistent with experimental evidence, this assumption cannot be discarded at this stage because it is probable that if all of the transient strain model parameters were included in the calibration process, model results would be improved. Such a process shall take place in the work of chapter 6.

For the remaining simulations of this chapter, the TTS1 model assumption alone shall be applied. This assumption is chosen because it produces results consistent with

current practice automatically (in particular that total strain in unloaded conditions contains negligible transient strain) and is, therefore, likely to produce behaviour intended by the original authors without calibration of model parameters.

5.3 Predictions of models in various high temperature conditions

Although much can be deduced from the pure mathematical models presented in chapter 4, it is necessary to examine the results of application of these models realistically, such as within a hygro-thermo-mechanical model in a FE environment. There are some examples of this for each model in the literature, though the conditions in which the models are applied are not consistent with one another. Therefore, to compare the models, it is useful to perform parallel simulations using different transient strain models in a range of experimental conditions

The general multiaxial form of the transient strain models can be written as follows.

$$\Delta\boldsymbol{\varepsilon}_{tr} = \begin{cases} \mathbf{0} & , \quad \Delta T \leq 0 \\ \boldsymbol{M}\boldsymbol{\sigma}'\Delta T & , \quad \Delta T > 0 \end{cases} \qquad \text{Equation 5-7}$$

where $\boldsymbol{M}$ is a tensor that defines the temperature-dependence and the multiaxial nature of the model. Transient strain is assumed in this work to be isotropic in nature. Therefore, in general, $\boldsymbol{M}$ is a function of temperature and a transient strain Poisson's ratio parameter, υ_{tr}. In this work, υ_{tr} is assumed to be equal to 0.2 and independent of load and temperature.

The Bažant model is the only transient strain model considered in this work that cannot be written in the form of Equation 5-7. Thus, the general form if this model may be defined as follows.

$$\Delta\boldsymbol{\varepsilon}_{tr} = \boldsymbol{M}^{*}\boldsymbol{\sigma}'\Delta t \qquad \text{Equation 5-8}$$

where $\boldsymbol{M}^{*}$ is the tensor that defines the magnitude of transient strain that develops in time Δt due to effective stress $\boldsymbol{\sigma}'$. It is dependent on υ_{tr} in a similar manner to $\boldsymbol{M}$ due to the assumption of isotropy.

In the discussion to follow, two measures of axial transient strain shall be utilised. These are the value equal to the mean of the axial transient strain values calculated at

each Gauss point throughout the simulation and the value calculated directly from the total axial displacement results in loaded and unloaded conditions (and application of the mathematical model for temperature-dependent elastic strain). The latter measure is intended to reproduce the experimentally observed transient strain measure, while the former is intended to be representative of the actual transient strain active within the specimens during heating. For the purposes of clarity, the former measure of transient strain shall be referred to as the *actual transient strain*[9] and the latter measure as the *deduced transient strain*.

Results show that the peak temperature difference across the rapidly heated specimens is far larger than that across the slowly heated specimens. The temperature difference across the FHTHT specimens reaches a value of approximately $300°C$ at a late stage of the heating process, whereas the maximum temperature of the SHTHT specimens is about $10°C$ and occurs after a reduced time of heating relative to the surface temperature. As the heating rate differs by a factor of 50, these results are reasonable. The effect of this difference in temperature across the mesh can be considered to account for much of the differences in behaviour of the rapidly heated specimens and the slowly heated specimens. The FHTLT and SHTLT specimens do not acquire such large temperature differences (a maximum of about $10°C$ for the FHTLT specimens) due to the significantly reduced heating period.

Results of relative humidity averaged over the specimen show that the rapidly heated specimens dry out almost completely by the point at which the average temperature of the specimen is approximately $400°C$. The equivalent point for the slowly heated specimens occurs at an average specimen temperature of $300°C$. The lower temperature of drying can clearly be attributed to the increased time prior to the point at which any given temperature is reached of the SHTHT specimens.

It is necessary to calibrate the thermal strain parameters to the intended apparent thermal strain formulation in one set of conditions. As it is unimportant in which set of conditions this process is performed, the FHTHT conditions are chosen for this purpose. Through trial and error, the parameters of the thermal strain model can be

[9] This term should not be taken to literally mean that this measure is a true measure of transient strain. The Gauss-point averaging technique is itself inherently approximate when applied to 2D axisymmetric problems in the manner used here due to the lack of weighting factors in the calculation process.

chosen for each transient strain model such that the simulations produce results that fairly closely match the predictions of the thermal strain model of Equation 5-2, as shown in figure 5-12. Although the variation in values of thermal strain parameters by transient strain model is relatively small, the effect on total strain in loaded conditions may be significant.

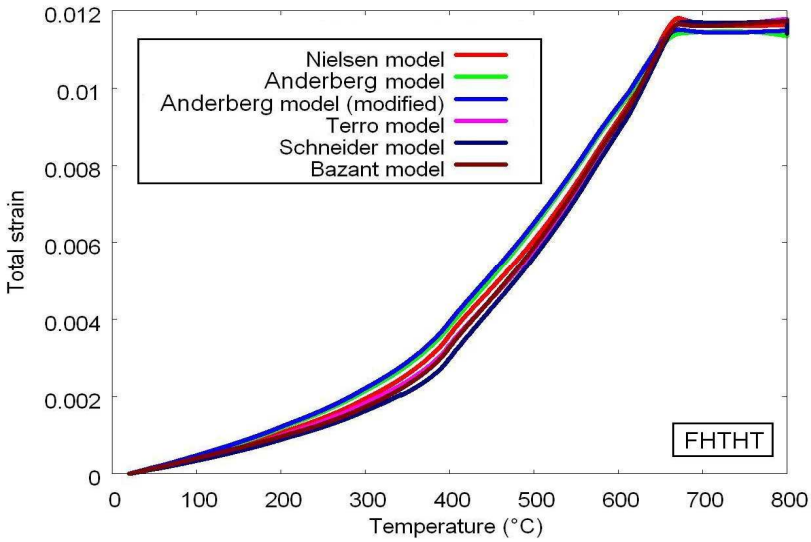

Figure 5-12: Total strain results in unloaded FHTHT conditions using all five transient strain models.

Comparison of the total strain results in unloaded SHTHT conditions, as shown in figure 5-13, indicates the effect of heating rate on the thermal strain results. These results, which are almost exactly simply the thermal strain component, demonstrate the influence of transient strain in the results of figure 5-12.

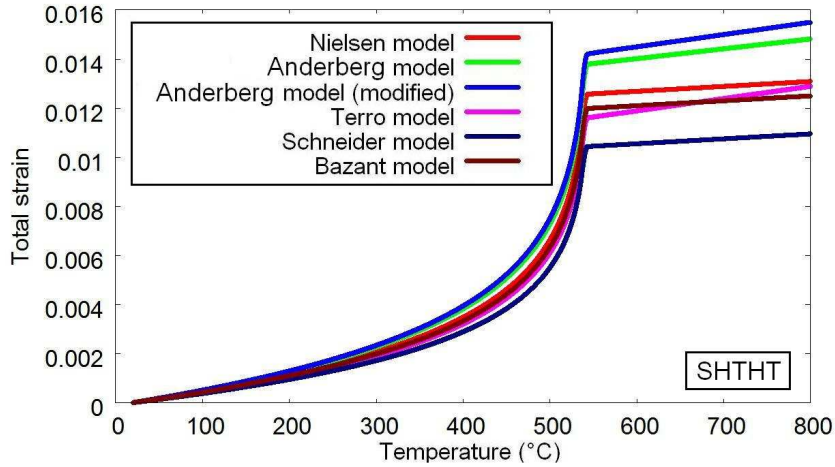

Figure 5-13: Total strain results in unloaded SHTHT conditions using all five transient strain models.

As shown in figure 5-14, the dependence of the total strain in unloaded conditions on the heating rate is fairly large. The temperature at which a transition in total strain development occurs is shifted by about 100℃ by use of a different heating rate. Also,

the rate of strain increase in the temperature range slightly below the transition temperature is consistently higher for the specimens that are heated more slowly.

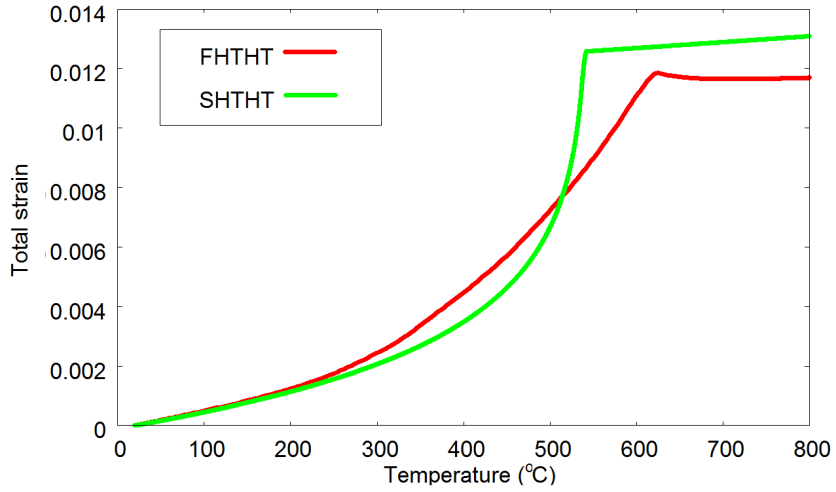

Figure 5-14: Total strain results for unloaded specimen in FHTHT conditions and SHTHT conditions, modelled using the Nielsen transient strain model.

The different total strain development of specimens in FHTHT conditions and those in SHTHT conditions is caused by several factors. Throughout the heating period, a large temperature differential exists across the specimen heated in FHTHT conditions, which is absent in the specimen heated more slowly. This means that the temperature measure associated with the specimen during this period is not representative of large volumes of the specimen. Thus, it is inevitable that the strain-temperature curve diverges from that associated with more slowly heated specimens.

Moreover, the thermal stresses induced in the specimens in the FHTHT conditions lead to the development of net transient strain in the specimens. The development of net transient strain is the reason that the two curves do not reach a consistent final total strain value at the end of the test. The measures of transient strain found appear to confirm this and show, as in figure 5-12, that the net transient strain measure that develops during heating of an unloaded specimen in FHTHT conditions is approximately the difference in total strain between the two curves of figure 5-14. This observation is valid for the results found for all transient strain models.

The difference in total strain results of figures 5-12 and 5-13 becomes most significant for temperatures above about $400℃$. Therefore, rapid heating to temperatures below this level should not be expected to produce significant self-induced thermal stresses and consequent transient strain, as is confirmed by figure 5-15. Indeed, the results of

cyclic heating at different rates to 200℃ (i.e. HC1 and HC2) under no load show no transient strain component in results.

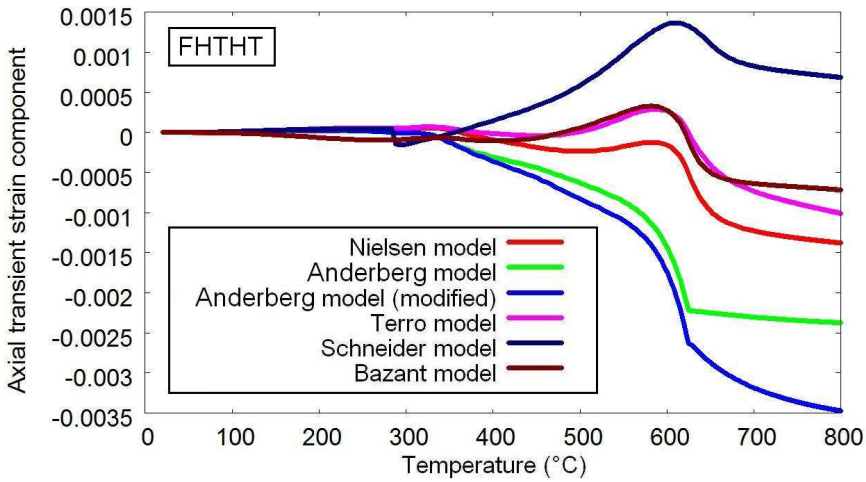

Figure 5-15: Average measures of transient strain that develops in unloaded specimens in FHTHT conditions, due to local thermal stresses calculated using all five transient strain models.

The transient strain curves induced by thermal stresses in the unloaded specimens can be seen in figure 5-15 to be highly dependent on the transient strain model used. Although the curves clearly undergo qualitatively very similar behaviour, the specific transient strain evolution is quite variable.

It should be noted that, of the three TTS model assumptions proposed in §5.2, these results are produced using the TTS1 model assumption, which is found to result in the lower bound net transient strain response in unloaded conditions (as positive and negative strain components approximately balance). Therefore, if evidence emerges that experimental results are more consistent with either the TTS0 assumption or the TTS2 assumption material, the effects of the net transient strain induced by thermal stresses observed here may underestimate the real effects.

Results show a fairly large deviation in total strain results for different transient strain models applied to specimens loaded and heated to 800℃. The Anderberg model (in both modified and unmodified forms) results in a much lower degree of negative strain in the high temperature region than all of the other models. As shown in figure 5-16, the Nielsen model, Terro model, and Schneider model appear to exhibit very similar total strain behaviour over most of the temperature range, whereas the Bažant model exhibits a larger development of negative strain in the high temperature range than most of the other models.

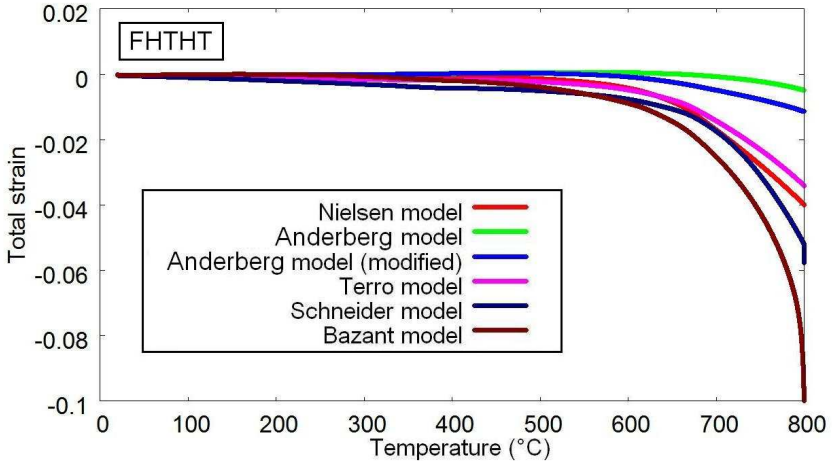

Figure 5-16: Total strain results for loaded specimens in conditions of FHTHT. Note that the Bažant model deforms at constant temperature beyond the minimum strain value shown in the graph.

Unlike each of the other models, the Bažant model undergoes a great deal of additional strain development in the period of time spent at constant temperature for the FHTHT conditions. The total strain at the point at which the mean specimen temperature reaches approximately $800℃$ can be seen in figure 5-16 to be approximately -0.1. However, after a period of 30 days from the start of heating, this value is found to increase further in magnitude to approximately -0.23. Note that this strain development at constant temperature is not observed in the unloaded specimens because thermal stresses are rapidly relaxed by transient strain.

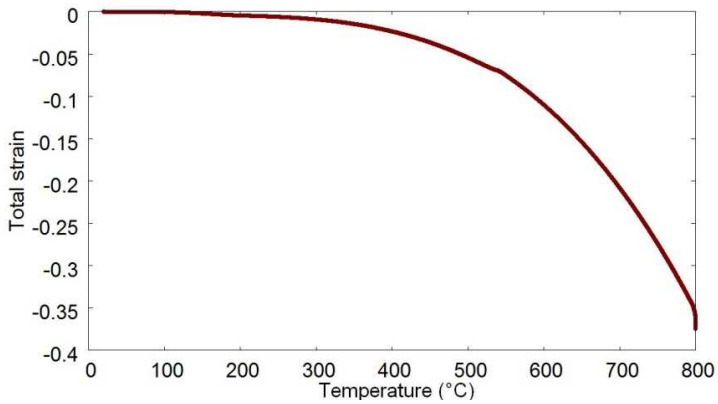

Figure 5-17: Total strain results for the loaded specimen in SHTHT conditions modelled using the Bažant transient strain model.

The loaded specimens in SHTHT conditions undergo similar behaviour to those of figure 5-16. However, the results for the Bažant model, shown separately in figure 5-17, are of an increased negative magnitude. This can be considered to be due to the increased development time for the transient strain mechanism of the Bažant model for any given temperature. It is noteworthy that, despite the very low heating rate, a

small degree of delayed transient strain develops in the period after constant temperature is reached.

The development of transient strain calculated using the Bažant model during the period of constant temperature observed for the specimens heated to $800℃$ in conditions of rapid heating and slow heating are similarly observed in the results of specimens heated to low temperatures, i.e. $80℃$. In both conditions of FHTLT and SHTLT, a significant development of negative strain occurs during the period of constant temperature, as is illustrated by the results of figure 5-18. This can be considered to be due to the finite length of time required for the microprestress to decay to a low value, which is due in part to the slow process of drying. Similar results are found for the specimens subjected to both HC1 and HC2 conditions.

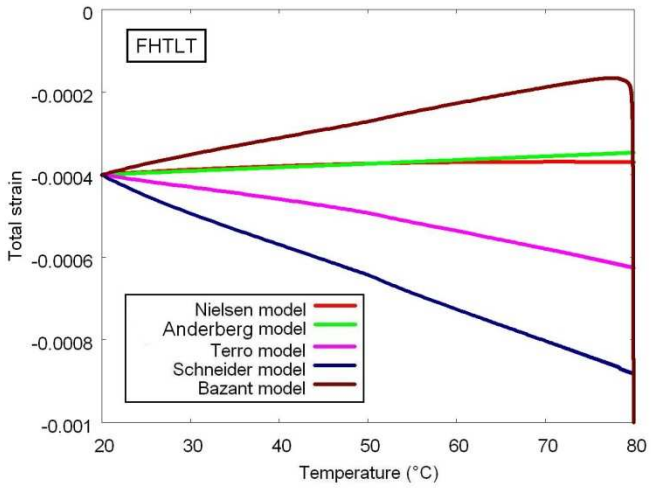

Figure 5-18: Total strain results for loaded specimens in FHTLT conditions. Note that the Bažant model develops at constant temperature beyond the minimum strain value shown in the graph.

The effect of heating rate on the axial transient strain evolution can be found through comparison of the deduced transient strain evolutions found for the SHTHT specimens and the FHTHT specimens. Results consistently show for the Nielsen model, Anderberg model, Terro model, and Schneider model that a very similar transient strain component develops in both sets of conditions with a slightly increased strain magnitude developing in the temperature region above about $400℃$. This general result is well represented by figure 5-19, which shows the set of results found for the Nielsen model.

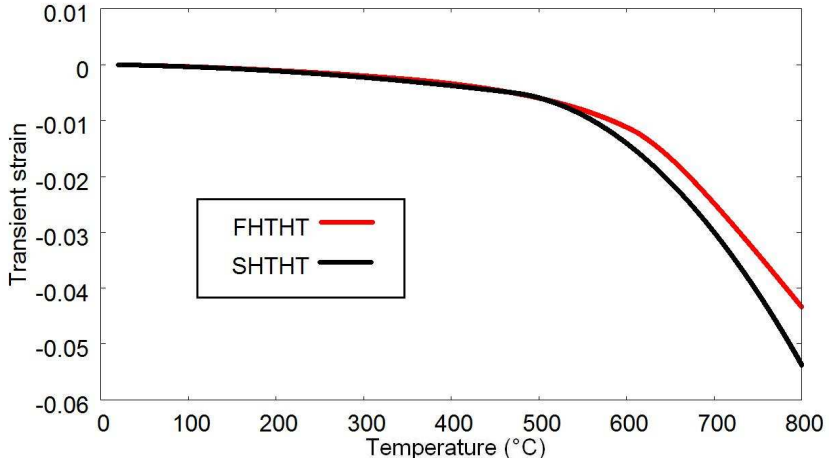

Figure 5-19: Deduced transient strain component that develops in the loaded specimens in FHTHT conditions, calculated using the Nielsen model.

The equivalent results for the Bažant model are shown in figure 5-20. It can be seen that the difference between the magnitude of transient strain that develops in FHTHT conditions and SHTHT conditions is very large and develops throughout the temperature range.

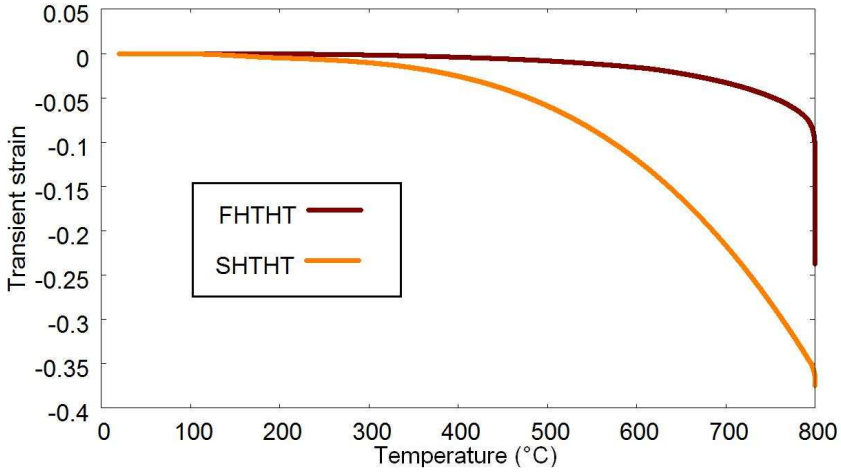

Figure 5-20: Deduced transient strain component that develops in the loaded specimens in FHTHT conditions, calculated using the Bažant model.

The heat cycle results give an indication of the effect of the transient strain models on the deformation of the specimens in conditions of cooling and re-heating. The unloaded HC1 results exhibit highly reversible behaviour during heating and cooling for all the models. This implies that no transient strain develops in these conditions. The loaded HC1 results are similar to the respective unloaded results for the Nielsen model, Anderberg model, Terro model, and Schneider model with the addition of transient strain to the results, though the curves differ from one another to a relatively high degree. It is noteworthy that the models that produce very similar total strain behaviour when under load in the high temperature range, i.e. the Nielsen model, the

Terro model, and the Schneider model, produce more distinct total strain behaviour in the low temperature range. Conversely, the Anderberg model, which produces a total strain behaviour that is dissimilar to those of the other models in the high temperature region results in a very similar total strain evolution to the Nielsen model in the temperature range below 200℃, as shown in figure 5-21.

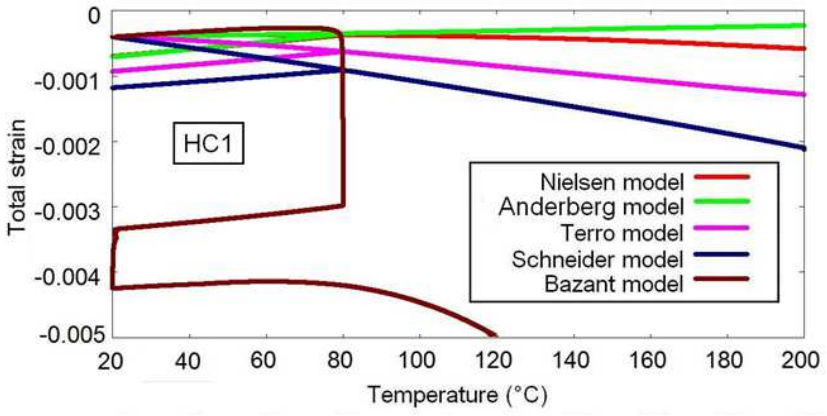

Figure 5-21: Total strain results for loaded specimens in HC1 conditions using all of the transient strain models.

Also shown in figure 5-21 is the total strain evolution of the Bažant model in loaded HC1 conditions. The results show that the total strain that develops is significantly different to that of any of the other models after the first temperature plateau value is reached. In particular, a very large negative strain develops in the total strain results in each of the constant temperature periods of the heat cycle.

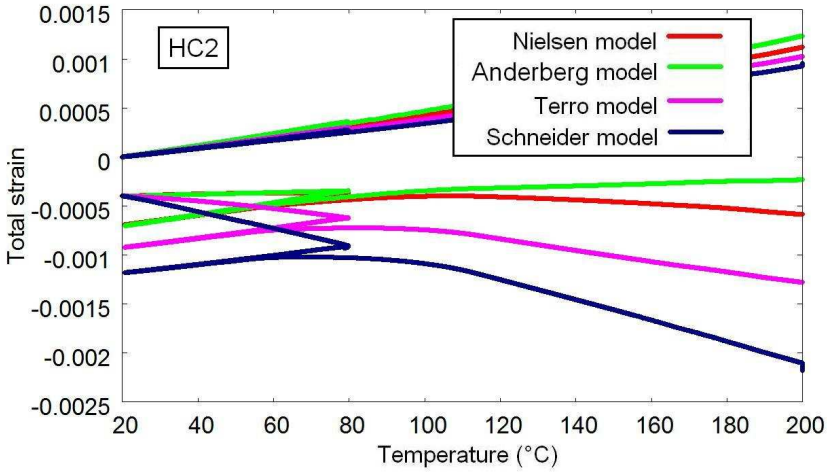

Figure 5-22: Total strain results for both loaded and unloaded specimens subjected to the HC2 conditions using the Nielsen model, the Anderberg model, the Terro model, and the Schneider model.

The more rapid heat cycle conditions (HC2) produce broadly similar total strain results. As shown in figure 5-22, the total strain behaviour of each model develops in an approximately identical manner to the respective curves of figure 5-21. One clear

difference is that, during the re-heating phase of the loaded specimens, total strain of each set of simulations does not appear to reversibly follow the total strain evolution of the first heating phase. There appears to be an additional negative component that develops in the period of time immediately preceding that at which the first temperature plateau is reached. It appears that there may be some development of transient strain in non-virgin heating conditions.

As shown in figure 5-23, the deduced transient strain measures for the HC2 conditions, which is determined using a process that intentionally replicates methods of determination of the transient strain component as if from experimental observations, suggests that a small quantity of transient strain does apparently develop in non-virgin heating conditions. This is in contrast to the HC1 conditions which show no development of transient strain until the previous maximum temperature is exceeded.

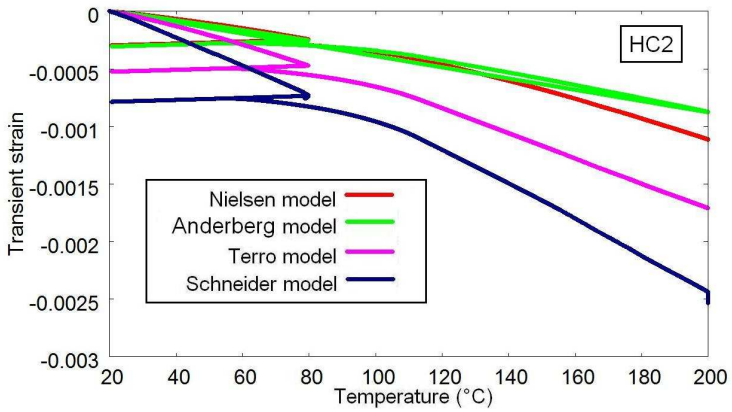

Figure 5-23: Deduced transient strain results for specimens loaded and subjected to the HC2 conditions using the Nielsen model, Anderberg model, Terro model, and Schneider model.

As the strain models used to produce the total strain models of figure 5-23 are formulated such that the development of transient strain in non-virgin heating conditions is forbidden, it can be deduced that the increase in transient strain shown in figure 5-23 is an apparent effect. In fact, this increase in deduced transient strain is due to the temperature differential across the specimen. During re-heating, the average specimen temperature does not exceed the previous maximum temperature until half of the volume of the specimen is at a temperature that exceeds this value. There is a period of time for which an outer portion of the cylinders is at a temperature above 80℃ (the previous maximum specimen temperature in this case) and therefore undergoes transient strain. Due to the previous heat cycle, this transient strain in excess of that associated with the mean value is not offset by the reduced transient

strain of material at temperatures below the mean value. Therefore, the mean transient strain measure of the specimen exceeds that which is expected for the mean specimen temperature.

Another observation that can be made with regard to the results shown in figure 5-23 is that the transient strain measure appears to increase in magnitude during cooling and decrease reversibly during re-heating. This phenomenon is also an apparent effect, which appears to be a result of the thermal stresses that develop during heating and cooling (which are not accounted for in the process of calculating the deduced measure of transient strain). Analysis of the components of elastic strain and transient strain confirms both the asymmetry of the axial thermal stresses during cooling and re-heating and that no transient strain develops on cooling respectively.

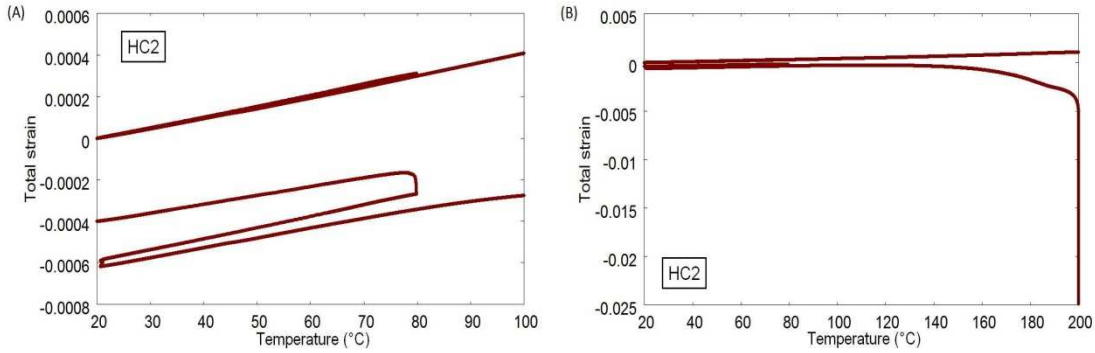

Figure 5-24: The total strain results of both loaded and unloaded specimens subjected to the HC2 conditions calculated using the Bažant model, shown in (a) the low temperature region only and (b) the entire temperature range of heating.

The equivalent results for the Bažant model, shown in figure 5-24 (a), demonstrate that the results in the early period of the HC2 experimental conditions are similar to those of the other models in magnitude although a significant quantity of negative strain develops in the period of time spent at the first temperature plateau. However, as shown in figure 5-24 (b), in the period of heating above about 100℃ and the second elevated temperature plateau, a negative strain of an extremely large magnitude develops and results in very different total strain behaviour than that of any other transient strain model, shown in figure 5-22.

It is also noteworthy from the results of figures 5-24 (a) and (b) that no significant degree of transient strain is found to develop during (or at the initial temperature after) cooling. This suggests that one major area of disagreement for this model with experimental observations (i.e. that transient strain does not develop in conditions of

temperature decrease) is found to be relatively unimportant, without application of explicit model constraints to ensure that this is the case.

5.4 Modifications of models

The results have shown that the transient strain models chosen for analysis in this work produce a varied response to loading and heating. There is some scope for some of the models to be modified in order to potentially better reproduce experimental observations. Therefore, some proposals are here made on potential modifications that can be made to the models.

5.4.1 *Modification of Bažant model*

There are two principal issues with the Bažant model that may be resolved by modification of the mathematical formulation of the model. Firstly, the constraint placed on the model that the microprestress value can never decrease to a negative value appears to be inconsistent with the prior development of the model. Secondly, the results of §5.3 suggest that the transient strain behaviour produced by this model may be qualitatively consistent with broad experimental observations that were discussed in section §2.1.2, that transient strain may develop slowly in the low temperature range ($T < 100℃$) but more rapidly for higher temperatures.

During development of the model, Bažant et al. [56] imposed absolute value bars on the microprestress evolution equation in order to prevent the microprestress from developing negative values (Equation 4-9). This is justified as it allows microprestress to evolve in such a way that an increase in transient strain may be predicted in cooling conditions, despite an acknowledged likely overestimate in transient strain that this causes.

Alternatively, it is here suggested that the result intended by the authors may also be obtained if the microprestress evolution equation is defined as initially suggested.

$$\dot{S} + \psi_S c_0 S^2 = k_1 \left(\dot{T} \ln h + T \frac{\dot{h}}{h} \right) \qquad \text{Equation 5-9}$$

In addition to use of Equation 5-9, modification of the viscosity model (such that the absolute value of microprestress is the argument of the function) allows negative

values of microprestress to develop as the 'natural' form of the model appears to allow, without the development of a negative viscosity term, which would make no physical sense.

$$\frac{1}{\eta(S)} = 2c|S| \qquad \text{Equation 5-10}$$

However, there is also a potential issue with the modifications of Equations 5-9 and 5-10. In some conditions of temperature and relative humidity change, a model formulated in this manner may predict that the microprestress value develops to be lower in magnitude than the hypothetical value used to determine the specific component of transient strain calculated by the model. This may result in an apparent reduction in creep rate due to the change in conditions and thus to transient strain recovery, which has never been reported. Tests may be necessary to determine if this issue is likely to be significant.

If the Bažant model is modified in the manner detailed above and found to be reliable, it is possible to speculate that insights may be provided into the absence of transient strain in cooling conditions and the development of transient strain in non-virgin heating conditions. However, this work is not generally accepted by most researchers, and not pursued by Bažant et al. [56]. In a model, such as that defined above, prolonged cooling may be required for a sufficient decrease in microprestress that the sign is reversed and the magnitude of the term increases.

With regard to the second principal issue determined in this work with regard to the Bažant model (i.e. that the delayed transient strain observed is not generally supported by experimental observations, particularly in the high temperature range), it may be possible to modify the mathematical model in order to retain some time-dependence in the low temperature behaviour, while modifying the high temperature behaviour to avoid the significant delayed component of transient strain here found to be predicted by this model for loaded specimens.

As can easily be shown through mathematical simulation, the value of k_1 is of extremely large importance in defining the influence of changing temperature and relative humidity on the increase in microprestress (and subsequent transient strain).

Therefore, as changes in relative humidity only affect the microprestress evolution in the lower temperature region and changes in temperature affect the microprestress evolution in the entire temperature region, the model may behave in a manner more qualitatively similar to experimental observations if the term representing changing temperature and that representing changing relative humidity are coupled using separate parameters to the microprestress evolution. Therefore, the modification here suggested is that microprestress evolution (Equation 4-9) is rewritten.

$$\dot{S} + \psi_S c_0 S^2 = \left| k_1^T \dot{T} \ln h + k_1^h T \frac{\dot{h}}{h} \right| \qquad \text{Equation 5-11}$$

where k_1^T and k_1^h represent separate coupling parameters introduced in place of k_1 in Equation 4-9. If the values of k_1^h and k_1^T are chosen carefully, the qualitative behaviour of the model may be consistent with experimental observations. Specifically, the value of k_1^T can be chosen such that a changing temperature leads to a smaller increase in microprestress than is implied by the original model. This may result in a reduced development of transient strain in high temperature conditions during heating and in the period at constant elevated temperature. However, a future investigation may be necessary to demonstrate if such a qualitative change in model behaviour can be effected in this manner.

5.4.2 *Modification of Anderberg model*

The results of application of the FE simulations of this work suggest that the component of transient strain predicted at high temperatures by the Anderberg model may be too weak. Whereas the total strain results of this model appear to be very similar to those of the Nielsen model, the Terro model and the Schneider model in the low temperature range, these models develop a significantly increased magnitude of model output in the high temperature region.

A further issue with the Anderberg model is that transient strain is found to be of a lower degree of variation between different concretes than thermal strain. This shall certainly be an issue when the model is used for predictions of different concrete types.

In terms of the first issue with regard to the Anderberg model, the modified form of the model is found to provide high temperature total strain behaviour of more similar behaviour to that of the other models. Therefore, it appears that this issue can be resolved easily with adoption of the modified form of the model and a change in the magnitude of the coupling parameters of the equation.

Regarding the objection to the model that the thermal strain behaviour and the transient strain behaviour of concretes do not appear to be related as suggested by this model, it may be necessary to introduce a dependence on the coefficient of thermal strain at a reference temperature to the definition of the transient strain coupling coefficient. If an appropriate value of the coefficient of thermal strain of a concrete used to define the model is found to be, say, $7\ mm/m$ at 500℃, then the general model can be redefined as follows.

$$\dot{\varepsilon}_{tr} = \beta_0 \frac{\sigma}{f_c(T_0)} \frac{7.0 \times 10^{-3}}{\alpha_{th}(500°C)} \alpha_{th} \dot{T} \qquad \text{Equation 5-12}$$

where the parameter β_0 may retain the default initial value.

If it is valid to apply a transient strain model that depends linearly on the thermal strain behaviour of the material, the modification of Equation 5-12 should result in transient strain predictions for different concrete types that are similar despite distinct thermal strain behaviour.

5.4.3 *Modification of Nielsen model*

No specific issues are found to be present in the Nielsen model in this work. However, it is here proposed that the transition temperature of the model may be considered to be a free parameter of the model. There is no theoretical argument to constrain the transition temperature to a value of 470℃. Therefore, based on experimental evidence, the value of this parameter may be re-defined.

5.4.4 *Modification of Terro model*

Aside from the issues discussed in §4.5 with respect to the load-dependence of the model and the use of the reduced temperature variable in the model calculations, there are no further modifications to be made to the Terro model.

5.4.5 *Modification of Schneider model*

The Schneider model may be interpreted as a model based on the principle of dehydration creep. As shown in §4.8, the major temperature-dependence of the model is here found to be appropriate as a mathematical description of the degree of a thermally-activated chemical reaction. As the Sabeur model (§4.4) is based on similar principles, it is consistent to examine this model for potential modifications of the model.

The Schneider model, which is intended in the original form to be applied to conditions of rapid heating, may therefore be modified such that time-dependence is incorporated into the model for heating at relatively low rates. As the dehydration process is not instantaneous, this modification is theoretically justified.

To modify the model in this manner, it is necessary to equate the function ϕ of the Schneider model (Equation 4-56) with the function m_{eq} of the Sabeur model (used in Equation 4-30 and defined in figure 4-11 (b)). Therefore, the function ϕ may be considered to be equivalent to the temperature-dependent limiting value of a sub-function (equivalent to the dynamic mass of dehydrated material, m_{dehyd}) which is used in the modified Schneider model in place of ϕ. The evolution of this function may be defined, analogously to Equation 4-30.

$$\dot{\psi} = \frac{\phi(T, w) - \psi}{\tau_{hyd}^{Sch}(T)} \qquad \text{Equation 5-13}$$

where ψ is the sub-function that defines the dynamic value of the hyperbolic tangent function and τ_{hyd}^{Sch} is the Schneider model dehydration relaxation time, which may be plausibly considered to be a function of temperature. The equivalent parameter of the Sabeur model [46, 64] is found to be well defined as a constant. However, this conclusion may be considered to remain open to investigation, particularly as the temperature range considered in the previous examination of the time-dependence of the dehydration process did not exceed $500℃$.

5.5 Closing remarks

This chapter aimed to explore the potential mathematical mechanisms for modelling the transient strain due to states of tension and to examine typical output of the models in realistic heating conditions chosen for the shortlist in §4.11. This was performed within the context of a hygro-thermo-mechanical model set in a FE environment (as defined in chapter 3).

In order to examine the most appropriate tensile transient strain model, three assumptions were defined for this aspect of the model (TTS0, TTS1, and TTS2). These three assumptions, which are significantly different from one another, represent three potential mathematical formulations for TTS that may be considered reasonable.

By FE modelling of realistic conditions of rapid heating applied to concrete cylinders, it has been shown that significant net transient strain may develop in unloaded specimens. Moreover, it was shown that the magnitude of this strain component depends strongly on the TTS assumption applied. Specifically, a net negative (positive) strain component of a magnitude of about one third of the thermal strain magnitude is found to develop for the TTS0 (TTS2) assumption.

Due to the significant magnitude of this net transient strain, it is necessary to recalibrate the thermal strain model parameters such that total strain in unloaded conditions is consistent with the intended behaviour. It is as a result of this recalibration that the TTS assumption applied influences the total strain behaviour of concrete in loaded conditions. In this work, it is found that, for consistency, use of the TTS0 assumption requires a more thermally expansive concrete and TTS2 a less thermally expansive concrete. When external loading is applied to these concretes, the axial transient strain component that develops due to thermal stresses is found to be negligible (in contrast to the case for unloaded specimens) and, thus, total strain results in loaded conditions deviate from those obtained by superposition of total strain in unloaded conditions and the mechanical strain that develops in loaded conditions. Therefore, in order to produce similar predictions in both loaded and unloaded cases, a process of simultaneous calibration of thermal strain and transient strain models is necessary. The success of such a procedure for each TTS assumption in

comparison to experimental data may provide evidence for the most appropriate TTS assumption to adopt in practice. This work shall be performed in chapter 6.

Preliminary evidence suggests that use of both TTS0 and TTS1 assumptions can produce results consistent with experimental observations. However, generally distinct parametric sets must be allowed for the transient strain model. Model results produced using the TTS2 assumption could not be made here fully consistent with experimental observations, though the methodology of this investigation may not have been sufficient to allow this to occur. In chapter 6, more sophisticated methodology shall be applied that shall demonstrate whether it is possible to apply the TTS2 assumption and produce results consistent with experimental behaviour.

The quantitative analysis of each of the shortlist of transient strain models showed that the development of net transient strain in unloaded conditions occurs for all transient strain models. As this strain component has been directly examined in this work using the novel methodology that produces GPM values of the strain components throughout the FE simulations (§3.5), it is proposed here that such a tool should be implemented in general. In the absence of such a technique, it is not possible that this strain component could be examined directly and interpretation of model results would have been more difficult.

Some of the results of heat cycling (HC2) appear to support the development of a small quantity of transient strain in non-virgin heating conditions. However, this is explained here as an apparent effect caused by the development of transient strain in the volume of the specimen that is at a temperature sufficient to lead to further transient strain, while the volume-averaged temperature measure is insufficient to lead to this behaviour.

Most of the transient strain models produce results consistent with experimental evidence. Use of the Bažant model, however, leads to behaviour that may not be regarded as realistic. In particular, according to the Bažant model, a great deal of transient strain develops in constant temperature conditions under applied load, particularly at elevated temperatures. While this is not observed for unloaded specimens (as transient strain rapidly relaxes thermal stresses), even heating to

relatively low temperatures ($80°C$) leads to development of significant delayed transient strain.

No significant degree of transient strain is found to develop for simulations of the Bažant model in the cooling phase of the heat cycle tests. As this is a potential area of strong disagreement between this model and experimental observations, this is an important observation.

As a result of this qualitative investigation, several model modifications are proposed for the models. Two potential modifications are suggested for the Bažant model. These are to combat the potential issues in the model that have been highlighted by this work. Firstly, it is suggested that the microprestress term should not be constrained such that it may take negative values. It may be argued that this is more consistent with the original development of the mathematical model. In order to avoid absurd predictions, such as development of a negative value of viscosity, the viscosity term of the model may also be modified such that it is dependent on the absolute value of the microprestress term.

Secondly, it is suggested that the parameter that couples changes in the temperature and relative humidity to the evolution of the microprestress term is decomposed into two separate terms that represent separately temperature change and relative humidity change. This is intended to address the issue observed here that the Bažant model consistently predicts unrealistic developments of transient strain in constant temperature conditions, particularly at high temperatures.

It is shown in this work that the modified form of the Anderberg model is necessary to produce results that are similar to those of the other models in the high temperature range. Thus, it is proposed that this model is applied in general.

It is a well known criticism of the Anderberg model that concretes that undergo a greater magnitude of thermal strain are not observed to undergo a similarly greater magnitude of transient strain in equivalent conditions. Therefore, a modification of the Anderberg model is here proposed in which the model is normalised by coefficient of thermal strain at a particular reference temperature. Thus, the magnitude of thermal strain does not affect the magnitude of transient strain that develops, though the

temperature-dependence of thermal strain still governs the temperature-dependence of the transient strain.

Chapter 6. Quantitative analysis of model performance

In chapter 4, a shortlist of five models to be considered in the remainder of the work was chosen based on a number of explicit criteria. The predictions of these models in different realistic heating conditions were explored in chapter 5, with modifications subsequently proposed to improve model performance. While this investigation has been useful in demonstrating typical model output and demonstrating qualitative agreement with experimental observations, it is the aim of this work to make an objective quantitative assessment of the ability of the models to reproduce experimental results.

The results of chapter 5 demonstrate that, in some conditions, thermal stresses induced by heating can lead to net transient strain in unloaded concrete specimens. In particular, it was shown that the nature of the TTS assumption applied in the transient strain model formulation can be significant in defining the magnitude of total axial strain observed in heated concrete. Although no firm conclusion could be drawn from this work about which of the three TTS assumptions implemented (Equations 5-4 and 5-5 (a–c)) leads to model behaviour most consistent with experimental results, it is clear that it is necessary to calibrate the thermal strain and transient strain model parameters for each of the TTS assumptions separately. Thus, when applied to a range of experimental results, predictions of the models may diverge and comparisons with experimental data sets may indicate which TTS assumption is most realistic.

In this chapter, the transient strain models shall be applied to realistic conditions of heating and compared to experimental data. In order for this procedure to be objective, however, it is necessary that uncertain error caused by ill-fitted parametric sets is minimised. Therefore, the parameters of each of the transient strain models shall be calibrated to the experimental data sets considered in this work. One of the transient strain models shall be simulated using each of the three TTS assumptions (defined in §5.2) in turn in order to attempt to provide evidence for which leads to the most consistency with experimental results.

In order to carry out such a process, it is necessary to apply a novel methodological framework that allows the simultaneous calibration of thermal strain and transient

strain to identical data sets. The framework developed here for this purpose is outlined in §6.1.

Furthermore, in order to ensure that the investigation to be performed in this chapter is reliable, it is necessary that the experimental data set used provides as much information as possible regarding relevant hygro-thermo-mechanical parameters. This ensures that all aspects of the model (aside from thermal strain and transient strain) can be accurately calibrated to the experimental data accurately prior to the investigation, which is important for an objective analysis. Details of the experimental data sets considered in this work are provided in §6.2. Moreover, aspects of the model that are selected to ensure that the FE simulations reproduce experimental behaviour well are discussed in §6.3.

The results of application of the present methodology to the experimental data sets for each of the transient strain models are presented and discussed in §6.4. Finally, a further short piece of work performed into the load-dependence of transient strain implied by the experimental data is outlined in §6.4.7. Transient strain is almost always assumed to be linear in load-dependence (in the loading range of interest). Thus, any deviation from linearity may have important consequences for the field of transient strain modelling.

In the following work, the term '*principle of monotonic transient strain increase*' is used. This term is used in reference to the general observation that $\frac{\partial|\varepsilon_{tr}|}{\partial T} \geq 0$ for all temperatures.

6.1 Methodology

In order to carry out an objective analysis of the transient strain models of interest here, it is necessary to explicitly define the objective of this investigation. A set of parametric values shall be sought for each transient strain model that results in the axial strain history that most closely matches the experimental data sets. The set of parametric values that achieve this shall be considered to be the *best set* of parameters for the model.

Due to the component of transient strain found in this work to consistently develop in unloaded heated specimens due to interaction between thermal stresses and the

transient strain model, mutually consistent parametric values must be found for both the thermal strain model and the transient strain model. Thus, calibration of the thermal strain model must be carried out simultaneously with the calibration of the transient strain model over all available experimental data sets.

Therefore, a methodology is required that allows a systematic and objective search for suitable parameters for each of the models. Broadly, there are two main methods of fitting model parameters to experimental results; these are '*trial and error*' and direct curve fitting. In this context, trial and error means that several different sets of parametric values are employed in a realistic model (e.g. FE modelling) until eventually a parametric set is found for which the model results are close to the experimental results. At this point, the values of the parameters may be refined until a close enough fit is obtained. Alternatively, direct curve fitting is a conventional method of directly calibrating model parameters to data sets. However, as a realistic model, like a FE model, cannot be used, some realistic effects (e.g. thermal stresses) must be ignored.

The former technique requires significant resources to carry out and the model may not fit the experimental data in a fully satisfactory manner, even after many trials. The latter technique, which effectively assumes negligible inhomogeneity of model variables across the modelled specimen throughout the test, may lead to significant errors if applied to inappropriate examples, such as rapidly heated large specimens.

The general process to be employed in this work, referred to as the *iterative feedback technique (IFT)*, is a hybrid of these two approaches, discussed in greater detail in §6.1.1. A key component of the IFT is a novel computer program, named the *Parametric Permutation Iterator* (*PPI*), which automates the trial and error process. When applied to the experimental data for each transient strain model, the PPI identifies the parametric set that produces the most accurate results. To account for the effects of inhomogeneity on the results, the program utilises data files produced using previous FE simulations. Thus, for example, this technique may account for the net effect of thermal stresses on the total strain results.

6.1.1 *The iterative feedback technique*

The IFT is a process here developed in order to calibrate both the thermal strain model and the transient strain model to experimental data sets simultaneously. This is achieved through successive calibrations of each model (an iteration) until subsequent calibrations no longer affect the match between the model and the experimental data. Thus, upon completion of the IFT, a mutually consistent solution should be obtained.

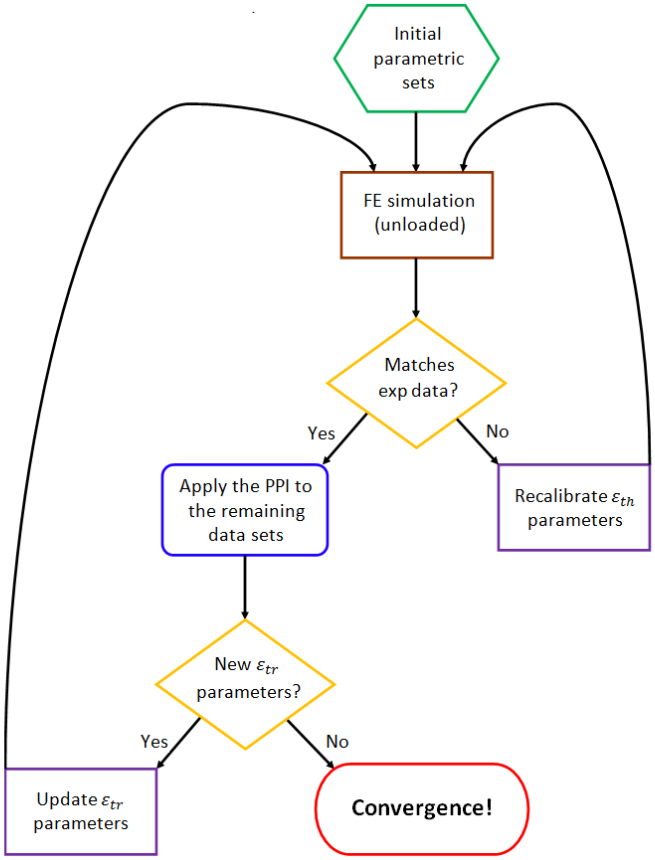

Figure 6-1: Flow diagram representing the IFT procedure.

As shown in figure 6-1, before applying the IFT, an initial set of parametric values are defined for the thermal strain and transient strain models. Using these values, the first stage of the IFT process may be carried out, i.e. the FE simulation of the concrete specimen in unloaded heated conditions.

The next stage of the IFT is the analysis of these results in comparison with the experimental data. If the results are visibly poor, the thermal strain model is recalibrated (§6.1.3) and the FE simulation of the concrete specimen in unloaded heated conditions is repeated. This process is repeated until the results of the FE simulation match the experimental data well.

Upon completion of this stage of the IFT, a set of thermal strain parameters should have been obtained that reproduce the experimental data for unloaded heated concrete, with the initial transient strain parametric set. The next stage of the IFT is to calibrate the transient strain data to the remaining experimental data sets (obtained in loaded conditions). This is achieved through FE simulations of the remaining data sets to produce input data sets for the PPI, which may then be applied. This stage is explained in more detail in §6.1.2.

The result of application of the PPI is that a set of transient strain parameters are selected that produce the closest match to the experimental data. If this parametric set is different from that which was applied during the earlier stage of FE modelling of unloaded heated concrete specimens (or if the change in value of the error measure given by the PPI is not negligible), the transient strain parameters are updated with these new values and a new iteration of the IFT takes place. Otherwise, the IFT is considered to be completed and the thermal strain and transient strain models may be considered to have been calibrated.

6.1.2 *The Parametric Permutation Iterator (PPI)*

The *PPI* is a method that is integral to the operation of the IFT. It is used to determine the transient strain model parameters that result in the closest match to experimental data. This is achieved through a '*brute force*' type process in which simulations of strain history (for each set of experimental conditions to be considered) are performed sequentially until a set of strain histories for every unique permutation of parameters (within certain bounds defined in advance) has been simulated. Through comparison of the total strain history produced for each set of parameters and the intended experimental data set, an error measure is calculated for each.

The simulations made by the PPI program may be considered to be simplified as all variables applied to the model are necessarily representative mean values (e.g. the temperature of the specimen is represented by one value at any point in time). Thus, it is assumed by applying the model that all model variables are homogeneous fields. As this is generally a poor approximation, all model variables applied in the PPI are calculated by interpolation of GPM data generated by FE simulations performed in advance. Thus, for instance, variation of axial load throughout the tests is modelled by

linear interpolation of GPM axial stress data produced in advance for the appropriate set of experimental conditions. This allows realistic effects, such as thermal stress, to be implicitly taken into account globally by the PPI program.

The PPI is a novel technique that is intended to be a hybrid of FE simulations and direct application of parametric calibration, such that the process is more rapid than multiple FE simulations and more realistic than direct curve fitting. To ensure that the PPI program consistently produces realistic results, FE simulations are always performed after the results are obtained.

For the strain calculations of the PPI program, total strain is decomposed into thermal strain, elastic strain, basic creep and transient strain. This strain decomposition is identical to that proposed by the researchers [1] who performed the experiments on which the investigation is based (§6.2).

As for the model variables (such as temperature), the strain components (other than transient strain) are modelled by linear interpolation of GPM data produced in advance by FE simulations of the experimental conditions. This ensures that very little error may be present in the PPI program results due to poor performance of the calculations of these strain components. On a practical level, it also speeds up the execution of the PPI by a significant factor.

The error measure calculated by the PPI program is defined as a weighted sum of the squares of the differences in strain values at each of the temperature values of the experimental data set. In order to calculate this value, the experimental data must be split into a number of subsets of experimental data (10 is chosen for this work). These subsets are split evenly over the entire temperature range in order to remove any bias towards temperature ranges that contain a larger number of data points.

The error measure is expressed mathematically as follows.

$$\delta = \frac{1}{10}\sum_{i=1}^{10}\sum_{j=1}^{N(i)} \kappa_{i,j}\left[\varepsilon_{tot}^{exp}\left(T_{i,j}^{exp}\right) - \varepsilon_{tot}^{sim}\left(T_{i,j}^{exp}\right)\right]^2 \qquad \text{Equation 6-1}$$

where δ is the error measure, $\kappa_{i,j}$ is the weighting factor, ε_{tot}^{exp} and ε_{tot}^{sim} are the experimental and simulated total (axial) strain data sets respectively, $T_{i,j}^{exp}$ is 'jth' temperature value of the 'ith' subset of data points, and $N(i)$ is the total number of experimental data points in the 'ith' subset of data points. The value of δ calculated using Equation 6-1 is representative of the transient strain parameters used to produce ε_{tot}^{sim} and the experimental conditions simulated.

The weighting factor, $\kappa_{i,j}$, of Equation 6-2 is defined as follows.

$$\kappa_{i,j} = \begin{cases} 0 & , \quad N(i) = 0 \\ \dfrac{1}{N(i)} & , \quad N(i) > 0 \end{cases} \qquad \text{Equation 6-2}$$

A value of δ is calculated for each permutation of parameters and each experimental data set. Upon completion of the execution of the PPI program, these values may be examined to determine the permutation of transient strain parameters that resulted in the closest match between simulated and experimental data.

The aim of the execution of the PPI program is the simultaneous calibration of the transient strain model parameters to all experimental data sets available. Thus, the comparisons of the values of δ for each permutation of parameters should involve the sum of the values of δ for each experimental data set. However, it is found that a straightforward summation introduces bias towards the experimental data set that is generally associated with the highest values of δ. Therefore, to remove this bias, a normalisation procedure is applied such that each calculated value of δ is multiplied by a common factor equal to the inverse of the minimum value of δ calculated for each experimental data set to give a normalised set of error measures δ_{norm} (the minimum value of which is unity). Thus, comparison of the sum total of δ_{norm} for any permutation of parameters across all experimental data sets yields the parametric set that is identified by the PPI program as that which best matches the experimental data sets.

The full set of permutations of transient strain parameters to be simulated by the PPI program are defined by three variables for each model parameter, a minimum parametric value, a maximum parametric value, and the total number of

permutations. The values of each parameter are linearly distributed in the range defined by these variables. Where possible, the values of these three variables should be based on rational arguments. Often, this can be achieved by constraining the model results to be consistent with the *principle of monotonic transient strain increase* (as analysis shows that some permutations of transient strain values may lead to violations of this principle).

It is not always possible to argue a priori for limits on the values that can be taken by the model parameters. In these instances, a heuristic approach is taken, i.e. preliminary limits are defined in a manner consistent with parametric values used elsewhere. If the bounds on the model parameters are found to be restrictive, the upper and/or lower limits can be modified and the analysis repeated.

6.1.3 *Conventional fitting technique*

As stated in §6.1.1, in operation of the IFT, it is necessary to recalibrate the thermal strain model to account for the net components of transient strain, elastic strain, and basic creep that may develop during heating. This is achieved through conventional fitting techniques.

After the FE simulation, the results obtained for axial strain can be expressed as follows.

$$\varepsilon_{tot}^{FE} = \varepsilon_{th}^{FE} + \varepsilon_{el}^{FE} + \varepsilon_{cr}^{FE} + \varepsilon_{tr}^{FE} \qquad \text{Equation 6-3}$$

where ε_{tot}^{FE}, ε_{th}^{FE}, ε_{el}^{FE}, ε_{cr}^{FE}, and ε_{tr}^{FE} are the total strain, thermal strain, elastic strain, basic creep, and transient strain histories calculated by the FE simulations respectively.

It is required that ε_{tot}^{FE} matches the experimental data for total strain history of the unloaded heated concrete specimen, ε_{tot}^{exp}. Therefore, Equation 6-3 can be rewritten as follows.

$$\varepsilon_{tot}^{exp} = (\varepsilon_{th}^{FE} + \varepsilon_{tot}^{exp} - \varepsilon_{tot}^{FE}) + \varepsilon_{el}^{FE} + \varepsilon_{cr}^{FE} + \varepsilon_{tr}^{FE} \qquad \text{Equation 6-4}$$

where the terms in parentheses may be considered to be the 'target' for the behaviour of the thermal strain model, $\varepsilon_{th}^{target}$.

$$\varepsilon_{th}^{target} = \varepsilon_{th}^{FE} + \varepsilon_{tot}^{exp} - \varepsilon_{tot}^{FE} \qquad \text{Equation 6-5}$$

Thus, using conventional fitting techniques, the thermal strain model parameters are recalibrated to the data set, $\varepsilon_{th}^{target}$, defined by Equation 6-5. This is achieved using a modified form of the Levenberg-Marquardt algorithm to fit functions to data [2, 3], implemented in software named *gnuplot* [4].

6.2 *The Experimental Data Sets*

In order to perform some objective detailed analysis of the transient strain models, it is necessary that suitable experimental data sets are selected. Several criteria are explicitly identified here as desirable for such data sets:

- A full set of relevant parameters that defines the material properties of the specimens, particularly those that define the mechanical, thermal transport, and hygral transport behaviour, should be readily available.
- Experimental parameters, including heating rate, specimen dimensions, details of data measurement, and details of load application should be provided.
- Data should be available for materially-identical specimens heated under no load.
- Several data sets using identical specimens under several different applied load levels should be available.
- The temperature range over which the specimens are tested should be relatively large (say, $T > 500$°C).

A further criterion may be identified that appears at first sight to be so fundamental that it does not require attention. However, the issue of interpretation of experimental results depends quite strongly on the explicit definition of parameters. Frequently, for instance, results are presented in which the variable ‘temperature’ is undefined. There are generally several possible and quite distinct interpretations of the measured variable that may be named ‘temperature’, e.g. specimen core temperature or furnace temperature. It is important, particularly when large specimens are tested, that this variable is well-defined as the temperature across a specimen can vary substantially.

In modelling terms, the mean specimen temperature can be considered to be the most reasonable temperature value with which to develop models based on experimental results. Therefore, it is preferable if temperature distribution is provided by experimental investigations. However, if this is unfeasible, the temperature evolution at a specific value is also useful. A reasonable match with simulations can later be found and, therefore, the mean temperature can be derived from the simulations.

In reality, few experimental investigations exist that can be considered ideal in that all possible criteria are achieved. In many cases, it is the first (and most challenging) of the criteria that is unsatisfied. As the parameters demanded by this criterion are high in number, a partial satisfaction should be considered satisfactory. However, it is clear that there are unavoidable uncertainties in the results of analysis using most experimental data sets.

An experimental investigation in which all criteria are met, except for the first, is the influential piece of experimental and theoretical work of Anderberg and Thelandersson [1]. The experimental test program consisted of the application of several different sets of experimental conditions to specimens of concrete composed of aggregates of high quartz content and OPC (of water/cement ratio 0.6).

The specimens used in tests most relevant to this analysis are cylinders of diameter $75\ mm$ and height $150\ mm$. These were manufactured with a central cylindrical cavity of diameter $10\ mm$ in which quartz tubes are positioned for axial deformation measurements. This allows some moisture to escape from the specimens but the role played in the heating of the specimens is unclear (§6.3.1).

The specimens used in the tests are produced using material from several different batches. The compressive strength parameter is experimentally determined for material of each of the batches of concrete using $150\ mm$ cubes. Some small variation is found in the value of this parameter for material of different batches (within a range of approximately $12\ MPa$). Due to structural effects, this parameter is expected to be equal to approximately four thirds of that of the cylinders used in testing. Therefore, for consideration of the cylindrical specimens, the cube strength is multiplied by a factor of three quarters. No other variation in material properties between materials of different batches is reported in the work.

Table 6-1: Material properties given by Anderberg and Thelandersson [1] for relevant experimental tests.

Material property	Initial value
Young's modulus	$21.5\ GPa$
Compressive strength	Various (between 39.3 and $48.0\ MPa$)
Thermal conductivity	$1.79\ Wm^{-1}K^{-1}$
Density	$2160\ kgm^{-3}$
Moisture content (by mass)	1.9%
Age	Various (between 21 and 26 weeks)

All material properties specified for the data set are reproduced in table 6-1. Important parameters that are unspecified are the intrinsic permeability, the initial porosity, Poisson's ratio, and specific heat capacity[10]. However, within reasonable bounds, the axial strain found to develop in unloaded conditions due to differences in the values of these parameters is relatively invariant to the specific values. Therefore, typical values are used in the analysis to follow.

The experimental test program of interest to this analysis is that in which concrete specimens are placed under compressive axial preload and heated to failure (or $800℃$). The parameters of the experimental program are given in table 6-2. Four separate data sets are relevant to this work, achieved using different compressive axial load levels applied to concrete cylinders. The data sets are labelled '*AT225'*, '*AT35'*, '*AT45'*, and '*AT675*' for those obtained using load levels of 22.5%, 35%, 45%, and 67.5% respectively[11].

The temperature measurement made in this investigation is given as the temperature value recorded at a sensor embedded in the concrete specimen placed at a distance of 70% of the outer radius of the cylinder. This position appears to have been chosen as it lies approximately on the surface of an imaginary cylinder of identical height and 50% volume to the actual cylinder centred on identical axis. Moreover, simple calculations show that if the temperature distribution across the specimen is

[10] An approximate model is given for enthalpy of the material derived from tests of experimental data of an investigation using different materials. This approximation is not here assumed more valid than that of the present model.

[11] The 'AT' prefix refers to the first letters of each of the authors who carried out the experimental work, *Anderberg* and *Thelandersson*.

approximately quadratic, the temperature recorded at this position is approximately the volume-averaged measure of temperature.

It is found in simulations that this temperature is very accurately described by the Gauss point average measure of temperature automatically output by the FE model when applied to the heating conditions of table 6-2. This allows the analysis of results to be performed very easily. However, the accuracy of this approximation should always be checked when different experimental conditions are considered.

Table 6-2: Experimental parameters of tests performed by Anderberg and Thelandersson [1].

Experimental parameter	Value
Initial temperature	$19.8℃$
Initial relative humidity	65%
Heating rate	$5Kmin^{-1}$
Axial load applied	22.5%, 35%, 45%, and 67.5% of f_c[12]

Several issues regarding the experimental data remain to be resolved before these experimental conditions can be investigated using the IFT. These issues concern the role of the central quartz tube in the interaction between the concrete specimen and the external conditions, the method of accounting for the temperature-dependent basic creep observations provided by the authors [1], and the effect of preload on the degradation of Young's modulus of the material. These issues are considered in §6.3.

6.3 Details of application of model

There are several issues to consider before the IFT can be applied to the experimental data sets of Anderberg and Thelandersson [1]. Specifically, a brief investigation is necessary to determine the most appropriate modelling method to represent the concrete cylinders as regards the axial cylindrical cavity (§6.3.1). Then, the basic creep model presented by the authors is integrated into the strain decomposition to be applied here (§6.3.2). Following this, experimental results provided by the original authors [1] that shows the softening behaviour of the material used in the tests is used to calibrate the thermal damage model to be applied in this work (§6.3.3). Finally, it is

[12] Note that the value of f_c varies by test performed.

necessary to ensure that the FE model parameters are appropriate to produce a stable and reliable solution.

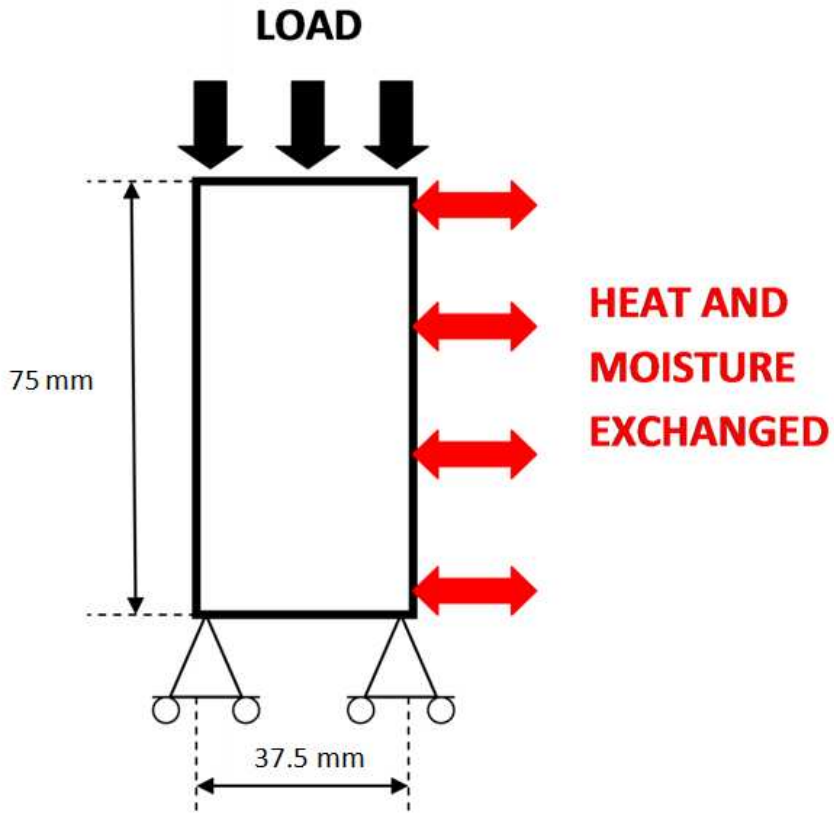

Figure 6-2: The finite element mesh used to simulate the experimental conditions of §6.2.

As mentioned previously, FE modelling is necessary to carry out the investigation. The concrete specimens shall be represented by a two-dimensional mesh consisting of eight-noded serendipity elements using the axisymmetric analysis type, as in chapter 5. Symmetry is assumed between the upper and lower halves of the cylinders. Therefore, the mesh dimensions are required to be of the radial length in one direction and half of the axial length of the specimens in the other, as shown in figure 6-2.

Note that figure 6-2 represents the mesh used for the solid cylinder approximation of the concrete specimens used in the experimental investigation. For the cases in which the cylindrical cavity is explicitly considered in the model, the radial dimensions are decreased by $5.0\ mm$ from the central axis. Furthermore, the radial displacement of the inner surface is no longer constrained.

6.3.1 *Accounting for the cylindrical cavity*

The presence of a central cavity in the concrete cylinders poses a problem from the point of view of FE modelling. The quartz tube present within the central axis of each specimen cannot be explicitly modelled. It is unclear from the description provided by the original authors which boundary conditions (BCs) are most appropriate for the inner surface of the mesh. It is clear that the experimental set up is not designed to apply the furnace conditions to the central core of the specimens. However, anecdotal evidence suggests that moisture is transferred at the inner surface (water is observed to flow down the length of the quartz tubes during the tests [1]). Therefore, some degree of moisture flux is apparent, though almost certainly not the free transfer that is present at the outer surface. Indeed, the local relative humidity within the cavity is likely to be greatly affected by any moisture that escapes from the specimen due to the severely restricted volume available (the tube within the cavity is of approximately the same diameter as the cavity) and the apparent inability for moisture transfer with the furnace.

In order to accurately reproduce the experimental conditions in a FE environment, it is necessary to make a simplifying assumption. There are three potential assumptions that are here identified to represent heat and moisture transfer across the inner surface:

1. The central cavity within the cylinder can be ignored in the analysis such that the specimens are modelled as solid cylinders (i.e. no cavity is modelled).
2. The surface of the cavity can be treated in an identical manner to the outer surface (i.e. identical BCs).
3. The surface of the cavity can be modelled as sealed to the external conditions (i.e. no transfer of heat or moisture is allowed across the cavity surface).

Each of these assumptions is not fully satisfactory. The first method (*filled*) allows the specimens to lose some heat to the central core (i.e. the central cylinder of material, which is absent in the actual experiments), which could be argued to represent the heat that must be transferred to the central quartz tube in the experiments. However, if the cavity is ignored in this manner, the stress distribution in the cylinder may be significantly altered and the moisture distribution is likely to be significantly changed.

If the second method (*unsealed*) is applied, the specimen shall be heated from the inner surface as well as from the outer surface. Hence, the temperature across the specimen shall be close to uniform throughout the tests. This result is not unsatisfactory as the specimen size is fairly small, so temperature gradients across the specimen should be relatively weak. However, the experimental set up appears to suggest a heat sink is more appropriate than a heat source at the inner surface. Also, transfer of moisture across the cavity surface, though consistent with anecdotal observations [1], is likely to be calculated to be excessive through use of the unsealed BCs. In the experiments, the limited volume into which moisture can move (from inside the concrete) likely significantly hinders moisture transfer across the cavity surface. This effect cannot be reproduced by use of the unsealed BCs.

The final option (*sealed*), to allow no transfer of heat or moisture at the inner surface has the advantage that the cavity is explicitly modelled and thus no additional issues arise regarding the stress distribution or increased temperature gradients. However, the lack of any moisture loss contradicts the anecdotal observations and the lack of heat loss is physically unreasonable (unless, for instance, the quartz tubes slowly increase in temperature due to contact with an external heat source, such that they are constantly in thermodynamic equilibrium with the inner surface of the concrete).

Clearly, none of the models constitute perfect representations of the experimental conditions. However, it is useful to examine which of the three representations is most appropriate. As this cannot be deduced a priori, FE analysis shall be applied. For the purposes of this investigation, the most realistic representation shall be considered to be that which reproduces most accurately the temperature distributions experimentally determined by the authors for a slow heating rate, the heating rate of interest to this work, and the most rapid heating rate possible with the experimental apparatus, i.e. $1℃/min$, $5℃/min$ and '*Max*' respectively.

Using a mesh of 400 elements (with a time step of $5\ s$), the results show that the temperature profiles produced most closely match the experimental results if the 'sealed' BCs are applied to the inner surface. The match between the simulated results and the experimental results is particularly good for the $5°C/min$ heating rate, shown in figure 6-3 (b). The 'filled' set of conditions produce results that are very similar to

the ‘sealed’ BCs but are visually less well matched to the experimental data. The ‘unsealed’ BCs consistently produce temperature profiles in advance of the experimental results (except for the slow heating rate which is underestimated by all simulations throughout the test).

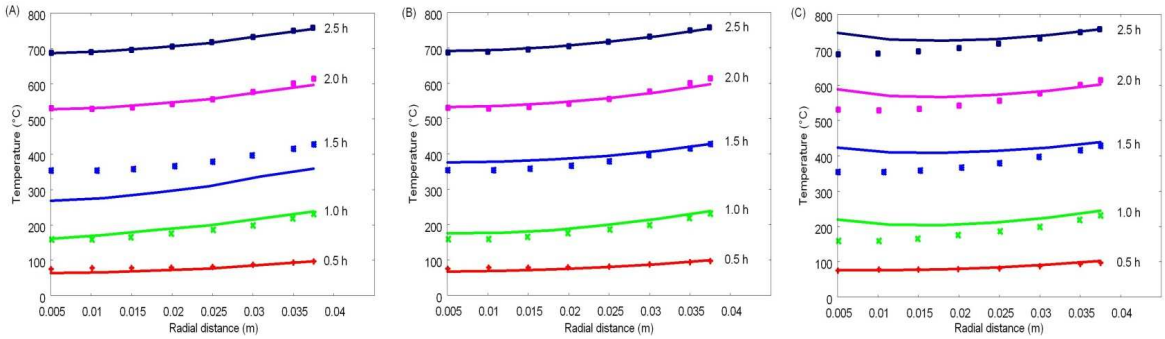

Figure 6-3: Comparison of the simulation of the evolution of the radial temperature profile of the concrete specimens heated at 5°C/min for use of (a) the *filled* BCs, (b) the *sealed* BCs, and (c) the *unsealed* BCs.

As demonstrated in figures 6-3 (a)-(c) for the heating rate to be considered in the work to follow, the experimental temperature profile is consistently well described by the thermal transport model applied in this work, particularly with the ‘sealed’ BCs applied at the surface of the inner cavity. Thus, these BCs shall be adopted for the FE simulations to be applied in the analysis to follow.

6.3.2 *Applying the basic creep model*

From the point that a concrete specimen is placed under load, basic creep begins to develop. Usually, the development of this strain component is ignored in the analysis of transient strain experimental results as the period of loading tends to be insufficient for a significant component to develop. Moreover, no reliable predictive models exist for basic creep (which may be partially stochastic in nature). Thus, the component of basic creep present in LITS experiments is difficult to identify in experimental data and, as a result, it is rare that basic creep is considered explicitly.

Although this practice has also been adopted in this work so far, this shall not be the case for the work within this chapter. Due to the availability of experimental data that allow the development of basic creep to be extrapolated to the conditions of interest for this investigation, a reliable model to account for this component of axial strain can be implemented. This is valuable as it allows the transient strain contribution to the experimental results to be identified more accurately.

Anderberg and Thelandersson [1] performed experimental tests to determine the short term basic creep behaviour of the concrete type used in their work. Based on these data, a model was developed for the magnitude of basic creep after three hours of loading. In uniaxial form, this is given as follows.

$$\varepsilon_{cr,3} = \frac{\sigma}{f_c(T)} \beta_{cr} e^{k_{cr}(T-20°C)} \qquad \text{Equation 6-6}$$

where β_{cr} and k_{cr} are constants set equal to 0.53×10^{-3} and $3.04 \times 10^{-3}°\text{C}^{-1}$ respectively. The model is generalised for all time values with multiplication by a time factor to give the generalised form of the model.

$$\varepsilon_{cr} = \varepsilon_{cr,3} \left(\frac{t}{t_r}\right)^{p_{cr}} \qquad \text{Equation 6-7}$$

where p_{cr} is a constant, given as 0.5 and t_r is a reference time, given as 3 hours. It should be noted that this basic creep model is intended only for use as a short term creep model; application of this model to long term loading (say, over the period of several days) would be likely to produce unreliable results.

The authors [1] propose a method to generalise the model to arbitrary heating and loading conditions. According to this model, to calculate the increment in creep at any time, the current value of total axial creep is assumed to have developed due to the constant application of (the current values of) σ and T. In this framework, to bring consistency with the creep predictions of Equations 6-6 and 6-7, the time variable must be replaced with an effective time variable, known as the '*material time*', t_m. Rearrangement of Equation 6-7 allows this variable to be calculated.

$$t_m = t_r \left(\frac{\varepsilon_{cr}}{\varepsilon_{cr,3}}\right)^{\frac{1}{p_{cr}}} \qquad \text{Equation 6-8}$$

Upon calculation of this value, the increment of basic creep, $\Delta\varepsilon_{cr}$, may be calculated as follows.

$$\Delta\varepsilon_{cr} = \varepsilon_{cr,3}\left[\left(\frac{t_m + \Delta t}{t_r}\right)^{p_{cr}} - \left(\frac{t_m}{t_r}\right)^{p_{cr}}\right] \quad \text{Equation 6-9}$$

where Δt is the time step used in the calculations.

However, this model, which is intended for uniaxial problems, is not generally valid for multiaxial stress states (and corresponding creep strains). It can easily be envisaged that it may not always be possible to calculate a consistent value of t_m for different components of ε_{cr}.

Thus, it is necessary to calculate a value of t_m for each component of basic creep to avoid this problem to avoid this problem in calculations. In this work, the multiaxial basic creep model includes no Poisson-effect to simplify the analysis. This is justified on the basis that the experimental tests are always uniaxial in applied load and therefore that the Poisson's ratio effect on the axial component of creep shall be of a relatively low magnitude.

Furthermore, it is plausible that, at a given point in the analysis, a state may exist in which $sgn(\sigma) \times sgn(\varepsilon_{cr}) < 0$. Thus, in these conditions, Equation 6-8 yields a complex value of t_m if $p_{cr} = 2$. Upon insertion into Equation 6-9, it is not difficult to show that this complex value may lead to mathematical difficulties in the calculation of $\Delta\varepsilon_{cr}$.

The solution to this problem applied in this work is to assume that tensile stresses do not cause basic creep (similar to the TTS0 assumption for transient strain). This avoids the potential issue of parametric complexity and is found also to improve stability of the basic creep model when implemented in a FE model.

One final aspect of this model to consider is that the model requires as input a model for the temperature-dependent compressive strength of concrete. This should be determined using experimental data presented by the authors [1].

Based on the available experimental data, it can be seen that the degradation of compressive strength with heating is independent of the presence of preload and can therefore be considered to be a function of temperature only. A piecewise model appears to be appropriate as a mathematical description of the experimental data. The model found to fit the data well is given as follows.

$$\frac{f_c(T)}{f_c(T_0)} = \begin{cases} 1.0 + \dfrac{(T - 20°C)}{(T_1 - 20°C)}(C_0 - 1.0) & , \quad T \leq T_1 \\ K + (C_0 - K)exp\left[-\dfrac{(T - T_1)}{\lambda_1}\right] & , \quad T_1 < T \leq T_2 \\ \left\{K + (C_0 - K)exp\left[-\dfrac{(T_2 - T_1)}{\lambda_1}\right]\right\} exp\left[-\dfrac{(T - T_2)}{\lambda_2}\right], & \quad T_2 < T \end{cases}$$

Equation 6-10

where C_0, K, λ_1, and λ_2 are free parameters of the model, with T_1 and T_2 the transition temperatures.

The results of fitting the free parameters of Equation 6-10 to the experimental data are shown in figure 6-4. As shown in figure 6-4, the first phase of development of the high temperature compressive strength is a slight linear increase in the strength parameter up to the first critical temperature (found to be approximately $190℃$). This is followed by a relatively rapid exponential decay to a constant value up to around $390℃$. The final phase of the compressive strength evolution is a further stage of exponential decay that is relatively slow in development in comparison to the previous stage of decay but that produces a far larger decrease in the strength parameter.

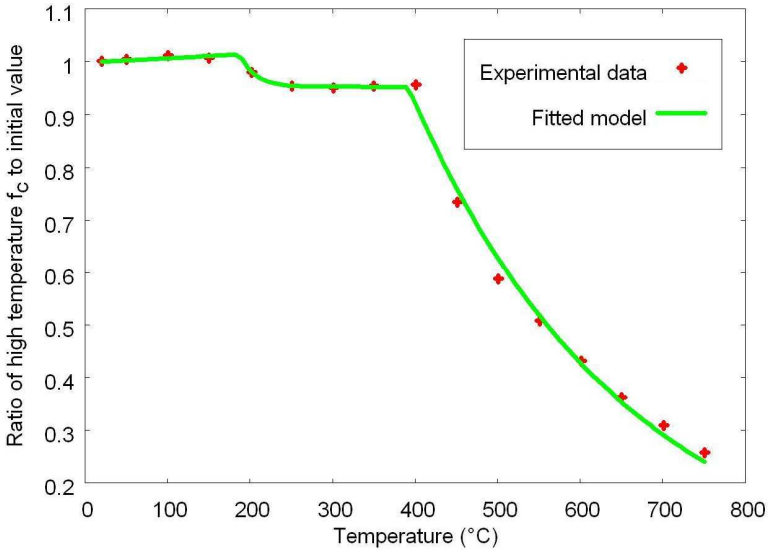

Figure 6-4: Comparison of the mathematical model for the changing compressive strength parameter with increasing temperature and experimental data on which it is based.

It is of interest to note that the rapid and slow phases of exponential decay coincide roughly with the temperature ranges in which the dehydration of C-S-H and CH occur respectively. If a causal link is postulated, the weakening effect of C-S-H dehydration can clearly be considered to be of lesser importance in this particular concrete in

comparison to that of the CH dehydration. In this theoretical framework, the initial small increase in strength may be considered to be due to the beneficial effects of consolidation caused by the loss of moisture from the smallest pores and the inter-hydrate layers of the cement matrix.

However, Caution should be exercised in assuming that a strong causal link exists between the dehydration of C-S-H and CH and the two distinct phases of strength loss. The dehydration of CH is generally considered to take place over a fairly narrow temperature range and that of C-S-H over a fairly broad temperature range. This is in contrast to the supposed effects on the strength parameter shown in figure 6-4. The strength parameter is an extremely complicated parameter to define due to the various factors that contribute to the failure mechanisms in concrete. Therefore, the similarity between the temperature ranges of the distinct strength decay phases and the dehydration processes may be insignificant.

6.3.3 *Thermal damage*

Tests were performed to determine the softening effects of heating on the concrete specimens to be used in this analysis, in both unloaded and preloaded conditions [1]. To ensure that the effects of transient strain are absent in the results for the preloaded specimens, the change in secant elastic modulus (measured at a load level of about $0.3f_c$) was used to measure thermal damage in these tests.

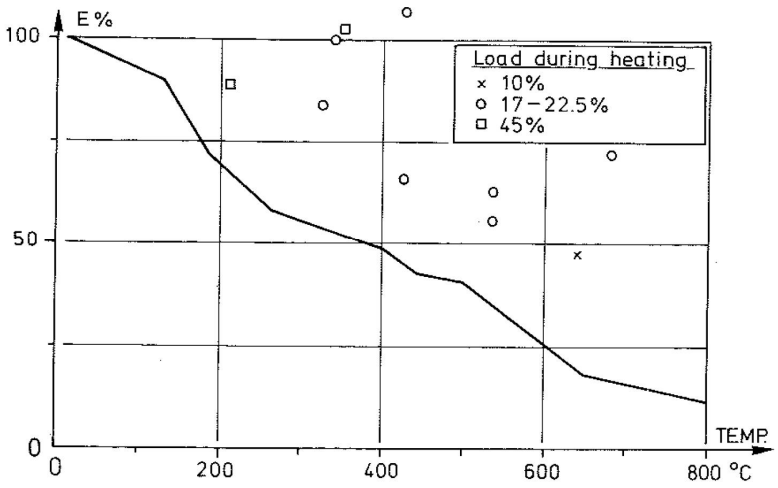

Figure 6-5: The experimental results for the evolution of the elastic modulus in heated conditions. The line represents the average behaviour found experimentally for unloaded concrete and the data points that of preloaded concrete.

The results, shown in figure 6-5, suggest that the presence of a preload consistently causes a reduction in loss of stiffness when compared to a specimen heated to the same temperature in unloaded conditions. This is consistent with observations commonly reported elsewhere [5-9]. It is worthwhile to attempt to account for the effects of applied load in the degradation of Young's modulus.

No relationship appears to exist in the results of figure 6-5 between the magnitude of the applied preload and evolution of thermal damage. Therefore, a conservative approach is taken here, such that

- the effects of preload on thermal damage development are assumed to be independent of the magnitude of preload and
- a subset of the data points of figure 6-5 that constitute a lower bound measure of the effect of preload on thermal damage development are used to calibrate the model for thermal damage development in preloaded conditions.

As stated in §3.3.1, a modified form of the thermal damage model applied by Pearce et al. [10] is proposed in this work to represent thermal damage development in preloaded concrete specimens, defined as follows.

$$1-\chi_\sigma = \begin{cases} 1, & \theta < \theta_\chi^* \\ \left[1-\zeta_\sigma\left(\theta-\theta_\chi^*\right)\right]^2, & \theta \geq \theta_\chi^* \end{cases} \qquad \text{Equation 6-11}$$

where χ_σ is the thermal damage parameter that describes the decrease in the elastic modulus of concrete when preloaded, ζ_σ and θ_χ^* are free parameters that may be calibrated to experimental data.

In the literature [10], Equation 6-11 is applied to unloaded heated concrete specimens, with $\theta_\chi^* = 0$ and $\zeta_\sigma = 0.1$. When applied to the data of figure 6-5 for unloaded heated specimens, values of 0 and 0.084 are obtained by data fitting for these parameters respectively. Similarly, for the preloaded heated specimens, values of 1.2 (equivalent to $140℃$) and 0.059 are obtained respectively.

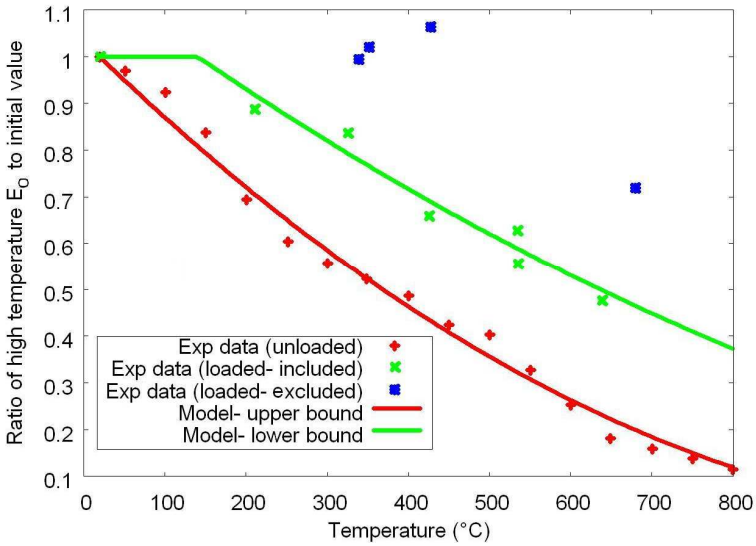

Figure 6-6: The output of Equation 6-11 calibrated to the unloaded and loaded specimens.

Broadly, when calibrated to preloaded heated specimens and to unloaded heated specimens, Equation 6-11 may be considered to represent a lower bound and an upper bound of thermal damage development respectively. As discussed briefly in §3.3.1, the former evolution of the thermal damage parameter is here considered to be *intrinsic thermal damage*, with the latter representative of the combined effects of *intrinsic thermal damage* and *thermal mismatch damage*.

The value of θ_χ^* for the lower bound thermal damage development, 140°C, is generally consistent with this model. No intrinsic thermal damage is expected to develop in this model framework until the chemo-thermal processes develop sufficiently such that a non-negligible fraction of the C-S-H has undergone transformation. A temperature of 140°C, determined objectively using data fitting techniques, is a realistic value at which this point may be reached.

The additional thermal damage observed to develop when the concrete specimens are heated in unloaded conditions (i.e. the difference between the upper bound thermal damage parameter and the lower bound thermal damage parameter) is here postulated as developing due to the thermal mismatch that is known to exist between the various components of concrete. These components, particularly aggregate inclusions and cement paste, expand to generally different magnitudes when heated, particularly if moisture loss is allowed and the cement paste component undergoes significant contraction [11]. Tensile stresses develop in the phase that expands to a

lesser extent than the surrounding phase, which leads to microcracking and therefore material softening. The role of compressive preload, in this model, is to reduce or remove entirely these tensile stresses (referred to as *parasitic* by Khoury [12]) and to reduce the microcracking and related softening as a result.

It should be noted that it is highly likely that microcracking due to thermal stresses occurs in sufficiently heated preloaded concrete specimens also. Due to cement paste contraction in particular, it appears to be unlikely that tensile stresses can be removed from the matrix phase throughout the entire temperature range. However, it is plausible that compressive preload slows the progress of microcracking and reduces its influence on material stiffness.

This model (Equation 6-11) is intended to be applied for the analysis of the experimental data sets here considered (§6.2). The separately calibrated forms of Equation 6-11 are explicitly applied, depending on the known preload conditions for the intended simulation. Clearly, this is not ideal and the model should be robust enough to be applied unmodified for arbitrary loading conditions. However, preliminary attempts at developing and integrating such a form of the model lead to various numerical issues. Thus, further development of this model, though beyond the scope of this work, should be the subject of future work.

6.3.4 *Test of FE model parameters*

In order to reliably apply FE modelling to the experimental conditions considered in this investigation, it is necessary that the results of the FE analysis are reliable and the results are not affected by the FE model parameters, the mesh discretisation and the time step value used in specific tests.

In order to investigate suitable parameters for the time step and the mesh discretisation, an example problem is simulated for several different values of these parameters (as in §5.1.3). The experimental conditions here considered are those of concrete specimens heated under no applied load to $800℃$ at the constant heating rate of $5℃/min$. Unloaded conditions are chosen as the effects of thermal stresses on the results are larger in specimens under no applied load.

The simulations performed to investigate the mesh discretisation parameters are performed using a time step value of $5\ s$. The mesh coarseness property is varied between that of 100 body elements (10×10) and that of 1600 body elements (40×40). The simulations carried out to investigate the value of the time step are performed on specimens of 400 body elements (20×20) with 20 line elements used to represent the flux boundary of the specimens. The specific time step values investigated range between $0.5\ s$ and $30\ s$. Consistent with previous findings (§6.3.1), no moisture flux or heat flux is allowed at the inner surface of the mesh.

The results, analysed principally using the Gauss-point mean variables, indicate that the total strain is practically invariant to all the time step values used, although the results for the highest time step resulted in significant numerical instability. Results for the strain components indicate that the basic creep and elastic strain components found to develop during heating are almost identical for the results produced using a time step less than $10.0\ s$, while the effect on these results of use of a time step of $10.0\ s$ is very minor. Thermal strain, transient strain, temperature, and relative humidity are observed to develop identically for all values of the time step. Finally, the axial load level evolution is almost identical for results obtained using a time step value less than $10.0\ s$.

Similar results were found for the mesh test. The total strain measure, transient strain, temperature, and relative humidity measures appear to be practically identical for all meshes tested. Very slight variations are found to develop in all meshes tested of fewer elements than 400 (20×20). The deviations however are of a very low magnitude.

On the basis of these tests, it is recommended that a time step of any value below $10.0\ s$ and a mesh of a fineness of that of a mesh of 400 elements (20×20) or greater are appropriate for this analysis.

6.4 Results and Discussion

In this section of work, each of the five transient strain models identified in chapters 4 and 5 is compared with the experimental data sets described in §6.2. In order to ensure that the analysis is objective, it is necessary that the values of the parameters

of the models are chosen to maximise the performances of the models. To achieve this, the methodology of §6.1 shall be applied to each model in turn.

The analysis for the first transient strain model to be considered here (the Nielsen model) shall be performed three times, each time using a different TTS assumption in order to investigate whether the experimental data sets provide evidence for the nature of the tensile transient strain response that most closely reflects reality. As the nature of the transient strain model applied is unlikely to be important to the investigation into the most appropriate transient strain model response to states of tension, only the Nielsen model is subjected to this methodology for each TTS assumption (for reasons specified in §4.11). Following this analysis, the IFT is applied to each of the remaining transient strain models in turn.

6.4.1 *The Nielsen model/TTS analysis*

As already mentioned, the IFT is here applied to the Nielsen model to calibrate the model to the experimental data separately for each of the three TTS assumptions identified in this work as potential mathematical descriptions for the transient strain response of concrete under states of tensile stress (Equations 5-4 and 5-5 (a)–(c)). To recap, the three TTS assumptions, named *TTS0*, *TTS1,* and *TTS2,* are defined as follows.

- According to the TTS0 assumption, transient strain does not develop due to net tensile stresses.
- According to the TTS1 assumption, transient strain develops due to both net tensile stresses and net compressive stresses. Moreover, the load-dependence of transient strain is governed by the stress/compressive strength ratio for both net tensile and net compressive stresses.
- According to the TTS2 assumption, transient strain develops due to both net tensile stresses and net compressive stresses. However, the load-dependence of transient strain is governed by the stress/compressive strength ratio for net compressive stresses only. For net tensile stresses, the load-dependence is governed by the stress/tensile strength ratio.

This work is intended to allow critical analysis of the performance of the transient strain model and to allow an examination of the experimental data for evidence of the

most appropriate TTS assumption. The experimental observable on which this analysis is based is axial strain.

The Nielsen model is applied in the form presented in §4.6 without modification, aside from the explicit consideration of the transition temperature as a free parameter of the model. As there is no theoretical basis for fixing the transition temperature at the default value (470℃), there is no justification for restricting the values that this parameter can take.

$$\boldsymbol{\varepsilon}_{tr} = \begin{cases} \dfrac{(A\theta^2 + B\theta)}{f_c(T_0)}\boldsymbol{Q}:\boldsymbol{\sigma}, & \theta \leq \theta^* \\ \dfrac{[C(\theta-\theta^*)^2 + A\theta^*(2\theta-\theta^*) + B\theta]}{f_c(T_0)}\boldsymbol{Q}:\boldsymbol{\sigma}, & \theta > \theta^* \end{cases} \quad \text{Equation 6-12}$$

The Nielsen model is a fairly simple model that is computationally very stable. Therefore, the implementation of this model is not expected to require any additional considerations. The nature of the model is also such that the shape of the strain-temperature curve varies smoothly and predictably with small changes in the values of the parametric set. Therefore, it can be expected that application of the IFT to this model shall be efficient.

According to the IFT method, the analysis commences with two sets of model parameters as unknowns, those of the thermal strain model and those of the transient strain model. As described in §6.2, the first step in the analysis is to find values of the parameters of the thermal strain model that produce total strain results in unloaded conditions that match well the related experimental data set (using the default set of transient strain parameter values in the first stage). The initial default values of the thermal strain parameters (Equation 5-2), used for all applications of the IFT, are defined in table 6-3. The initial transient strain parameters, previously applied for concretes containing quartzite aggregate [13], are defined in table 6-4.

For the Nielsen model, it is possible to define parametric values for the model that lead to violations of the principle of monotonic transient strain increase. As such sets of parametric values cannot be considered to be valid in this analysis, calculation of the associated error measures is inefficient and should be avoided.

Table 6-3: Values of default initial thermal strain parameters used in FE simulations.

Parameter	Default value
α_{th}	6.0×10^{-3}
β_{th}	0.0 [$^{\circ}C^{-1}$]
θ_{tr}	6.0
θ_2	7.0

Through differentiation of the temperature function of the Nielsen model with respect to temperature, the minimum values of the model parameters can be defined as in Equations 6-13 (a)–(c).

$$A \geq -\frac{B}{2\theta^*} \quad \text{(a)}$$

$$B \geq 0 \quad \text{(b)} \qquad \text{Equation 6-13}$$

$$C \geq -\frac{B + 2A\theta^*}{2(\theta_{max} - \theta^*)} \quad \text{(c)}$$

Adherence to these inequalities guarantees that the principle of transient strain monotonic increase is not violated in the temperature range $0 \leq \theta \leq \theta_{max}$, the temperature range of the experimental procedure (approximately $20^{\circ}C$ to $800^{\circ}C$). Note that no minimum value of θ^* is suggested by the above considerations. However, a negative value is not allowed on the grounds that the temperature function would not necessarily be equal to zero at the initial temperature. In any case, such low values of the transition temperature are not considered plausible; mention is made simply for rigour.

It can be seen, from Equation 6-13 (a), that the values of A allowed depend on the concomitant value of B. Hence, the minimum value of A that can be considered in the analysis is related to the maximum value of B. In a similar manner, the minimum value of C depends on the values of all the remaining parameters according to Equation 6-13 (c).

The PPI program identifies any parametric permutations that violate Equations 6-13 (a)–(c), assigns a very large value of the error measure, and iterates the parametric

values to another set. This prevents the program from making absurd predictions and is efficient with computer resources.

Table 6-4: Values of default initial transient strain parameters used in the FE simulations.

Parameter	Default value
A	0.6×10^{-3}
B	1.0×10^{-3}
C	1.3×10^{-2}
θ^*	4.5

No restrictions analogous to those of the minimum values can be justifiably placed on the maximum values of the parameters. Combinations of parameter values that result in unrealistically strong transient strain development should be avoided. Hence, maximum values are chosen heuristically.

The ranges of the values of the transient strain model parameters, along with the values of the parametric increments, found in preliminary tests to be of sufficient parametric fineness and subsequently applied in the analyses, are shown in table 6-5. The proportion that represents valid permutations is just over 50%. As the program essentially ignores these permutations, their inclusion within the range of the procedure does not cause inefficiency.

Table 6-5: Range of values of parameters and incremental values used in the PPI procedure.

Parameter	Minimum value	Maximum value	Incremental value
A	-0.2×10^{-3}	1.8×10^{-3}	0.1×10^{-3}
B	0.0	2.0×10^{-3}	0.1×10^{-3}
C	-2.0×10^{-2}	2.0×10^{-2}	0.1×10^{-2}
θ^*	2.5	7.5	0.25

Application of the IFT to the experimental data sets for the Nielsen model is found to require only the minimum number of iterations for each TTS assumption (two), i.e. the process of fitting thermal strain parameters to data files is repeated once, as is the process of searching for most appropriate transient strain parameters using the PPI

program[13]. It is likely that this reflects the relative stability of the technique when applied to these experimental conditions using this transient strain model. Other experimental examples, particularly those in which specimens of larger dimensions are used, may require a greater number of iterations.

The values of the thermal strain parameters found for each of the TTS assumptions are very similar. Figure 6-7 (a), which shows the calibrated thermal strain models for each assumption, demonstrates that the difference in thermal strain behaviours between the three assumptions is only non-negligible in the high temperature region. This reflects the observation that, due to the relatively small dimensions of the specimen, significant thermal stresses across the specimens, which drive the deviation in total strain from that due to pure thermal strain, do not develop until a temperature close to the thermal strain transition temperature is reached (i.e. around $610°C$). Examination of figure 6-7 (b), which shows the axial transient strain component confirms both that the magnitude of transient strain that develops is relatively small, particularly for TTS1, and that the bulk of the final strain magnitude develops in the later heating period.

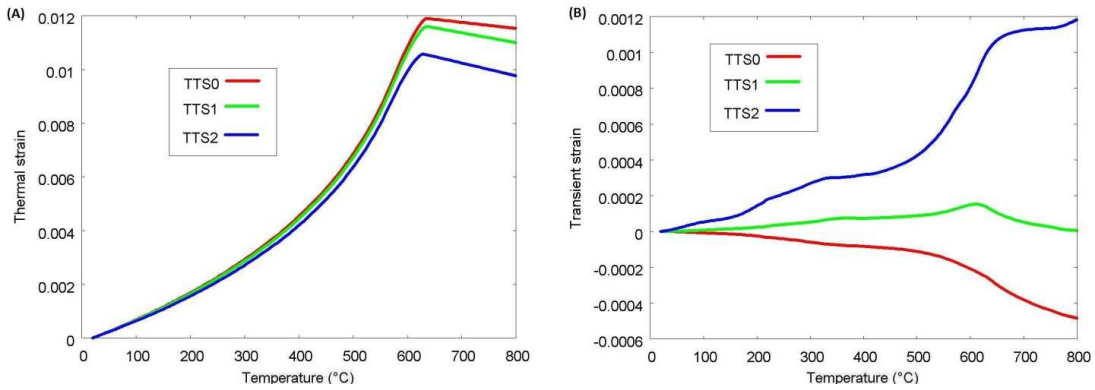

Figure 6-7: Comparison of the different evolutions of (a) thermal strain and (b) transient strain that develop during heating of specimens described by transient strain models of differing TTS assumptions.

Despite the observation that the difference in thermal strain for each of the TTS assumptions is relatively small, illustrated in figure 6-7 (a), when compared with the resultant total strain in identical conditions, shown in figure 6-8, it is clear that practically no difference exists between the total strain curves. Thus, consistency between the different approaches and the experimental results is achieved despite

[13] The second iteration results in an identical set of parametric values as the first iteration, so it may be considered that one iteration is necessary to find the parameter values and one is required to confirm the result.

differences in the strain decomposition of each. The mutual calibration of thermal strain and transient strain is achieved due to the IFT.

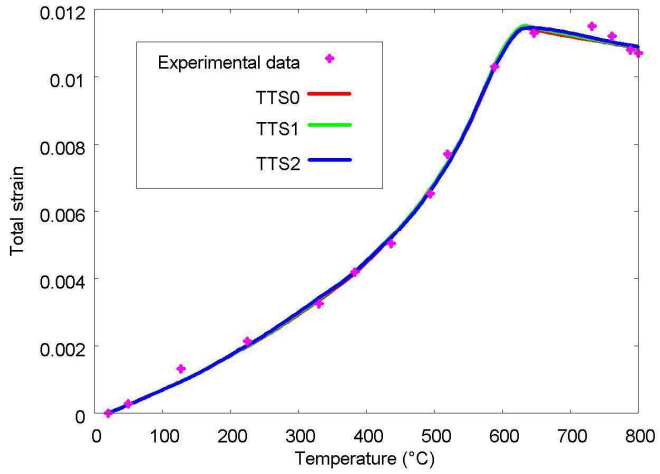

Figure 6-8: Comparison of simulated total strain in unloaded heated conditions and experimental data.

The results of application of IFT show that calibration of the Nielsen model to each of the data sets individually produces strain-temperature curves that are generally highly dependent on data set. As an illustration, figure 6-9 shows the transient strain curves found to be the most appropriate when each of the loaded cases is analysed individually using the TTS0 assumption. These results, which are very similar to the results found for both the TTS1 and TTS2 assumptions, are produced through application of the models to an axial load equivalent to 50% of the initial compressive strength.

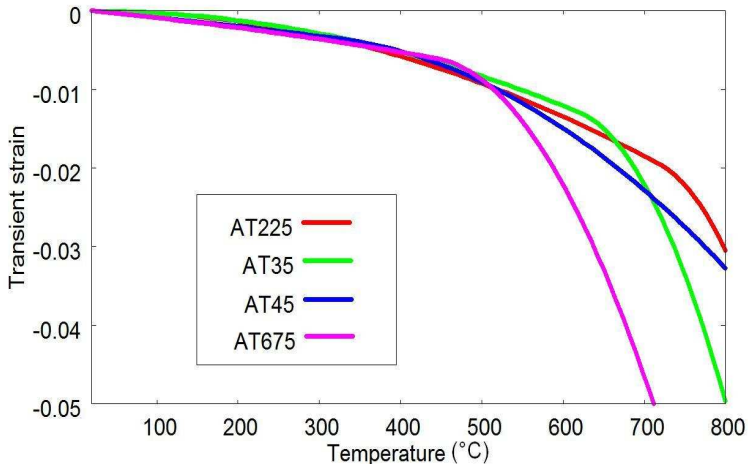

Figure 6-9: Comparison of the transient strain (TTS0) curves found to be most appropriate for the total strain results using each of the individual loaded data sets.

It can be seen from figure 6-9 that the main differences in the transient strain curves develop in the temperature region above about $500℃$. This suggests that the main differences between the curves are caused by the values of θ^* and C.

For the sets of parameter values chosen using individual data sets, as for the transient strain curves shown in figure 6-9, the transition temperature, not previously generally considered to be a free parameter of this model, is found to vary in value depending on the data set considered. It is therefore worthwhile to briefly examine the effect of the value of this parameter on the performance of the model.

If the mean error measure obtained for each value of the transition temperature is plotted against the transition temperature[14], as shown in figure 6-10, it can be deduced that all data sets record a significantly reduced mean measure of error for transition temperatures above approximately 5.0.

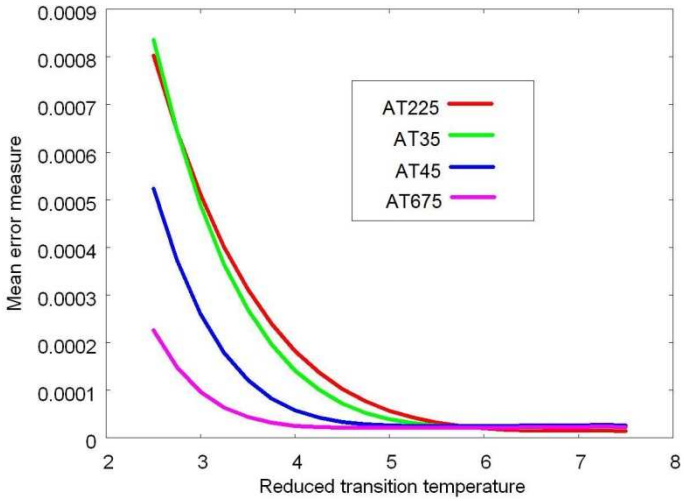

Figure 6-10: Mean error calculated across all permutations of parameter values for each value of the transition temperature considered (TTS0 assumption applied).

However, the results of figure 6-10, shown for the TTS0 assumption but found to be almost identical for both the TTS1 and TTS2 assumptions, do not indicate with certainty that the performance of the model is greatest for transition temperatures of a relatively large magnitude. Instead, the results of figure 6-10 indicate simply that the use of a transition temperature in the relatively high temperature region is more likely to contain a large number of parametric orientations associated with a relatively low

[14] Note that any permutations of values of parameters that violate the principle of transient strain monotonic increase are discounted from the analysis. Therefore, the large values of error associated with them by the PPI program are not included in the calculation of the mean value.

measure of error within the limits of the values of parameters applied in this analysis (defined in table 6-5).

In order to examine the values of transition temperature for which the model is most effective at each load level and to determine the importance of the value of the transition temperature parameter in this respect, a plot of the minimum error measure associated with each transition temperature is more instructive. Results of this type are shown for each TTS assumption and each data set in figures 6-11 (a)-(d).

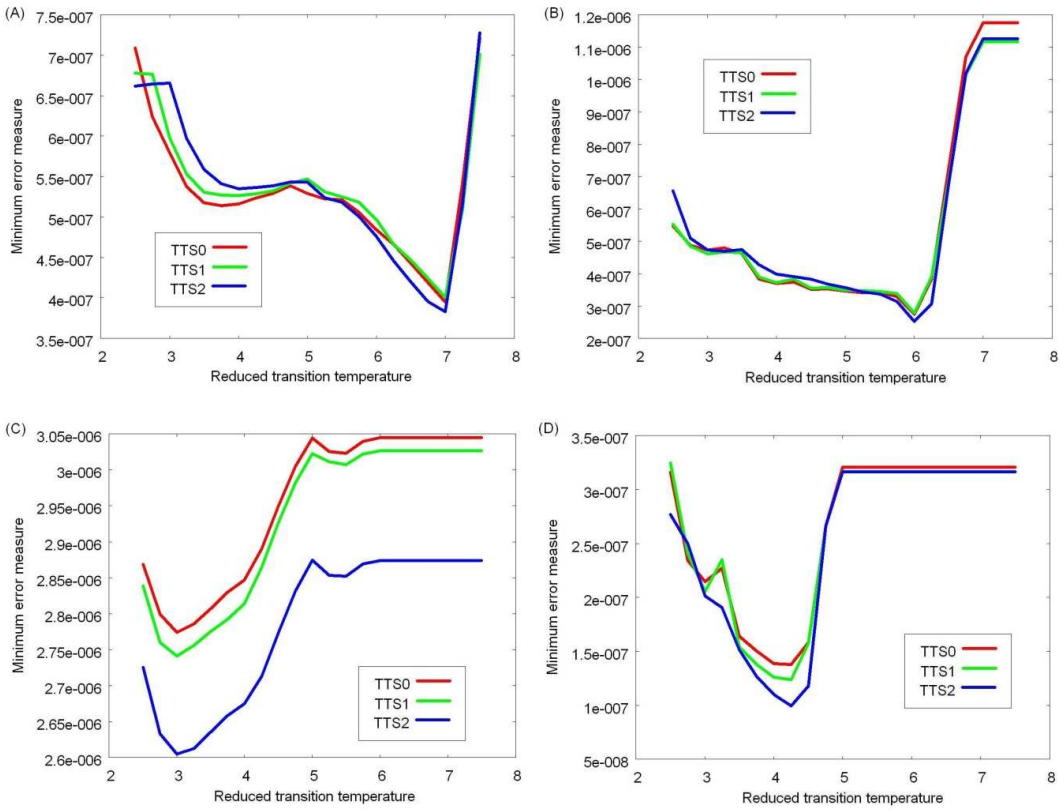

Figure 6-11: Minimum error associated with each transition temperature for (a) AT225, (b) AT35, (c) AT45, and (d) AT675 data sets.

It can be seen from figures 6-11 (a)-(d) that there exist clear values of the transition temperature at each load level for which the minimum error measure is found to be at the lowest possible value[15] with no dependence of the value of transition temperature (at which this minimum error is found) on the TTS assumption employed. It is quite apparent that a transition temperature above about 7.0 (720°C) and below 3.0 (320°C) shall not be found to be associated with the minimum error measure as the

[15] This is true with respect to the specific sets of parameter values applied to the data sets by the PPI program.

error measures found in these temperature ranges tend to be the largest values of minima found.

It can further be observed from figures 6-11 (a)-(d) that the range of transition temperatures considered in the analysis is sufficient to detect the error measure minima in the results. The results do not suggest that there would be further minima found if the range of transition temperatures were wider, nor do they suggest that sharp minima would be found in values of transition temperature intermediate to those used in the analysis (as suggested by the apparent relatively smooth shapes of the curves).

Based on the results of figures 6-11 (a)-(d), in which the transition temperature at which the lowest value of the minimum error measure is found is dependent on the data set, it is valid to investigate whether the improvement in model performance if the transition temperature is allowed to vary by data set (or, more specifically, by applied load) justifies this type of modification of the model.

In the experimental and theoretical work of Anderberg and Thelandersson from which the data sets used here are derived [1], the authors speculate on the apparent load-dependence of the critical temperature (i.e. the temperature at which the concrete specimens fail due to heating under constant load). While no conclusions are reached, it may be speculated that a load-dependent transient strain transition temperature would cause the critical strain associated with failure to be reached at a temperature dependent upon the applied load and thus to a clear explanation for the observations.

Hence, it is worthwhile examining if the data sets provide any evidence that the transition temperature of the transient strain model may be best described as dependent on load applied. In order to investigate this possibility rationally, it is assumed that the values of the remaining parameters of the Nielsen model (A, B, and C) are independent of applied load.

The results of this analysis suggest that the error measure is reduced most if the transition temperature is allowed to reduce with an increase in applied load (though, no change is found necessary between the load levels of 45% and 67.5%). The transition temperature is found to vary between $470℃$ and $395℃$ for the analyses

applying both the TTS0 and TTS1 assumptions, whereas the corresponding values are $545℃$ and $420℃$ for the analysis applying the TTS2 assumption. The results of application of the Nielsen model with a load-dependent transition temperature and each of the TTS assumptions are shown in figures 6-12 (a)-(c).

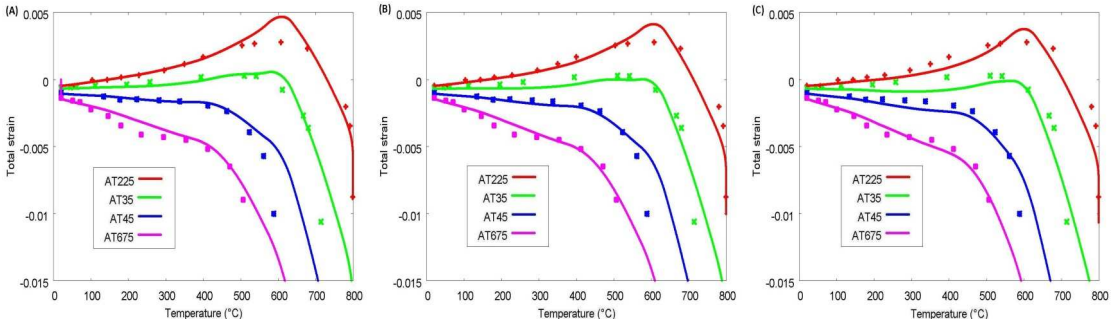

Figure 6-12: The total strain predicted for each load level in comparison with the experimental data sets using the Nielsen model and (a) the TTS0 assumption, (b) the TTS1 assumption, and (c) the TTS2 assumption. The parameters A, B, and C for each graph are chosen according to the data of all four load levels with θ^* chosen independently for each individual load level.

The total strain results can be observed to reproduce the experimental results very well for each load level. The qualitative features of each data set are present in the model results. The error measure results suggest that the TTS2 assumption produces the most accurate predictions over all the data sets, followed by the TTS1 assumption and then the TTS0 assumption. While the relative differences in the values are low, approximately 2%, the results for TTS2 appear visually to be the most similar to the experimental results.

The improvement in the model performance produced by the assumption of variable transition temperatures between data sets, in terms of the error measure, is an improvement of approximately 6%, 11%, and 18% for the TTS0, TTS1, and TTS2 assumptions respectively. These values, which are in reference to the model performances when calibrated to all data sets simultaneously, show that the improvement in model performance is reasonably good.

Comparison of figures 6-12 (a)–(c) with the corresponding total strain results found for the original model (in which transition temperature does not vary by applied load level), shown in figures 6-13 (a)–(c), shows visually that the improvement in the results, though of a relatively low magnitude, is noticeable. Without the load-dependence of transition temperature, the model is capable of reproducing the experimental results fairly accurately, though the shape of the strain-temperature

curves in figures 6-13 (a)–(c) appear to match the data more poorly in the temperature region above about $500℃$ for the AT45 data set than in figures 6-12 (a)–(c).

Therefore, while it should be noted that these results suggest that the performance of the Nielsen model is improved with the introduction of a load-dependent transition temperature[16], the modification is not further pursued in this work. This is due to the good performance of the model with a constant transition temperature and the lack of a strong physical justification for the modification.

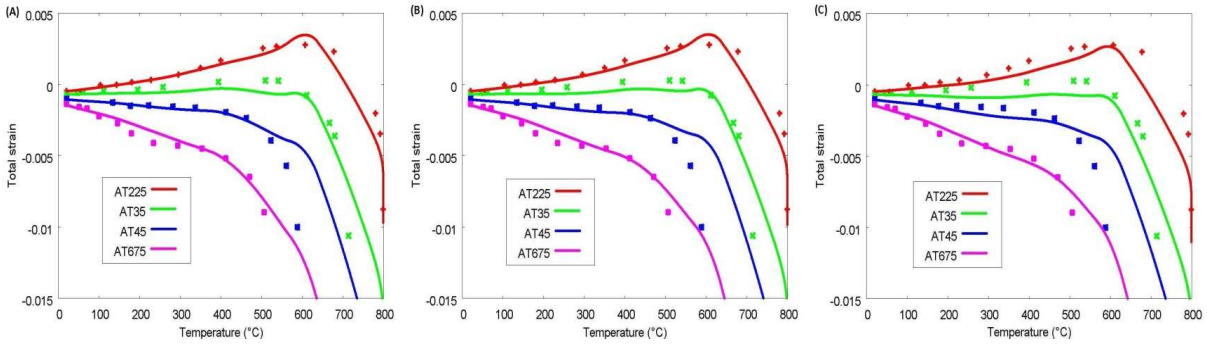

Figure 6-13: The total strain predicted for each load level in comparison with the experimental data sets using the Nielsen model and (a) the TTS0 assumption, (b) the TTS1 assumption, and (c) the TTS2 assumption. The parameters for each graph are chosen according to the data of all four load levels.

The results of figures 6-13 (a)–(c) demonstrate that the Nielsen model is capable of reproducing experimental results over the load range $22.5\%–67.5\%$ to a high degree of accuracy. It is instructive to compare these results to the most accurate reproduction of experimental data that is possible for each individual load level using the method here applied. This allows both the capacity of the model to reproduce these data and the robustness of the results (to differing applied load levels) to be evaluated.

The total strain results calibrated by each individual data set, plotted in figures 6-14 (a)–(c) for each TTS assumption, show that the experimental data can be very well reproduced quantitatively by the current total strain model. All data, except for the final data point of the AT45 data set, are very closely matched by the strain-

[16] It should perhaps be noted that the performance of the modified model may be further improved than the results here presented. This would require a further iteration of the IFT in which the transient strain model applied to the thermal strain is plotted consistent with the modified model. It would be necessary to explicitly assume the correct value of the transition temperature in the zero applied load condition; either extrapolation or the assumption of an equal value to that associated with the AT225 data set appear the most justified.

temperature curve. This suggests that the model is very capable of reproducing the experimental results.

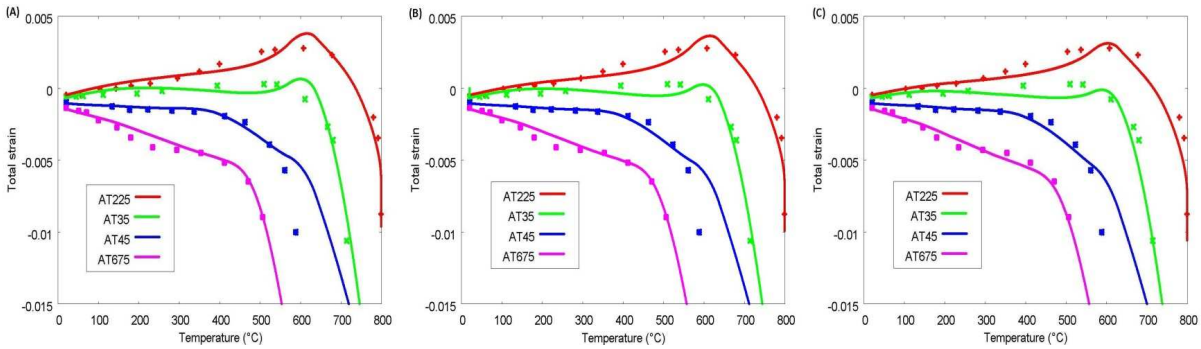

Figure 6-14: The total strain predicted for each load level in comparison with the experimental data sets using the Nielsen model and (a) the TTS0 assumption, (b) the TTS1 assumption, and (c) the TTS2 assumption. The parameters for each curve are chosen according to each individual data set.

Comparison of the results of figures 6-14 (a)-(c) with those of figures 6-13 (a)-(c) suggests that the improvement achieved by calibrating the parameters by each individual data set is relatively low. It can be seen that the results of figures 6-13 (a)-(c) are not significantly less closely matched to experimental data than those of figures 6-14 (a)-(c) and it can be further argued that the qualitative match is improved in the total strain results in which the set of parameter values are chosen for all data sets simultaneously (note, in particular, the positive strain gradient for the AT35 data set for temperatures in the range $500 - 600℃$ in the results of figures 6-14 (a)-(c)). Therefore, the robustness of the Nielsen model in terms of applied load levels appears to be good.

In terms of the TTS investigation, there are two sets of model performances to analyse, those produced by model calibration to all data sets simultaneously (figures 6-13 (a)–(c)) and those produced by model calibration to each data set individually (figures 6-14 (a)–(c)).

When the Nielsen model is calibrated by all data sets at once, as can be seen in figures 6-13 (a)–(c), the dependence of the model performance is only very weakly dependent on the TTS assumption applied. The strain-temperature curves are relatively accurately described in each application. In terms of the overall error measures calculated for each, the TTS0 assumption is found to produce the most accurate results with those of the TTS2 assumption found to be least accurate. If the error measure of TTS0 is

normalised to 1.00, those of TTS1 and TTS2 are evaluated as approximately 1.07 and 1.13 respectively.

In a similar manner, the visual inspection of the results of figures 6-13 (a)–(c) suggests that the model performance is invariant to the TTS assumption applied. However, examination of the error measure results found when results are calibrated by each individual data set shows that the performance of the TTS2 assumption is consistently that which leads to the lowest level of error measure for each data set. In a similar manner of expressing the error measure, in which the lowest value is considered to be 1.00, the error measures for AT225 for TTS0 and TTS1 respectively are 1.03 and 1.05, for AT35 are 1.08 and 1.12, for AT45 are 1.07 and 1.05, and for AT675 are 1.40 and 1.20.

Hence, the relative error measures for each different type of analysis suggest that the TTS2 assumption allows the model to most closely match any single experimental data set and that the results of application of the model using the TTS0 assumption produces the most accurate results when calibrated to all data sets. Therefore, it is here concluded that these results support the application of the TTS0 assumption to transient strain modelling. Thus, no transient strain shall be considered to result from states of net tensile stress in application of the IFT to the remaining transient strain models in this work. However, the results show that the differences between model output and experimental results are very low for each of the TTS assumptions. Visually, no significant difference appears to be made to the model performance of the TTS assumption applied. Therefore, this aspect of the model should be subjected to further research.

6.4.2 *The Anderberg model*

The IFT is here applied to the Anderberg model in order to investigate the performance of the model in comparison with experimental data. The form of the model used is that, detailed in §4.2, in which the magnitude of the transient strain increment that develops is modelled as directly proportional to that of the corresponding thermal strain increment in the temperature range below a transition temperature only. Above this temperature, the transient strain develops proportionally to temperature increase.

$$\dot{\boldsymbol{\varepsilon}}_{tr} = \begin{cases} \dfrac{\beta_A}{f_c(T_0)} \dfrac{\partial \varepsilon_{th}}{\partial T} \boldsymbol{Q} : \boldsymbol{\sigma} \dot{T} \ , & T \leq T_{cr} \\ \dfrac{\mathrm{B}_A}{f_c(T_0)} \boldsymbol{Q} : \boldsymbol{\sigma} \dot{T} \ , & T > T_{cr} \end{cases}$$ Equation 6-14

The model modification proposed in §5.4.2, that in which the magnitude of the proportionality constant β_A is normalised by the magnitude of thermal strain at a reference temperature, is not here applied. This modification is proposed to be used for application of the model to different concrete types (with corresponding different thermal strain behaviour). As only one concrete type is investigated in this section of work, this modification would not affect results.

It is worthy of note that the implementation of the model here applied explicitly uses the 'true' measure of thermal strain to define the temperature-dependence of the transient strain model ($T < T_{cr}$). Previous applications of this model apply the total strain in unloaded conditions as this temperature-dependent parameter [14-16], a strain measure that was shown in §5.2 to generally contain non-thermal strain components in certain conditions. However, this distinct approach to this model is likely to be insignificant in this work as appreciable non-thermal strain components are found to develop in unloaded concrete specimens principally in the high temperature region, above the transition temperature of this model (i.e. $T > T_{cr}$). Thus, these non-thermal strain components are of negligible influence on the model output, as defined by Equation 6-14.

Due to the relative simplicity of the Anderberg model, implementation of this model shall not require any additional considerations. Small changes in the values of the three parameters of the model cause fairly predictable changes to the strain output. Therefore, the application of the PPI program to this model is expected to be efficient.

The form of the Anderberg model applied in this analysis (Equation 6-14) has three free parameters, the transition temperature and the two coupling parameters. Default initial values of these parameters, shown in table 6-6, reflect values used by other researchers in the literature [17].

Table 6-6: Default initial values of the free parameters of the Anderberg transient strain model (Equation 6-14).

Parameter	Default initial value
β_A	2.35
B_A	1.0×10^{-4}
T_{cr}	550°C

Violation of the principle of monotonic increase in transient strain can be avoided easily by restriction of the coupling parameters of the model to positive values only. This ensures that an increase in temperature leads to an increase in transient strain, provided that thermal strain also increases with temperature increase for T< T_{cr}. This condition is met if T_{cr} is of a lesser value than the transition temperature of the thermal strain model. If this is not the case, due to the behaviour of the thermal strain model in this temperature region, it is possible that transient strain may violate the principle of monotonic transient strain increase. Therefore, to avoid this potential forbidden behaviour, the model is modified to remove this potential behaviour.

$$\dot{\boldsymbol{\varepsilon}}_{tr} = \begin{cases} \dfrac{\beta_A}{f_c(T_0)} \mathrm{E}' \boldsymbol{Q} : \boldsymbol{\sigma} \dot{T} \ , & T \leq T_{cr} \\ \dfrac{\mathrm{B}_A}{f_c(T_0)} \boldsymbol{Q} : \boldsymbol{\sigma} \dot{T} \quad , & T > T_{cr} \end{cases} \qquad \text{Equation 6-15}$$

where E' is defined as follows.

$$\mathrm{E}' = \begin{cases} 0 \quad , & \dfrac{\partial \varepsilon_{th}}{\partial T} \leq 0 \\ \dfrac{\partial \varepsilon_{th}}{\partial T} , & \dfrac{\partial \varepsilon_{th}}{\partial T} > 0 \end{cases} \qquad \text{Equation 6-16}$$

The ranges of parameter values used in the IFT and the incremental values are shown in table 6-7. These values, chosen heuristically, are based on the observed dependence of the transient strain model on the values of the parameters and on the results of preliminary tests using the PPI program.

Table 6-7: Range of values of parameters and incremental values used throughout the PPI procedure.

Parameter	Minimum value	Maximum value	Incremental value
β_A	1.5	3.0	2.5×10^{-2}
B_A	0.0	2.0×10^{-4}	0.5×10^{-5}
T_{cr}	450°C	600°C	5°C

It is of particular interest to analyse the Anderberg model using the IFT because this model was originally developed based on these experimental data. Therefore, it should be expected that the model is well suited to these data and that the parameters should be fairly well calibrated to the data sets at the outset of the analysis.

Application of the IFT to each of the individual data sets for the Anderberg model is most successful, in terms of the resultant error measure, for the AT675 data set. Expressing the minimum error measure of this data set as 1.0, those of the AT225, AT35, and AT45 data sets are expressed approximately as 3.06, 2.19, and 8.72 respectively. Thus, these results are consistent with the results of §6.4.1 in which, across the experimental data sets analysed, the lowest error measure is found for the highest applied load level and the highest error measure is found for the conditions of 45% applied axial load.

A potential weakness in the application of the PPI program is clear in application to the Anderberg model and the AT45 data set. As shown in figure 6-15, the parametric orientation identified by the PPI program as that which produces the lowest error measure results in a very poor fit to data in the temperature range above approximately $550℃$. The cause of the apparent error is that the behaviour of the transient strain model in the post-transition temperature region (above $590℃$) does not affect the strain-temperature curve evaluated by the PPI program in the temperature region in which the experimental data are available. Therefore, the value of B_A does not affect the error measure calculated and, by default, a null value is selected. However, the effect of the value of B_A on the strain-temperature curve that develops in FE simulations is apparent in the pre-transition temperature region (as the temperature of the mesh is not uniform). As a result, a significant deviation is found between the FE results and the experimental data in the temperature range close to the transition temperature, as shown in figure 6-15. This can be easily corrected by application of the FE model by modifying the value of B_A to a non-zero value. When this is done, the results significantly improve.

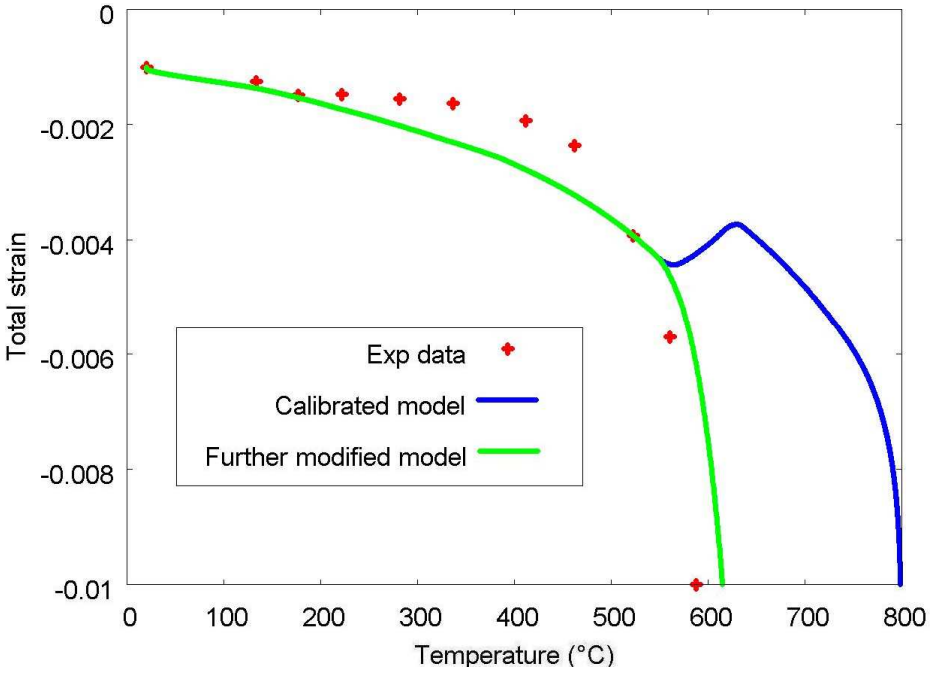

Figure 6-15: Comparison of the total strain results obtained through FE simulations using the transient strain model (Anderberg) calibrated to the experimental data (AT45) via the PPI program. The further modified model results are for a similar simulation in which a non-zero value of $\mathbf{B_A}$ is applied.

As the most important results of the IFT are those obtained through application of a consistent set of transient strain parameters over several data sets, the aberration in model performance without further modification, shown in figure 6-15, is unimportant as the results of other data sets consistently indicate a non-zero value of B_A produces a lower overall error measure. However, this example demonstrates that the results of the PPI program should always be checked using the FE model to ensure that the predictions are reliable.

The total strain results for each load level calibrated to the experimental data, shown in figure 6-16, show that the results fairly accurately match the experimental data. Therefore, the capacity of the Anderberg model, despite its inherent simplicity to accurately reproduce experimental data appears to be fairly good.

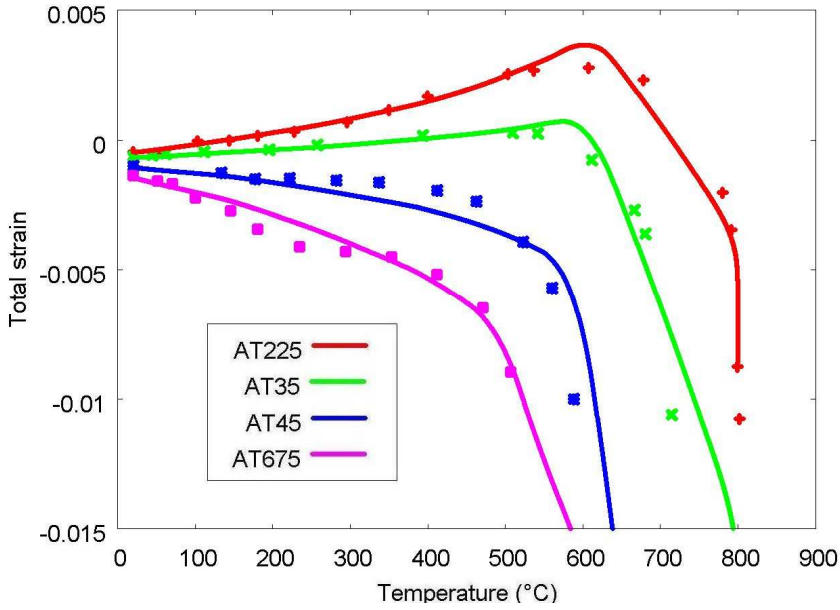

Figure 6-16: The total strain predicted by FE simulations for each load level in comparison with the experimental data sets using the Anderberg model. The parameters for each graph are chosen according to each individual data set.

The transient strain model parameter values used to produce the total strain results of figure 6-16 (see Appendix B) vary between data sets to produce the lowest error measure to a fairly low degree. The values of the parameter β_A are all within 16% of the mean value, with a value of approximately 31% and 7% for the parameters B_A and T_{cr} respectively.

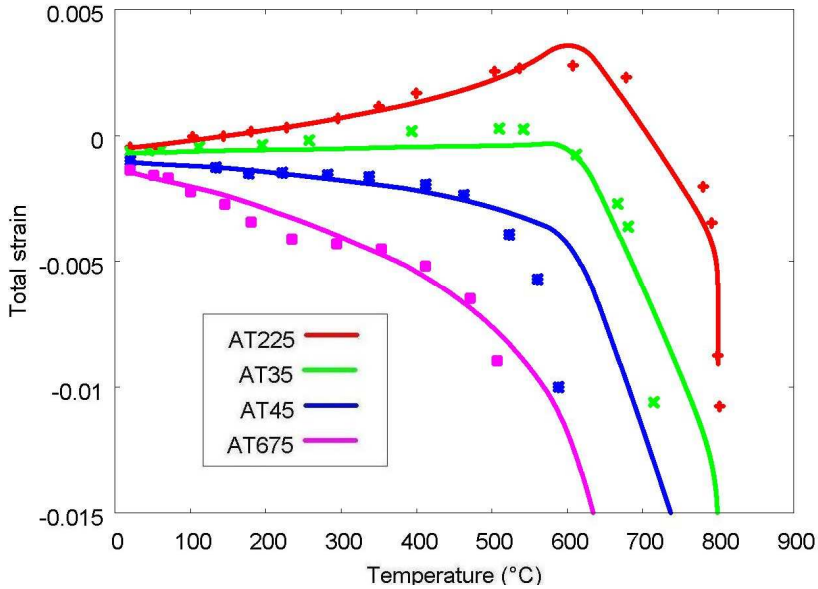

Figure 6-17: The total strain predicted for each load level in comparison with the experimental data sets using the Anderberg model. The parameters for each graph are chosen according to the data of all four load levels.

The total strain curves for the set of parameter values found to produce the error measure of lowest magnitude, shown in figure 6-17, appear not to be significantly less

well matched to the experimental data than the results of figure 6-16. This is true of all data sets except for the AT45 data set, which performs relatively poorly in comparison to the experimental data.

The values of the parameters found to minimise the (normalised) error measure over the four loaded data sets suggest that a transition temperature of around $465℃$ is most appropriate with values of the coupling parameters of 1.775 and 1.15×10^{-4} for the low temperature and high temperature regions respectively. In comparison to the default initial values, this represents a modification of the difference in transition temperature of around $85℃$ and a change in magnitude of the coupling parameters of approximately 25% and 15% respectively. As stated earlier, the original values of the parameters were chosen by the authors using these experimental results. Therefore, this modification of the parameters, found here to reduce the error measure over all the data sets, shows the usefulness of the IFT.

6.4.3 *The Terro model*

The IFT is applied to the data sets using the Terro transient strain model (implementing the TTS0 assumption). The polynomial function of the model is fourth order and uses the reduced temperature measure in place of temperature, as suggested in §4.5.

$$\varepsilon_{tr} = -10^{-6} \times \frac{(A'_1\theta + A'_2\theta^2 + A'_3\theta^3 + A'_4\theta^4)}{f_c(T_0)} \boldsymbol{Q}:\boldsymbol{\sigma} \qquad \text{Equation 6-17}$$

Polynomial functions, despite their relative lack of complexity, can be extremely difficult to fit to data sets in a unique manner. This is particularly true of functions of relatively high order (e.g. fourth order). Two separate polynomial curves may be fitted to a data set, for instance, that are of similar accuracy but that are defined by entirely distinct sets of polynomial coefficients. Thus, there are likely to be a large number of dissimilar parametric sets that produce results of comparable error measure. Therefore, each iteration of the IFT may produce dissimilar parameter values without significantly affecting the transient strain curve. Hence, a stationary value of error measure is used to identify the point at which iterations of the IFT may cease.

Furthermore, it is not generally possible to define a rigid and succinct set of conditions which, when imposed, constrain the performance of the function such that the principle of monotonic transient strain increase is obeyed in the entire temperature range of interest, without imposing conditions that are unduly restrictive. As the temperature function of the Terro model is a fourth order polynomial, differentiation with respect to temperature results in a polynomial of third order.

$$A'_1 + 2A'_2\theta + 3A'_3\theta^2 + 4A'_4\theta^3 \geq 0, \qquad 0 \leq \theta \leq \theta_{max} \qquad \text{Equation 6-18}$$

No general solution is possible (of which the author is aware) by which all four polynomial coefficients of Equation 6-18 can be constrained to ensure that the inequality remains true without also preventing valid solutions (e.g. the imposition of the constraint that A'_1, A'_2, A'_3, and $A'_4 > 0$ guarantees that the inequality of Equation 6-18 is true but may rule out a valid solution where some of these coefficients may be negative).

It is evident from inspection of Equation 6-18 that $A'_1 \geq 0$ to ensure that the principle of monotonic transient strain increase is not violated for temperatures in proximity to the initial temperature. However, restrictions on the three remaining parameters are dependent on the simultaneous values of the remaining parameters. Therefore, the ranges of values of the parameters cannot generally be chosen in a manner that guarantees adherence to the principle of monotonic transient strain increase. Hence, the procedure of the application of the IFT must be slightly modified for the use of the Terro model. The ranges of the values of parameters are chosen based on a set of parameter values determined, through application of conventional fitting techniques.

Firstly, as usual, a set of default initial transient strain parameters is used to calibrate the set of thermal strain parameters. After this stage, the loaded cases are simulated to generate data that allow the 'target' transient strain data to be defined by comparison with experimental data. By normalisation with respect to applied load level, the data can be combined and used to calibrate the parameters of the temperature function of Equation 6-17. Through application of PPI using parametric values close to these values (specifically, within 0.9–1.1 of these fitted values), predictions for the model parameters can be generated for the next iteration of the

IFT. The values applied for the first iteration are shown in table 6-8 (new parameters should be evaluated for each iteration).

Table 6-8: The maximum, minimum, and incremental values of the model parameters applied in the first application of the PPI program within the IFT analysis of the Terro model.

Parameter	Minimum value	Maximum value	Incremental value
A_1'	3669.1740	4484.5460	81.5372
A_2'	−1942.3360	−1589.1840	35.3152
A_3'	426.1203	520.8137	9.46934
A_4'	−27.716920	−22.677480	0.503944

For each permutation of the parameter values, a calculation is performed to check whether the parameters result in violation of the inequality of Equation 6-18. If this is found to be the case, a default (large) error measure is assigned to the permutation of parameters and the PPI iterates to the next set of parameters. Thus, solutions that violate the principle of monotonic transient strain increase are not considered in this analysis.

Application of the IFT to the experimental data sets requires three iterations for a stationary solution to be found. The total strain results obtained for each data set (where the parameters are separately calibrated to each data set) are shown in figure 6-18.

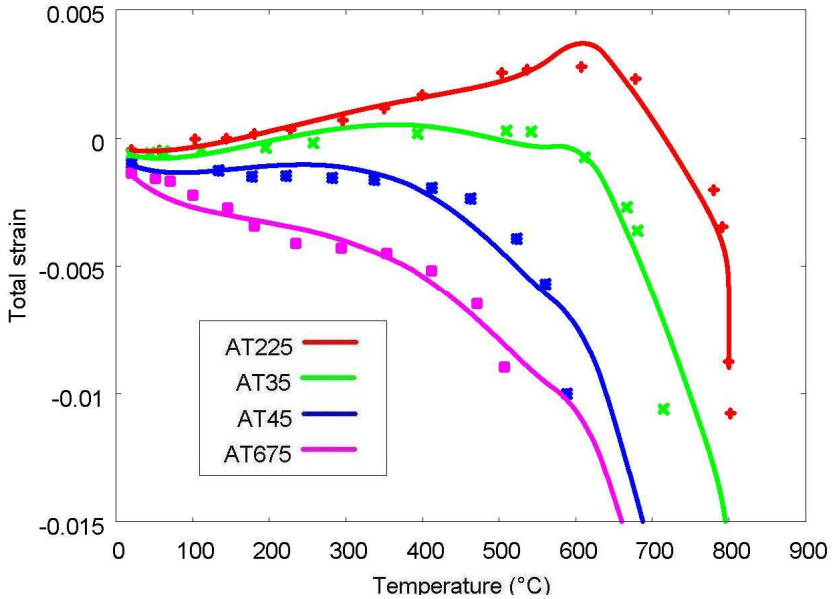

Figure 6-18: The total strain predicted by FE simulations for each load level in comparison with the experimental data sets, using the Terro model. The parameters for each graph are chosen according to each individual data set.

Consistent with application of the IFT to the other models, when the minimum error measures found for each data set are compared, the lowest value is found for the AT675 data set. In comparison, the relevant error measures found for AT225, AT35, and AT45 relative to that of AT675 are approximately 2.65, 2.40, and 3.95 respectively.

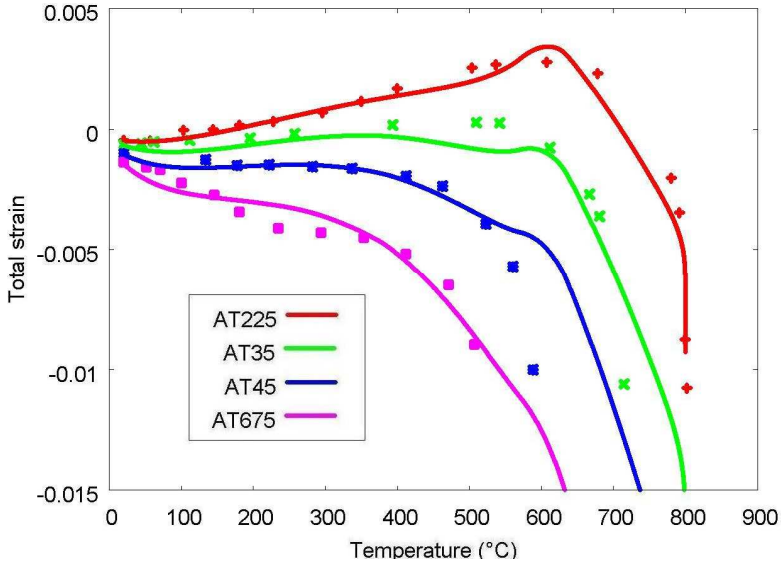

Figure 6-19: The total strain predicted by FE simulations for each load level in comparison with the experimental data sets, using the Terro model. The parameters for each graph are chosen according to the data of all four load levels.

The total strain results associated with these minimum values of the error measure, shown in figure 6-18, demonstrate that the total strain model incorporating the Terro

transient strain model is capable of reproducing the experimental data fairly well. Therefore, the model can be considered to have the potential to accurately reproduce experimental results.

The improvement in the model performance provided by the selection of transient strain parameters for each data set can be found by comparison of the results of figure 6-18 with those produced using the parametric set calibrated to all data sets, shown in figure 6-19. The results of figure 6-19 show that the total strain results are reasonably well matched to the experimental data. Thus, the Terro model appears to be capable of accurately reproducing realistic experimental data over a range of load levels.

It is noteworthy that, as is often found in fitting polynomial functions to data sets, some small degree of oscillation about the data curves is apparent in the results of figures 6-18 and 6-19[17]. The process of fitting polynomial functions to data sets often results in this type of behaviour. While this is undesirable, it is not here considered to be a significant model weakness.

6.4.4 *The Schneider model*

The IFT is now applied to the Schneider transient strain model (§4.8). A potential modification was proposed in §5.4.5 that may improve consistency between the Schneider model predictions and experimental observations, i.e. the introduction of a time function into the mathematical model to represent the time-dependence of the dehydration process. While this modification has the potential to lead to model output that is able to reproduce the time-dependence of the strain development of the transient strain of concrete specimens heated to low temperatures, the experimental data considered here in the investigation of the relative performances of the models do not allow for this parameter of the model to be reliably chosen. Therefore, this modification shall not be included in the model formulation considered in this investigation.

However, a slightly modified form of the mathematical model is here applied. The moisture-dependence of the hyperbolic function, γ_w, is found to be fairly unimportant to the model output. Therefore, this parameter is replaced with a parameter of

[17] It should be noted that the oscillation in the transient strain curve in some temperature regions is about a mean gradient above zero (with the minimum gradient also above zero).

constant value, $\gamma_{w,0}$. As the moisture-dependent form of the model requires two free parameters to be fixed, this also simplifies the parametric investigation.

$$\varepsilon_{tr} = \frac{\left[1.0 + \frac{(T - T_0)}{100}\Sigma_{0.3}(\sigma)\right]\phi(T) + \frac{(T - T_0)}{100°C}\Sigma_{0.3}(\sigma)}{E(T,\sigma)}\sigma \quad \text{(a)}$$

$$\phi(T) = C_1 \tanh\left[\gamma_{w,0}(T - T_0)\right] + C_2 \tanh\left[\gamma_0\left(T - T_g\right)\right] + C_3 \quad \text{(b)} \qquad \text{Equation 6-19}$$

$$\Sigma_{0.3}(\sigma) = \begin{cases} \frac{\sigma_c}{f_c(T_0)}, & \frac{\sigma_c}{f_c(T_0)} \leq 0.3 \\ 0.3, & \frac{\sigma_c}{f_c(T_0)} > 0.3 \end{cases} \quad \text{(c)}$$

The temperature-dependence of the Schneider model is strongly defined by ϕ, defined in Equation 6-19 (b). While the temperature-dependence of the elastic modulus is also important in this respect, the parameters of this model are defined by high temperature stiffness data and are therefore not subject to modification.

As is evident from Equation 6-19 (b), the Schneider model has five free parameters, C_1, C_2, $\gamma_{w,0}$, γ_0, and T_g (the value of C_3 is fixed to ensure that $\phi(T_0) = 0$). The values of none of these parameters can be justifiably set equal to a constant value throughout the analysis and each plays an important role in defining the development of transient strain with increasing temperature. Therefore, it is necessary to find the values of five free parameters in the IFT.

The form of the transient strain model ensures that the strain output produced by the model does not violate the principle of transient strain monotonic increase provided each of the parameters is defined to be positive. Although this may appear to be an unnecessarily restrictive condition (e.g. if the remaining parameters are suitably defined, a value of $C_2 < 0$ may not lead to violation of the principle of monotonic transient strain increase), tests demonstrate that use of a negative value of any of the parameters results in visibly poor results. Hence, a heuristic approach is taken and all free parameters must be positive in value.

Preliminary tests show that, in a similar manner to the Terro model, it is extremely difficult to find a stationary set of limits to the parameter values for each individual data set within which a set of parameter values can be selected using the PPI program

that produces a minimum quantity of error[18]. Moreover, the ranges of the parameters for each data set tend to become quite different from one another. Therefore, the application of the PPI program to this problem over a range of values for each parameter that allows the 'best' set for each individual data set to be analysed requires a very large number of parametric permutations.

Similarly to the application of the IFT to the Terro model, the values of the parameters are therefore initially fitted using conventional fitting techniques to all of the data sets simultaneously (normalised by load level). Subsequently, parametric values close to those found via this calibration are simulated using the PPI program. The default initial transient strain parameters used are identical to those suggested by Schneider [5] for concretes containing quartzite aggregates shown in table 6-9.

Table 6-9: Default set of transient strain parameters for the Schneider model.

Parameter	Default initial value
C_1 [-]	2.6
C_2 [-]	1.4
$\gamma_{w,0}$ [°C^{-1}]	17.2×10^{-3}°C^{-1}
γ_0 [°C^{-1}]	7.5×10^{-3}°C^{-1}
T_g [°C]	700°C

The process of fitting the parameters conventionally is also very challenging. Parameters of magnitudes that appear to be unrealistically large in value (or negative) may be predicted. When the final results are observed, any improvement in model performance is very low. Therefore, the data fitting procedure is modified slightly to ensure that such high values of the parameters are forbidden.

Using a heuristic approach, the limits for each parameter necessary for reasonable results to be found are fairly wide. In particular, it is found that the value of γ_0 should be allowed to assume a value of about three orders of magnitude lower than the default value.

[18] The value of at least one of the parameters is found to be equal to a limiting value, which implies that the limits should be modified and the analysis restarted.

As with the Terro model, the values of the parameters that are applied to the PPI program are defined using the fitted parametric set and multiplicative factors, 0.9 and 1.1. Example values found in preliminary tests to allow sufficient freedom in the shape of the strain-temperature curve around at directly fitted to the normalised 'target' data are given in table 6-10.

Table 6-10: Range of values of parameters and incremental values used in the PPI analysis procedure (third iteration).

Parameter	Minimum value	Maximum value	Iterative value
C_1 [-]	3.591	4.389	0.0798
C_2 [-]	2.340	2.860	0.0460
$\gamma_{w,0}$ [°C^{-1}]	1.746×10^{-3}	2.134×10^{-3}	3.88×10^{-5}
γ_0 [°C^{-1}]	0.900×10^{-6}	1.100×10^{-6}	0.20×10^{-7}
T_g [°C]	632	758	12.6

As with the application of the IFT to the Terro model, three iterations are required to produce a stationary error measure. This increased in procedural repetition in comparison with, say, the Anderberg model reflects the higher mathematical complexity of this model.

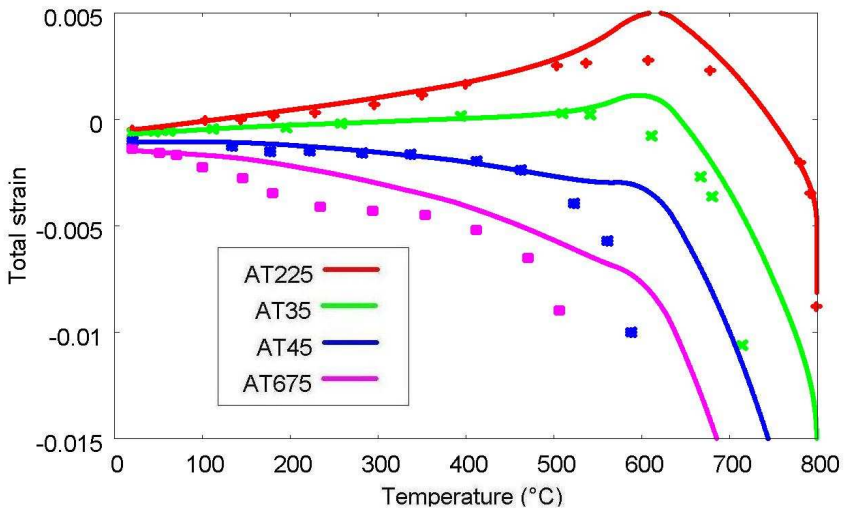

Figure 6-20: The total strain predicted by FE simulations for each load level in comparison with the experimental data sets, using the Schneider model. The parameters for each graph are chosen according to each individual data set.

Consistent with application of the IFT to the other models, when the minimum error measures found for each data set are compared, the lowest value is found for the AT675 data set. In comparison, the relevant error measures found for AT225, AT35,

and AT45 relative to that of AT675 are approximately 2.03, 2.00, and 5.70 respectively.

The total strain results associated with these minimum values of the error measure, shown in figure 6-20, demonstrate that the total strain model incorporating the Schneider transient strain model is capable of approximately reproducing the experimental data. However, the model output appears to be incapable of achieving a good quantitative match to the experimental data.

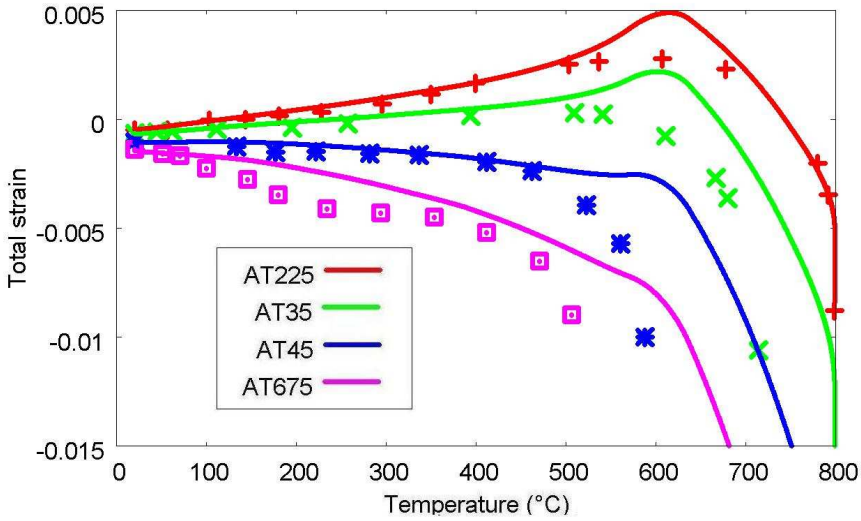

Figure 6-21: The total strain predicted for each load level in comparison with the experimental data sets using the Anderberg model. The parameters for each graph are chosen according to the data of all four load levels.

The main goal of the IFT analysis is to produce a consistent set of parameters across all data sets. The identification of parametric sets that best match individual experimental data sets is only an approximate solution (as each iteration is intended to reduce the error measure determined over all data sets). The results of application of the set of parameter values that produces the lowest overall error across all data sets are shown in figure 6-21.

The results of figure 6-21 show that the total strain results match the experimental data qualitatively well. The quantitative match, similar to the results of figure 6-20, is not particularly good. However, the reason that this model is not well matched to the experimental data may be a result of a failure of the methodology to find a sufficiently favourable parametric orientation.

6.4.5 *The Bažant model*

The Bažant model is the final transient strain model to be analysed using the IFT. The model here applied is a modified form of that originally proposed by the Bažant et al. [18]. As found in §5.3, the original version of the model, formulated for use at temperatures below $100℃$, predicts extremely large transient strain measures to develop in the post-heating period of time for specimens heated to high temperatures. While this appears at first sight to be consistent with the nature of the model (i.e. that transient strain is an additional component of basic creep), much of the creep that forms after heating to high temperature ceases is properly modelled as basic creep. In fact, the Bažant model must be modified to reduce the magnitude of the excessively large strain that develops to be useful for transient strain modelling over a wide range of temperatures.

The cause of the additional strain development can be determined from an examination of the results of simulations to be the extremely large values of microprestress values that develop, particularly at high temperatures. The cause of this behaviour is the relative humidity dependence of the model shown in Equation 6-20, which is assumed to be valid in the entire temperature range, including that in which the concrete specimen is almost completely dry. The FE model predicts an extremely low finite value of relative humidity in this temperature range, which leads to the development of an extremely large value of S.

$$\dot{S} + \psi_S c_0 S^2 = k_1 \left| \dot{T} \ln h + T \frac{\dot{h}}{h} \right| \qquad \text{Equation 6-20}$$

As can be deduced from Equation 6-20, a very low value of the relative humidity parameter h leads to a magnification of the effects of a changing temperature on the microprestress evolution. This model behaviour seems to be unreasonable. In fact, the effects of relative humidity on transient strain should not continue in this temperature range. Hence, it is clear that the model must be modified to remove this behaviour. Replacing the relative humidity parameter applied to Equation 6-20 with a value-limited effective relative humidity, such as that of Equation 6-21, allows the behaviour of the model to be constrained in the desired manner.

$$h^{lim} = \begin{cases} h_{min}, & h < h_{min} \\ h, & h \geq h_{min} \end{cases}$$ Equation 6-21

The value of the value-limiting parameter h_{min} should be set based on observations. The effect of the value of this parameter on the development of microprestress can be found by inspection of figure 6-22 (a) which is produced using experimental conditions considered in this work.

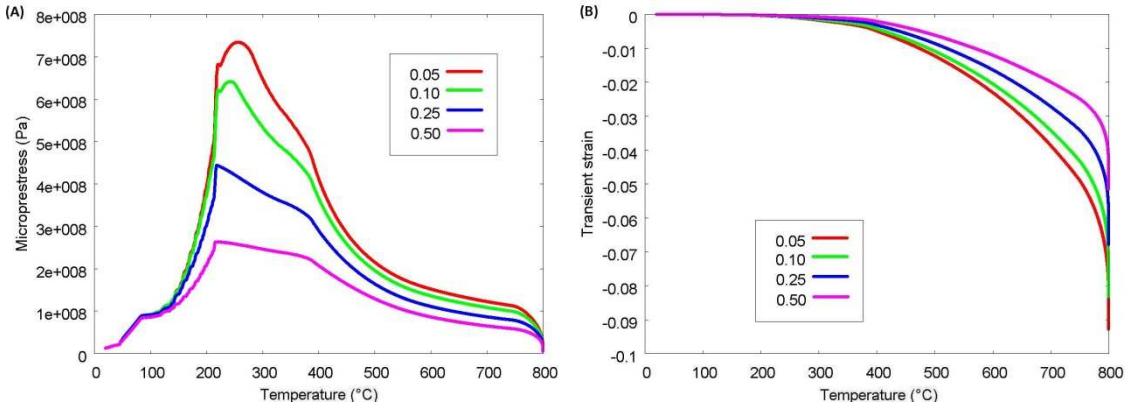

Figure 6-22: Development of (a) microprestress and (b) transient strain during heating to 800°C at 5°C/min heating for a range of minimum values of the model relative humidity parameter.

It can be clearly seen from figure 6-22 (a) that the main effect of the value of the minimum relative humidity model parameter is to decrease the peak in microprestress that occurs at a temperature of around $200℃$. Qualitatively, the results remain essentially the same. Moreover, the results of figure 6-22 (b) suggest that the magnitude of transient strain that develops is affected to a relative low extent by a fairly large range of values of $h_{min} > 0$. Therefore, it is concluded that the value of h_{min} applied is of relatively low order importance and that appropriate selection of the remaining parameters should ensure that model predictions are essentially invariant to the particular value used. The value chosen for use in this work is 0.10.

The transient strain model proposed by Bažant et al. [18] is also modified, as suggested in §5.4.1, by the decoupling of the k_1 parameter into two parameters, k_1^T and k_1^h. This modification, intended to allow the relative magnitudes of the effects on the model output of a changing temperature and of a changing relative humidity to be modified to most closely match experimental data, increases the number of free parameters of the model.

The behaviour of the Bažant model is extremely difficult to predict a priori. Tests suggest that the PPI program is not an appropriate method of reproducing the predictions of the FE simulations for the Bažant model. The predictions of the evolution of microprestress are dissimilar to those found applying the FE model. This is likely to be caused by the inadequacy of the process of calculation of a microprestress variable by the PPI program, which is based on mean temperature and mean relative humidity history. In particular, the use of the rate of change of mean temperature and mean relative humidity to define the microprestress variation (Equation 6-20) is likely to be a significant source of the error in the microprestress evaluation. Thus, the mean microprestress calculated in the FE simulations is at variance with the value calculated in the PPI program.

Furthermore, tests show that, even if the mean microprestress data are generated by a FE simulation and provided to the PPI program, sufficient agreement cannot be obtained between the total strain histories calculated by the PPI program and the FE model. Thus, the error measures generated by the PPI program cannot be used to determine the set of Bažant model free parameters that yield total strain results that match the experimental data.

Therefore, the critical role played by the PPI program in the IFT must be replaced with another method to determine parametric values that provide a good match with experimental results. However, no such method is known, so the conventional technique of trial and error using the FE model must be implemented.

As a result of the complexity of the Bažant model, it is particularly difficult to impose constraints on the allowed values of the model parameters in order to ensure realistic behaviour. In fact, the model, in the form proposed by the authors initially, is found to produce monotonically increasing transient strain in heated conditions, provided that the value of the parameter k_1 is positive.

The full set of parameters considered to be free in this analysis consists of seven variables. The nature of the variables and their default initial values are shown in table 6-11. It is a difficult task to find values of each of these parameters that produce a close representation of experimental results. It is necessary to attempt to determine the roles that each parameter plays in defining the shape of the strain-temperature

curve by observing the model output when values of various magnitudes are defined for each. Once the role of each parameter is established, the parameters can be varied in turn (with the FE output compared with 'target' transient strain data, calculated in the usual way) until the model predictions are found to have become sufficiently similar to the desired behaviour. This process, which is imperfect, time-consuming and difficult to execute, shall play the role of the PPI program in the application of the IFT to the Bažant model.

Table 6-11: Default initial parameter values for the Bažant model.

Parameter	Initial value
$Q_v/_R$	$5000K$
$Q_s/_R$	$3000K$
k_1^T	$3.0\ MPa/K$
k_1^h	$3.0\ MPa/K$
c_0	$4.6296 \times 10^{-14}(Pa.s)^{-1}$
c	$3.4722 \times 10^{-22}(Pa^2.s)^{-1}$
S_0	$13.0\ MPa$

Results of attempts to find a parametric orientation of the Bažant model suggest that this model is not presently reliable for the process of calculation of transient strain that develops in high temperature conditions. The shape of the strain-temperature curve, although superficially similar to that observed in experimental results, is too dissimilar to experimental data when examined quantitatively. Specifically, the development of transient strain is unrealistically slow for temperatures of heating lower than about $200℃$. Subsequently, the model tends to predict very rapid development of transient strain for temperatures above about $400℃$. Although this is generally observed in results, the development of strain tends to be too rapid. It is possible to impose parametric values on the model such that the strain-temperature curve is sufficiently shallow to yield a good fit with experimental data in the high temperature region, as demonstrated in figure 6-23. However, there is no similar method found by the present author that allows a similar improvement in the results in the low temperature region. This includes the decomposition of the k_1 parameter

that was proposed in part in an attempt to improve the model performance for low temperature applications of the model.

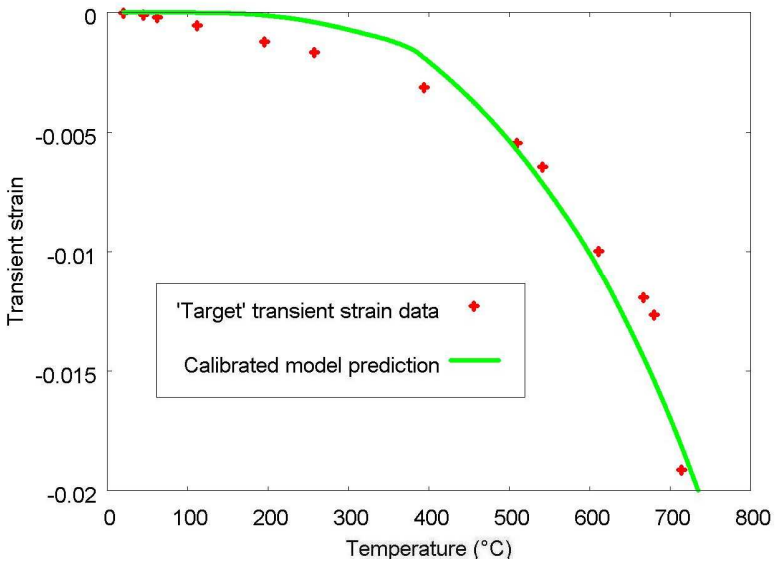

Figure 6-23: Comparison of the experimental data (AT35) and model output.

The results of figure 6-23 are achieved using only one modification from the default set of parameter values; the value of c is reduced to one half of the initial value. Many different trials of sets of parameter values were attempted in order to attempt to find a parametric orientation that could improve on the results of figure 6-23. However, none could be found. Therefore, the set of parameters found to produce the results of figure 6-23 are considered in this work to represent the 'best' set of parameters. Application of these values of the parameters to all data sets leads to the total strain results shown in figure 6-24.

Comparison of the experimental results and model output, shown in figure 6-24, confirms that the low temperature transient strain behaviour of the model underestimates that observed to develop in the experimental data. If temperature is allowed to remain constant at the temperature level of each data point, the Bažant model may be capable of accurately reproducing similar final values of total strain. However, this is not an accurate reflection of the method of data collection performed in the experimental tests. Hence, this would not represent a fair examination of the model performance.

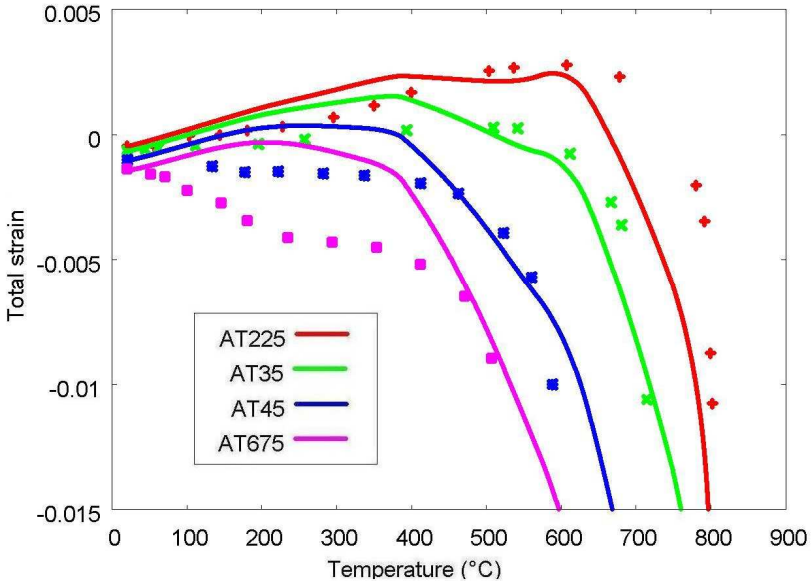

Figure 6-24: Comparison of the experimental data and simulated results using the Bažant transient strain model calibrated to results using trial and error.

The high temperature behaviour of the model appears, in contrast to that of the low temperature, to be reasonably close in matching the experimental results. In comparison to the total strain results obtained by use of the initial default set of values of the parameters, shown in figure 6-25, the improvement is clear.

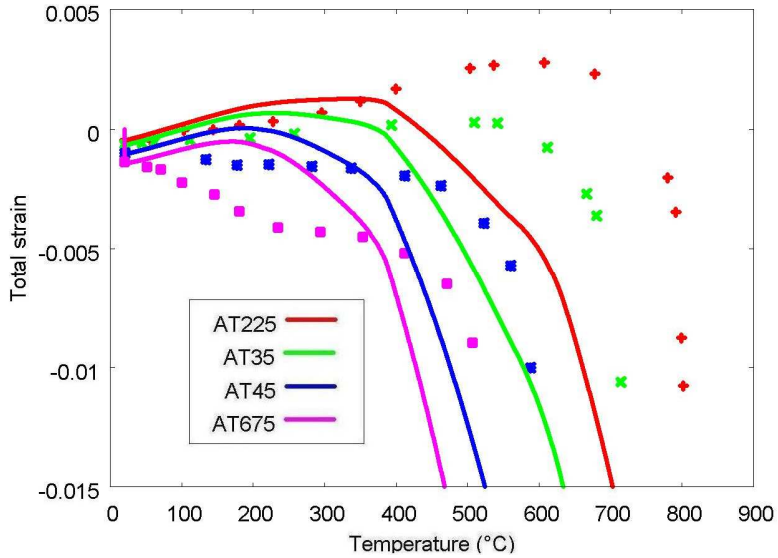

Figure 6-25: Comparison of experimental data and the model predictions using the Bažant transient strain model calibrated with the initial default set of values of parameters.

There may be further developments in the Bažant model formulation that results in increased model performance in the low temperature region. However, the nature of these developments is not apparent at this stage. Therefore, the results of figure 6-24 are here considered to be the best performance of the model that is possible.

6.4.6 *Overall discussion*

When distinct sets of parameter values for each transient strain model are found that minimise the error measure for the individual data sets, it is consistently found that the data set for which the lowest error measure is evaluated is the AT675 data set. This is true for all models (and all TTS assumptions), e.g. for the Nielsen model, the minimum error measure for the AT675 data set is roughly half that of the AT35 data set and one third that of the AT225 data set.

The reason that the AT675 data set is most well matched by the models is highly likely to be mostly due to the limited temperature range of the data set in comparison to the others. The highest temperature for which total strain results are available for the AT675 test is approximately $500℃$ (failure occurs before a higher temperature can be reached). This compares with corresponding values of $800℃$, $714℃$, and $588℃$ for the AT225, AT35, and AT45 data sets respectively.

The Nielsen model and Anderberg model (and, to an extent, the Schneider model[19]) suggest that a transition occurs in the development of the transient strain with increasing temperature. Furthermore, the temperatures at which this transition takes place can plausibly be considered to be typically close to that at which the experimental data for the AT675 data set ceases. Therefore, it is plausible that the entire data set is within the pre-transition temperature region and, thus, that two factors cause the reduction in the error measure calculated for this data set.

Firstly, the models applied to this data set are required to fit a data set that is inevitably more uniform in development from the initial temperature to the final temperature of the data set as the transition is absent in the results. Secondly, models that are designed for a temperature range up to a high temperature, such as $800℃$, are composed of a sufficient number of parameters to control the shape of the model strain-temperature curve over a relatively large temperature range. Therefore, the application of such a model to a data set of a much reduced range of temperatures allows parameters intended to define the strain development in the post-transition

[19] This depends on the calibration of the model. If the parameters are chosen such that the high temperature hyperbolic tangent function develops gradually with temperature increase, then the model results do not exhibit any transition in strain development.

temperature region to be active earlier and thus to improve the fit of the model considerably. This is well illustrated by the Nielsen model for which the parameter C is active only after the transition temperature is reached. Results of application of the PPI program consistently suggest that the value of the transition temperature is below $500℃$ for the AT675 data set such that this parameter can allow the strain-temperature curve to better match experimental results (in contrast with the value found for the AT225 data set, for instance, of $720℃$).

Clearly, a potential methodological weakness is identified. Some individual data sets may exist almost wholly in the temperature range below the 'true' transition temperature. When the analysis is applied to these data sets, results of application of the PPI program shall always find that the 'best' transition temperature is within the temperature range of the data set. Therefore, the PPI program shall almost certainly identify that a set of parameter values different from the 'true' set of parameter values result in a lower measure of error.

Therefore, to minimise the importance of this issue, the results of application of the PPI program to multiple data sets in parallel is always, where possible, applied to produce sets of parameter values that minimise the error measure across several conditions of loading. Furthermore, some of the data sets must be of a sufficiently high maximum temperature to ensure that the prediction of an unnaturally low value of the transition temperature is very unlikely. These conditions are met in the analysis of this work but are worthy of note for future investigations.

In contrast with the consistently low values of error measure found when the data set AT675 is analysed in isolation using the PPI program, the error measures found for each model for the AT45 data set are consistently much higher than those of the other data sets. In some situations, the difference in error measure is one order of magnitude larger than that of the next highest error measure. The reasons for this consistently observed result are unclear. Examination of an example group of 'target' transient strain data sets calculated for application of the IFT to the Schneider model, shown in figure 6-26, suggests that the shape of the transient strain curve for this data set is not too dissimilar to those of other data sets.

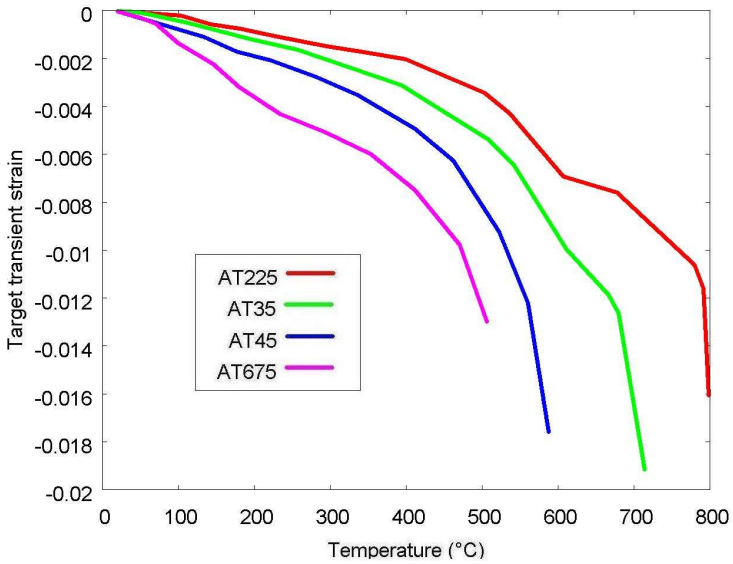

Figure 6-26: Target transient strain data calculated for each of the four data sets.

The results of figure 6-26 suggest that the AT45 data set requires a transient strain development typical of the other data sets when compared in the same temperature range. Therefore, it is unclear why the error measure is consistently of a higher value for this data set in comparison to those typical of the other data sets.

The larger value of the best error measure found for the AT45 data set illustrates that the use of weighting factors to calculate the overall error measure (for multiple data sets) is very important. If weighting is ignored, the sets of values of parameters are consistently very different from those otherwise found, due to the intrinsic bias in the calculation process in favour of minimising the error measure of the AT45 data set.

The application of the IFT to this group of experimental data sets suggests that the role of the TTS assumption in unloaded heated concrete specimens is relatively unimportant. In contrast to the example simulations of §5.2, values of the thermal strain parameters fitted to the experimental data set for the unloaded specimens are fairly similar for all TTS assumptions.

It is likely that the cause of the apparent relative unimportance of TTS in unloaded specimens is due to the small dimensions of the specimens used in the experimental procedure used in this work, which were chosen to be sufficiently small that temperature gradients remain low throughout the test and to be sufficiently large that concrete specimens can be used (rather than mortar). Therefore, the conclusion that

TTS0 is most consistent with these experimental results should be subject to future investigation.

The Nielsen and Anderberg models require only two iterations of the IFT to produce a stationary set of model parameter values. This indicates that these models are very well suited to this type of technique, due to the stability of the predictions of the models (i.e. slight perturbations of the parameters produces only a corresponding slight perturbation of the strain-temperature curve). This allows a relatively smooth error surface to be defined in parametric space which can be systematically investigated using many trials of parameter values to produce a set of parameter values that result in a good correlation between total axial strain history calculated by the FE model and the experimental data.

Conversely, the Terro model and the Schneider model are found to require three iterations to find a set of parameters that produce a stationary error measure. This reflects the complexity of the strain output of the models in terms of the values of the parameters. Moreover, the Bažant model is found to produce an intractable problem as regards application of the IFT. The complexity of the mathematical formulation of the model ensures that control of the model through definition of the values of the parameters is extremely difficult and must be performed using multiple FE analyses.

Results of the analysis of individual data sets can be considered to demonstrate the mathematical suitability of the functional forms of the transient strain models to reproduce the experimental data. These results can be analysed in terms of the error measures calculated in the investigation of each model.

The error measures found for the use of transient strain models calibrated to each individual data set, shown in table 6-12 in normalised form, suggest that the model that is most mathematically suitable for reproduction of the transient strain phenomena is the Nielsen model. The Terro model performs to a very similar standard. The performance of the Anderberg model, though fairly strong for all data sets except AT45, is weak in comparison to these two models. The Schneider model is evaluated to reproduce the experimental results in the least realistic manner, ignoring the Bažant model for which an error measure is not calculated.

Table 6-12: The relative error measures calculated for each of the transient strain models calibrated to each individual data set.

Model	AT225	AT35	AT45	AT675	Mean
Nielsen	1.00	1.00	3.51	1.00	1.38
Anderberg	1.54	1.59	3.32	1.43	1.97
Terro	1.36	1.78	1.00	1.43	1.39
Schneider	1.56	2.22	2.16	2.14	2.02
Bažant[20]	–	–	–	–	–

However, it should be noted that the results of table 6-12 can be considered to provide a rough guide only to the capacity of the models to reproduce experimental results. The sets of parameters found to reduce the error measure for each individual data set are strictly approximate. This is not the principal aim of this investigation which is to calibrate the model parameters for reproduction of multiple data sets. If the investigation were to be performed in a manner to investigate each individual data set, the IFT would be required to be applied to each data set individually (such that each would be permitted to have separate thermal strain parameter values). However, the application of these results to multiple load levels would not be valid, so the value of such an investigation is not high.

It is more accurate to consider the results of table 6-12 to demonstrate the capacity of the models to reproduce each separate experimental data set using sets of parameter values close to those found to produce a close fit to multiple data sets simultaneously. Subject to these criteria, the Nielsen model and Terro model can be considered to perform to the highest standard.

The performances of the models when calibrated to multiple data sets can be evaluated in a similar manner. These results, shown in table 6-13, demonstrate that the Nielsen model and Terro model are the models that produce results over all data sets in the most accurate manner, with the Anderberg model performing fairly well and the Schneider model worst.

[20] As the Bažant model cannot be reliably implemented in the PPI program, no error measure is calculated.

Table 6-13: The relative error measures calculated for each of the transient strain models calibrated to all data sets.

Model	AT225	AT35	AT45	AT675	Mean
Nielsen	1.05	1.02	1.82	1.00	1.22
Anderberg	1.09	1.00	1.98	1.50	1.39
Terro	1.00	1.15	1.00	1.63	1.20
Schneider	1.19	1.74	1.08	1.88	1.47
Bažant[21]	–	–	–	–	–

The relative error measure results confirm the observations that the models that are most able to reproduce the experimental data over the full set of loaded conditions are the Nielsen model, the Anderberg model, and the Terro model. The performances of the more complicated models, those of Schneider and Bažant, are found to be poorer. The Schneider model reproduces the experimental results in a manner that is of a lower standard than the simpler models. The Bažant model, the most complex of all the models, is found to be entirely incapable of reproducing any significant quantity of the transient strain component that is found to develop below a temperature of $200℃$ during heating at $5℃/min$.

It is noticeable from the results that the AT45 data set is the cause of the largest contribution of the relative error measure for both the Nielsen model and the Anderberg model, which appear to be poorly formulated to reproduce these data. If this data set were discounted from analysis, the mean values of relative error would be re-evaluated as 1.02, 1.20, 1.26, and 1.60 for the Nielsen model, the Anderberg model, the Terro model, and the Schneider model respectively. Clearly, the issues that cause the error measure of this data set to be higher for application of all transient strain models are of a lesser relative importance when the Terro model or the Schneider model are applied.

From a modelling perspective, the transient strain model that this investigation has shown to be the most effective for application to simulation of experimental conditions is the Nielsen model. It is the model that produces the lowest mean relative error when calibrated to individual data sets and is very nearly the most accurate

[21] As the Bažant model cannot be reliably treated using the PPI program, no error measure is calculated.

model when calibrated to all the data sets here considered. The procedure of application of the model is straightforward, with parameters that play clear roles with regard to definition of the transient strain development due to increasing temperature.

Use of the Anderberg model can be a very simple and effective technique to predict transient strain development in heated concrete specimens. Accurate solutions can be found and application of the model is found to be very simple. However, the model appears to be accurate only in the modified form applied here and the robustness of the model for applying to different concretes must be investigated to determine whether the value of the first coupling constant can be predicted in advance of tests.

It is very difficult to calibrate the parameters of the Terro model with confidence as there appears to be no unique 'best' set of parameter values. However, if the model can be applied in conditions in which it is unnecessary to calibrate the parameters, the Terro model, here modified to utilise the reduced temperature variable, represents an accurate and reliable method to account for transient strain.

The Schneider model, though formulated in a manner that is appealing due to the apparent link with a chemo-thermal source of transient strain identified in this work, is found to produce total strain results that are relatively inaccurate in comparison to the simpler transient strain models. Moreover, it is found to be extremely difficult to calibrate the model parameters to experimental data.

Based on the results found here, the final model here investigated, the Bažant model, appears to be fundamentally incapable of reproducing the experimental results in the present form. It seems that this conclusion can be firmly made even in the absence of a suitable method, such as that of the PPI program, to generate values of the model parameters that reproduce the error measure between model results and experimental data.

6.4.7 *The load-dependence*

Transient strain is almost always considered to be linearly related to applied load. While this practice is supported by most experimental evidence, some results suggest

that the load-dependence is slightly altered for low and high levels of applied load [19]. Thus, some small deviation from linearity may be present in experimental results.

In order to determine if deviation of the transient strain model from linear load-dependence occurs, the IFT can be applied to the experimental data sets with several different assumed forms of load-dependence. Due to the low number of data sets at unique load levels and the necessary small deviation from the standard linear model, it is preferable to define simple load-dependent functions with only one free parameter, as defined in Equations 6-22 (a)–(e).

$$g_1 = \frac{\sigma}{f_c} + k_1 \quad \text{(a)}$$

$$g_2 = -\left(\frac{\sigma}{f_c}\right)^2 + k_2 \quad \text{(b)}$$

$$g_3 = -\left|\frac{\sigma}{f_c}\right|^{k_3} \quad \text{(c)} \qquad \text{Equation 6-22}$$

$$g_4 = -\left(\frac{\sigma}{f_c}\right)^2 + k_4\left(\frac{\sigma}{f_c}\right) \quad \text{(d)}$$

$$g_5 = -k_5\left(\frac{\sigma}{f_c}\right)^2 + \left(\frac{\sigma}{f_c}\right) \quad \text{(e)}$$

where k_1, k_2, k_3, k_4, and k_5 are the free parameters of each of the load-dependent functions.

Using Equations 6-22 (a)–(e) to define load-dependence, the Nielsen model can be modified in order to allow an investigation of the load-dependence suggested by the experimental data to be performed, as shown in Equation 6-23 for the uniaxial case.

$$\varepsilon_{tr} = \begin{cases} \dfrac{(A\theta^2 + B\theta)}{f_c(T_0)} g_i(\sigma), & \theta \le \theta^* \\ \dfrac{[C(\theta - \theta^*)^2 + A\theta^*(2\theta - \theta^*) + B\theta]}{f_c(T_0)} g_i(\sigma), & \theta > \theta^* \end{cases}, i = 1, \ldots, 5 \qquad \text{Equation 6-23}$$

Using the IFT, the free parameters of the five transient strain models of Equation 6-23 may be calibrated to the experimental data. This process allows the load-dependence suggested by the experimental results to be examined. This methodology is applied to only one transient strain model as the nature of the transient strain model is not

expected to be important to the general outcomes of such an investigation; the Nielsen model is chosen for the reasons given in §4.11.

It should be noted that additional parametric degrees of freedom (where a certain combination of values of all additional parameters can remove any influence of the additional parameters) must necessarily either increase model performance or have no effect. Therefore, in order for the results to be considered to reveal that the experimental results suggest that use of any of the load-dependent functions of Equations 6-22 (a)–(e) is more appropriate than the default function, a significant improvement in performance is required.

It is difficult to determine the appropriate improvement necessary to justify the addition of a free parameter to a model. It depends, to a large extent, on the performance of the model with a fixed parametric value relative to that of the model with a free value. For instance, in the results of figures 6-11 (a)–(d), the effect of use of different values of the transition temperature parameter to the Nielsen model are shown. It can be seen that the minimum error measures found for each value of the transition temperature parameter vary over a fairly wide range for each data set, e.g. for the AT225 data set (figure 6-11 (a)), the difference in error measures between minimum and maximum values within the graph are approximately 75% of the minimum value.

Table 6-14: The values of the free parameters of the load-dependent functions applied to the data sets using the IFT.

Parameter	Minimum value	Maximum value	Incremental value
k_1	-0.10	0.10	0.02
k_2	-0.27	-0.15	0.01
k_3	0.75	1.35	0.06
k_4	0.36	0.48	0.01
k_5	-0.24	0.24	0.04

As it is recognised that deviation from linearity must be relatively small, the range of parameters over which the IFT is applied are chosen such that the output of the function deviates from the default output by no more than a threshold parameter, chosen here to be 10%, for any of the applied load levels of the experimental data

sets. Thus, the values of the free parameters of Equations 6-22 (a)–(e) shown in table 6-14 are applied to the data sets using the IFT.

The results show that improvements are obtained in overall model performance for all load functions of Equations 6-22 (a)–(e), except Equation 6-22 (b). This is consistent with the aforementioned principle that additional degrees of freedom always lead to an improved performance because this function cannot reproduce the output of the default model for any values of the free parameter g_2. Similarly, the function defined by Equation 6-22 (d) cannot reproduce the default output; despite this, an improvement in performance is obtained using this function.

The functions, applied using the free parameter values found to most closely reproduce the experimental data sets, are shown in figure 6-27, along with the default function. As it can be seen, the functions deviate from the default output by only a small margin within the loading range of the experimental data sets, a condition explicitly imposed by the free parameter values applied.

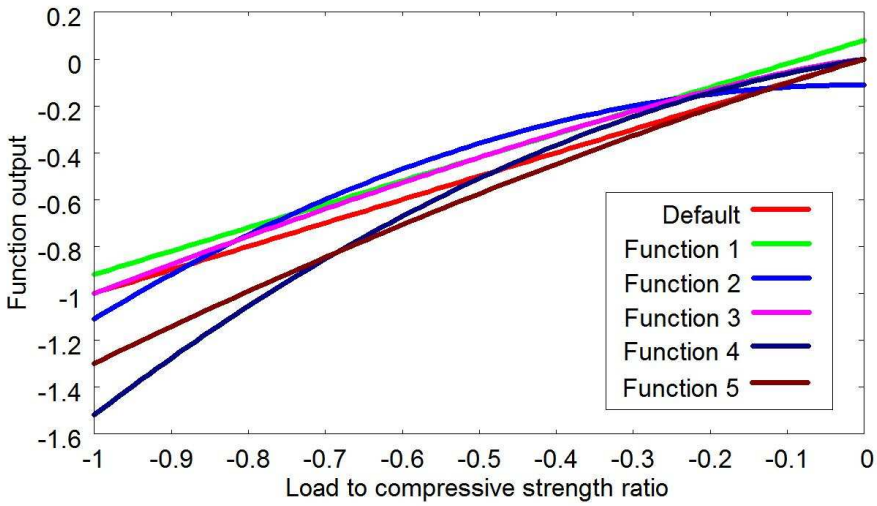

Figure 6-27: Comparison of the load-dependent functions found to best describe the experimental data sets using the IFT applied to the data sets and Equations 6-22 (a)–(e).

The overall error measures, relative to the default value, for the various functions of figure 6-27 are shown in table 6-15, along with the values of the free parameters found to produce these values. It can be seen that function g_1 improves model performance by the largest quantity.

Table 6-15: The parameters of the loading functions found to produce the lowest overall error using the IFT.

Function	Best parameter[22] (k_i)	Overall error relative to that of default
g_1	0.08	83.5%
g_2	−0.11	118.8%
g_3	1.25	84.7%
g_4	0.52	92.9%
g_5	0.30	95.3%

As shown in the values of table 6-15, the improvements in the overall error measure for each of the loading functions is relatively modest. However, as experimental results consistently show that the default loading function is a fairly good description of the load-dependence of the transient strain component, a large improvement in performance should not be expected.

It is of interest that inspection of figure 6-27 shows that the two functions that produce the lowest overall error measure, as shown in table 6-15, g_1 and g_3, are almost identical for the range of loads associated with the experimental data sets. This may explain the similar error measures associated with the two functions. Thus, the two model descriptions can be considered to be quasi-equivalent to one another. However, the function g_3 produces reasonable predictions of zero transient strain development for no applied load. Thus, as it is likely to be valid over a wider range of applied load levels, this function may be considered to be preferred by this method. Application of g_1 would probably require modification for low load levels to ensure that these predictions are removed.

As the number of experimental data sets on which these results are obtained is low, the findings here reported should be considered to be preliminary. However, these results appear to suggest that a modest improvement in model performance can be achieved using a modified loading function. Although these loading functions shall not be adopted for remaining simulations, further work should focus on widening the

[22] It may be noted that two of the parametric values lie outside of the range of allowed values, as defined in table 6-14. This is a result of the procedure in which if an iteration of the IFT suggests that the best parameter is equal to the maximum or minimum value applied, the limits are changed and the iteration repeated.

scope of this investigation to examine the deviation from linearity that may be suggested by these results.

Chapter 7. Structural case studies

In chapter 6, five transient strain models were subjected to an objective quantitative investigation. This allowed the performances of the models to be objectively assessed with respect to experimental data sets. In this chapter, the three transient strain models[23] found to most effectively reproduce experimental results are applied to realistic examples of concrete structures that are subjected to high temperature conditions. These conditions are a rapidly heated ($5℃/min$) restrained concrete beam (both under no preload and preloaded), a column of concrete subject to fire conditions, and a nuclear reactor pressure vessel (NPV) in service conditions.

The values of the transient strain model parameters are based on those found using the IFT (§6.1.1) for the experimental set up used by Anderberg and Thelandersson [1]. While a basic creep model (§6.3.2) and a load-dependent thermal damage model (§6.3.3) were applied in chapter 6, the model assumptions defined in chapter 3 are applied in this chapter. Thus, no basic creep model is assumed and thermal damage is governed by the thermal damage parameter defined by Equation 3-27. The former assumption is assumed in order to simplify interpretation of results, while the latter assumption is assumed as the preload-dependent thermal damage model must be developed further for application to general loading conditions (though, for comparison, results of implementation of this model are shown in §7.1).

It should be noted that, consistent with the evidence of chapter 6, the TTS0 assumption (Equation 5-5 (a)) is assumed for the simulations. However, no tensile stresses should develop in the restrained beam simulations, while it is likely that tensile stresses develop in the NPV simulations only during cooling. Thus, direct TTS effects should be absent for these sets of simulations. However, previous results (such as §5.2) have consistently shown that TTS effects tend to develop when unloaded specimens are heated rapidly. Therefore, it is possible that the particular TTS assumption applied shall affect the simulations considerably. The simulations are repeated for each TTS assumption (defined in Equations 5-5 (a)–(c)) using the Nielsen model.

[23] For perspective on the magnitude of any differences in results found to occur for different transient strain models, each of the example sets of conditions are also run without an active transient strain model.

7.1 Restrained beam

Three separate sets of slightly varied heating and loading conditions are applied to a concrete beam here. In the first set of conditions, the specimen is heated at $5℃/min$ to $800℃$ in conditions of full axial restraint. In the second set of conditions, identical conditions are applied with the addition of an initial applied prestress equal to 30% of the compressive strength in the axial direction.

It should be noted that, due to the application of certain simplifying assumptions, FE modelling is not strictly necessary for the simulation of these experimental conditions. The motivation for application of this technique is the convenience associated with consistency with the modelling practice applied throughout the rest of this work.

In terms of the mesh used for FE modelling, the plane stress condition is invoked, as is standard for beams. For similar reasons, temperature change is assumed to occur homogeneously throughout the mesh. Therefore, temperature throughout the mesh is prescribed (rather than through use of flux elements).

As a consequence of the simple conditions of the analysis, there are no temperature gradients across the specimen, so a fairly coarse mesh can be used to describe the beam problem. Specifically, a mesh composed of nine eight-noded serendipity elements, shown in figure 7-1, is applied.

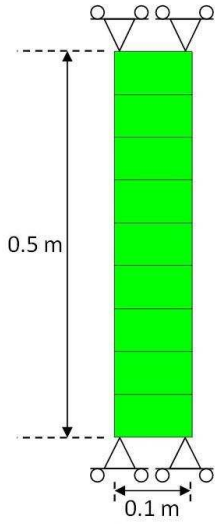

Figure 7-1: FE mesh used to simulate the heated restrained concrete beams (plane stress).

The observable of interest in this test is the axial stress evolution. This simulation has previously been performed by Pearce et al. [2]. Following a similar procedure, the thermal strain model applied to the problem is given by the value-limited logarithmic temperature function fitted to the results of a quartzite concrete, as shown in figure 7-2 and defined by Equations 3-32 and 3-33.

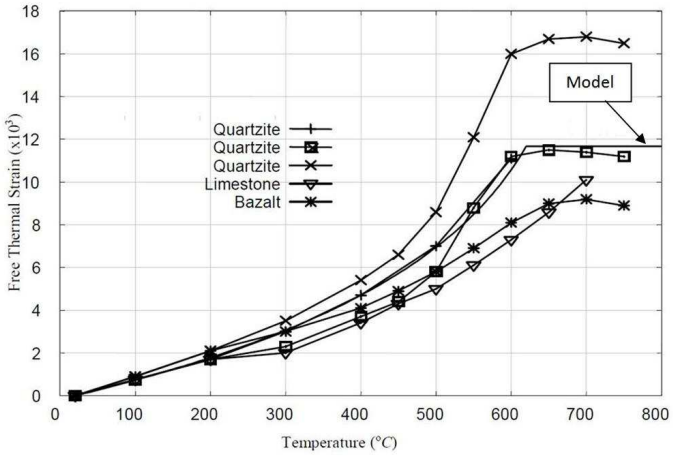

Figure 7-2: Thermal strain data for various concrete types and the derived thermal strain model applied to the beam specimens (modified to indicate the model curve) [2].

As the thermal strain component is of leading order importance to the axial stress development in the beam elements in this example, the thermal strain model is a critical consideration to the results. It should be noted that, though experimental data that show the axial stress evolution are available, similar data that indicate the thermal strain behaviour of the beam are unavailable. Assuming that the thermal strain model shown in figure 7-2 is applicable and, using the Nielsen model for transient strain, Pearce et al. [2] obtained the results shown in figure 7-3.

As can be seen in figure 7-3, the development of transient strain is extremely important in this example. Without transient strain, it can be seen that the axial stress in the column would lead to complete failure at a temperature of around $350℃$. Thus, the application of the Nielsen model is significant appears to broadly match the qualitative development of stress suggested in the experimental data fairly well particularly for temperatures larger than $470℃$. However, it can be seen that an underestimation of the magnitude of stress development is consistently made for both loading cases.

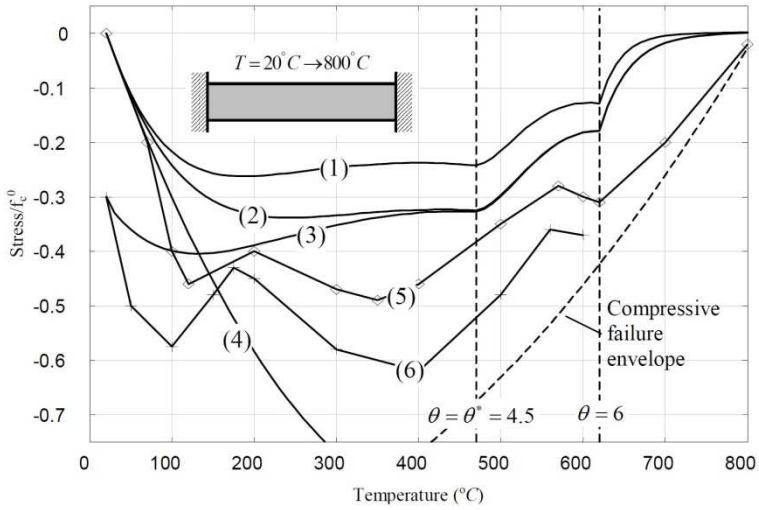

Figure 7-3: Axial stress evolution obtained by Pearce et al. [2], using (1) the Nielsen model with a lower bound set of parameter values (no preload), (2) the Nielsen model with an upper bound set of parameter values (no preload), (3) the Nielsen model with an upper bound set of parameter values (preloaded), (4) no transient strain model (no preload), and experimental data obtained for (5) specimens with no preload [3] and (6) preloaded specimens [4].

Results obtained here using the Nielsen model are shown in figure 7-4 (a). Though any quantitative improvement in the results in comparison to the results of figure 7-3 is relatively small, an improved qualitative agreement can be found. For both sets of preloading conditions, a local maximum in compressive stress magnitude is found in the model results produced here at a temperature between about $350℃$ and $400℃$. This coincides well with local maxima found in the experimental results for each of the loading conditions. Conversely, the local maxima (that are also significantly shallower) for the results of fig 7-3 occur at a temperature of around $470℃$. Indeed, it is not obvious from figure 7-3 that the maxima of the experimental data and the model results are of the same origin, likely to be the increased magnitude of $\frac{\partial \varepsilon_{tr}}{\partial T}$ in the high temperature region. This suggests that these experimental results support the use of a Nielsen model transition temperature of around $370℃$, suggested by the results of chapter 6 (rather than the original value of $470℃$ [2]).

A further indication that use of the Nielsen model parameters found in this work using the IFT may be more appropriate for these experimental data than the original values is the local maximum in axial stress encountered at a temperature of around $620℃$, clearly visible in both sets of experimental data sets. The results of figure 7-4 (a) reproduce the qualitative behaviour more closely than those of figure 7-3. Although the cause of the local maximum is principally the transition in thermal strain behaviour

in this temperature range, not a transition in transient strain behaviour, the transient strain model is found to play an important role in the definition of the shape of the curve in this region.

In contrast, results of application of the Anderberg model, shown in figure 7-4 (b), are found to behave qualitatively very poorly in comparison to the experimental data. These results appear to suggest that an approximately constant stress level is established in the temperature range $300 - 600℃$, despite the nonlinearity of thermal strain in this range. As this behaviour does not agree with the experimental data, it appears that these results do not support the use of the Anderberg model as a description of the transient strain behaviour.

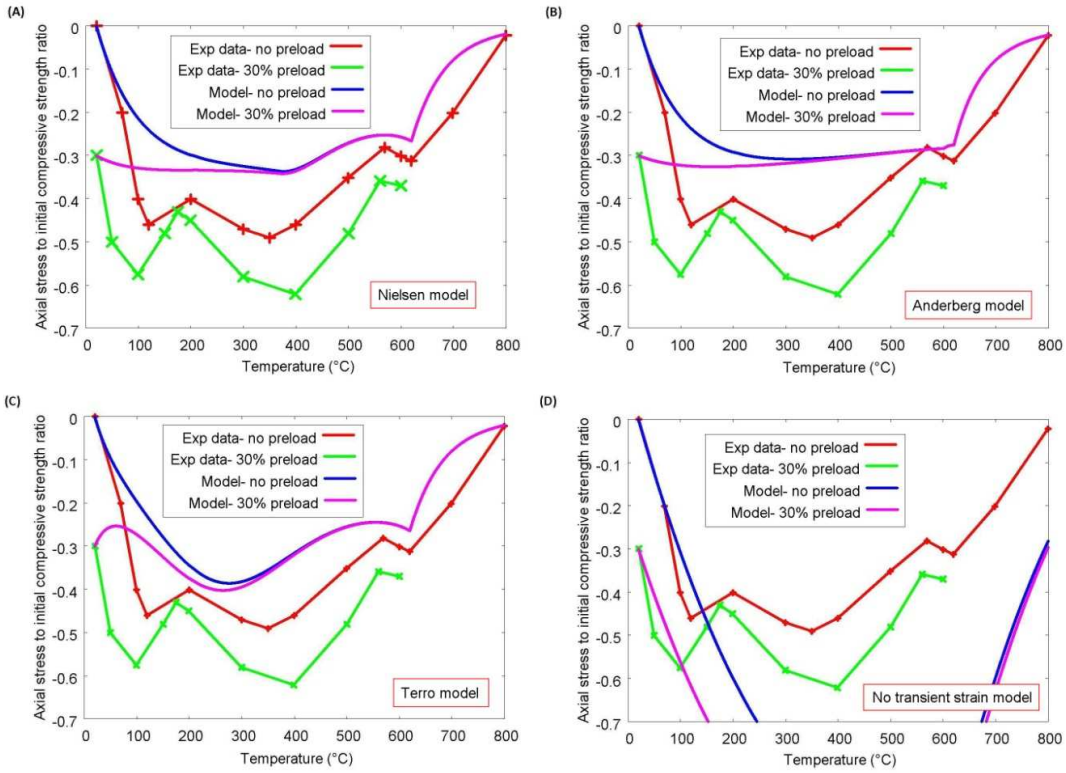

Figure 7-4: Comparison of the experimental results for the heated concrete beam in both unloaded and preloaded conditions and model results for (a) the Nielsen model, (b) the Anderberg model, (c) the Terro model, and (d) no transient strain model.

Results of application of the Terro model, shown in figure 7-4 (c), reproduce the qualitative behaviour of the experimental results to a similar level as the Nielsen model. The local maximum in experimental axial stress at about $350℃$ is found to occur at a temperature of around $250℃$. This is a considerable temperature when compared to the results of use of the Nielsen model. However, the larger peak

associated with the Terro model is more similar to that found in the experimental results.

As shown in figure 7-4 (d), the results of application of no transient strain model demonstrate that transient strain is critical to the stress development in the concrete beams. The maxima in axial stress found to develop are of the order of the initial compressive strength of the material, far larger than those found in the experimental data.

It is worthy of note that the experimental stress values are found to be larger than those of the simulated results for temperatures less than about $100℃$ in figure 7-4 (d). As transient strain, active as a relaxing agent in the experimental test, is omitted from model calculations, axial stress should consistently be of a greater magnitude in the simulated results than in the experimental results. This may be a strong suggestion that the magnitude of applied thermal strain model is inadequate in this temperature range[24]. This may partially explain the reduced magnitude of axial stress development in the model results in comparison to the experimental data observed over the full temperature range for all transient strain models.

There are three points to consider regarding the application of a thermal strain model based on the results of figure 7-2 to these examples. Firstly, the thermal strain model most appropriate for the concrete of the beams may be more similar to the curve associated with the more expansive quartzite concrete of figure 7-2. Results obtained using a model calibrated to this curve show that an improvement in the magnitude of stress development is obtained with this thermal strain curve. However, significant differences continue to exist.

Secondly, it was demonstrated in chapter 5 that, accounting for transient strain, the thermal strain curve necessary to reproduce the results of tests on unloaded heated concrete specimens may be different to that obtained from simple curve fitting of the thermal strain model. Thus, as the TTS0 assumption is applied here, 'true' thermal

[24] Another potential cause of the increased stress values in the experimental results is that the thermal damage formulation applied is unrealistically large in this temperature range. However, the difference in stress in this temperature range directly caused by thermal damage is roughly 15%. As some degradation of elastic modulus is likely to occur, the deviation from this relatively low value is unlikely to be significant. Therefore, thermal damage is unlikely to be the source of the disagreement in the results.

strain may be larger than that of figure 7-2 due to the net negative component of transient strain that also develops due to thermal stresses. However, deviation caused by this effect is mostly found to develop in the high temperature range, so modification of the thermal strain model based on this effect is unlikely to lead to a vastly improved model.

Finally, it is assumed that the thermal strain behaviour of a heated cylinder is the same as that of a heated beam. Depending on the specific dimensions of the examples, there may be significant differences in behaviour due to the different rates of drying of the specimens, likely to be particularly significant in the low temperature range.

Results for the preloaded restrained specimen clearly indicate that the stress in the specimen strongly increases due to initial heating. None of the simulated results in which a transient strain model is applied reproduce this behaviour to any significant degree. Furthermore, the simulated results consistently show that the axial stress curves of preloaded specimens converge to that of the unloaded specimens at a temperature of around $350℃$, behaviour that is not reproduced in the experimental results.

This disagreement is very likely to be a result of the identical thermal strain models applied for both examples, a condition that is unlikely to be true of the two materials used[25]. Based on the results of figure 7-4 (d), it appears that thermal strain should be of a larger magnitude than that used in the simulations in the low temperature range. It is also possible that application of a thermal damage model that accounts for the effects of preload would allow the results of each to remain distinct throughout. However, the unloaded specimen is essentially preloaded for most of the period of heating due to the restraint. Hence, with identical thermal strain formulations, very similar thermal damage should develop in each of the specimens, even if preload is considered.

It should be noted, however, that modification of the thermal strain model affects the simulated results when the Nielsen model and Terro model are applied, the effects on the Anderberg model are comparatively very small. It is found that the results of the

[25] The experimental data sets are derived from separate sources.

Anderberg model are relatively indifferent to the magnitude of the thermal strain model, with similar results to those of figure 7-4 (b) consistently found.

In order to allow independent modification of the results, the Anderberg model must be modified in a manner such as that suggested previously (Equation 4-19), where the temperature-dependence of transient strain is identical to that of thermal strain but the absolute magnitude of transient strain that develops is independent of the magnitude of thermal strain (at a reference temperature). Alternatively, the coupling coefficient may be considered to be material-dependent (as is implied by the original authors [1]).

The experimental results suggest that there should be a local maximum in stress at a temperature of around $100℃$. This may be caused by a reduction in the apparent coefficient of thermal strain in this temperature region caused by rapid drying, an effect not reproduced by the present thermal strain model (which is based on thermal strain of heated cylinders). Another potential reason is a finite rate of transient strain development for temperatures below about $100℃$, as suggested by some experimental work (see §2.1.2). Thus, the combination of a weaker thermal strain development and a stronger transient strain development in the temperature range around $100℃$, which are not reproduced in the models, may be the cause of the local maximum.

As was previously mentioned, the unloaded specimen is essentially preloaded for the entire temperature range. Therefore, it may be appropriate and more accurate to simulate the axial stress evolution using a thermal damage formulation based on preloaded specimens, such as that of Equation 6-6. The results of such a modification are shown in figures 7-5 (a)–(d).

Although the Anderberg model continues to produce qualitatively poor results, a clear general improvement in the performance of the simulated results is found for the other transient strain models, as shown in figures 7-5 (a)–(c), particularly for the unloaded specimens. As already stated, it appears to be very likely that a stronger thermal strain formulation is required for the preloaded specimens to more accurately reproduce the experimental results, particularly for the preloaded specimen.

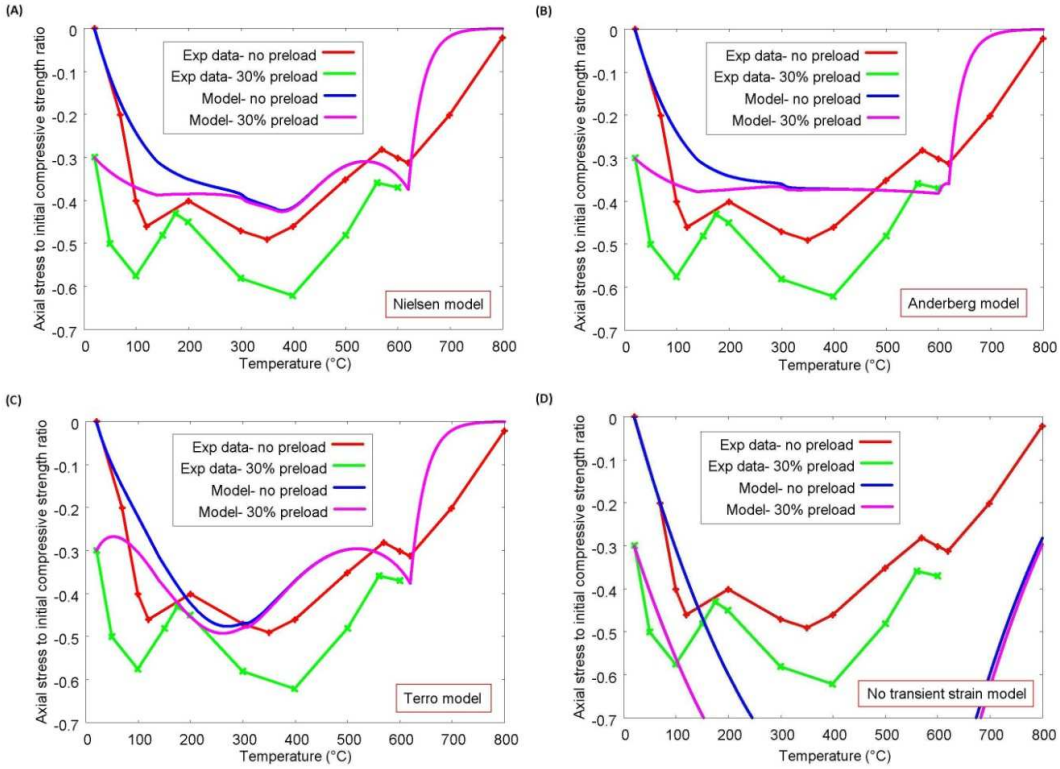

Figure 7-5: Comparison of the experimental results for the heated concrete beam in both unloaded and preloaded conditions and model results, using a thermal damage model that accounts for preload, for (a) the Nielsen model, (b) the Anderberg model, (c) the Terro model, and (d) no transient strain model.

The stress behaviour in the temperature range above 600°C undergoes more rapid relaxation in the simulations of figure 7-5 (a)–(c) in comparison to the experimental data, whereas the behaviour found using the original thermal damage model (figure 7-4 (a)–(c)) appears to be more appropriate. This suggests that, while an overall improvement is found using the thermal damage model of Equation 6-11, further work is required to establish the most appropriate form of this model for use in these simulations. However, of higher order importance are the thermal strain models.

7.2 Column in fire conditions

This set of conditions simulates a concrete column placed in fire conditions. The column is considered to be square in prismatic dimension of width $0.4\ m$, and of considerably greater height. Therefore, the standard plane strain condition is applied to the FE mesh.

The ISO fire curve is used to simulate the external temperature conditions, with flux elements used to simulate the resultant heating. This heating regime, as shown in

figure 7-6 (a), is characterised by a rapid initial period of heating with a diminishing, though consistently substantial, rate of temperature increase throughout the test.

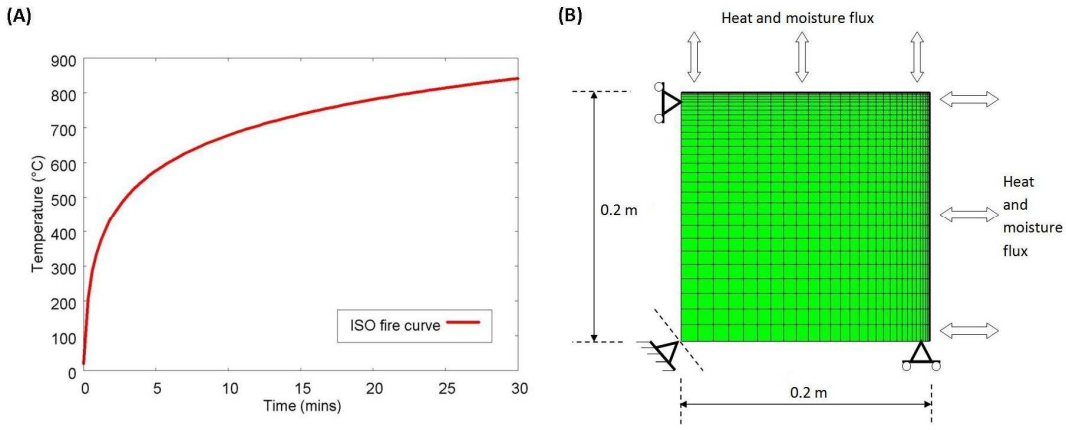

Figure 7-6: (a) The ISO fire curve, as applied to the concrete cylinder in the numerical simulation and (b) FE mesh used (plane strain).

In order to simulate these conditions, a FE mesh is applied containing 900 eight-noded serendipity elements, with a non-uniform discretisation as, reproduced in figure 7-6 (b). This is found to increase model stability significantly.

Application of the model to the column in fire is characterised by a rapid temperature increase of the outer material with relatively little increase in the internal temperature within the timeframe of interest. Due to the resulting differences in thermal expansion across the mesh, the outer material is partially restrained by neighbouring material. This results in a state of compression in the regions near to the outer surfaces, with a general state of tension throughout the remaining area of the mesh, as shown in figures 7-7 (a)–(c).

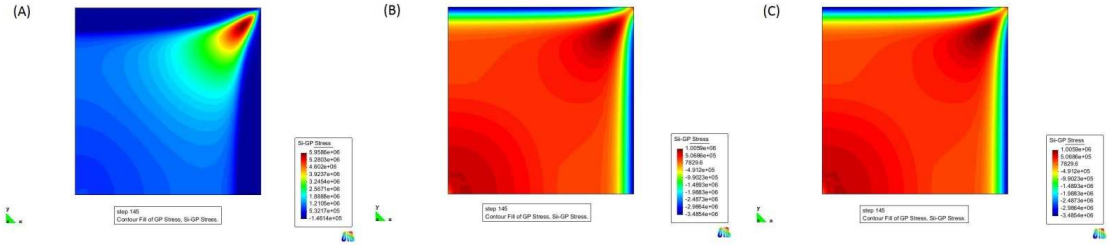

Figure 7-7: Profiles of the (a) first, (b) second, and (c) third principal stress components in the column cross section five seconds prior to the initiation of mechanical damage in the region of the upper right hand corner (Nielsen model).

A particular concentration of tensile stresses develops in the region of the corner of the mesh where the two outer surfaces meet, as can be seen in figures 7-7 (a)–(c). After a time, the magnitude of the tensile stresses in this region become large enough

to lead to a localised zone of high values of mechanical damage. This damaged zone, which can be interpreted as a crack, spreads moderately rapidly orthogonal to the diagonal connecting the centre of the column cross section with the outer corner. After a short time, the crack ceases to grow in size and reaches a stable configuration, which is shown in figure 7-8 (a).

The crack appears to effectively decouple the two regions of the mesh that it separates, due to the inefficiency of stress transfer across the heavily damaged region. Thus, the corner region, which is also the location of the most rapid temperature increase, undergoes subsequent increases in stress magnitudes and significant mechanical damage. The development of damage in this manner may be one of the causes of thermal spalling in rapidly heated concrete. Therefore, it is possible that, in practice, sections of the cross section would be ejected from the column at this point. This would modify the subsequent evolution of the hygro-thermo-mechanical state of the concrete body significantly. However, the current model cannot simulate this type of behaviour, so it is here assumed that no such process occurs.

A short time later, a second major region of localised damage develops in the mesh parallel to the initial crack, as shown in figure 7-8 (b). This region, which can also be considered to be a crack, develops rapidly in a similar manner to the previous crack.

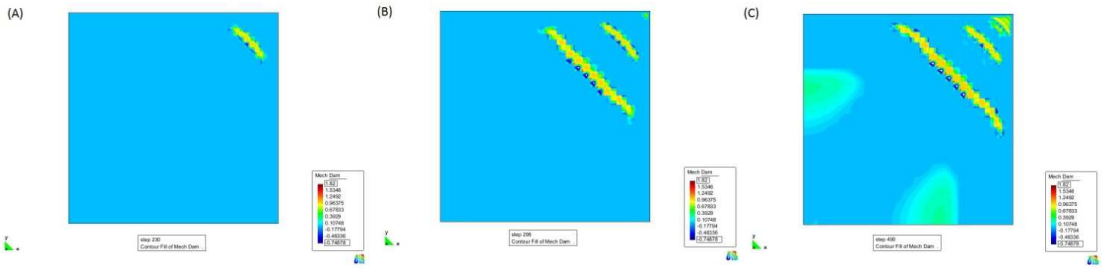

Figure 7-8: Profile of mechanical damage in the column cross section after (a) 230 seconds, (b) 295 seconds, and (c) 490 seconds of exposure to fire conditions (Nielsen model).

In the period following the formation of the second major crack, stresses induced by heating continue to build in the mesh. However, the decoupling effects of the cracks restrict interaction between these stresses induced by the expansion of the heated outer surfaces. As a result, the diagonal that bisects these two surfaces (i.e. the diagonal from the centre to the outer corner) is not the region in which mechanical damage is initiated as with all previous damage. Instead, two regions of relatively low

magnitude mechanical damage develop on the inner surfaces at a point that is at least midway between the centre of the cross section and the outer edge, as shown in figure 7-8 (c). This damage is spread over a relatively wide area and remains of a low value. The model fails to run beyond this point for all simulations except that using the Anderberg model. In this simulation, the two damaged regions are found to spread gradually towards the central region. When the damaged zones combine, the overlapping region becomes the most damaged.

Results of the simulations show that applications of a transient strain model increases the time at which any mechanical damage develops in the mesh. Whereas a characteristic time of roughly 150 seconds of fire conditions passes before the initial crack is initiated when any of the transient strain models are applied, this time is approximately 130 seconds for simulations in which no transient strain model is active. Similarly, approximately 240 seconds pass before mechanical damage develops in the corner region for simulations in which a transient strain model is applied, whereas a time of approximately 210 seconds is found for simulations in which no transient strain model is active[26].

Simulation of identical conditions using the Nielsen model and the TTS1 assumption produces similar development of damage over the mesh, though the periods of time that elapse before the first and second major cracks appear are increased to 155 seconds and 280 seconds respectively. Similarly, use of the TTS2 assumption leads to increased periods of time at which these major cracks appear. The first crack appears after 185 seconds of heating, with 405 seconds of heating found to elapse before the second major crack appears. The second major crack appears in a slightly different location within the cross section, as can be seen in comparison of figures 7-9 (a) and (b).

Thus, the results suggest that the action of transient strain has a fairly large effect on the capacity of the concrete columns to be subjected to fire conditions without development of mechanical damage. Moreover, although the nature of the transient

[26] No further comparisons can be made as the simulations in which no transient strain model is applied fail to run beyond 260 seconds. It is reasonable to expect that the damage mechanism that would lead to the second major crack would initiate at around this time as the time is consistent with the previous comparisons with the other simulations.

strain model appears to be of low order importance in this respect, the nature of the response of the transient strain model to tensile states of loading is very important in terms of the duration of time before mechanical damage develops and potentially in the location of the centres of damage (which may be a particularly important consideration for design purposes).

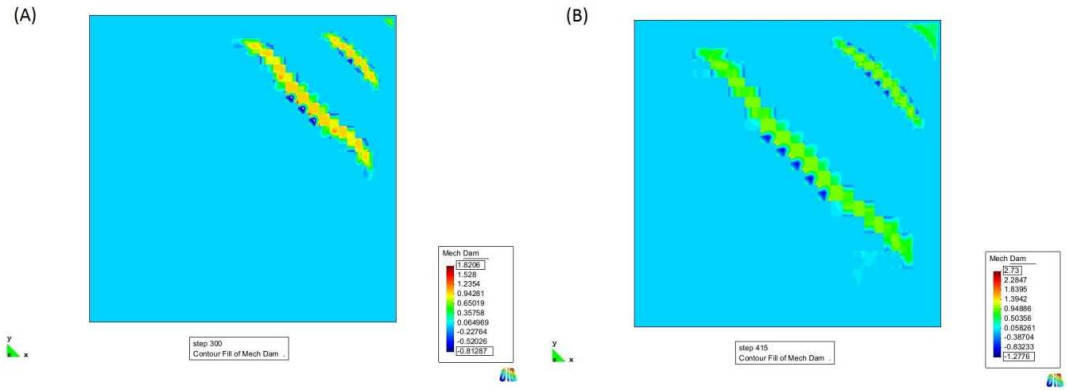

Figure 7-9: The mechanical damage profile for the column in fire conditions (a) after 300 seconds of heating (Nielsen model and TTS1) and (b) after 415 seconds of heating (Nielsen model and TTS2).

The geometry of the mesh is highly likely to contribute to the configurations of the cracks that develop in the mesh. As has been noted, the interaction of the two stress fields induced by the perpendicular expanding surfaces (equal in magnitude and orthogonal in direction of application) is important in the development of mechanical damage. In effect, the location of superposition of these stress fields 'seeds' the location at which mechanical damage occurs. Therefore, if the mesh is of an overall shape that does not allow this superposition to occur at a single location, such as a circular cross section, the distinct cracking behaviour should not be observed to develop. Indeed, simulations of cylindrical column cross sections performed here (results not shown) suggest that damage does not develop in localised cracks as found for the geometry of 7-6 (b).

7.3 Nuclear reactor pressure vessel in service conditions

In this section, the hygro-thermomechanical state of a nuclear pressure vessel (NPV) subject to service conditions is simulated using each of the three transient strain models. The NPV considered here, though of an irregular shape, is $35.585\ m$ in height and $30.328\ m$ in diameter. The contained area, cylindrical in shape, is $19.691\ m$ in height and $18.898\ m$ in diameter, as shown in figure 7-10.

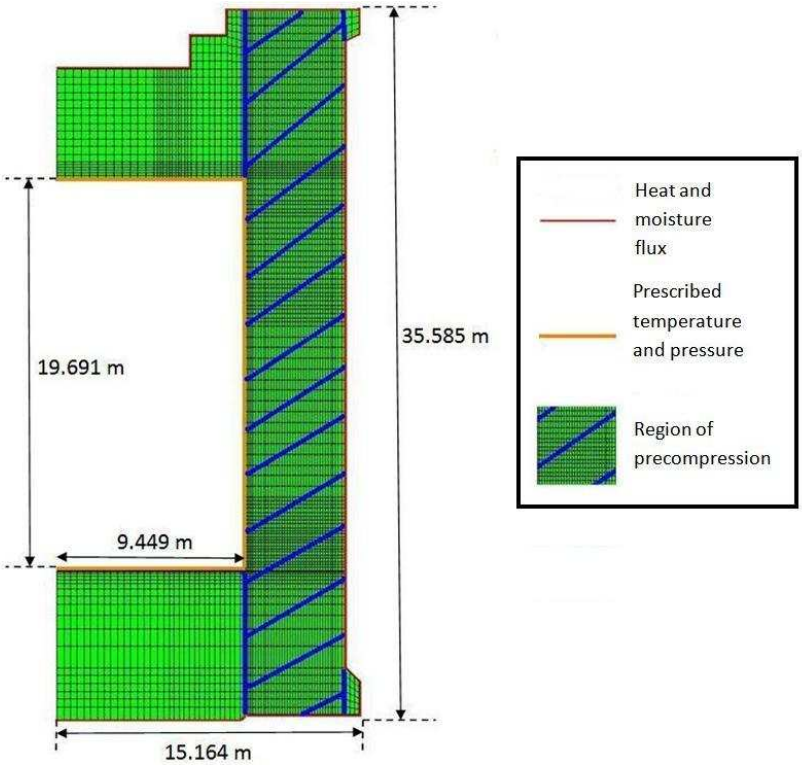

Figure 7-10: The FE mesh used for numerical modelling of NPV in service conditions.

The specific temperature and loading conditions applied to the structure are somewhat complex and based on empirical measurements [5]. In order to increase the capacity of the structure to sustain tensile deformation, radial and axial tendons are present in the material column, identified in figure 7-10, which provide precompression to the structure. It should be noted that the region of precompression within the structure is likely to be more diffuse in practice than it appears in figure 7-10. Due to basic creep, the stress in these tendons reduces with time. This is explicitly simulated in the model using an empirical time function for the prescribed nodal forces within this region of the mesh. Similarly, the temperature and internal pressure applied to the inner surface of the NPV due to regular nuclear reactor operation are prescribed to the nodes in this region using empirical time functions. Two temperature cycles are simulated in which the contents of the NPV is linearly heated to (and subsequently cooled from) a maximum temperature of $85℃$ (temperature change occurs over the course of approximately 100 days) and held at temperature for a period of 400 days. As an initial period of 201 days in ambient conditions is simulated, the length of time of the simulation is 1401 days.

Due to the large mass of the structure, it is not appropriate to consider the surface on which the structure rests to be infinitely stiff. Instead, the boundary restraint on the lower edge of the mesh is modelled as elastic. This allows deformations of this surface to occur in an axial direction, despite the resistance provided by the ground.

To account for realistic heat transfer, the temperature increase of the concrete material in contact with the heating agent is position-dependent, as demonstrated in figure 7-11, which shows the temperature profile across the mesh at the peak temperature in the cycle. It may be noted that, due to heat transfer between the NPV and the external atmosphere (imposed on the FE mesh using flux elements, as indicated in figure 7-10), the temperature of a large portion of the mesh does not significantly increase in temperature, despite the relatively high temperature of the contents of the pressure vessel. Thus, stationary temperature gradients are characteristic of the NPV during operation.

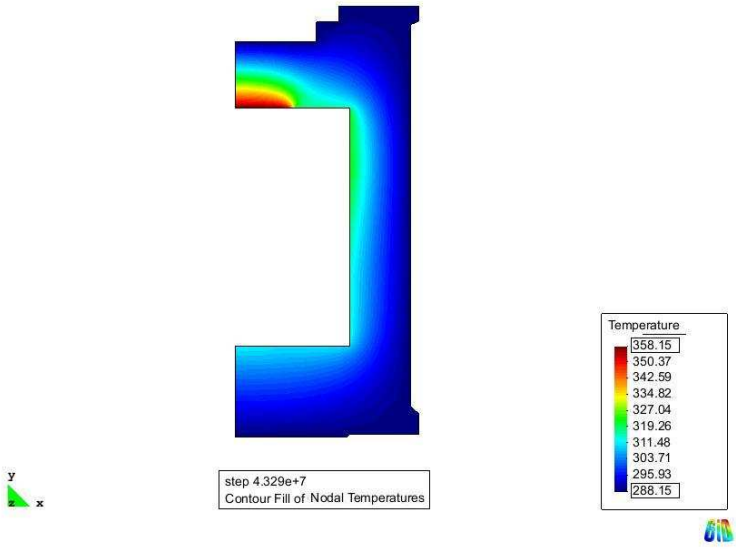

Figure 7-11: The stationary temperature profile at the peak operating temperature of the service conditions.

Results show that the specific transient strain model applied plays a relatively minor role in the thermomechanical state of the NPV in service conditions. As each of the models is active during the first heating cycle only, transient strain develops only within this short time period. Moreover, as the heating is very slow, the development of thermal stresses during heating is negligible. Although effects of the transient strain model may be expected to propagate throughout the test, very little difference is

found for the simulations applying different models, in terms of the complex stress and strain profiles that develop throughout the simulations.

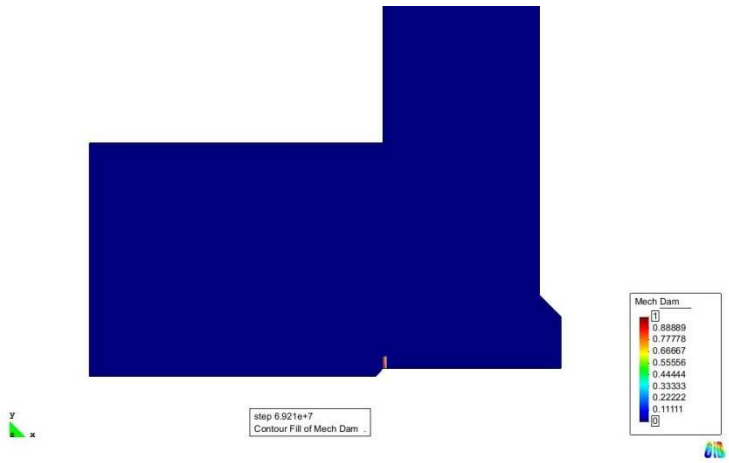

Figure 7-12: The profile of mechanical damage that develops in the NPV in the absence of the transient strain development after the first period of cooling is complete.

That transient strain is a significant strain component is clear from results of simulations performed with no active transient strain model. A localised region of total mechanical damage is found to develop in the base of the structure due to local bending caused by the specific deformation of the structure after the first period of cooling is complete, as shown in figure 7-12.

It may be noted that no basic creep model is explicitly applied in the simulation of the nuclear pressure vessel simulation (though the prescribed preload is explicitly defined to relax due to creep). As the time scale over which the simulation takes place is relatively large and the magnitude of temperature increase is relatively low, the assumption that basic creep can be ignored may be of questionable validity. However, it is unclear if the action of a basic creep model would lead to significant effects beyond the relaxation of precompression.

Moreover, the possibility that transient strain may develop in conditions of non-virgin heating, as suggested by some experimental results [6], may be considered to potentially significantly modify these results. Two possible scenarios were identified in the review of the literature as those in which transient strain may re-develop in non-virgin heating conditions: a second heat cycle that occurs after a significant period of time following the first heat cycle and a second heating period for which the time spent at high temperature during the first cooling cycle was relatively short. The NPV

service conditions may satisfy the first condition. Thus, it may be appropriate to consider transient strain to develop during the second heating period, which may have an effect on the development of stresses within the NPV.

Therefore, further work in the areas of basic creep modelling and the physical origins of transient strain may be useful to increase the reliability of simulations of the NPV in service conditions. It appears that the nature of the transient strain model applied is relatively unimportant to model performance.

7.4 Final remarks

In this chapter, the three transient strain models found to result in strain behaviour most consistent with the experimental data sets considered in chapter 6 were applied in simulations of three sets of realistic conditions of concrete structures subjected to heating conditions.

The simulations of the heated restrained concrete beam were very useful due to the availability of experimental data. While a direct quantitative comparison of the model results and the experimental data would not be fair due to the uncertainty surrounding critical aspects of the strain model (particularly, the thermal strain behaviour), the data indicate qualitative behaviour that should be broadly reproduced by the simulations. In this manner, it is found in this work that the experimental data support the use of the value of the Nielsen model parameter θ^* found in chapter 6. The similarity of the peak in stress at this temperature (due to this value of θ^*) and the peak observed in the experimental data appears to support this view.

Moreover, the experimental data associated with the heated restrained concrete beam indicate that the Anderberg model provides a poor description of transient strain. Despite significant changes to model parameters, it appears that it is not possible to significantly modify the quantitative evolution of stress in simulations using this model. Thus, the poor quantitative consistency with experimental data achieved using this model appears to be unavoidable.

Considerable improvement to the results of the simulations is achieved using the preloaded thermal damage model developed in §6.3.3. Results show that, after a very short period of time, the axial load is of sufficiently large that use of a preloaded

thermal damage model may be justified. Thus, due to promising results such as these, the preload-dependent thermal damage model should be developed further in future work.

Results of simulations of a concrete column subjected to fire heating conditions demonstrate that the development of transient strain plays a significant role in preventing the onset of mechanical damage. Moreover, though the nature of the transient strain model applied in this work is found to be of low order importance, the TTS assumption applied is found to be very significant to the evolution of mechanical damage in the mesh, both in terms of the positions within the mesh at which damage develops and the periods of time that elapse from the start of heating before damage develops. Clearly, such considerations may be important for design purposes. Therefore, further research into the TTS aspect of concrete behaviour may be considered to be relevant.

Results for the simulation of the NPV in service conditions demonstrate that the nature of the transient strain model applied in the analysis is unimportant to the evolution of the overall hygro-thermo-mechanical state of the structure. Due to the low values of both heating rate and maximum temperature, very little transient strain develops in normal service conditions. However, results indicate for each model that the development of transient strain during the first heat cycle prevents the development of mechanical damage in a small region of the mesh. Clearly, this finding may be highly significant for such a structure.

Chapter 8. Conclusions and further work

8.1 Conclusions

A review of the literature suggests that, although a multitude of transient strain models exists, no objective analyses on which models perform most accurately in comparison with experimental data have been performed. Given that the physical origin of transient strain remains an active area of research interest, numerical modelling may provide some evidence for the physical nature of transient strain that can guide future investigative work. Moreover, recommendations for the most accurate transient strain models are inherently valuable as most researchers that require a transient strain model for simulations, though do not focus on the transient strain aspect of the simulations, apply the most simple model available (i.e. the Anderberg model [1]). An investigation into the performances of selected models may either support this practice or justify an adoption of other models to be used as default.

Another important aspect of transient strain research identified in a review of the literature that has not so far been considered in detail is the transient strain response to states of tension. Although experimental tests applying loading states that are in part tensile (such as tests on specimens under flexural loading) to heated CM specimens have been performed, no thorough analysis of these results has been carried out to investigate the nature of the transient strain response of concrete to states of tension. Whereas this may be justified as concrete structures are designed to avoid the application of direct tension to concrete, due to well known material weakness, local states of tension may develop in regions of heated concrete specimens, particularly those under no applied load. The magnitude of the potential relaxing effect of transient strain may be significant on the overall evolution of the mechanical performance of these specimens.

This work has been performed to attempt to address these issues objectively, chiefly using a sophisticated thermo-mechanical model for concrete behaviour implemented in a finite element environment.

8.1.1 *Analytical review of proposed transient strain models*

In chapter 4, ten currently-used transient strain models were defined in turn. Each of these models was subjected to detailed analysis and, in order to determine model behaviour not clear from published work, simple graphical investigations of model output. Through this process, in which several valuable insights were gained, the expected behaviour of the models when applied in FE analysis could be determined. Finally, based on an explicit set of evaluation criteria, the list of transient strain models for further investigation was determined.

For the transient strain model developed by Bažant et al. [2], investigations into model behaviour are particularly useful as it is difficult to determine model output without performing simulations due to the complexity of the model. It is determined here that the relative humidity evolution of the specimen is extremely important to model output. The effect of drying on the transient strain output of this model may increase transient strain by one order of magnitude (when compared to an identical non-drying specimen). Moreover, a similar increase in the period of time required for full development of transient strain is also found to be associated with this model, with a period of 30 days from the start of heating typical for drying specimens. In comparison, the effect of heating rate on transient strain development and magnitude was found to be relatively minor.

The basis for the calibration of the transient strain model proposed by Gawin et al. [3] was found by analysis to be unreliable due to the necessary derivation of a particular strain component in the results of an unloaded specimen, thermo-chemical strain. This strain component is defined by removal of free thermal strain and drying shrinkage from total strain results obtained on unloaded heated concrete specimens. However, the transient strain model is defined such that the Bishop's effective stress parameter acts to produce transient strain when thermo-chemical strain simultaneously increases. Therefore, a component of transient strain of similar magnitude to the drying shrinkage (also modelled to be a result of Bishop's effective stress) must develop in unloaded conditions.

The transient strain model proposed by Sabeur et al. [4, 5] is governed by a function that defines the equilibrium mass of dehydrated water as a function of temperature

level. It was shown in this work that this function may be well represented by a weighted sum of hyperbolic tangent functions, similar to the main temperature-dependent function of the transient strain model proposed by Schneider [6]. Thus, the physical origin for transient strain for each was inferred to be essentially the same, dehydration of cement paste.

It is difficult to determine the precise load-dependence of the transient strain model of Schneider [6], though it was shown here using simple plotting techniques that deviation of load-dependence from linearity is extremely small. Moreover, the moisture-dependence of the model, considered at first to account for drying creep, was here shown to be inconsistent with this assumption.

The model proposed by Terro [7] is here re-written using normalised temperature variables for improved computation of the function. Furthermore, the factor included to account for aggregate content is here found to be formulated to produce a larger model output for materials of increased aggregate content, counter to intended results. Similarly, the load-dependence of the model requires modification for implementation in a general model due to the non-zero LITS predictions in unloaded conditions.

The set of five models chosen for further analysis in this work are the Nielsen model [8], the Anderberg model [1], the Schneider model [6], the Bažant model [2], and the Terro model [7].

8.1.2 *Qualitative investigation of model behaviour*

For the five chosen models, the insights gained from the analysis of chapter 4 were supplemented by a qualitative investigation of the behaviour of the models in various high temperature conditions in chapter 5. Based on comparison of the qualitative behaviour of the model results and experimental observations detailed in the review of the literature (chapter 2), suggestions for modifications of the models were made.

Furthermore, using the Nielsen model, the effects on total axial strain results of the magnitude of the transient strain response to states of tension could be found using three assumptions (temperature-dependence was assumed to be the same as in compression), labelled TTS0, TTS1, and TTS2. These assumptions are associated with

no tensile transient strain, tensile transient strain of equal magnitude to that under an equivalent compressive applied load, and tensile transient strain of equal magnitude to that under an equivalent compressive load level (i.e. normalised by tensile strength) respectively.

Through analysis of Gauss point mean measures of strain components, it was found that a significant component of net transient strain may develop in unloaded specimens due to the thermal stresses that develop during heating. For TTS0 specimens, this component is compressive, whereas the reverse is true for TTS2 specimens. The component is relatively minor for TTS1 specimens. Based on comparisons between the simulated results in both unloaded and loaded conditions and 'hypothetical' data sets, it was determined that the TTS1 assumption is the most consistent with experimental practice. However, the TTS0 assumption may also be consistent with experimental practice if 'true' thermal strain is distinct from the experimentally determined measure.

Using analysis of model predictions in simplified conditions, it was shown that drying can make a very large difference to the transient strain predictions of the Bažant model. As a result, it is very important that the evolution of the moisture state of concrete is accurately described to prevent poor parametric calibration.

Moreover, although results of the low level analysis of chapter 4 suggests that heating rate makes a relatively small difference to transient strain predictions (as a function of temperature), FE results suggests that this is not generally true in large temperature ranges in which a relatively large difference in transient strain may be observed between two specimens heated at different rates.

While the observations that the full transient strain component of the Bažant model may require up to approximately 30 days to develop are consistent with some experimental results for temperatures below approximately $100°C$, periods of shorter duration should generally be required for higher temperature ranges. The FE model results suggest that a major delayed component of transient strain develops after the cessation of heating for all temperature ranges. Moreover, the magnitudes of the final transient strain values predicted by the Bažant model are extremely large, particularly for high temperatures, when compared with those of the other models. Thus, it

appears that the original model is both qualitatively and quantitatively poor. Therefore, the model must be modified and the parameters calibrated to experimental data.

Several such modifications are here proposed, including the use of a minimum value of the relative humidity parameter applied to the model, a slight re-formulation of the microprestress evolution equation, and use of separate parameters to define the relative magnitudes of the effects of changing temperature and changing relative humidity on transient strain development.

Based on the results of the FE simulations, the Anderberg model is found to produce the weakest transient strain behaviour in the high temperature range. This may suggest that an additional degree of model freedom is required in these conditions, such as that of the modified form of the model, defined by Equation 4-19.

No modifications are proposed for the Nielsen model based on the results of the FE simulations, though the transition temperature of the model is here considered a free parameter as there is no theoretical justification for maintaining the default value. Thus, the model is considered to have four free parameters. Also, the effects of the moisture-dependent parameter of the Schneider model are found to be of minor importance. Thus, this parameter is replaced with a constant value.

8.1.3 *Quantitative analysis of model performance*

A technique that applies the methodology of FE analysis in conjunction with simple fitting techniques, named the 'iterative feedback technique' (IFT), was here developed in order to perform quantitative analysis of the transient strain models in comparison to the results of a comprehensive experimental investigation. The IFT is developed to be more reliable than simple mathematical fitting and more efficient than trial and error.

Results of application of the IFT to the experimental data sets using the Nielsen model suggests that the TTS0 assumption produces total strain results that are most consistent with experimental data sets. Though the difference is very small due to the relatively small thermal stresses that develop in the specimens, the TTS0 assumption is applied for subsequent analysis for the remaining models.

Using the IFT, the performances of each of the five transient strain models on the shortlist were compared objectively. It was found that the lowest overall error measure, which is defined using a weighted mean of the square of the differences in total strain data between experimental data sets and simulated strain histories, is obtained using either the Nielsen model or the Terro model. Each of these models is found to produce very similar levels of the error measure, both for results calibrated to individual data sets and to all data sets simultaneously. The performances of the remaining three models in order are found to be the Anderberg model, the Schneider model, and the Bažant model.

In support of the proposal that the transition temperature is a free parameter of the model, it was found, based on experimental evidence, that a value that is approximately 100°C lower than the default value is appropriate. The results also support the use of the modified form of the Anderberg model as the thermal strain behaviour at high temperatures is not found to increase sufficiently rapidly to reproduce observed transient strain behaviour. However, the error measures typically associated with this model are higher than those of the Terro model and the Nielsen model, even when the modified form of the model is applied.

This work has found that the Bažant model is unable to reproduce experimental data in the low temperature range ($T < 500℃$) despite the range of temperatures initially intended for application of the model ($T < 100℃$). Previously, it appeared that this behaviour may be suitable for concrete as transient strain is considered to be slower in development at low temperatures. However, these experimental results suggest that this model does not reproduce transient strain at a realistic rate in the low temperature range.

Moreover, although the modifications to the model prevent significant quantities of the delayed transient strain from developing, particularly by the use of a minimum value of the relative humidity parameter applied in the model calculations, it is found that reliable calibration of the associated parameters generally requires far more experimental data. Thus, no significant calibration of the parameters applied was performed.

The IFT was also utilised in this work to investigate the experimental data to provide evidence for the most appropriate load-dependent function of transient strain. A reduction in the error measure of up to approximately 16% in comparison to the default linear model was found for two functions. In particular, the loading function defined as the load level raised to a non-unity power produces good results, while resulting in a load-dependence that is linear in the mid-loading range and a reducing function of load in the low load range, which is consistent with some observations [9]. Moreover, no modifications are required to ensure that sensible predictions are made for conditions of zero local stress.

8.1.4 *Structural case studies*

In chapter 7, the Nielsen model, Anderberg model, and Terro model were applied to three realistic applications of concrete structures that may undergo heating. These examples, a heated and restrained beam, a column in fire conditions, and a nuclear reactor pressure vessel (NPV) in service conditions, were performed to demonstrate the consequences of the nature of the transient strain model to the performance of concrete as an engineering material.

The models were applied in the calibrated forms found most appropriate in chapter 7, though linear load-dependence is assumed. While the nature of the TTS assumption is not directly relevant to the results for the restrained beam and the NPV, some effects may be found for the column in fire conditions, so this example is performed using each TTS assumption in turn.

For the restrained beam, the axial stress evolutions produced using the Nielsen model and the Terro model are more consistent with observed results. Though not completely appropriate to directly compare the model predictions with the experimental results due to lack of information regarding thermal strain development, it can be seen that the behaviour of the Anderberg model is fundamentally unable to reproduce the shape of the stress-time curve, whereas results of the other two models show significant promise that, with further calibration of relevant parameters, a fairly good qualitative match may be possible (as demonstrated through use of the preloaded form of the thermal damage model defined in chapter 6). The results also

provide evidence for use of the value of the transition temperature of the Nielsen model found appropriate in the work of chapter 6.

For the column in fire, the results suggest that a relatively small difference is made by the nature of the model used. Very similar damage development occurs in the column cross section for each model, though slight differences occur in the time of development of damage in each region and slight differences in position of localised damage centres, particularly for use of the TTS1 and TTS2 assumptions. However, in comparison with the development of mechanical damage in the absence of transient strain, the importance of the nature of the transient strain model appears to be relatively small.

The NPV in service conditions does not undergo a great deal of transient strain as a relatively modest increase in temperature occurs during the first temperature cycle and is not exceeded during any subsequent heating cycle. It is found that the activity of a transient strain model prevents the development of mechanical damage that otherwise develops in a very small localised area of the cross section.

8.1.5 *Wider implications*

The implications of this work for the physical origins of transient strain are that it appears that the failure of the Bažant model suggests that the hypothesis that transient strain is a result of a temporary increase in basic creep compliance is unlikely to be valid. Similarly, the necessary modification of the Anderberg model suggests that any potential direct link between thermal strain and transient strain must be discounted. Beyond these two potential physical origins, no support is explicitly here provided for any remaining physical origin for transient strain.

Despite the potential link identified in this work between the Schneider model and a physical model in which transient strain is driven by a thermally-activated chemo-thermal process (such as dehydration), the relatively poor performance of the Schneider model should not be considered to indicate that transient strain cannot be strongly related to the dehydration process; this is for three main reasons. Firstly, it is possible that the calibration of the Schneider model may be further improved. Significant difficulties were established in applying the IFT to this model. Secondly,

despite the potential similarity between the general temperature-dependence of the Schneider model and the progress of the dehydration process indicated, there is no indication that the model was formulated on these principles. Thus, re-development of the model may be necessary to properly test this hypothesis. Finally, the link between the dehydration process and transient strain may not be properly characterised by the 'order' of the set of chemical reactions. Therefore, even if a model based on these principles were found to be invalid, the proposed physical origin of transient strain would not be disproved.

In fact, it is possible that the origin of transient strain is the dehydration of cement paste but that the complexity of the interaction between the changing chemical and physical natures of the material on the microscale and the apparent inelastic deformability of the material on the macroscale cannot be adequately described using macroscopic (or mesoscopic) parameters. Changes of configuration of the phases due to chemical interactions that occur under load, which could be a major source of transient strain, may plausibly be highly dependent on the nature of the chemical phases taking part in the interactions. Thus, the use of the specific mass of dehydrated water or the order of the dehydration process as dynamic variables of a model may be inappropriate.

Hence, as the macroscopic parameters or experimental observables that define the behaviour of such a model are presently unknown, significant levels of further research into the microstructure of cement gel during heating and the interactions between microstructural changes and behaviour on higher scales of observation may be required before a reliable mathematical model directly based on physical principles may be found.

Although use of the IFT for the Bažant model and the Schneider model produced relatively poor model results in comparison to the experimental data sets, some caution should be exercised in concluding that these models are relatively poor as significant difficulties were encountered in the parametric calibration of these models. The '*Parametric Permutation Iterator*' stage of the IFT is found to be inappropriate for the Bažant model as predictions of this program do not reproduce predictions of a FE

simulation. Therefore, the parameters were calibrated using 'trial-and-error' in a FE environment.

In terms of modelling practice, according to the evidence of this work, the Nielsen model and the Terro model produce results that are most similar to the experimental data sets examined. Therefore, it is recommended that one of these models is implemented when a transient strain model is required, in place of the Anderberg model which is generally applied. Although it may be possible that the Schneider model may be made to produce results more consistent with experimental results than achieved here, the evident difficulties of implementation, application, and manipulation of this model are significant disadvantages.

8.2 Further work

It is a significant strength of the methodology of the work performed here that the experimental data sets investigated are derived from the same experimental investigation [1], in which comprehensive information is provided with regard to the transport properties, mechanical properties, and the transient strain components that develop in heated conditions of the concrete specimens used in the analysis. This significantly aids efforts to identify the true transient strain component within the total axial strain results reported. However, future work should aim to apply this methodology to further experimental data sets in order to determine the robustness of the model predictions.

In particular, the analysis of further experimental data sets may provide evidence for the most appropriate nature of the response of transient strain models to states of tension. While the results of chapter 5 suggest that the TTS assumption applied may play a large role in the development of axial strain in some conditions, it was found in the work of chapter 6 that this role is fairly small in the experimental conditions of interest. This is highly likely to be principally due to the relatively small radial dimensions of the concrete specimens. Thus, analysis of experimental investigations performed on larger specimens is an area of interest for future work.

Moreover, verification of the most appropriate relationship between transient strain and load requires further experimental data of an increased range and number of

distinct applied load levels. Any deviation of load-dependence from linearity is necessarily fairly small. However, a deviation may be important in accurately defining values of the parameters of the temperature-dependent function of transient strain models and may significantly affect TTS analysis to be performed in future work.

For the purposes of application of the IFT to experimental results in chapter 6, two different mathematical formulations of thermal damage were applied. One of the formulations represents unloaded heated specimens, while the other represents preloaded heated specimens. Through use of the same mathematical formulation (Equation 6-11) with slightly different parameters, it was possible to represent the slightly different evolutions of thermal damage suggested by experimental data for the two distinct loading conditions. Use of disparate thermal damage evolutions in the two loading states is justified by the experimental data provided [1]. However, practical implementation of the two model configurations using one model proved to be very difficult. Attempts using switching or transitional techniques were found to produce poor results, probably due to feedback between varying local stresses and stiffness across small regions of the mesh. Therefore, for reasons of robustness and realistic thermal damage modelling of distinct local regions within large structures, further model development is necessary to implement a realistic thermal damage model that evolves according to preload in a stable manner.

Appendix A

$$C_{TT} = \left(\underline{\rho C}\right) + (\lambda_D + \lambda_E)\left(\epsilon_D \frac{\partial \rho_L}{\partial T} + \rho_L \frac{\partial \epsilon_D}{\partial T}\right) - \lambda_E\left(\epsilon_L \frac{\partial \rho_L}{\partial T} + \rho_L \frac{\partial \epsilon_L}{\partial T}\right) \quad \text{Equation A-1}$$

$$C_{TV} = -\lambda_E \rho_L \frac{\partial \epsilon_L}{\partial \tilde{\rho}_V} \quad \text{Equation A-2}$$

$$C_{TP} = 0 \quad \text{Equation A-3}$$

$$C_{AT} = \tilde{\rho}_A\left(\frac{\partial \phi}{\partial T} - \frac{\partial \epsilon_L}{\partial T}\right) - \frac{\epsilon_G P_G}{R_A T^2} \quad \text{Equation A-4}$$

$$C_{AP} = \frac{\epsilon_G}{R_A T} \quad \text{Equation A-5}$$

$$C_{AV} = -\frac{\epsilon_G R_V}{R_A} - \tilde{\rho}_A \frac{\partial \epsilon_L}{\partial \tilde{\rho}_V} \quad \text{Equation A-6}$$

$$C_{MT} = \tilde{\rho}_V \frac{\partial \phi}{\partial T} + (\epsilon_L - \epsilon_D)\frac{\partial \rho_L}{\partial T} + (\rho_L - \tilde{\rho}_V)\frac{\partial \epsilon_L}{\partial T} - \rho_L \frac{\partial \epsilon_D}{\partial T} \quad \text{Equation A-7}$$

$$C_{MP} = 0 \quad \text{Equation A-8}$$

$$C_{MV} = \epsilon_G + (\rho_L - \tilde{\rho}_V)\frac{\partial \epsilon_L}{\partial \tilde{\rho}_V} \quad \text{Equation A-9}$$

$$K_{TT} = k + \lambda_E \frac{\epsilon_L K K_L \rho_L}{\mu_L} \frac{\partial P_C}{\partial T} \quad \text{Equation A-10}$$

$$K_{TP} = -\lambda_E \epsilon_L \rho_L \frac{K K_L}{\mu_L} \quad \text{Equation A-11}$$

$$K_{TV} = -\lambda_E \frac{\epsilon_L K K_L \rho_L}{\mu_L} \frac{\partial P_C}{\partial \tilde{\rho}_V} \quad \text{Equation A-12}$$

$$K_{AT} = -\frac{\epsilon_G D_{AV} \tilde{\rho}_V P_G}{\tilde{\rho}_G R_A T^2} \quad \text{Equation A-13}$$

$$K_{AP} = \frac{K K_L}{\mu_G} \epsilon_G \tilde{\rho}_A + \frac{\epsilon_G D_{AV} \tilde{\rho}_V}{\tilde{\rho}_G R_A T} \quad \text{Equation A-14}$$

$$K_{AV} = -\frac{\epsilon_G D_{AV}}{\tilde{\rho}_G}\left(\tilde{\rho}_A + \frac{R_V}{R_A}\tilde{\rho}_V\right) \quad \text{Equation A-15}$$

$$K_{MT} = \frac{\epsilon_G D_{AV} \tilde{\rho}_V P_G}{\tilde{\rho}_G R_A T^2} - \frac{\epsilon_L K K_L \rho_L}{\mu_L} \frac{\partial P_C}{\partial T} \quad \text{Equation A-16}$$

$$K_{MP} = \frac{K K_G}{\mu_G} \epsilon_G \tilde{\rho}_V - \frac{\epsilon_G D_{AV} \tilde{\rho}_V}{\tilde{\rho}_G R_A T} + \epsilon_L \rho_L \frac{K K_L}{\mu_L} \quad \text{Equation A-17}$$

$$K_{MV} = \frac{\epsilon_G D_{AV}}{\tilde{\rho}_G}\left(\tilde{\rho}_A + \frac{R_V}{R_A}\tilde{\rho}_V\right) - \frac{\epsilon_L K K_L \rho_L}{\mu_L}\frac{\partial P_C}{\partial \tilde{\rho}_V}$$ Equation A-18

Appendix B

In order to find an appropriate mesh discretisation and time step value for the simulations of chapter 5, a set of heating conditions (in fact, those expected to be most challenging for solution convergence) are simulated for a range of values of the total number of body elements. In accordance with good practice, a maximum elemental aspect ratio of 3:1 is maintained throughout.

The transient strain model implemented for this purpose is strongly expected to cause little or no difference to the results of this procedure. The Nielsen model is applied as it uses relatively few parameters, it is entirely distinct from other phenomena (e.g. the magnitude of thermal strain), and it has a well-defined point at which transient strain development ceases.

The results show that if the time step value is about 2.0 s or less, the solution (in terms of displacement) is within $\pm$0.1% of the solution given by a time step of 0.1 s, as shown in figure B-1 (a). This indicates that no significant loss of accuracy occurs with use of a time step of 2.0 s and lower.

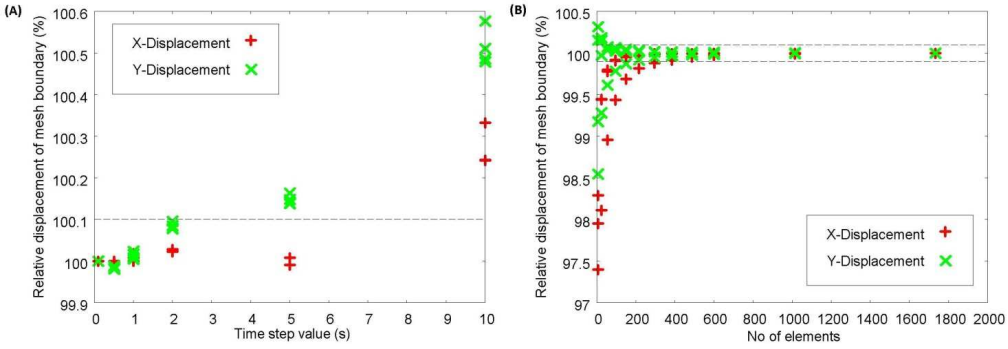

Figure B-1: Comparison of the displacement values found at the surface of the mesh approximately (a) one day after start of heating for 30x20 mesh simulated using various values of the time step parameter, and (b) two days after start of heating for a mesh composed of various numbers of elements simulated using a time step of 2 s.

Furthermore, the results of figure B-1(b) show that a mesh composed of a total number of elements greater than roughly 400 produces displacement results which are within $\pm$0.1% of the solution produced by using a mesh of 1734 elements (51×34).

On this basis, the mesh to be used in the simulations shall be composed of 30×20 elements with a time step value of 2.0 s. This combination produces results which are not significantly at variance with much finer meshes and lower time step magnitudes respectively. Also, apart from producing near-identical displacements at the mesh

boundaries, a mesh discretisation given by a 30×20 mesh also produces a mesh in which the stress and strain profiles can be closely inspected for results analysis if necessary.

The dependences of the results for temperature, gas pressure, and vapour content on mesh discretisation and time step value are very similar to those for displacement. Thus, a mesh of 30×20 elements and a time step of 2.0 s is sufficient to produce results of a very similar value to those of the high mesh fineness and low time step.

Appendix C

The error measures found in the simulations of experimental conditions (performed in chapter 6) are as recorded in tables C-1–6. The error measures are calculated within the PPI program (6.1.2) using the simulated total strain histories associated with each permutation of parameters. The error measure is given by the weighted mean of the sum of the squares in strain difference between the simulated strain results and experimental strain results. The weighting procedure is chosen to reduce any bias in the methodology towards temperature ranges in which more experimental data are available.

The terminology applied to refer to the data sets are defined as follows. The prefix 'AT' labels the individual experimental data sets, with the following number referring to the applied axial load associated with the experimental procedure. '4AT' is the label for all data sets. The presence of parentheses and subscript 'n' implies that the error measure is calculated over the data sets using a normalisation procedure. Finally, the symbol '4ATθ' references the tests performed for the Nielsen model in which the parameters are fitted to all data sets, with the transition temperature allowed to assume any value for any data set to minimise the error measure.

Table B-1: Parameter values associated with minimum error values for results of each data set and combinations of data sets, where the Nielsen model is implemented, with the TTS0 assumption.

Data set(s)	A [-]	B [-]	C [-]	θ^* [-]	Error measure [-]
AT225	8.0×10^{-4}	0.0	2.0×10^{-2}	7.00	0.39×10^{-6}
AT35	7.0×10^{-4}	1.0×10^{-4}	1.8×10^{-2}	6.00	0.27×10^{-6}
AT45	1.0×10^{-4}	2.0×10^{-3}	2.0×10^{-3}	3.00	2.77×10^{-6}
AT675	2.0×10^{-4}	2.0×10^{-3}	1.1×10^{-2}	4.25	0.14×10^{-6}
4AT	2.0×10^{-4}	2.0×10^{-3}	2.0×10^{-3}	3.50	1.08×10^{-6}
$(4AT)_n$	2.0×10^{-4}	2.0×10^{-3}	2.0×10^{-3}	3.50	1.51 (1.08×10^{-6})
4ATθ	3.0×10^{-4}	1.7×10^{-3}	3.0×10^{-3}	4.50 4.25 3.75 3.75	1.02×10^{-6}
$(4AT\theta)_n$	2.0×10^{-4}	1.9×10^{-3}	3.0×10^{-3}	4.50 4.25 3.75 3.75	1.37

Table B-2: Parameter values associated with minimum error values for results of each data set and combinations of data sets, where the Nielsen model is implemented, with the TTS1 assumption.

Data set(s)	A [-]	B [-]	C [-]	θ^* [-]	Error measure [-]
AT225	7.0×10^{-4}	4.0×10^{-4}	2.0×10^{-2}	7.00	0.40×10^{-6}
AT35	7.0×10^{-4}	1.0×10^{-4}	1.7×10^{-2}	6.00	0.28×10^{-6}
AT45	1.0×10^{-4}	2.0×10^{-3}	2.0×10^{-3}	3.00	2.74×10^{-6}
AT675	2.0×10^{-4}	2.0×10^{-3}	1.0×10^{-2}	4.25	0.12×10^{-6}
4AT	3.0×10^{-4}	1.7×10^{-3}	2.0×10^{-3}	3.75	1.12×10^{-6}
$(4AT)_n$	2.0×10^{-4}	2.0×10^{-3}	2.0×10^{-3}	3.75	1.61 (1.16×10^{-6})
4ATθ	2.0×10^{-4}	2.0×10^{-3}	3.0×10^{-3}	4.50 4.25 3.75 3.75	1.00×10^{-6}
$(4AT\theta)_n$	2.0×10^{-4}	2.0×10^{-3}	3.0×10^{-3}	4.50 4.25 3.75 3.75	1.32

Table B-3: Parameter values associated with minimum error values for results of each data set and combinations of data sets, where the Nielsen model is implemented, with the TTS2 assumption.

Data set(s)	A [-]	B [-]	C [-]	θ^* [-]	Error measure [-]
AT225	6.0×10^{-4}	4.0×10^{-4}	2.0×10^{-2}	7.00	0.38×10^{-6}
AT35	6.0×10^{-4}	3.0×10^{-4}	1.8×10^{-2}	6.00	0.25×10^{-6}
AT45	1.0×10^{-4}	1.8×10^{-3}	2.0×10^{-3}	3.00	2.60×10^{-6}
AT675	2.0×10^{-4}	2.0×10^{-3}	9.0×10^{-3}	4.25	0.10×10^{-6}
4AT	2.0×10^{-4}	1.9×10^{-3}	2.0×10^{-3}	3.75	1.20×10^{-6}
$(4AT)_n$	2.0×10^{-4}	2.0×10^{-3}	2.0×10^{-3}	4.00	2.02 (1.22×10^{-6})
4ATθ	2.0×10^{-4}	1.9×10^{-3}	3.0×10^{-3}	4.75 4.25 3.75 3.75	0.98×10^{-6}
$(4AT\theta)_n$	2.0×10^{-4}	2.0×10^{-3}	4.0×10^{-3}	5.25 4.75 4.00 4.00	1.42

Table B-4: Parameter values associated with minimum error values for results of each data set and combination of data sets, where the Anderberg model is implemented (with the TTS0 assumption).

Data set(s)	β_{tm}^{An} [-]	B_{tm}^{An} [°C^{-1}]	T_{tr}^{An} (°C)	Error measure [-]
AT225	2.300	1.45×10^{-4}	545	0.60×10^{-6}
AT35	2.150	1.95×10^{-4}	590	0.43×10^{-6}
AT45	2.825	0.00	590	1.71×10^{-6}
AT675	2.450	1.70×10^{-4}	495	0.20×10^{-6}
4AT	2.400	1.30×10^{-4}	500	1.13×10^{-6}
$(4AT)_n$	2.475	1.55×10^{-4}	600	1.23 (1.17×10^{-6})

Table B-5: Parameter values associated with minimum error values for results of each data set and combination of data sets, where the Terro model is implemented (with the TTS0 assumption).

Data set(s)	A_1' [-]	A_2' [-]	A_3' [-]	A_4' [-]	Error measure [-]
AT225	4286.152	-1921.485	475.0656	-22.48884	0.53×10^{-6}
AT35	3639.186	-1939.113	498.5837	-22.73872	0.48×10^{-6}
AT45	3720.057	-1868.600	517.3982	-22.48884	0.79×10^{-6}
AT675	4447.894	-1674.699	423.3258	-22.98859	0.20×10^{-6}
4AT	4407458	-1886.228	475.0656	-22.73872	0.78×10^{-6}
$(4AT)_n$	4447.894	-1886.228	470.3620	-22.48884	1.48 (0.79×10^{-6})

Table B-6: Parameter values associated with minimum error values for results of each data set ad combinations of data sets, where the Schneider model is used (with the TTS0 assumption).

Data set(s)	C_1 [-]	C_2 [-]	γ_w [°C^{-1}]	γ_0 [°C^{-1}]	T_g [°C]	Error measure [-]
AT225	3.591	2.340	1.746×10^{-3}	0.9×10^{-6}	632	0.61×10^{-6}
AT35	4.2294	2.860	1.746×10^{-3}	1.1×10^{-6}	632	0.60×10^{-6}
AT45	3.8304	2.860	1.746×10^{-3}	1.1×10^{-6}	632	1.71×10^{-6}
AT675	3.5910	2.340	1.746×10^{-3}	0.9×10^{-6}	632	0.30×10^{-6}
4AT	3.7506	2.860	1.746×10^{-3}	1.1×10^{-6}	632	0.94×10^{-6}
$(4AT)_n$	3.6708	2.860	1.746×10^{-3}	11×10^{-6}	632	1.24 (0.95×10^{-6})

Appendix D

List of publications:

- 2008 Annual Meeting of ACME, Newcastle University, 1-2 April 2008; "*Investigation into the form of the load-induced thermal strain model*"
- 2009 Annual Meeting of ACME, The University of Nottingham, 6-8 April 2009; "*Modelling the load-induced thermal strain of concrete*"
- 2010 EURO-C Conference, Rohrmoos/Schladming, Austria, 15-18 March 2010; "*Investigation into the form of the load-induced thermal strain model*"

Modelling the strain behaviour of heated concrete as a two-phase isotropic composite using the concept of effective stress

***C. J. Robson[1], C. T. Davie[2]**

School of Civil Engineering and Geosciences,
Newcastle University,
NE1 7RU
[1] c.robson@ncl.ac.uk

[2] colin.davie@ncl.ac.uk

Key Words: *Concrete, drying shrinkage, free thermal expansion, composite, finite element, finite difference, computational model.*

Introduction

Concrete is the World's most used manmade material. It is used in the construction of tall buildings, roads, bridges, tunnels and many other structures. As a result of this apparent ubiquity, it is important that the thermal-mechanical behaviour of concrete at high temperatures is well understood. High temperature situations can conceivably arise in a number of ways; fire situations are the most likely cause for applications such as tall buildings and tunnels but there are also examples whereby concrete structures must be designed to withstand moderately high temperatures for an extended amount of time such as nuclear pressure vessels which can be subject to cyclic thermal loading typically in the temperature range 15˚C-80˚C over the course of dozens of years.

The thermal-mechanical behaviour of concrete is a large subject with many different aspects. The purpose of this investigation is to model the free thermal strain, the drying shrinkage and the creep of the concrete in these situations. The free thermal strain is defined as the strain of non-drying concrete as a result of a change in temperature. The drying shrinkage is the strain of concrete as a result of a change in internal humidity. The concept of effective stress (otherwise known as Bishop's stress) accounts for the additional stress applied internally to concrete from the pore fluids and is to be used to model the drying shrinkage of concrete. Creep is defined as the time-dependent strain of concrete that is subject to a sustained mechanical load.

Furthermore, this investigation will explicitly take account of the separate strain behaviours of the cement matrix and the aggregate and use these to produce an overall composite strain. This is an improvement on models which ignore the separate strain behaviours of the aggregate and the cement paste as the hygro-thermo-mechanical behaviour of the separate components can be more readily understood than that of the concrete without reference to

the behaviour of its components. The aggregate phase will be assumed to undergo only free thermal strain in the conditions considered, whereas the cement paste will have components of free thermal strain, drying shrinkage, and creep.

Theory

Concrete is a composite material broadly consisting of an aggregate phase, a binding cement matrix phase, and pore space containing fluid phases. More specifically, these phases can be further subcategorized; the pore space is categorized by pore size which ranges from nanometres to millimetres; the aggregate consists of coarse and fine aggregate phases; the matrix phase consists of many different chemically distinct materials such as the main hydration product of Portland cement CSH (calcium silicate hydrates), both high and low density, and ettringite.

The interactions of these phases can cause complex hygro-thermo-mechanical behaviour in non-equilibrium situations. For instance, when concrete is heated the aggregate material expands linearly whereas the cement matrix initially expands linearly due to the temperature increase but, depending on the conditions, can lose moisture and eventually shrink as a result of a growth in the contractive effective stress (Gawin, Pesavento et al. 2007). Often, this is not observed however because the external heating drives the moisture into the concrete and, until equilibrium is reached, the cement paste does not lose moisture and can even gain moisture, so it does not contract. Clearly, it is desirable for the model to capture this complex behaviour.

For the purposes of modelling concrete, explicitly accounting for each separate phase would likely produce a robust model with a strong predictive potential but would be computationally challenging and logistically very difficult because of inherent randomness in phase distributions and phase properties.

On the other hand, treating concrete as a single phase material with averaged properties and using phenomenological data fits for the purpose of modelling would be much simpler computationally and a broad range of concretes could be modelled in a variety of non-equilibrium situations. However, the ability of the model to provide useful output would depend heavily on the availability of experimental data in specific situations and, where this is not available, data produced could not be so strongly relied upon as important phenomena may have been missed by the model. Furthermore, if conditions are different, some data fits may be inadequate, e.g. experiments performed under unsealed conditions may not produce reliable results for applications for which the concrete is sealed and, therefore, unable to exchange fluids with the environment.

A useful compromise between these two modelling extremes is to treat concrete as a two-phase medium, model the strain components of each phase and use this information to produce an effective strain behaviour of the concrete. A simple method to perform this is to use the Rosen-Hashin equation (Rosen and Hashin 1970). Originally intended to produce effective thermal expansion coefficients, this study uses a slightly modified version of the equation to produce a composite strain from the overall strains of the two components. For the case of an isotropic composite consisting of two isotropic components, this gives

$$\varepsilon^* = \bar{\varepsilon} + \frac{(\varepsilon_1 - \varepsilon_2)}{\left(\frac{1}{K_1} - \frac{1}{K_2}\right)}\left[\frac{1}{K^*} - \overline{\left(\frac{1}{K}\right)}\right], \qquad (1)$$

where ε^*, ε_1, ε_2, and $\bar{\varepsilon}$ are the effective composite strain, the strains of component 1 and component 2, and the average strain of the two components respectively; and K^*, K_1, K_2, and $\overline{\left(\frac{1}{K}\right)}$ are the effective bulk modulus of the composite, the bulk moduli of component 1 and component 2 and the average of the inverse of the bulk moduli of the two components respectively. The averaged quantities are calculated by weighting the strains of the separate components using their specific volumes.

The two components to be used are the cement matrix and the aggregate material. The strain components of the cement matrix considered by this investigation are free thermal strain, drying shrinkage and creep whilst the only strain component of the aggregate that is considered is the free thermal strain.

The free thermal strain of each component is modelled as a linear function of temperature, which agrees well with experimental data.

The drying shrinkage of the cement phase is modelled using the effective stress principle. As moisture is removed from the cement matrix, it is thought that three main processes act to increase the compressive strain on the solid skeleton. They are due to the capillary tension, the surface energy, and the disjoining pressure. The stress produced by these processes produces an immediate drying shrinkage strain component and a transient strain due to the creep of the cement matrix caused by this applied stress. The immediate strain given by this stress is given by

$$\boldsymbol{\varepsilon} = -\alpha\chi_s^{ws}\frac{p_c}{3K_T}\mathbf{I}, \qquad (2)$$

where $\boldsymbol{\varepsilon}$ is the drying shrinkage strain, α is the Biot constant, χ_s^{ws} is the solid surface fraction in contact with the wetting phase, p_c is the capillary pressure, and K_T is the bulk modulus of the cement paste.

The creep strain is modelled using Bažant's microprestress-solidification theory (Bažant, Hauggaard et al. 1997; Bažant, Hauggaard et al. 1997) whereby creep is modelled as the sum of a viscoelastic component and a viscous flow component. The viscoelastic component is affected by the continuing hydration of the cement paste and produces the creep strain using a Kelvin chain. The viscous flow component is affected by the changing apparent viscosity as a result of the relaxation of the microprestress (due to creep) and by moisture loss.

Numerical model

The above model is to be applied using an existing coupled model for concrete exposed to high temperatures (Davie, Pearce et al. 2006). This model is cast in a finite element framework and is implemented using an existing finite element program, FEAP.

The model is to be used to simulate the heating of a nuclear reactor type unsealed concrete exposed to increasing temperatures as reported in the literature by Khoury (Khoury 2006). This paper provides data regarding the strain behaviour of several different unsealed nuclear reactor type concretes under increasing thermal load both in conditions of applied stress and no applied stress. The concrete test specimens used are cylindrical of diameter 62 mm and height 186 mm.

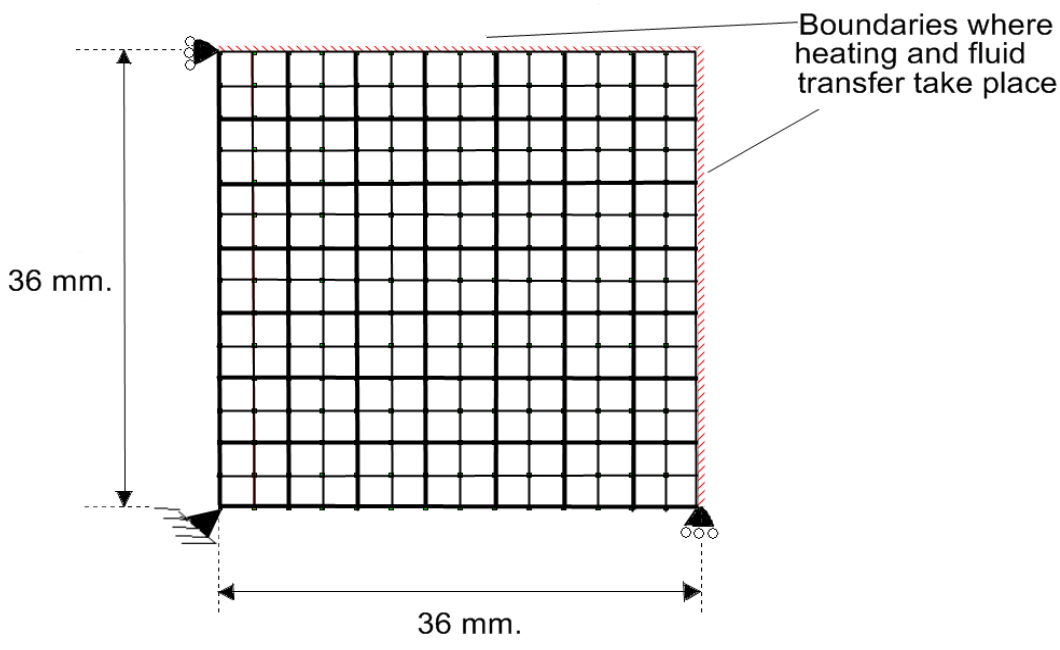

Figure 1 Finite element mesh used to model the experimental data of Khoury

For the numerical simulation, the hygro-thermal-mechanical behaviour of the cylindrical specimens will be assumed to be essentially 2 dimensional and the shape used will be a square rather than a circle. This is done for simplicity only and is considered valid as the surface length to area ratio of each are identical provided the width and height of the square are equal to the diameter of the circle. Quarter symmetry is assumed and a mesh consisting of 49 9-noded Lagrangian elements that form the main body of the mesh and 14 3-noded boundary elements is used, as shown in fig. 1.

Results and discussion

The validity of the model is demonstrated here through the reproduction of experimental results reported by Khoury. The model is used to simulate the strain of a concrete that is first heated to a moderately high temperature, held under this thermal load for a relatively long period of time and finally cooled in two stages until it reaches its original temperature as shown by the temperature evolution in fig. 2 (a).

The concrete used contains crushed dolomitic limestone and natural siliceous sands as the aggregate phases with ordinary Portland cement and a small amount of pulverized fuel ash as the cement binder phase. For the purposes of this investigation, the aggregate properties are taken as those of limestone and the binder properties are taken as those of ordinary Portland cement.

The results of imposing the heating conditions of fig. 2 (a) onto the concrete specimen have been modelled and are shown in fig. 2 (b) in comparison to the experimental results reported by Khoury, also plotted is the modelled strain behaviour of the aggregate and of the cement paste under the same conditions.

It should be noted that results indicated that the Rosen-Hashin equation was inappropriate as a means of plotting the strain components of drying shrinkage and creep and, therefore, is only used to produce the composite free thermal strain with reference to those of the aggregate and the cement paste. The remainder of the composite strain is a weighted sum of the other strain components based on the specific volume of the phase exhibiting the strain.

As can be seen in fig. 2 (b), the model produces results which reproduce the experimental data rather well qualitatively. This indicates that the most important hygro-thermal-mechanical behaviour has been taken into account by this model. It is worthy of note that a residual strain is observed after the concrete has been allowed to return to the starting temperature. This would usually not be found using a model that implicitly modelled drying shrinkage as a component of the free thermal strain. This further demonstrates the strength of this model.

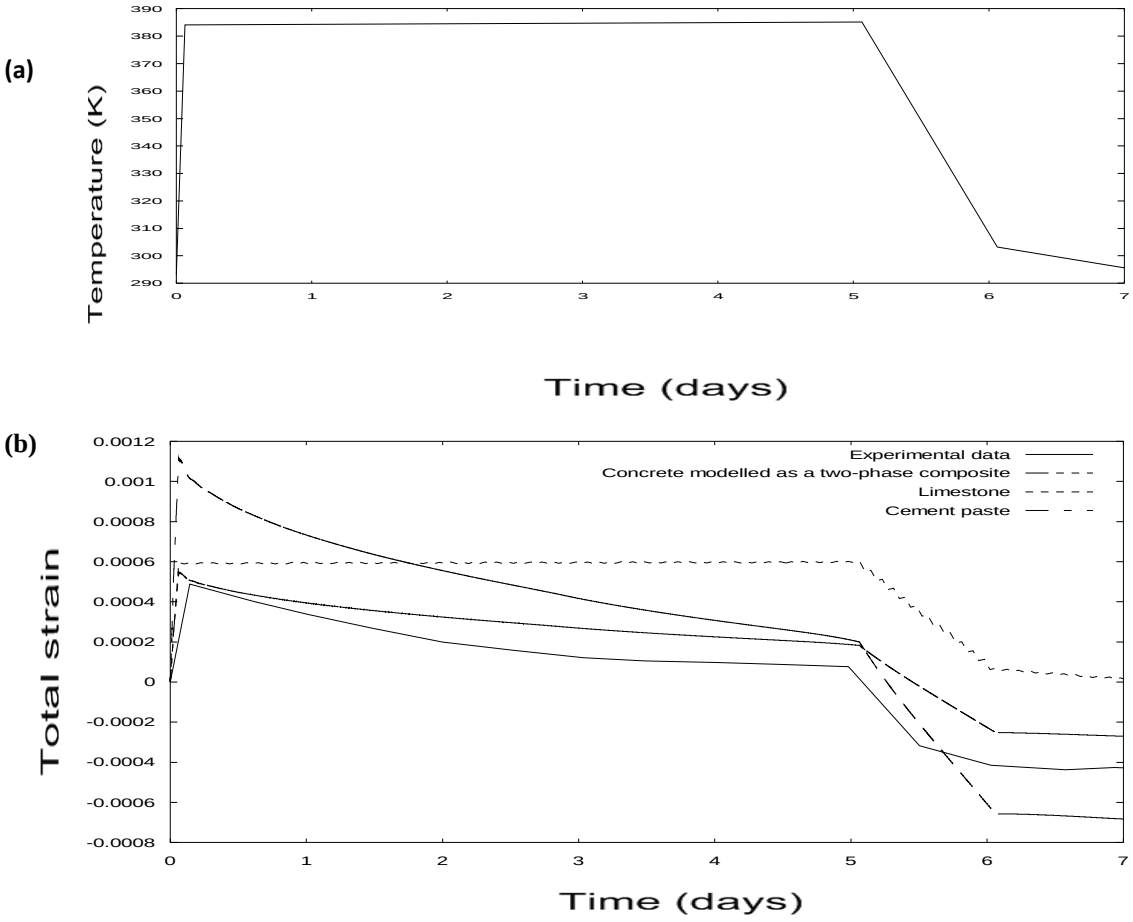

Figure 2 (a) The thermal loading applied to the boundary of the concrete specimen in (Khoury 2006) (b) The resultant strains of the thermal loading regime of (a) applied to the cement paste, the limestone, the two-phase model of concrete and the experimental data of Khoury for a limestone concrete

To make the model even more accurate, a more sophisticated composite strain model should be developed, one which accounts for the stiffness of the two different phases for all of the strain components. It may also be necessary that the porosity and the pore size distribution are explicitly taken into account, along with the composition and content of the sand component of the aggregate and any extra binding material used, e.g. pulverized fuel ash.

Acknowledgements

This work was based on an existing hygro-thermal mechanical model for concrete that was developed as part of the MAECENAS project. The contributions of Prof. N. Bićanić, Dr. C. J. Pearce and others to the development of that model are gratefully acknowledged.

References

Bažant, Z. P., A. B. Hauggaard, et al. (1997). "Microprestress-solidification theory for concrete creep. II: Algorithm and verification." Journal of Engineering Mechanics **123**(11): 1195-1201.
Bažant, Z. P., A. B. Hauggaard, et al. (1997). "Microprestress-solidification theory for concrete creep. I: Aging and drying effects." Journal of Engineering Mechanics **123**(11): 1188-1194.
Davie, C. T., C. J. Pearce, et al. (2006). "Coupled heat and moisture transport in concrete at elevated temperatures - Effects of capillary pressure and adsorbed water." Numerical Heat Transfer; Part A:

Applications **49**(8): 733-763.
Gawin, D., F. Pesavento, et al. (2007). "Modelling creep and shrinkage of concrete by means of effective stresses." Materials and Structures **40**: 579-591.
Khoury, G. A. (2006). "Strain of heated concrete during two thermal cycles. Part 1: strain over two cycles, during first heating and at subsequent constant temperature." Magazine of Concrete Research **58**(6): 367-385.
Rosen, B. W. and Z. Hashin (1970). "Effective thermal expansion coefficients and specific heats of composite materials." International Journal of Engineering Science **8**: 157-173.

Modelling the load-induced thermal strain of concrete

***C. J. Robson[1], C. T. Davie[2]**

School of Civil Engineering and Geosciences,
Newcastle University,
NE1 7RU
[1]c.robson@ncl.ac.uk
[2]colin.davie@ncl.ac.uk

Key Words: *Concrete, load-induced thermal strain, transitional thermal creep, high temperature, computational model.*

1 Introduction

Concrete is the world's most used manmade material. It is used, for example, in the construction of tall buildings, roads, bridges, tunnels and many other structures. As a result of this apparent ubiquity, it is important that the thermal-mechanical behaviour of concrete at high temperatures is well understood. High temperature situations can conceivably arise in a number of ways; fire situations are the most likely cause for applications such as tall buildings and tunnels but there are also examples whereby concrete structures must be designed to withstand moderately high temperatures for an extended period of time such as nuclear pressure vessels which can be subject to cyclic thermal loading typically in the temperature range 15˚C-80˚C over the course of dozens of years. These structures are often not only subject to elevated temperatures but concomitant loading. It is important that the behaviour of concrete in these service conditions, as well as in accident conditions is as well understood as possible.

There are many different active research fields currently ongoing dedicated to improving the understanding of the thermal-mechanical behaviour of concrete at elevated temperatures. This study aims to investigate the methods with which load-induced thermal strain (LITS) is currently modelled and how it may be modelled in the future. To do this, it is intended that the current models available in the literature will be explored and used to produce results which can be compared to reported experimental data. Also, the common assumption that LITS is linear in terms of the stress/strength ratio will be explored by comparing data found in different loading conditions. These objectives will be completed using computer programs written by the author.

LITS is one of the most important aspects of thermo-mechanical modelling of concrete, which was first detected in experimental results in 1966 [1]. LITS, defined as the difference in total strain of a heated loaded concrete body with the initial elastic strain removed and an identical concrete body in identical conditions under no applied load, is made up of several different strain components. Though there is no absolute consensus in the research field of what these strain components are, LITS can be said to consist of transitional thermal creep (TTC), drying creep, (temperature-dependent) 'conventional' creep, any plastic strain that develops and changes to the elastic strain due to heating of

concrete under load. TTC is a component of the strain behaviour of heated loaded concrete that is the least well understood. It provides a large contribution to the strain behaviour of heated loaded concrete and its main properties are that it is only present in the virgin heating of loaded concrete, it is not reversible on unloading or cooling, and it is seated in the cement paste. Drying creep is a component of LITS that is due to a coupling between drying and applied load. The temperature-dependent creep strain and the change in elastic strain components are relatively small in comparison to the other components of LITS, as is the plastic strain in most practical conditions.

2 Theory

LITS is always modelled empirically. There are examples of LITS models based on physical mechanisms (e.g. [2]) but the models always contain parameters which must be fitted to experimental data. Based on experimental results, Khoury et. al. [3] proposed a LITS 'master' curve, which is a curve that relates the LITS and the temperature level for a given applied stress/strength ratio. The curve was linear in stress/cold strength (the compressive strength in ambient temperature conditions) up to about 30%, and seemed to be insensitive to concrete type, age, heating rate, and initial moisture state. These results have been influential in the development of thermo-mechanical models of concrete. Many of the LITS models available in the literature contain the assumption that LITS is the product of a temperature function and the stress/strength ratio.

There are no thermo-mechanical models of concrete in the literature of which the author is aware which computes every strain component of LITS separately. The reason for this is that it is difficult to separate the components of LITS theoretically, which tend to appear together. Attempts to separate them experimentally inevitably introduce other forms of thermo-mechanical phenomena, such as strains due to micro-cracking, which obscure the results.

3 Model

Two computer models have been designed to achieve the aims of this investigation. The first is named Material Point and the second is named Linear.

Material Point is a computer program which reads an experimental data file containing the strain results of a heated loaded concrete body taken from the literature. It also reads a file which contains the strain results of a heated unloaded concrete body of an identical concrete specimen. The program then uses this data along with information about the concrete contained in the input file as regards the heating cycle, thermo-mechanical parameters, and the applied loading condition of the concrete specimen to find the parameters of the LITS equation which produce the best results. The parameters of the LITS equation are varied systematically and the total strain results are compared with those of the experimental data file to produce a measure of the error, which is recorded beside the specific permutation of the parameters in a file which is standardized. The program can be run for a whole array of experimental results and a simple computer program can read these files and deduce which permutation of the LITS parameters produces the lowest measure of error overall. This can be

performed outright or the measure of error in each file can be normalized to the lowest error in order that the overall result is not biased towards minimizing any particular data file.

Linear is a model which is similar to Material Point in that it accepts as input experimental data files which contain total strain measures from reported thermo-mechanical tests from the literature. It also accepts files containing unloaded thermal strain data taken from the same literature source. Linear produces files which contain only the LITS by removing the initial elastic strain and the linearly interpolated thermal strain from the results. The LITS model is assumed to be of the form,

$$\varepsilon_{LITS} = f(T)\left(\frac{\sigma}{f_c}\right)^k,$$

(1)

where ε_{LITS} is the LITS, $f(T)$ is a function of temperature hypothesised to be universal for all concretes, σ is the absolute value of the applied load, f_c is the measured compressive strength of the concrete at 20°C, and k is the exponent of the stress-strength ratio, which is often assumed equal to unity in the literature. Using this assumed form, the value of k can be varied and the function of temperature can be isolated for all variations of k and, then, those found for different load levels and even different concretes entirely can be compared using linear interpolation and evaluating the square of the differences at respective temperature points. The best value of k should produce the most similar functions of temperature for different load levels.

Both of the models mentioned above were tested against sets of data with known solutions. Material Point produced results that were not exactly correct but were within the smallest possible level of error (i.e. one increment away from the correct answer) and Linear produced the exact answer as expected.

4 Results and discussion

To investigate LITS, data were taken from the results of Anderberg and Thelandersson ([4] in [5]) (denoted data set 1) and data were taken from that used by Gawin et. al. ([6] in [7]) (denoted data set 2). These references provided in total 7 data sets in varying loading conditions from 15% to 67.5% of the compressive strength.

At this stage, the parameters of only one of the LITS models [8] available in the literature has been investigated using the Material Point program,

$$\varepsilon_{LITS} = \frac{\sigma}{f_c} y, \text{ where } y = \begin{cases} A\vartheta^2 + B\vartheta, & 0 \le \vartheta \le \vartheta^* = 4.5 \\ C\left(\vartheta - \vartheta^*\right)^2 + A\vartheta^*\left(2\vartheta - \vartheta^*\right) + B\vartheta, & \vartheta > \vartheta^* \end{cases}, \ \vartheta = \frac{T[^\circ C] - 20}{100}$$

. (2)

The parameters A, B, C were examined using the experimental data previously mentioned. Also, the model was used to find the values of the parameters which reproduce closely the LITS 'master' curve proposed by Khoury. This allowed the master curve to be used for comparison with the model results as is shown in fig. 1(a) for set 1 and fig. 1(b) for set 2. As can be seen in the figures, the master curve gives broadly correct behaviour. The data produced by the model with parameters chosen to reduce error is fairly good, particularly for the results of set 1. However, the parameters used for each load level were very different in some cases, so these curves are not suitable for a robust computer model. This suggests that either a compromise must be found whereby the model parameters take constant values that minimises the error over all of the load levels or the model must be altered to remove the necessity of varying the parameters with load.

In quantitative terms, the error produced by using the master curve to model the LITS of concrete was lower for stress/strength ratios of about 60% and above for both sets of data. For set 1, it had about one half of the error of the result with the next lowest amount of error (45%) and for set 2, it had about one quarter of the error of the result with the next lowest amount of error (45%). Not enough data have been used in the analysis at different load levels to draw any firm conclusions but the error seems to generally decrease when using the Khoury master curve for increasing stress/strength ratios.

It is also interesting to note that when the data files produced by Material Point are analysed to find the set of parameters which minimise the overall error for the group of results in set 1 and for the group of results in set 2, the Khoury master curve parameters produce lower quantities of error for two of the three and one of the four results. In fact, the relative quantities of error are approximately 50, 1/2, and 2/3 for set 1 and 5/2, 3/2, 2, and 3/4 for set 2. Considering that the optimised parameters are able to vary for the different sets of results, the error produced by the Khoury master curve are generally fairly good. When the data files produced by Material Point for both sets of experimental data are analysed to find the set of parameters which produces the lowest quantity of error overall for all seven of the sets of experimental conditions, the results using these parameters produce a lower measure of error in only 3 of the 7 of the sets of experimental conditions. This suggests that, as a model of LITS that is to be used universally for concrete, the Khoury master curve is arguably a better model than that produced using the Material Point program because more of the simulations matched the experimental data more accurately. However, it also suggests that the methodology of using the lowest overall error, even using a normalisation procedure for each set of conditions, is inadequate for finding the best model parameters. This deserves more thorough investigation.

The previous observation that the LITS model used seemed to fit the experimental data more accurately at load levels above sixty percent leads to a question about the assumed linearity of the LITS equation in terms of stress/strength. In order to investigate the possibility that LITS is not linear in stress/strength, the Linear model was used for data sets 1 and 2. According to the results, if equation 1 is assumed to be capable of describing the LITS behaviour of concrete, the exponent of the

stress/strength ratio for data set 1 is 1.25 and that for data set 2 is 0.85. When the model was used in tests to produce known results, the difference between the error measure for the known result and that of the next best exponent was roughly four orders of magnitude. For these results, the differences in error measures between the best exponent and the next best is significantly less than this, which suggests that the exact figure is far from convincing. The error measure for the best exponent compared to that associated with the value of the exponent being 1.0 for set 1 and for set 2 are approximately 1/10 and 3/10 respectively, which does suggest that a value for the exponent other than 1.0 may be the most appropriate.

(a)

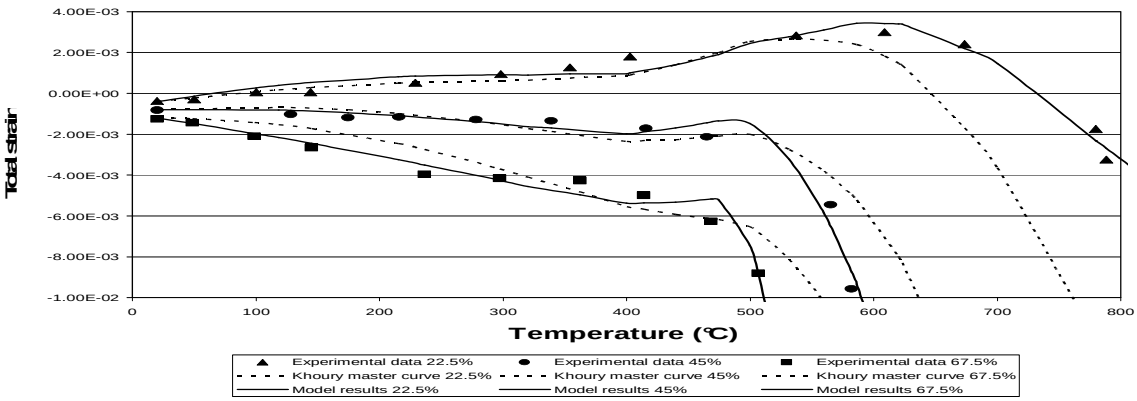

(b)

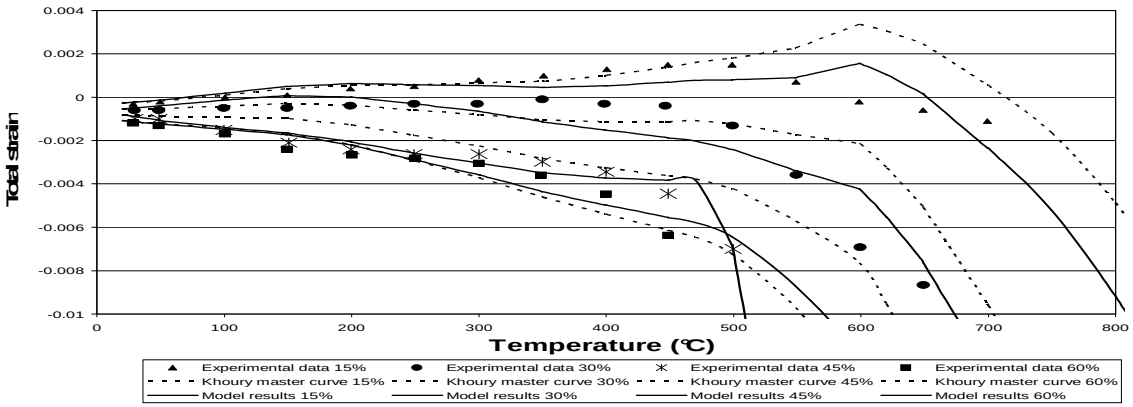

Fig. 1. The results of set 1 (a) and set 2 (b) in comparison with results produced using equation 2 with optimized parameters and those produced using the Khoury master curve

The functions of temperature produced by Linear for the optimal exponent for the data of set 1 (1.25) are shown as an example in fig. 2, alongside the necessary function of temperature if the exponent were 1.0.

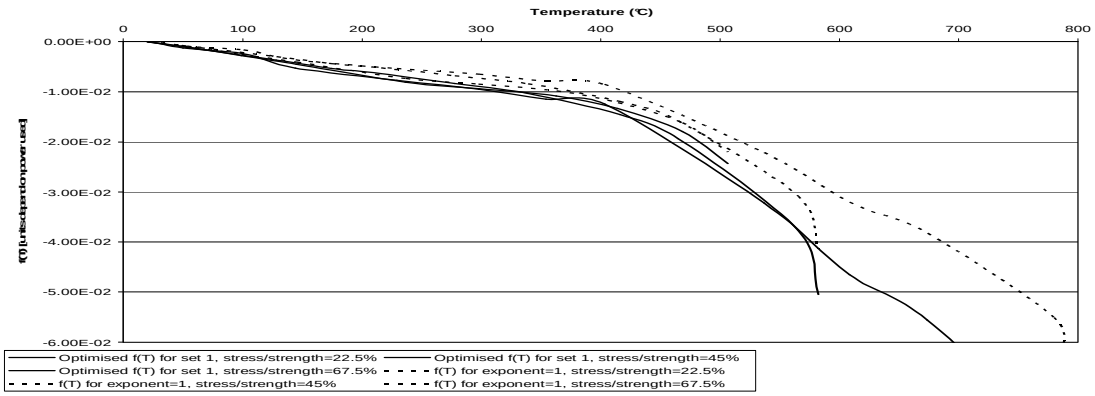

Fig. 2. The temperature functions (equation 1) produced when k=1.25 and when k=1.0 for results of set 1.

It is clear from fig. 2 that the functions of temperature for the optimised parameters are only slightly more uniform than those formed assuming that the exponent is 1.0. Visually, the difference does not appear to be a marked improvement, so no firm conclusions can be made at this time regarding the most appropriate exponent of the stress/strength term in the LITS equation.

This investigation has so far yielded some interesting preliminary results but any conclusions drawn from such a relatively modest volume of experimental data would be doubtful. In the future, it is intended that the investigation will include more data to be used to judge the universality of the LITS models, as well as the most appropriate form of the LITS equation by investigating more existing models and analysing experimental data with programs such as Material Point and Linear.

Acknowledgements

This work was performed with financial support provided by Halcrow Engineering Ltd and EPSRC through the CASE award programme. This support is gratefully acknowledged.

References

1. Hansen, T.C. and L. Eriksson, *Temperature change effect on behavior of cement paste, mortar, and concrete under load.* Journal of the American Concrete Institute, 1966. **63**(4): p. 489-504.

2. Sabeur, H. and F. Meftah, *Dehydration creep of concrete at high temperatures.* Materials and Structures, 2008. **41**(1): p. 17-30.

3. Khoury, G.A., B.N. Grainger, and P.J.E. Sullivan, *Strain of concrete during first heating to 600°C under load.* Magazine of Concrete Research, 1985. **37**(133): p. 195-215.

4. Anderberg, Y. and S. Thelandersson, *Stress and deformation characteristics of concrete at high temperatures*. 1976, Lund Institute of Technology, Sweden.

5. Thelandersson, S., *Modeling of combined thermal and mechanical action in concrete.* Journal of Engineering Mechanics, 1987. **113**(6): p. 893-906.

6. *Understand and industrial application of high performance concrete in high temperature environment-Final report*. 1999, Brite-Euram III BRPR-CT95-0065 HITECO.

7. Gawin, D., F. Pesavento, and B.A. Schrefler, *Modelling deformations of high-strength concrete at elevated temperatures.* Materials and Structures, 2004. **37**: p. 218-236.

8. Pearce, C.J., et al. *A transient thermal creep model for the hygral-thermal-mechanical analysis of concrete* in *VII International Conference on Computational Plasticity*. 2003. Barcelona: COMPLAS VII.

Investigation into the form of the load-induced thermal strain model

C.J. Robson, C.T. Davie
Newcastle University, Newcastle Upon Tyne, U.K.

ABSTRACT: Investigation into the temperature function and the normalised load level function, the product of which is postulated to form the equation which governs the load-induced thermal strain of cementitious materials. Using data from the literature, statistical methods and assumed forms of the equations involved, the normalised load level function is shown to be well modelled simply by the stress:cold compressive strength ratio and as a result, it is indicated that the temperature function cannot be universally plotted above a temperature of approximately 500°C.

1 INTRODUCTION

When a cementitious body is heated for the first time whilst under load, the largest strain component tends to be the load-induced thermal strain (LITS) for even relatively low levels of temperature increase and loading. The underlying mechanism which results in the occurrence of LITS is an ongoing research topic but it is known that the causes reside within the hardened cement paste phase itself. The role of the aggregate inclusions is simply one of restraint. It has also been widely accepted since the discovery of LITS in 1966 (Hansen and Eriksson 1966) that LITS is present only when the previous maximum temperature is exceeded, and that, consistent with this, LITS does not occur when the temperature is decreased (though, some studies have previously shown that creep increases in cooling which suggests that there may be a LITS-like effect at work, i.e. (Wallo, Yuan et al. 1965; Fahmi, Polivka et al. 1972) as referenced in (Bažant, Cusatis et al. 2004)). It is known that the excess deformation resulting from the coupling between loading and heating is far in excess of the additional strain which can be expected from the sum of the high temperature basic creep and the drying creep that is observed when concrete is simultaneously loaded and allowed to dry, though these two physical mechanisms surely contribute to LITS.

LITS can be defined as (Khoury, Grainger et al. 1985)

$$\varepsilon_{LITS}(T,\sigma) = \varepsilon_{tot}(T,\sigma) - \varepsilon_{ts}(T) - \varepsilon_{el}(T_0,\sigma), \quad (1)$$

where $\varepsilon_{LITS}(T,\sigma)$ is the LITS when a cementitious body is heated to temperature T whilst under load σ, $\varepsilon_{tot}(T,\sigma)$ is the total strain when the body is heated and loaded in the same conditions, $\varepsilon_{ts}(T)$ is the thermal strain when the body is heated to the same temperature under no applied load and $\varepsilon_{el}(T_0,\sigma)$ is the elastic strain produced by an identical load on the body with no change in temperature.

LITS is thought to consist of several separate deformation mechanisms, transitional thermal creep, drying creep, temperature-dependent basic creep and changes to the elastic strain. Of these components, TTC is dominant (Khoury 2006) and is also the least understood. Having said that, decomposing the LITS into all separate components is currently an inexact process likely to introduce errors unnecessarily, therefore LITS is generally modelled as a single component (e.g. (Khoury, Grainger et al. 1985; Thelandersson 1987; Terro 1998; Pearce, Davie et al. 2003)).

One of the most influential experimental studies to have guided attempts to model LITS was performed in 1985 at Imperial College in London (Khoury, Grainger et al. 1985). Results from this investigation suggested that the LITS behaviour of concrete is governed by a 'master' curve which is common to all cementitious materials of similar curing regimes and preheating conditions. Heating rate was shown to play only a minor role in defining the magnitude of LITS and the age was shown to be relatively unimportant, particularly for the temperature range below about 450°C. The study suggested that a linear relationship between LITS

and the stress: cold compressive strength ratio[1] was an accurate approximation for applied compressive loads between about 10% and 60% of the compressive strength at the initial temperature.

These results and others have influenced researchers attempting to produce realistic models for LITS. Some researchers have chosen to represent LITS as the product of a temperature function and the normalized load level (Thelandersson 1987; Terro 1998; Nielsen, Pearce et al. 2004). Other models for LITS have been proposed which are explicitly based on physical models (Sabeur and Meftah 2008), whilst others prefer to model LITS in the framework of creep models as an increase in magnitude of creep due to the changing temperature (Schneider 1988; Bažant, Cusatis et al. 2004).

2 AIMS & OBJECTIVES

The aims of this investigation are to investigate the universality of the form of the LITS temperature function and, by postulating that Equation 2 is the general form of the expression for LITS,

$$\varepsilon_{LITS}(T,\sigma) = f(T)g\left(\sigma/f_c\right) \quad , \qquad (2)$$

to find the most appropriate forms of the constituent temperature function f and normalised load level function g.

To achieve these aims, a material point-style model will be used to simulate experimental conditions to produce total strain results that can be compared to reported total strain values. The performance of a chosen LITS model compared with the performance of the same model optimised over several data files will provide evidence for the universality of LITS. The same model will be used to perform a similar investigation for three LITS models, each of which describes the temperature function of LITS in a different numerical method, to compare differing forms of the temperature function and the performance of these in comparison to experimental data.

Another model shall be used to determine the most appropriate form of the normalised load level function in a model for LITS. To do this, five possible forms of the function shall be assumed, each of which has one free parameter. Using strain ratios at corresponding data points, the free parameter can be fixed for every paired data point. Comparison of the values found via this method should indicate which model is the most accurate.

3 METHODOLOGY

3.1 *Details of numerical models used*

The material point model used here produces total strain results for any given heating and loading conditions using the strain components of Equation 1. Therefore, an initial elastic strain component, a thermal strain component and a LITS component must be calculated. The initial elastic strain can be calculated using the reported stiffness parameters. Data for the thermal strain behaviour in the same heating conditions are available in the literature. Therefore, using interpolation methods, the free thermal strain can be approximated at any temperature point. This method was assumed to be more accurate than fitting a polynomial to the data. Models from the literature were used to produce the LITS component in the model (see section 3.2 for details).

No previous information was assumed with respect to the parameters of the LITS models, other than taking note of prior values that have been used. This allowed a set of parameter maxima to be chosen that were far in excess of typical values. It was decided to choose parameters which resulted in no LITS as the parameter minima. Once chosen, the parameters were systematically varied between these extremes using a large number of permutations. The program the compared the total strain vs. temperature data produced with the experimental data file in order to calculate an error measure which could be recorded in a data file adjacent to the particular permutation of parameters used. The error was defined as the mean of the square of the strain differences between the simulated results and the experimental data. To remove bias towards temperature intervals which were more densely populated with data points, a weighting method was used in the error calculations. Potential error due to comparison of data points with misaligned temperature values was not present as the models used outputs results at the same temperatures as the experimental data files.

Once the data files containing the error measures were produced, the permutation of model parameters which produced the strain history most closely matching the reported data could be determined. Using multiple files, the model parameters could be optimised for more than one set of conditions. An error normalisation procedure was used in order to prevent bias towards files containing error minima of the largest magnitude.

The material point program was tested using numerically exact data to show how accurate the model is in terms of the forms of error inherent in the methodology (e.g. that due to the linear interpolation method). Thermal strain data files were produced by fitting fifth order polynomials to the

[1] referred to in the remainder as 'normalised load level'

original thermal strain files and replacing the strain values at each temperature point. Total strain data files were produced using the now fully characterised thermal strain, the loading and stiffness parameters from the reported data sets and Nielsen's LITS model (see section 3.2.1 for details) with known values of the parameters. The program was then applied to these data files. Results demonstrated that the model predicted that the values of optimal values of the LITS parameters were consistently very close to the known parameters. When the analysis was performed over all of the data sets, the accuracy increased and the parameters predicted were exactly correct.

Another model, to be referred to as the SRAP (strain ratio analysis program), was used to directly investigate the nature of the relationship between LITS and normalised load level. The total strain data of the reported experimental data sets (see section 3. 3 for details) were converted into LITS data by removing the thermal strain (calculated by linear interpolation of the reported thermal strain data) and the initial elastic strain. Assuming that LITS is the product of a temperature function f and a normalised load level function g, as in Equation 2, the ratios of the LITS values at the same temperatures are also the ratios of the normalised load level functions. Therefore, analysis of the experimental data can provide evidence as to which form of g is the most appropriate. To do this, the form of the function g must be assumed. Five different forms shall be investigated in this manner,

$$g\left(\sigma/f_c\right) = \left(\sigma/f_c\right) + k_1, \tag{3.1}$$

$$g\left(\sigma/f_c\right) = -\left(\sigma/f_c\right)^2 + k_2, \tag{3.2}$$

$$g\left(\sigma/f_c\right) = -\left(\sigma/f_c + k_3\right)^2, \tag{3.5}$$

$$g\left(\sigma/f_c\right) = -\left|\sigma/f_c\right|^{k_4}, \text{ and} \tag{3.4}$$

$$g\left(\sigma/f_c\right) = -\left(\sigma/f_c\right)^2 + k_5\left(\sigma/f_c\right), \tag{3.5}$$

where f_c is the initial compressive strength. By equating the values of the LITS and the ratios of the normalised load level function, a value of the free parameter k can be calculated for every pair of LITS data points which correspond to different load levels but identical temperatures, i.e.

$$k_1 = \frac{\left(\sigma/f_c\right)_1 - X\left(\sigma/f_c\right)_2}{(X-1)} \tag{4.1}$$

$$k_2 = \frac{-\left(\sigma/f_c\right)_1^2 + X\left(\sigma/f_c\right)_2^2}{(X-1)} \tag{4.2}$$

$$k_3 = \frac{\left(\sigma/f_c\right)_1 - \sqrt{X}\left(\sigma/f_c\right)_2}{(\sqrt{X}-1)} \tag{4.3a}$$

$$k_3 = \frac{\left(\sigma/f_c\right)_1 + \sqrt{X}\left(\sigma/f_c\right)_2}{(-\sqrt{X}-1)}, \tag{4.3b}$$

$$k_4 = \frac{\ln(X)}{\left[\ln\left(\sigma/f_c\right)_1 - \ln\left(\sigma/f_c\right)_2\right]}, \text{ and} \tag{4.4}$$

$$k_5 = \frac{-\left(\sigma/f_c\right)_1^2 + X\left(\sigma/f_c\right)_1^2}{-\left(\sigma/f_c\right)_1 + X\left(\sigma/f_c\right)_2} \tag{4.5}$$

where

$$X = \frac{\varepsilon_{LITS}(T,\sigma_1)}{\varepsilon_{LITS}(T,\sigma_2)}. \tag{4.6}$$

If the experimental data is produced by a product of two functions of the form of Equation 2 and the load function is given by one of Equations 3.1 to 3.5, then it would be expected that the value of k_i calculated using the corresponding equation from Equations 4.1 to 4.5 would be consistently calculated to be a very similar magnitude to that which best describes the LITS behaviour. Therefore, the model calculates the standard deviation of the calculated values of the free parameter k_i for each model for every data point available in order to evaluate the most consistent model. To ensure that the analysis is unbiased towards certain models of low k_i values, the standard deviation will be normalised to the magnitude of the calculated mean value of the free parameter for each model.

Note that there are two solutions for the free parameter of the third form of the function, Equation 3.3 as a result of the square root operator. Both of these solutions shall be found, Equations 4.3a and 4.3b, and the method which produces the best results, as previously defined, shall be taken as representative of this form of the loading function.

Two of the experimental data sets (see section 4.3) were obtained under identical normalised loading conditions. Hence, a model which conforms to the form of the LITS equation of Equation 2 would predict that the LITS curves of each should be identical. Therefore, the ratio of all of the respective LITS data points should clearly be 1.0. Hence, a value for the intrinsic error of the method can be found by statistical analysis of the actual ratio. If it is assumed that the error is entirely due to inaccuracy in the value of the free parameter of the normalised load level function and not due to inaccuracy in the loading conditions, temperature measurement, strain measurement (and interpolation) or the temperature function, an upper bound measure of the possible error in the free parameter is obtained.

Using the error measure term, a minimum and a maximum of the free parameter for each model can be calculated for each of the LITS ratios. This means that a set of error-adjusted values of the parameter

can be found and the standard deviation can be found in the usual way.

Clearly, there are more forms that g could take than simply the Equations 3.1-3.5, particularly if more than one free parameter is allowed. These forms can be possibly investigated in the future if necessary.

The SRAP methodology was tested in a similar manner to that in which the material point model was tested. As with the material point model test, fifth order polynomials were used to produce thermal strain data files, the known stiffness parameters were used to produce the initial elastic strain component and the LITS behaviour was produced using an equation with chosen parameters. The LITS equation was based on Equation 2 with a quadratic temperature function, chosen for simplicity. In order that each normalised load level model was directly tested, a set of data files was produced for each of the five assumed forms of the load level function of Equations 3.1-3.5.

The test was very useful as it demonstrated several issues with the methodology which were then able to be addressed. It became clear that the data in the low temperature range could not be included in the analysis as the strain ratios in this region tend to be much larger than in the rest of the temperature range due to numerical instability caused by the low values of the strain. The resultant predictions of the free parameter of the load function were wildly different from those of the remaining temperature region. Even comparisons of the G45 and the T45 data used to define the intrinsic error calculated relatively large error in this lower temperature region. Therefore, the temperature range used in comparisons of the LITS ratios was narrowed such that the minimum temperature allowable was set to at least 100°C which was roughly the temperature at which the strain ratios became more consistent. This replaced the original setting which was based on the minimum temperatures in the data files. When this issue was resolved, the intrinsic error was reduced from about 10% to about 1%.

Another issue highlighted by the tests is that comparisons between some of the data sets should be prevented as they tend to lead to erroneous values of the free parameter k (i.e. for comparisons of the results of the P44 test and the G45 or T45 test and of the T675 test and the G60 test). The predicted values of k can be very much larger than for other comparisons and, as a result, the mean value can be vastly different from the correct value. This is, again, a numerical issue which is due to the value of the LITS ratio being so close to 1.0. Therefore, results produced from the ratios of the aforementioned tests shall not be used in the process of finding the values of the free parameter k for each model.

When both of these issues were resolved, each calculated mean value of k was far closer to the correct value than they had been.

One final issue emerged from the testing of the model. This was that the relative standard deviation was not an indicator of the superior form of the normalised load level function. In fact, in one case, the model which was used to predict the results was, in fact, the model with the largest associated measure of relative standard deviation. This suggests that, whilst the methodology is valid, the principle that consistency of the calculated value of the free parameter is a reliable indicator of the most realistic model is highly questionable. Therefore, to quantify the quality of the data fit, a temperature function will be produced by inversion of Equation 2 to give the temperature function of the LITS equation. The function shall be calculated between a minimum temperature and a maximum temperature that is within the range of all of the data sets such that all of the data sets can be used to produce a mean temperature function. With reference to this mean, a standard deviation can be calculated which is taken as the error measure of the temperature function. The standard deviation can be made into a relative value using the magnitude of the mean temperature function for each temperature at which the quantity is calculated.

Some of the proposed models of Equations 5.1-5.5 can predict a non-zero value of LITS when no stress is applied, which seems objectionable, given that the definition of LITS used in this investigation is given by Equation 1. However, it should be noted that, according to experimental results (Khoury, Grainger et al. 1985), the relationship between normalised load level and LITS is approximately linear in the normalised load level range of 10% to 60% with the relationship tending towards a decreasing function of normalised load level for the lower stress range and an increasing function of normalised load level in the higher stress range. Hence, to fit experimental observations, the model for the mid-stress range would not be expected to pass through the origin when extrapolated to the state of zero applied stress. This possibility applies even if a loading function is approximated over the whole stress range. Thus, despite this conceptual problem, a model which is accurate in the mid-stress range may predict that LITS is present even when there is no agent present which can produce LITS. To avoid this problem, should a normalised load level function be selected with a value of k which produces non-zero LITS in situations of no applied stress, the range of applicability of the LITS model should explicitly remain in the normalised load level in which the investigation is carried out.

3.2 *Details of LITS models used*

As the material point model has no means of calculating the evolving hygral state of the cementitious material or explicit structural effects which may occur over the course of a test, only LITS models which do not explicitly require hygral parameters can be investigated with this method in its present form. Three models from the research field which fulfil this condition shall be investigated here using the material point-type model. The models shall be referred to as Nielsen's model (Nielsen, Pearce et al. 2004), Thelandersson's model (Thelandersson 1987) and Terro's model (Terro 1998). A brief description of each of these models is provided below. Each of the models conforms to the general form of the LITS model of Equation 2 with the normalised load level given by Equation 3.1 with k_1 set to zero.

3.2.1 *Nielsen's model*

The temperature function of the LITS model of Nielsen and colleagues is biparabolic with a transition temperature of 470°C. According to the model, LITS is given by

$$\varepsilon_{LITS}(T,\sigma) = \left({}^{\sigma}/_{f_c}\right) y(\theta), \tag{5.1}$$

where, for $0 \leq \theta \leq \theta^* = 4.5$,

$$y(\theta) = A\theta^2 + B\theta \tag{5.2a}$$

and, for $\theta > \theta^*$,

$$y(\theta) = C(\theta - \theta^*)^2 + A\theta^*(2\theta - \theta^*) + B\theta^* \tag{5.2b}$$

where A, B and C are the parameters of the model, and θ is a normalised measure of temperature given by

$$\theta \overset{\text{def}}{=} \frac{(T - T_0)}{100^{\circ}C}, \tag{5.2c}$$

where T is the elevated temperature of interest and T_0 is the initial temperature.

3.2.2 *Thelandersson's model*

Thelandersson's LITS model is given by

$$\varepsilon_{LITS}(T,\sigma) = \left({}^{\sigma}/_{f_c}\right) \beta \varepsilon_{ts}(T,0), \tag{5.3}$$

where β is the only parameter of the model. The temperature function of the model is directly proportional to the unloaded thermal strain, which is generally expressible as a nonlinear function of temperature.

3.2.3 *Terro's model*

The temperature function of Terro's LITS model is a fourth order polynomial in temperature (fifth order if Thames river gravel is used as aggregate) which was originally fitted to the 'master' curve of Khoury for a normalised load level of 0.3. The form of the normalised load level function of Equation 3.1 is used to model LITS in different loading conditions. An additional factor was also initially included to account for materials of different aggregate contents but this is ignored here as this effect is assumed to be intrinsically accounted for in the value of the initial compressive strength, an assumption presumably inherent in the previous two models. With this in mind, according to Terro's model, LITS is given by

$$\varepsilon_{LITS}(T,\sigma) = \left(k + \frac{\sigma}{f_c}\right) \sum_{n=0}^{n=4} (A_n T^n), \tag{5.4}$$

where A_i and k are the parameters of the model.

Terro's model should be investigated by finding a value for the parameter k first of all using the SRAP methodology, then the coefficients can be found for the polynomial temperature function.

3.3 *Details of experimental data sets used*

In order to conduct this investigation effectively, data for a broad range of load levels is required, as well as over a large temperature range. Experimental conditions which minimise gradients within the cementitious specimen would be advantageous as the material point-style model does not include structural effects, which should ideally, therefore, be kept to a minimum.

Table 1. Details of the parameters of the test data used in the investigation

Test code	Normalised load level	Temperature range (°C)	Ratio of elastic modulus to compressive strength
G15	-0.150	20-400	455.7
G30	-0.300	20-700	455.7
G45	-0.450	20-500	455.7
G60	-0.600	20-450	455.7
T225	-0.225	20-800	540.0
T45	-0.45	20-600	540.0
T675	-0.675	20-500	540.0
P44	-0.440	20-250	558.4

As a result of the experimental observation that LITS is only present when the temperature exceeds the previous maximum temperature, the curing regime of the concrete can be very important for attempts to model the LITS of concrete. For instance, the central regions of large concrete structures can develop temperatures as high as 80°C during hydration (Neville 1995). Therefore, a

prediction of LITS in future heating could be absent in this low temperature region (assuming the subsequent heating does not allow sufficient time to pass that LITS recovery takes place). Therefore, experimental conditions which do not allow the hydration process to cause significant temperature increase are necessary for this investigation.

Eight sets of experimental data, from the literature, were chosen to perform the analyses of this investigation [four were found in (Gawin, Pesavento et al. 2004), three were found in (Thelandersson 1987), and one found in (Petkovski and Crouch 2008)]. The experimental details are shown in Table 1.

4 RESULTS & DISCUSSION

4.1 *Investigation into the form of the LITS temperature function*

4.1.1 *Results of using temperature function of Nielsen's model*

The parameters found by the material point model to produce the total strain behaviour most closely matching each set of experimental results using Nielsen's LITS model are shown in Table 2.

Table 2. The LITS parameters found to reproduce the strain with the least error for each individual set of test conditions

Test code	Parameter			Error measure
	A (10^{-4})	B (10^{-3})	C (10^{-2})	(10^{-6})
G15	10.0	0.0	0.9	0.605
G30	9.4	0.0	0.7	1.490
G45	1.7	2.8	7.7	0.113
G60	4.1	1.4	*	0.224
T225	7.5	0.3	0.2	0.116
T45	2.5	2.1	1.6	0.139
T675	1.0	2.8	4.4	0.149
P44	7.3	0.0	*	0.004

* The highest temperature for the test used does not reach the region in which the parameter C is active.

The optimal parameters for each data set vary to a fairly high degree as is shown in the table. However, the actual LITS produced by each set of parameters is similar as is demonstrated in Fig. 1, which shows the LITS produced by applying each set of parameters to a representative stress/strength of 45%. Note that the optimal parameters produced for data sets G60 and P44 are not plotted beyond 470°C because no information is available regarding the value of the model parameter C in this region.

Clearly, the results of the graph suggest that each of the optimised sets of parameters produce results which are in fairly close correlation for the lower region of the temperature range. For the higher range of temperatures, there is a relatively large degree of scatter which should be expected because the quantity of experimental data available in this range is much more sparse. In two cases (G45 and T675), there is only one data point in this range. Therefore, the model will favour a value of the parameter C which results in a curve which passes very close to this point, regardless of the subsequent projection of the curve. This can clearly be seen for the data sets G45 and T675 as the optimal value of the final parameter for both is substantially higher than those of the other data sets.

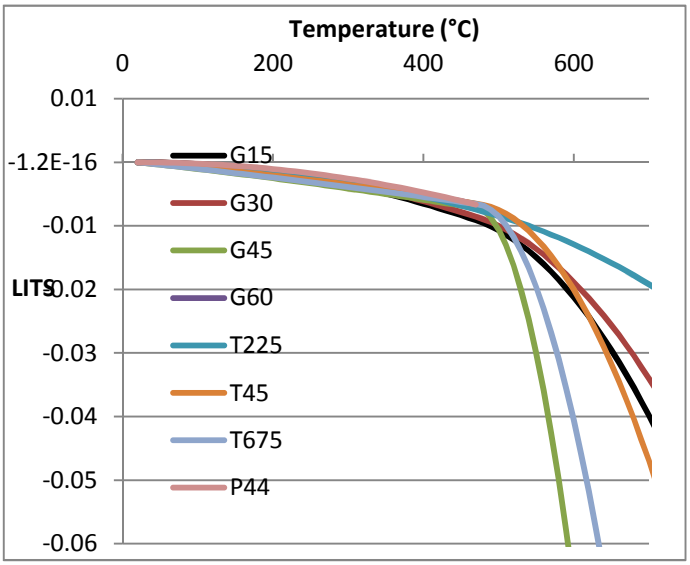

Fig. 1. Graph shows the LITS produced by the model parameters optimised for each different data set with an applied normalised load level of -0.45.

When more than one data set is analysed at once, the best LITS model parameters that are found should result in the most accurate version of the LITS model for the data sets analysed. If there is a universal LITS function, then the parameters produced when multiple data sets are analysed like this should converge to the same or a very similar set of parameters. To investigate if there is any evidence in these data sets for a universal LITS function, multiple data sets were analysed simultaneously in order to find evidence for a convergence of parameters.

Table 3. The optimised LITS parameters obtained when seven data sets are analysed at once.

Test code missed out	Parameter			Normalised error
	A (10^{-4})	B (10^{-3})	C (10^{-2})	
G15	8.8	0.0	0.2	7.083
G30	8.8	0.0	0.2	7.209
G45	8.6	0.0	0.2	6.574
G60	8.9	0.0	0.2	7.537
T225	8.5	0.0	1.0	4.525
T45	8.6	0.0	0.2	5.890
T675	8.8	0.0	0.2	6.768
P44	7.3	0.8	0.2	6.317
None*	8.8	0.0	0.2	6.985

*"None" means that all eight data sets were analysed at once.

The data in Table 3 suggests that there may be a universal LITS function. The optimised parameters barely change at all when one any one of the data sets is removed from the analysis which suggests the parameter set produces good results for all the data files.

4.1.2 *Results of using temperature function of Thelandersson's model*

Thelandersson's model was the most simple to fit to data as there was only one free parameter. Similarly to the results of section 4.1.1, the optimised parameter for one data set is not the same for any of the others.

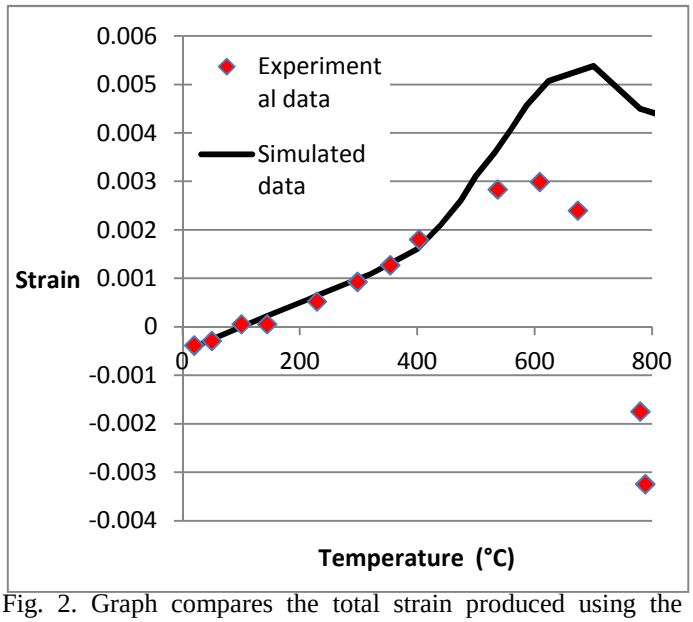

Fig. 2. Graph compares the total strain produced using the Thelandersson LITS model optimised to the data plotted on the same graph (data set is T225)

However, problems were found with this model. The model can match the experimental data fairly well up to a temperature of approximately 500°C but, after this point, the LITS curves appear to qualitatively change in a manner that the curves produced using the Thelandersson model are unable to capture. It was found that, initially, in order to minimise values of the error measure (i.e. the sum of the squares of the difference in strain between the predicted curves and the experimental curves), the model was producing values of the free parameter β which would cause the total strain curve to pass through a midpoint of the total strain curve. This would cause the error measure to be lower overall than it would if the parameter were chosen such that the region of the strain curve in the lower temperature region were well simulated. To avoid this unsatisfactory situation, the model had to be run only in the lower temperature region. This produced a better model in this region of the temperature field but the total strain in the large temperature region was very inaccurate. As can be seen as an example in Fig. 2, the Thelandersson model cannot produce the downturn in strain that is observed in practice.

4.1.3 *Results of using temperature function of Terro's model*

Details of the calculation of the optimal parameter k are presented in section 4.2. The best value of the parameter which was found was 0.0. Therefore, the temperature function of the LITS model of Equation 2 can be expressed in terms of the LITS data divided by the normalised load level. Collating all results from all of the data sets of section 3.3, a group of data is produced. Using the plotting software 'gnuplot', a fourth order polynomial was fitted to the group of data. The parameters, of the Terro model, are therefore shown in Table 4.

Table 4. The optimised parameters of the Terro equation.

k	A_0	A_1	A_2	A_3	A_4
	(10^{-3})	(10^{-4})	(10^{-6})	(10^{-9})	(10^{-12})
0	-6.25157	1.99317	-1.23681	2.85134	-1.85289

In general, application of this model was reasonably successful. However, the error measures are consistently higher than those of the Nielsen model. Also, the fourth order temperature function appears to be possibly inadequate. The LITS function actually decreases in magnitude slightly between 150°C and 350°C. This behaviour is not observed in experimental data and may be a result of the temperature range over which the parameters were set (20°-250°C).

4.1.4 *Discussion of the temperature function investigation*

The results of this investigation demonstrated that there is a qualitative change in the behaviour of LITS at high temperatures. The one parameter model of Thelandersson does not have the versatility to capture this high temperature behaviour. Fig. 2 is a typical result from the investigation which shows that, while the model seems ideally suited to capturing the behaviour of the LITS in the lower temperature range and seems to have a plausible physical footing, the strain behaviour in the higher temperature conditions implies that the model must be developed with perhaps another parameter included in the model in order that it can simulate the strain behaviour over a wider range of temperature.

The basis for Thelandersson's model seems to be that LITS is a coupling between the temperature increase and the loading. Hence, it is a natural progression to attempt to model the LITS behaviour as being proportional to the product of the strain produced by loading the cementitious body without

heating and the strain produced by the heating of the cementitious body without loading. If this is the cause of the LITS in a direct way then perhaps the improvements to be made to this model are in analysing the conditions that are perhaps incorrectly taken as the same in the low temperature conditions as in the high temperature conditions, e.g. the compressive strength of the material is perhaps reduced significantly at high temperatures. This would result in an increased normalised loading level in the higher temperature region and perhaps could partially explain the increasing difference between the model predictions and the observed strain data in the high temperature regions.

Nielsen's model already has the ability to track the increased LITS at high temperatures with an extra parameter. This is a welcome addition to the model as it allows for steep gradients in the higher temperature regions without the requirement of high powers of temperature as the Terro model has. However, just as with the Thelandersson model, more research is required in order to ensure that the model is able to find a reliable way to model the high temperature LITS behaviour accurately without the requirement of changing the parameter C to fit the data available.

4.2 *Investigation into the form of the LITS normalised load level function*

4.2.1 *Results of the strain ratio analysis program*

In order to assess the intrinsic accuracy of the method, the LITS ratios of the G45 and T45 tests were compared between a temperature minimum and maximum (100°C and the lower of the two temperature maxima in the results files) at a set number of equally spaced temperature values. The largest strain in magnitude was assigned as the numerator term and the other was assigned as the denominator term. This meant that the ratio was taken such that it was always larger than 1.0; this was in order to reflect the subsequent investigation of the LITS ratios whereby the larger strain and the smaller strain are always taken to be the numerator term and the denominator term of the strain ratio respectively. The intrinsic error in the strain ratios was then taken to be the mean of the difference between this value and 1.0. The result is shown in Fig. 3 along with the mean error, which was calculated to be about 0.21.

The subsequent program determined the ratios of the LITS values found from the reported experimental data. The previously calculated mean error was then applied to the ratios such that a maximum and minimum possible value of the parameter was found for each model according to the maximum and minimum possible values of the LITS ratio. Table 5 shows the calculated mean values of the free parameter k for each normalised load level model.

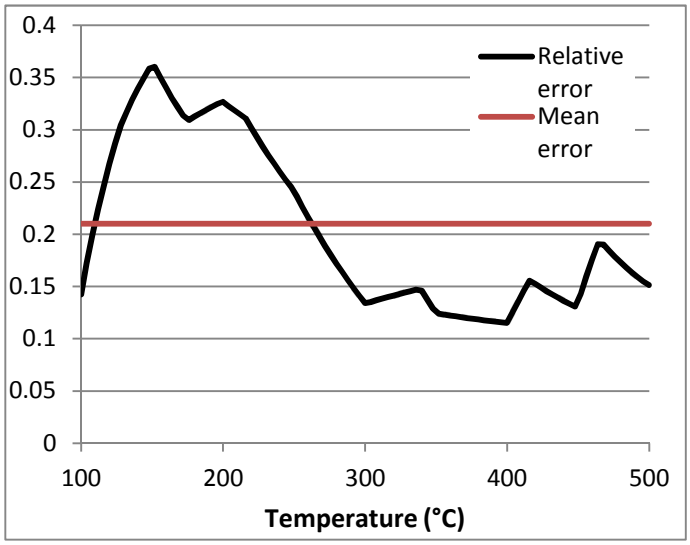

Fig. 3 Graph showing the erratic nature of the LITS ratio of the two sets of test data produced using the same normalised load level

Table 5. Mean values of free parameter k calculated both with and without the anomalous results for each form of the normalised load level function

Model number	Initial mean value of k	Mean value of k after removal of anomalous results*
1	1.007	0.072(1)
2	0.480	-0.074(1)
3	1.644	-0.230(1)
4	1.135	0.888(2)
5	1.029	-0.076(1)

*figure in parentheses represents number of anomalous results removed to produce new mean value of k.

Analysis of the results show that, for each model, values calculated for k for a small number of the pairs of tests are anomalously large. These values are so different from the remainder of the calculated values of k that the mean is significantly altered. As shown in table 5, the mean values of k after the removal of the anomalous results leads for all models to far more moderate quantities when compared with the load levels of use in the functions. This method of selecting which results to use is somewhat arbitrary and far less objective than is desirable. Nonetheless, the mean values obtained after removing the few values of k considered to be anomalies are noted along with another statistical quantity which can be objectively calculated from the data sets of k values without being significantly skewed by the presence of the anomalous results, the median. The median values of k found for each form of the normalised load level function are shown in Table 6.

By inverting the LITS equation and calculating the temperature function which results from using these forms of the normalised load level functions, a standardised measure of error can be calculated for

each of the values of k applied for the respective models as shown in Table 7. According to the results, the third load level model produces the most similar temperature functions over the experimental data are used in this investigation and a lower level of error is achieved by using the median value of k rather than the mean value. The resultant temperature function is shown in Fig. 4.

Table 6. Median values of the free parameter k found for each form of the normalised load level function

Model number	Median value of k
1	0.051
2	-0.077
3	-0.245
4	1.133
5	0.039

Table 7. Error measure found for the mean and median values of k by using relative standard deviation methodology

Model number	k	Relative standard deviation
1	0.072	37.639
1	0.051	34.465
2	0.123	32.771
2	0.121	32.740
3	0.076	32.598
3	0.071	32.503
4	0.077	35.341
4	0.092	33.127
5	1.252	89.669
5	0.434	59.966

*Relative standard deviation calculated at 100 evenly spaced temperature intervals. The values quoted are the sum of these values over the entire temperature range. For the mean value, simply divide by 101.

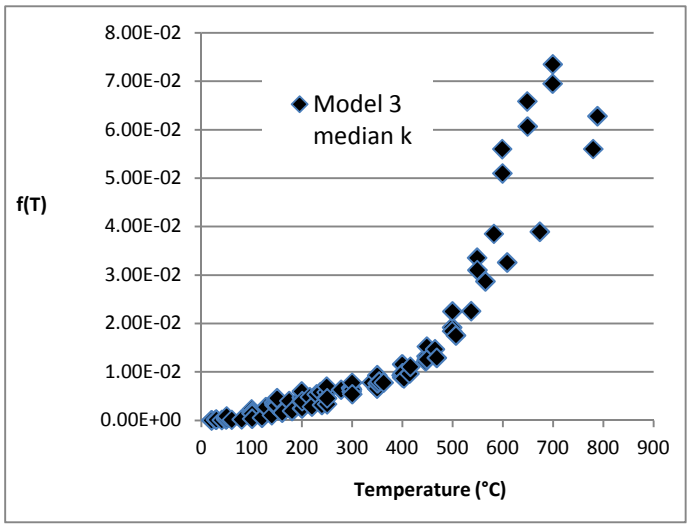

Fig. 4. The temperature function produced by inversion of the LITS data using Equation 3.3 and k=0.071.

The relative standard deviation produced for the first form of the load function with k set equal to zero is 33.667. This is the form of the function that is assumed by several models (e.g. Nielsen's model and Thelandersson's model). When compared with values of the relative standard deviation calculated for various forms of the load function in Table 7, it can be seen that it is among the best observed. The scatter graph of temperature functions produced by each model also looks very similar in terms of variance from a mean of the functions produced. In actual fact, the normalised load level functions produce very similar results with most of the divergence occurring at the higher load levels.

4.2.2 *Discussion of the normalised load level investigation*

The relatively modest increase in accuracy (as defined in the methodology) gained by using the normalised load level function Equation 3.3 in the general LITS equation given by Equation 2 suggests that the assumption of a simple form of the normalised load level function, such as that of Equation 3.1 with k set equal to zero, is a relatively good one in the mid-stress range considered here. The investigation provides no strong evidence statistically that the other simple forms which the function could take provide any kind of significant improvement.

Fig. 4 is evidence that a quite clear temperature function is produced by the methods employed in this investigation but only in the temperature range below approximately 500°C. Above this temperature, as already noted earlier when discussing the Thelandersson model, the LITS behaviour seems to change qualitatively in these high temperature conditions. As a result, it is fully expected that no normalised load level function could significantly improve on the temperature function produced as the LITS of the high temperature region is perhaps governed by a different equation than Equation 2 or possibly by a modification of this equation.

Fig. 3 shows the relative error that is produced using the methodology of this investigation from two data sets which should have identical LITS behaviour according to Equation 2. The clearly erratic behaviour that is identified here and, at times, in the subsequent investigation suggests that this method, though plausible in theory, may be too heavily reliant on the accuracy of the data to produce reliable results. However, the methodology has produced some results that can guide future research efforts.

The results produced consistently shows that the temperature function shows far more scatter in the temperature region greater than about 500°C than in the lower temperature region. This is in agreement with the previous observations (Khoury, Grainger et al. 1985) that the common behaviour of cementitious materials is present only in temperatures below about 450°C. Above this temperature, the LITS

behaviour seems very much dependent on the specific concrete used. In the higher temperature region of Fig. 4, the divergent data can clearly be seen to be separated into two distinct curves, the upper set of data points belongs to the experimental data sets G15 and G30 while the lower set of data points belong to the experimental data set T225. This clear distinction in LITS behaviour between different types of concrete may be due to dissimilar damage-type behaviour occurring in the two respective concretes. Also possible is that the reaction of the aggregate material to the increasing load placed on it over the course of a LITS test due to the stress relaxation in the cement paste phase is responsible for a proportion of the deformation and, hence, a disparity between the LITS observed for concretes made with different aggregate materials may tend to grow with time as a result of this. However, this hypothesis would not explain why the difference in LITS only seems to become noticeable in the temperature range above 500°C rather than a steady increase with time and it is questionable whether the increased load on most typical aggregate materials would cause such a difference in observed strain. The question of the role of the stress state of the cement paste phase however is of high interest as regards LITS analysis. As the cement paste phase is known to be the phase which undergoes LITS, the role of the variation of the average stress in the cement paste phase is an area to be explored in the future. Further to this, future work in this area shall investigate the relationship between damage evolution and the LITS behaviour in the higher temperature region. A greater understanding on the effects of damage should improve the modelling potential of all of the LITS models used in this investigation so far. Also, the current investigation will be continued such that further LITS models are examined, such as those of Bažant, Schneider, and Sabeur, certainly with changes in the methodology employed in this investigation, such as finite element modelling to allow structural effects and explicit hygral phenomena.

5 CONCLUSIONS

This investigation has provided evidence that the concept of a universal temperature function for LITS is limited to the temperature region below approximately 500°C, at which a qualitative change occurs in the behaviour of LITS. The investigation has determined that the three LITS models used in this paper are ill-equipped to model LITS in these high temperature conditions.

It has been shown that whilst minor improvements can be made to the normalised load level function, use of the normalised load level in itself as the loading function in Equation 2 is probably sufficient. The next area of research to be carried out in the field of LITS modelling is in reliably modelling the high temperature strain behaviour without necessity of changing parameters for different tests.

REFERENCES

Bažant, Z. P., G. Cusatis, et al. (2004). "Temperature effect on concrete creep modeled using microsprestress-solidification theory." Journal of Engineering Mechanics **130**(6): 691-699.

Fahmi, H. M., M. Polivka, et al. (1972). "Effect of sustained and cyclic temperature on creep of concrete." Cement and Concrete Research **2**: 591-606.

Gawin, D., F. Pesavento, et al. (2004). "Modelling deformations of high-strength concrete at elevated temperatures." Materials and Structures **37**: 218-236.

Hansen, T. C. and L. Eriksson (1966). "Temperature change effect on behavior of cement paste, mortar, and concrete under load." Journal of the American Concrete Institute **63**(4): 489-504.

Khoury, G. A. (2006). "Strain of heated concrete during two thermal cycles. Part 1: strain over two cycles, during first heating and at subsequent constant temperature." Magazine of Concrete Research **58**(6): 367-385.

Khoury, G. A., B. N. Grainger, et al. (1985). "Strain of concrete during first heating to 600°C under load." Magazine of Concrete Research **37**(133): 195-215.

Khoury, G. A., B. N. Grainger, et al. (1985). "Transient thermal strain of concrete: literature review, conditions within specimen and behaviour of individual constituents." Magazine of Concrete Research **37**(132): 131-144.

Neville, A. M. (1995). Properties of Concrete. Harlow, Essex, Pearson Education Limited.

Nielsen, C. V., C. J. Pearce, et al. (2004). "Improved phenomenological modelling of transient thermal strains for concrete at high temperatures." Computers and Concrete **1**(2): 189-204.

Pearce, C. J., C. T. Davie, et al. (2003). A transient thermal creep model for the hygral-thermal-mechanical analysis of concrete VII International Conference on Computational Plasticity, Barcelona, COMPLAS VII.

Petkovski, M. and R. S. Crouch (2008). "Strains under transient hygro-thermal states in concrete loaded in multiaxial compression and heated to 250°C." Cement and Concrete Research **38**.

Sabeur, H. and F. Meftah (2008). "Dehydration creep of concrete at high temperatures." Materials and Structures **41**(1): 17-30.

Schneider, U. (1988). "Concrete at high temperatures- A general review." Fire safety journal **13**(1): 55-68.

Terro, M. J. (1998). "Numerical modeling of the behaviour of concrete structures in fire." ACI Structural Journal **95**(2): 183-193.

Thelandersson, S. (1987). "Modeling of combined thermal and mechanical action in concrete." Journal of Engineering Mechanics **113**(6): 893-906.

Wallo, E. M., R. L. Yuan, et al. (1965). Sixth progress report: Prediction of creep in structural concrete from short time tests. T&AM. Urbana, Illinois, University of Illinois.

Acknowledgements

This work was carried out with the financial support of Halcrow Group Ltd. This contribution is gratefully acknowledged.

References

1. Mindess, S., L.F. Young, and D. Darwin, *Concrete*. Second Edition ed. 2003, London: Prentice Hall.
2. Neville, A.M., *Properties of Concrete*. 4 ed. 1995, Harlow, Essex: Pearson Education Limited. 844.
3. Phan, L.T., *Fire Performance of High-Strength Concrete: A Report of the State-of-the-Art*, in *Fire Performance of High-Strength Concrete*. 1996, NISTIR 5934: Gaithersburg, Maryland.
4. Kalifa, P., F.D. Menneteau, and D.A. Quenard, *Spalling and pore pressure in HPC at high temperature.* Cement and Concrete Research, 2000. **30**: p. 1915-1927.
5. Phan, L.T., J.R. Lawson, and F.L. Davis, *Effects of elevated temperature exposure on heating characteristics, spalling, and residual properties of high performance concrete.* Materials and Structures, 2001. **34**: p. 83-91.
6. Kalifa, P., G. Chéné, and C. Gallé, *High-temperature behaviour of HPC with polypropylene fibres: From spalling to microstructure.* Cement and Concrete Research, 2001. **31**(10): p. 1487-1499.
7. CEB-FIP, *CEB-FIP Model Code 1990*. 1993: Thomas Telford Services Ltd.
8. CEN, *BS EN 1992-1-2: 2004 Eurocode 2: Design of concrete structures part 1-2: General Rules- Structural Fire Design*, E. Standards, Editor. 2004.
9. Anderberg, Y. and S. Thelandersson, *Stress and deformation characteristics of concrete at high temperatures*. 1976, Lund Institute of Technology, Sweden. p. 1-84. Bulletin No. 54.
10. Johansen, R. and C.H. Best, *Creep of concrete with and without ice in the system.* RILEM Bulletin, 1962. **16**: p. 47-57.
11. Ross, A.D., G.L. England, and R.H. Suan, *Prestressed concrete beams under a sustained temperature crossfall.* Magazine of Concrete Research, 1965. **17**(52): p. 117-126.
12. Hansen, T.C. and L. Eriksson, *Temperature change effect on behavior of cement paste, mortar, and concrete under load.* Journal of the American Concrete Institute, 1966. **63**(4): p. 489-504.
13. Arthanari, S. and C.W. Yu, *Creep of concrete under uniaxial and biaxial stresses at elevated temperatures.* Magazine of Concrete Research, 1967. **19**(60): p. 149-156.
14. Ilston, J.M. and P.D. Sanders, *The effect of temperature change upon the creep of mortar under torsional loading.* Magazine of Concrete Research, 1973. **24**(84): p. 136-144.
15. Fahmi, H.M., M. Polivka, and B. Bresler, *Effect of sustained and cyclic elevated temperature on creep of concrete.* Cement and Concrete Research, 1972. **2**: p. 591-606.
16. Ilston, J.M. and P.D. Sanders, *Characteristics and prediction of creep of a saturated mortar under variable temperature.* Magazine of Concrete Research, 1974. **26**(88): p. 169-179.
17. Khoury, G.A., B.N. Grainger, and P.J.E. Sullivan, *Strain of concrete during first heating to 600°C under load.* Magazine of Concrete Research, 1985. **37**(133): p. 195-215.
18. Parrott, L.J., *A study of transitional thermal creep in hardened cement paste.* Magazine of Concrete Research, 1979. **31**(107): p. 99-103.

19. Petkovski, M. and R.S. Crouch, *Strains under transient hygro-thermal states in concrete loaded in multiaxial compression and heated to 250°C.* Cement and Concrete Research, 2008. **38**.
20. Hassen, S. and H. Colina, *Transient thermal creep of concrete in accidental conditions at temperatures up to 400°C.* Magazine of Concrete Research, 2006. **58**(4).
21. Colina, H. and J. Sercombe, *Transient thermal creep of concrete in service conditions at temperatures up to 300°C.* Magazine of Concrete Research, 2004. **56**(10): p. 559-574.
22. Nishizawa, N. and H. Okamura, *Strength and inelastic properties of concrete at elevated temperatures. Concrete for nuclear reactors.* ACI Special Publication, 1972. **SP-34**(Paper 22): p. 407-421.
23. Ehm, C. and U. Schneider, *The high temperature behaviour of concrete under biaxial conditions.* Cement and Concrete Research, 1985. **15**: p. 27-34.
24. Bernard, O., F.J. Ulm, and E. Lemarchand, *A multiscale micromechanics-hydration model for the early-age elastic properties of cement-based materials.* Cement and Concrete Research, 2003. **33**: p. 1293-1309.
25. Xi, Y., K. Willam, and D.M. Frangopol, *Multiscale modeling of interactive diffusion processes in concrete.* Journal of Engineering Mechanics, 2000. **126**(3): p. 258-265.
26. Lea, F.C. and R.E. Stradling, *The resistance to fire of concrete and reinforced concrete.* Engineering, 1922. **114**: p. 341-344, 380-382.
27. Bažant, Z.P., A.A. Asghari, and J. Schmidt, *Experimental study of creep of hardened Portland cement paste at variable water content.* Materials and Structures, 1976. **9**(52): p. 279-290.
28. Thelandersson, S., *Mechanical behaviour of concrete under torsional loading at transient high-temperature conditions*. 1974, Institute of Technology: Lund. p. 81. Bulletin No. 46.
29. Parrott, L.J. and R.M. Symmons, *Concrete in the Oceans: Deformation properties of an oil storage vessel: Concrete subjected to fluctuating stresses and temperatures. Report No. P3/I4*. 1977, Cement and Concrete Association. p. 13.
30. Khoury, G.A., B.N. Grainger, and P.J.E. Sullivan, *Transient thermal strain of concrete: literature review, conditions within specimen and behaviour of individual constituents.* Magazine of Concrete Research, 1985. **37**(132): p. 131-144.
31. Khoury, G.A., *Strain of heated concrete during two thermal cycles. Part 1: strain over two cycles, during first heating and at subsequent constant temperature.* Magazine of Concrete Research, 2006. **58**(6): p. 367-385.
32. Anderberg, Y. and S. Thelandersson, *Stress and deformation characteristics of concrete at high temperatures: 2. Experimental investigation and material behaviour model.* 1976, Institute of Technology: Lund. p. 86. Bulletin No. 54.
33. Thelandersson, S., *Modeling of combined thermal and mechanical action in concrete.* Journal of Engineering Mechanics, 1987. **113**(6): p. 893-906.
34. Schneider, U., *Concrete at high temperatures- A general review.* Fire safety journal, 1988. **13**(1): p. 55-68.
35. Jumppanen, U.-M., U. Diederichs, and K. Hinrichsmeyer, *Material properties of F-concrete at high temperatures*. 1986, Technical Research Centre of Finland.

36. Thienel, K.-C. and F.S. Rostásy, *Transient creep of concrete under biaxial stress and high temperature.* Cement and Concrete Research, 1996. **26**(9): p. 1409-1422.
37. Thienel, K.-C., *Festigkeit und Verformung von Beton bei hoher Temperatur und biaxialer Beanspruchung- Versuche und Modellbilding*. 1993, Dissertation Technical University Braunchweig.
38. Khoury, G.A., *Strain components of nuclear-reactor-type concretes during first heat cycle.* Nuclear Engineering and Design, 1995. **156**: p. 313-321.
39. Terro, M.J., *Numerical modeling of the behaviour of concrete structures in fire.* ACI Structural Journal, 1998. **95**(2): p. 183-193.
40. Fu, Y.F., et al., *Numerical tests of thermal cracking induced by temperature gradient in cement-based composites under thermal loads.* Cement and Concrete Composites, 2007. **29**: p. 103-117.
41. Khoury, G.A., P.J.E. Sullivan, and B.N. Grainger, *Radial temperature distributions within solid concrete cylinders under transient thermal states.* Magazine of Concrete Research, 1984. **36**(128): p. 146-156.
42. Khoury, G.A., et al., *Modelling of heated concrete.* Magazine of Concrete Research, 2002. **54**(2): p. 77-101.
43. Dias, W.P.S., G.A. Khoury, and P.J.E. Sullivan, *Basic creep of unsealed hardened cement paste at temperatures between 20°C and 725°C.* Magazine of Concrete Research, 1987. **39**(139): p. 93-101.
44. Khoury, G.A., W.P.S. Dias, and P.J.E. Sullivan, *Deformation of concrete and cement paste loaded at constant temperature from 140 to 724°C.* Materials and Structures, 1986. **19**(110): p. 97-104.
45. Grainger, B.N., *The effect of increase in temperature on the creep of a limestone concrete*. 1973, Central Electricity Research Laboratories: Leatherhead. p. 12.
46. Sabeur, H., et al., *Correlation between transient creep of concrete and its dehydration.* Magazine of Concrete Research, 2008. **60**(3): p. 157-163.
47. Khoury, G.A., *Strain of heated concrete during two thermal cycles. Part 2: strain during first cooling and subsequent thermal cycle.* Magazine of Concrete Research, 2006. **58**(6): p. 387-400.
48. Schneider, U., *Zur kinetik festigkeitsmindernder Reaktionen in Normalbetonen bei hohen Temperaturen*. 1973, Dissertation presented to Technische Universität Braunschweig. p. 94.
49. Schneider, U. and K. Kordina, *On the behaviour of normal concrete under steady state and transient temperature conditions*, in *Proceedings of the Third International Conference on Structural Mechanics in Reactor Technology*. 1975, North-Holland Publishing Company: London. p. Paper H1/6.
50. Schneider, U., *Creep effects under transient temperature conditions.* Fundamental research on creep and shrinkage of concrete, ed. F.H. Wittmann. 1982, The Hague: Martinus Nijhoff Publishers.
51. Anderberg, Y. and S. Thelandersson, *A constitutive law for concrete at transient high temperature conditions.* ACI Special Publication, 1978. **SP-55**: p. 187-205.
52. Weigler, H. and R. Fischer, *Influence of high temperatures on strength and deformation of concrete. Concrete for nuclear reactors.* ACI Special Publication, 1972. **SP-34**: p. 481-493.
53. Khoury, G.A., *Strain of heated concrete during two thermal cycles. Part 3: isolation of strain components and strain model development.* Magazine of Concrete Research, 2006. **58**(7): p. 421-435.

54. Kordina, K., C. Ehm, and U. Schneider. *Effects of biaxial loading on the high temperature behaviour of concrete*. in *Fire Safety Science- Proceedings of the First International Symposium*. 1985.
55. Kordina, K., W. Wydra, and C. Ehm, *Analysis of the developing damage of concrete due to heating and cooling*, in *ACI Symposium on 'Evaluation of Fire Damage of Concrete and Repair of Damage'. ACI SP 92-6*. 1986: San Francisco. p. 87-113.
56. Bažant, Z.P., G. Cusatis, and L. Cedolin, *Temperature effect on concrete creep modeled using microprestress-solidification theory.* Journal of Engineering Mechanics, 2004. **130**(6): p. 691-699.
57. Neville, A.M., *Creep of concrete as a function of its cement paste content.* Magazine of Concrete Research, 1964. **16**(46): p. 21-30.
58. Neville, A.M., *Theories of creep in concrete.* Journal of the American Concrete Institute, 1955. **27**(1): p. 47-60.
59. Counto, U.J., *The effect of the elastic modulus of the aggregate on the elastic modulus, creep and creep recovery of concrete.* Magazine of Concrete Research, 1964. **16**(48): p. 129-138.
60. Šmilauer, V. and Z.P. Bažant, *Identification of viscoelastic C-S-H behavior in mature cement paste by FFT-based homogenization method.* Cement and Concrete Research, 2010. **40**: p. 197-207.
61. Alizadeh, R., J.J. Beaudoin, and L. Raki, *Viscoelastic nature of calcium silicate hydrate.* Cement and Concrete Composites, 2010. **32**(5): p. 369-376.
62. Granger, L.P. and Z.P. Bažant, *Effect of composition on basic creep of concrete and cement paste.* Journal of Engineering Mechanics, 1995. **121**(11): p. 1261-1270.
63. Li, L.-Y. and J. Purkiss, *Stress-strain constitutive equations of concrete material at elevated temperatures.* Fire Safety Journal, 2005. **40**: p. 669-686.
64. Sabeur, H. and F. Meftah, *Dehydration creep of concrete at high temperatures.* Materials and Structures, 2008. **41**(1): p. 17-30.
65. Parrott, L.J., *Basic creep, drying creep and shrinkage of a mature cement paste after a heat cycle.* Cement and Concrete Research, 1977. **7**(5): p. 597-604.
66. Bažant, Z.P. and J.-C. Chern, *Concrete creep at variable humidity: constitutive law and mechanism.* Materials and Structures, 1985. **18**: p. 1-20.
67. Fares, H., et al., *High temperature behaviour of self-consolidating concrete. Microstructure and physicochemical properties.* Cement and Concrete Research, 2010. **40**: p. 488-496.
68. Parrott, L.J., *Increase in creep of hardened cement paste due to carbonation under load.* Magazine of Concrete Research, 1975. **27**(92): p. 179-181.
69. Hirljac, J., Z.Q. Wu, and J.F. Young, *Silicate polymerization during the hydration of alite.* Cement and Concrete Research, 1983. **13**(6): p. 877-886.
70. Dent Glasser, L.S., et al., *A multi-method study of C3S hydration.* Cement and Concrete Research, 1978. **8**(6): p. 733-739.
71. Mohan, K. and H.F.W. Taylor, *A trimethylsilylation study of tricalcium silicate pastes.* Cement and Concrete Research, 1982. **12**(1): p. 25-31.
72. Bentur, A., et al., *Structural-properties of calcium silicate pastes: 2. Effect of curing temperature.* Journal of the American Ceramic Society, 1979. **62**(7-8): p. 362-366.

73. Lentz, C.W., *The silicate structure analysis of hydrated portland cement paste*. 1966, Highway Research Board, Special Report 90: Washington. p. 269-285; cited in Khoury (1983).
74. Young, J.F., *Investigations of calcium silicate hydrate structure using silicon-29 nuclear magnetic resonance spectroscopy.* Journal of the American Ceramic Society, 1988. **71**: p. C-118-C-120.
75. Ishida, H., et al., *Highly-reactive β-dicalcium silicate: III, Hydration behaviour at 40°C-80°C.* Journal of the American Ceramic Society, 1992. **75**: p. 2541-2546.
76. Parrott, L.J., *Recoverable and irrecoverable deformation of heat-cured cement paste.* Magazine of Concrete Research, 1977. **29**(98): p. 26-30.
77. Brooks, J.J., *A theory for drying creep of concrete.* Magazine of Concrete Research, 2001. **53**(1): p. 51-61.
78. Grassl, P. and C.J. Pearce, *Mesoscale approach to modeling concrete subjected to thermomechanical loading.* Journal of Engineering Mechanics, 2010. **136**(3): p. 322-328.
79. Gal, E. and R. Kryvoruk. *Properties of concrete: A two step homogenization approach*. in *Computational Modelling of Concrete Structures*. 2010. Rohrmoos/Schladming, Austria: CRC Press.
80. Stroeven, P. and J. Hu, *ITZ's structural evolution during hydration in model concrete.* Magazine of Concrete Research, 2009. **61**(5): p. 371-377.
81. Hashin, Z. and P.J.M. Monteiro, *An inverse method to determine the elastic properties of the interphase between the aggregate and the cement paste.* Cement and Concrete Research, 2002. **32**: p. 1291-1300.
82. Li, G., et al., *Effective Young's modulus estimation of concrete.* Cement and Concrete Research, 1999. **29**: p. 1455-1462.
83. Yang, C.C., *Effect of the transition zone on the elastic moduli of mortar.* Cement and Concrete Research, 1998. **28**(5): p. 727-736.
84. Rainford, E.C. and J. Timusk, *Creep of hardened portland cement paste under cyclic temperature.* Journal of the American Ceramic Society, 1978. **61**(9-10): p. 380-385.
85. Youssef, M.A. and M. Moftah, *General stress-strain relationship for concrete at elevated temperatures.* Engineering Structures, 2007. **29**: p. 2618-2634.
86. Nielsen, C.V., C.J. Pearce, and N. Bicanic, *Theoretical model of high temperature effects on uniaxial concrete member under elastic restraint.* Magazine of Concrete Research, 2002. **54**(4): p. 239-249.
87. Gawin, D., F. Pesavento, and B.A. Schrefler, *Modelling deformations of high-strength concrete at elevated temperatures.* Materials and Structures, 2004. **37**: p. 218-236.
88. Terro, M.J., *Numerical modelling of thermal and structural response of reinforced concrete structures in fire*, in *Civil Engineering Department*. 1991, University of London: London.
89. Nielsen, C.V., C.J. Pearce, and N. Bićanić, *Improved phenomenological modelling of transient thermal strains for concrete at high temperatures.* Computers and Concrete, 2004. **1**(2): p. 189-204.
90. Pearce, C.J., et al. *A transient thermal creep model for the hygral-thermal-mechanical analysis of concrete* in *VII International Conference on Computational Plasticity*. 2003. Barcelona: COMPLAS VII.
91. Gerstle, K.H., *Simple formulation of biaxial concrete behaviour.* ACI Journal, 1981. **78-5**(1): p. 62-68.

92. Gerstle, K.H., *Simple formulation of triaxial concrete behavior.* ACI Journal, 1981. **78-34**(5): p. 382-387.
93. Stankowski, T. and K.H. Gerstle, *Simple formulation of concrete behavior under multiaxial load histories.* ACI Journal, 1985. **82**(2): p. 213-221.
94. Pearce, C.J., C.V. Nielsen, and N. Bicanic, *Gradient enhanced thermo-mechanical damage model for concrete at high temperatures including transient thermal creep.* International Journal for Numerical and Analytical Methods in Geomechanics, 2004. **28**(7-8): p. 715-735.
95. Davie, C.T., C.J. Pearce, and N. Bicanic, *Coupled heat and moisture transport in concrete at elevated temperatures - Effects of capillary pressure and adsorbed water.* Numerical Heat Transfer; Part A: Applications, 2006. **49**(8): p. 733-763.
96. Davie, C.T., C.J. Pearce, and N. Bićanić, *A fully generalised, coupled, multi-phase hygro-thermo-mechanical model for concrete.* Materials and Structures, 2010.
97. Tenchev, R.T., L.Y. Li, and J.A. Purkiss, *Finite Element Analysis of Coupled Heat and Moisture Transfer in Concrete subjected to Fire.* Numerical Heat Transfer, Part A, 2001. **39**: p. 685-710.
98. Gawin, D., C.E. Majorana, and B.A. Schrefler, *Numerical analysis of hygro-thermal behaviour and damage of concrete at high temperature.* Mechanics of Cohesive-Frictional Materials, 1999. **4**: p. 37-74.
99. Bažant, Z.P., *Constitutive equation for concrete creep and shrinkage based on thermodynamics of multiphase systems.* Materials and Structures, 1970. **3**(13): p. 3-36.
100. Bažant, Z.P., *Numerically stable algorithm with increasing time steps for integral-type aging creep*, in *Proceedings of 1st International Conference on Structural Mechanics in Reactor Technology (SMiRT-1)*, T. Jaeger, Editor. 1971. p. 119-126.
101. Bažant, Z.P. and S.T. Wu, *Thermoviscoelasticity of aging concrete.* Journal of the Engineering Mechanics Division, 1974. **100**(3): p. 575-597.
102. Bažant, Z.P., *Viscoelasticity of solidifying porous material- concrete.* Journal of the Engineering Mechanics Division, 1977. **103**(6): p. 1049-1067.
103. Bažant, Z. and S. Prasannan, *Solidification theory for concrete creep I: Formulation.* Journal of Engineering Mechanics, 1989. **115**(8): p. 1691-1703.
104. Bažant, Z. and S. Prasannan, *Solidification theory for concrete creep II: Verification and application.* Journal of Engineering Mechanics, 1989. **115**(8): p. 1704-1725.
105. Carol, I. and Z.P. Bažant, *Viscoelasticity with aging caused by solidification of nonaging constituent.* Journal of Engineering Mechanics, 1993. **119**(11): p. 2252-2269.
106. Bažant, Z. and Y. Xi, *Continuous retardation spectrum for solidification theory of concrete creep.* Journal of Engineering Mechanics, 1995. **121**(2): p. 281-288.
107. Bažant, Z.P., A.B. Hauggaard, and S. Baweja, *Microprestress-solidification theory for concrete creep. II: Algorithm and verification.* Journal of Engineering Mechanics, 1997. **123**(11): p. 1195-1201.
108. Bažant, Z.P., et al., *Microprestress-solidification theory for concrete creep. I: Aging and drying effects.* Journal of Engineering Mechanics, 1997. **123**(11): p. 1188-1194.
109. Nechnech, W., F. Meftah, and J.M. Reynouard, *An elasto-plastic damage model for plain concrete subjected to high temperatures.* Engineering Structures, 2002. **24**: p. 597-611.

110. Khennane, A. and G. Baker, *Thermoplasticity model for concrete under transient temperature and biaxial stress.* Proceedings: Mathematical and Physical Sciences, 1992. **439**(1905): p. 59-80.
111. Ring, T., M. Zeiml, and R. Lackner. *Structural behavior of tunnels under fire loading including spalling and load induced thermal strains*. in *Computational Modelling of Concrete Structures*. 2010. Rohrmoos/Schladming, Austria: CRC Press.
112. Ali, F., A. Nadjai, and S. Choi, *Numerical and experimental investigation of the behavior of high strength concrete columns in fire.* Engineering Structures, 2010. **32**: p. 1236-1243.
113. Weigler, H. and R. Fischer, *Beton bei Temperaturen von 100°C bis 750°C.* Beton, 1968. **2**: p. 33-46.
114. Kodur, V.K.R. and M.A. Sultan, *Effect of temperature on thermal properties of high-strength concrete.* Journal of Materials in Civil Engineering, 2003. **15**(2): p. 101-107.
115. Thelandersson, S., *On the multiaxial behaviour of concrete exposed to high temperature.* Nuclear Engineering and Design, 1983. **75**(2): p. 271-282.
116. Pickett, G., *The effect of change in moisture-content of the creep of concrete under a sustained load.* Journal of the American Concrete Institute, 1942. **38**: p. 333-356.
117. Parry-Jones, G., et al., *^{29}Si MAS-NMR hydration and compressive strength study in cement paste.* Cement and Concrete Research, 1989. **19**(2): p. 228-234.
118. Khoury, G.A., *Transient thermal creep of nuclear reactor pressure vessel type concretes*. 1983, University of London: London.
119. Schneider, U., M. Schneider, and J.-M. Franssen. *Consideration of nonlinear creep strain of siliceous concrete on calculation of mechanical strain under transient temperatures as a function of load history*. in *Fifth International Conference Structures in Fire*. 2008. Singapore.
120. Wu, B., et al., *Creep behavior of high-strength concrete with polypropylene fibers at elevated temperatures.* ACI Materials Journal, 2010. **107**(2): p. 176-184.
121. Gawin, D., M. Wyrzykowski, and F. Pesavento, *Modeling hygro-thermal performance and strains of cementitious building materials maturing in variable conditions.* Journal of Building Physics, 2008. **31**(4): p. 301-318.
122. Witek, A., et al., *Finite element analysis of various methods for protection of concrete structures against spalling during fire.* Computational Mechanics, 2007. **39**(3): p. 271-292.
123. Fares, H., A. Noumowé, and S. Remond, *Self-consolidating concrete subjected to high temperature: Mechanical and physicochemical properties.* Cement and Concrete Research, 2009. **39**: p. 1230-1238.
124. Chen, B., C. Li, and L. Chen, *Experimental study of mechanical properties of normal-strength concrete exposed to high temperatures at an early age.* Fire Safety Journal, 2009. **44**: p. 997-1002.
125. Picandet, V., A. Khelidj, and H. Bellegou, *Crack effects on gas and water permeability of concretes.* Cement and Concrete Research, 2009. **39**: p. 537-547.
126. Noumowé, A.N., R. Siddique, and G. Debicki, *Permeability of high-performance concrete subjected to elevated temperature (600°C).* Construction and Building Materials, 2009. **23**: p. 1855-1861.

127. Pijaudier-Cabot, G., F. Dufour, and M. Choinska, *Permeability due to the Increase of Damage in Concrete: From Diffuse to Localized Damage Distributions.* Journal of Engineering Mechanics, 2009. **135**(9): p. 1022-1028.
128. Lammertijn, S. and N. De Belie, *Porosity, gas permeability, carbonation and their interaction in high-volume fly ash concrete.* Magazine of Concrete Research, 2008. **60**(7): p. 535-545.
129. Meddah, M.S. and A. Tagnit-Hamou, *Pore structure of concrete with mineral admixtures and its effect on self-desiccation shrinkage.* ACI Materials Journal, 2009. **106**(3): p. 241-250.
130. Gawin, D., F. Pesavento, and B.A. Schrefler, *Towards prediction of the thermal spalling risk through a multi-phase porous media model of concrete.* Computer Methods in Applied Mechanics and Engineering, 2006. **195**(41-43): p. 5707-5729.
131. Dal Pont, S., et al., *An experimental relationship between complete liquid saturation and violent damage in concrete submitted to high temperature.* Magazine of Concrete Research, 2005. **57**(8): p. 455-461.
132. Nokken, M.R. and R.D. Hooton, *Using pore parameters to estimate permeability or conductivity of concrete.* Materials and Structures, 2008. **41**: p. 1-16.
133. Robert, F. and H. Colina, *The influence of aggregates on the mechanical characteristics of concrete exposed to fire.* Magazine of Concrete Research, 2009. **61**(5): p. 311-321.